

**A METHOD FOR THE PLY-LEVEL ELASTIC CHARACTERIZATION OF COMPOSITE  
MATERIALS USING THICK TUBULAR ANGLE-PLY SPECIMENS**

By

E.R. George

Thesis Submitted to the Faculty of the

Virginia Polytechnic Institute and State University

in partial fulfillment of the requirements for the degree of

Master of Science

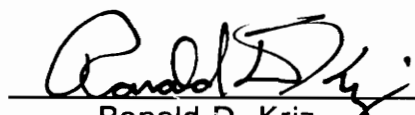
in

Engineering Mechanics

APPROVED:

  
Kenneth L. Reifsnieder, Chairman

  
G. Hayden Griffin

  
Ronald D. Kriz

December, 1993

Blacksburg, Virginia

C.2

LD  
5655  
V855  
1993  
9467  
C.2

# **A METHOD FOR THE PLY-LEVEL ELASTIC CHARACTERIZATION OF COMPOSITE MATERIALS USING THICK TUBULAR ANGLE-PLY SPECIMENS**

By

E.R. George

Kenneth L. Reifsneider, Chairman

Engineering Mechanics

(ABSTRACT)

Accurate mechanical properties are critical to the design and use of composite material structures. Due to the available processing methods, the properties of ceramic matrix materials are especially sensitive to the geometry of the component and how it is made. A method is presented by which the ply-level elastic properties of a composite material can be obtained for a common structure; a thick, laminated tube. The mechanical and thermal response of the tubes is modeled by a planar cylindrical elasticity solution. Properties are determined from surface strain measurements of a thick tube subject to axial, torsional, pressure, and thermal loads. All elastic properties (including thermal expansion coefficients) can be obtained except the out-of-plane shear moduli ( $G_{13}$ ,  $G_{23}$ ) which are not involved in the planar elasticity solution employed. The ply-level properties are estimated by inversion of the elasticity solution in terms of the global strain measurements. A Least Squares optimization approach is used for the inversion of the elasticity solution. Application of the method for a filament wound aluminum oxide-aluminum oxide tube is presented. Advantages and limitations of the method are identified.

## Acknowledgements

I would like to thank Dr. Reifsneider for providing this opportunity, and also, for his insight, assistance, patience and constant optimism. I also thank Kin Liao and Jack Lesko for their work on the experimental efforts of this project, and for their tolerance of my constant requests for more (and better!) data. Thanks also to Babcock & Wilcox for providing the experimental specimens and support and to my committee for their review and recommendations of this thesis. And finally, thanks to my father, who wanted to be an engineer, but is doing more by inspiring others as a teacher.

Table of Contents

1.0 Introduction . . . . . 1

1.1 Introduction . . . . . 1

1.2 Summary of Objectives . . . . . 2

1.3 Overview of the Thesis . . . . . 3

2.0 Theoretical Formulation . . . . . 4

2.1 Literature Review . . . . . 4

2.1.1 Characterization methods . . . . . 4

2.1.2 Strain response model . . . . . 5

2.2 Forward Solution . . . . . 6

2.2.1 Single Layer Solution . . . . . 7

2.2.2 Multi-Ply Solution . . . . . 15

2.3 Inverse Solution . . . . . 20

2.3.1 Use of Optimization . . . . . 20

2.3.2 Objective Function . . . . . 20

2.3.3 Derivation of Least Squares Method . . . . . 21

3.0 Method Verification . . . . . 23

3.1 Sample Geometry and Properties . . . . . 23

3.1.1 CASE I . . . . . 23

3.1.2 CASE II . . . . . 28

3.1.3 CASE III . . . . . 29

3.4 Conclusions . . . . . 32

<b>4.0 Experimental Specimens and Apparatus</b>	<b>33</b>
4.1 Experimental Specimens	33
4.1.1 Manufacturing, Porosity and Voids	33
4.1.2 Gross Geometry	34
4.2 Specimen Preparation and Instrumentation	40
<b>5.0 Experimental Results</b>	<b>44</b>
5.1 Applied Loads	44
5.2 Data Reduction	44
5.3 Final Data	63
<b>6.0 Inversion of Experimental Data</b>	<b>66</b>
6.1 Introduction	66
6.2.1 Effect of Porosity	66
6.2.2 Rule-of-Mixtures	68
6.3 Initial Inversion Attempt	69
6.3.1 Initial Adjustment to $\gamma_{x0}(F_x)$	70
6.3.2 Discussion of Convergence Problem	71
6.3.1 Initial Adjustment to $\epsilon_1(T_x)$ and $\epsilon_2(T_x)$	79
6.4 Inversion within "Convergence Zones"	80
6.3.1 Properties Along "Convergence Line"	84
<b>7.0 Summary, Conclusions and Recommendations</b>	<b>90</b>
7.1 Summary and Conclusions	90
7.2 Recommendations	92
7.2.1 Specimen Geometry and Characteristics	92
7.2.2 Experimental Data	93
7.2.3 Inversion Method	94
<b>References</b>	<b>95</b>

**Appendix A: Strain Property Influence Plots . . . . . 98**

**Appendix B: Experimental Data . . . . . 120**

**Appendix C: Effect of Gauge Position . . . . . 145**

**Appendix D: Codes . . . . . 150**

**D.1 BASIC Code . . . . . 150**

**D.2 C Code . . . . . 163**

**D.3 Pattern Search Code . . . . . 176**

**Vita . . . . . 181**

# 1.0 Introduction

## 1.1 *Introduction*

The increased efficiency of many systems and processes at higher temperatures has created a demand for high strength, high temperature materials. Ceramic matrix composites have great potential in these areas, combining the high strength and tailoring of properties available through continuous fiber composites with the thermal properties of ceramics. However, many unique engineering challenges are faced in the implementation. The problem of determining the ply level elastic properties of the material system is addressed in this study.

Ceramic matrix composite materials are very sensitive to processing conditions. Changes in specimen geometry effect the thermodynamics (and possibly chemistry) of the processing.[1] Flat coupon specimens may not accurately represent the material, especially when the primary components are tubes. The strain field in flat coupon specimens is also influenced by edge effects which complicates the interpretation of results.

The surface strain response of thick ( $R/h \leq 15$ ) cylinders subject to axisymmetric

loads is a function of all of the elastic properties except  $G_{13}$ ,  $G_{23}$ . Therefore, if the solution can be inverted, all of the properties (except  $G_{13}$  and  $G_{23}$ ) can be obtained in terms of the known (measured) strains. A single tubular specimen subject to three independent loads (axial, torsional and internal pressure loads) can be used to recover all of the available elastic constants. With the addition of thermal loading the coefficients of thermal expansion ( $\alpha_i$ ) can also be obtained. Mechanical and thermal testing of flat coupons yields only in-plane properties and requires several specimens of different geometries. Out-of-plane properties must be obtained by other methods (ultrasonic, etc.) or estimated from in-plane properties for that case.

## **1.2 *Summary of Objectives***

The specific study objectives were:

1. Development of a method by which the ply level, elastic properties of a thick, axisymmetric, laminated angle-ply cylinder can be determined from the strain response of the tube subject to axisymmetric thermal and mechanical loading.
2. To use the analysis to calculate the ply level mechanical properties of experimental specimens from measured surface strains.

Objective 1. was met by developing an numerical inversion scheme for the planar, cylindrical elasticity solution employed to model the strain response. This was accomplished by using a non-linear optimization method to find the "best" set of properties needed to reproduce the measured strains.

Objective 2. was complicated by details of the specimen geometry and limitations regarding the accuracy of strain measurements. Eventually a parametric approach was used to obtain a range of specimen properties.

## **1.3 *Overview of the Thesis***

In Ch. 2 the choice of the strain response model is discussed, and previous methods using cylindrical characterization specimens are referenced. The strain response model and inversion approach are developed including the derivation of the optimization method and its implementation for this problem.

In Ch. 3 sample inversions of analytical data are shown for a generic case. Case I shows the inversion employing axial, torsional, pressure, and thermal loads. Case II uses only axial and torsional loads to obtain a more limited set of properties. Case III examines the inversion as applied to a thin wall cylinder. The effect of variations in strain measurement are examined for all cases.

Chapter 4 details the specimen geometries. Experimental apparatus, testing procedures and data collection and analysis are discussed.

In Ch. 5 the experimental data are presented and reduced to a form suitable for the inversion method.

Chapter 6 covers the actual inversion of the experimental data. Final property ranges are presented. The assumptions and approximations necessary to the application of the method are examined.

Chapter 7 presents conclusions and recommendations for further study and use of the method presented.

Appendices include listings and details of the computer codes developed with sample input and output, strain-property curves and graphical presentations of the experimental data.

## 2.0 Theoretical Formulation

### 2.1 Literature Review

#### 2.1.1 Characterization methods

No general method for fully characterizing a material using laminated tubular specimens has been previously presented. However, tubular specimens have been previously suggested in the literature[2-8] as an efficient means of characterization. The extent of their application is summarized below.

Whitney and Halpin [2] published the most general of the previous characterization methods. They use Donnell Shell Theory to calculate the Classical Lamination Theory **A** matrix for symmetrically laminated cylinders subject to axial, torsional, and internal pressure loads. From the **A** matrix the in-plane "equivalent engineering constants" for the *laminate* are calculated. Ply-level properties are not obtained. The method is limited to thin wall cylinders, especially when considering expansional strains. Reference 3 is an extension of this effort.

Foley [4] calculates the in-plane shear modulus and strength for  $\pm 45^\circ$  filament wound Kevlar/epoxy and glass/epoxy *laminates*. Thickness effects were neglected and lamination theory was not employed. The strength calculations required thick cylinders

to prevent buckling. The stresses were calculated at the mid-plane yielding conservative strength estimates (assuming failure initiated at the outer surface). Other in-plane properties and ply-level properties are not obtained.

Bartkus and Humphrey [5] use thin, pressurized, hoop-wound specimens to calculate  $E_1$ ,  $\nu_{12}$  and the tensile fiber direction strength from surface strain measurements. Longitudinal fibers or random chopped fiber plies were also included in the laminate to prevent premature transverse cracking. Lamination theory was not used for this study. The dependence of the method on the specialized laminate (hoop-wound) and the limited properties preclude the use of the method for this study.

Swanson [6, 7, 8] has also done extensive laminate characterization work for both stiffness and strength using thin, laminated cylindrical specimens.

### **2.1.2 Strain response model**

The specimens of interest are thick walled ( $R/h \approx 8$ ) filament wound tubes (fig. 2.1). An exact planar elasticity solution[9] (referred to as the *forward solution*) is employed to model the strain response of the thick laminated cylinder. Several modified shell theories were considered, but the elasticity solution was chosen due to its flexibility and ease of formulation.

The elasticity solution, however, cannot account for the lack of axial symmetry (tow cross-overs, figure 2.2) inherent in filament wound cylinders. No analytical solution could be found in the literature which accounts for the effect of this geometry on the surface strain response of a thick cylinder. A finite element model might be possible and could be applied with the inversion scheme developed; however, the computational power and time required would be prohibitive. The formulation of the forward solution is summarized in Section 2.2.

## 2.2 Forward Solution

Geometry, nomenclature, and sign conventions are shown in fig. 2.1. The plies are numbered from inner to outer. Strains are given in either tube coordinates ( $\epsilon_x$ ,  $\epsilon_\theta$ ,  $\gamma_{x\theta}$ ) or material coordinates ( $\epsilon_1$ ,  $\epsilon_2$ ,  $\gamma_{12}$ ). The x axis is parallel to the cylinder axis and axial displacement is denoted  $u$ . The circumferential direction is  $\theta$  and the circumferential displacement is denoted  $v$ . The radial coordinate is  $r$  and radial displacement is denoted  $w$ . In the material coordinate system the fiber direction is denoted 1 and the transverse direction is denoted 2. The ply orientation angle ( $\phi$ ) is the angle between the x axis and the fiber direction (1 axis). A positive angle,  $\phi$ , rotates toward the positive y axis. The derivation of the elasticity solution is summarized below.

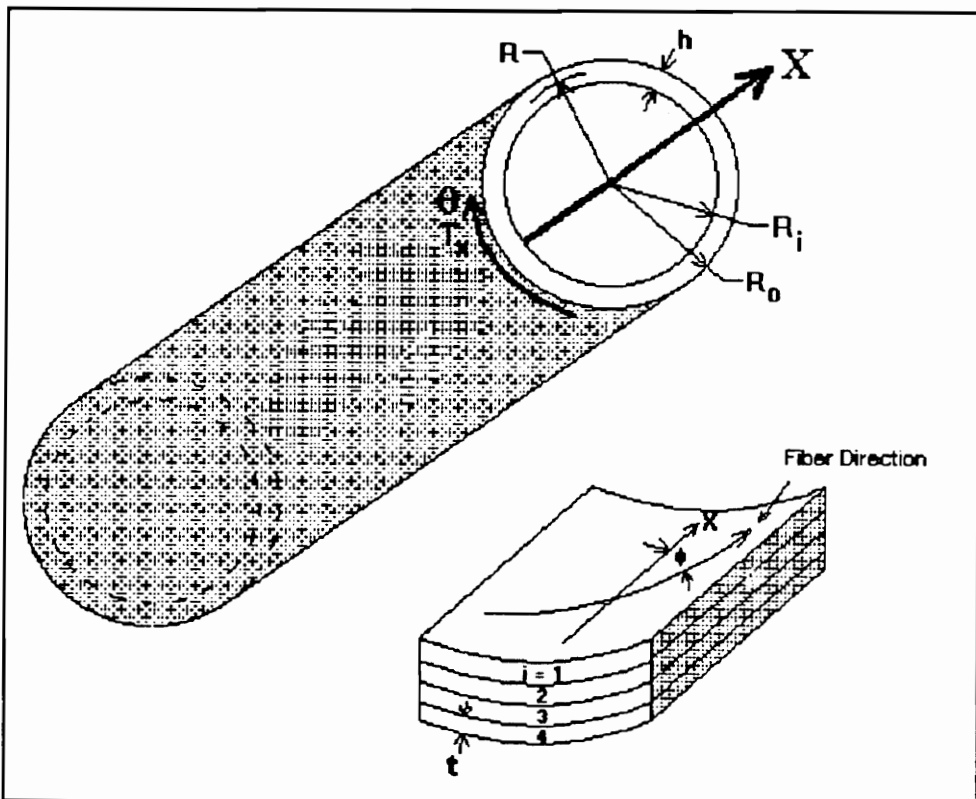


Figure 2.1 Geometry and Sign Conventions

### 2.2.1 Single Layer Solution

In general, the ply displacements are a function of all three coordinates.

$$\begin{aligned} u &= u(x, \theta, r) \\ v &= v(x, \theta, r) \\ w &= w(x, \theta, r) \end{aligned} \quad (1)$$

The strain-displacement relations for cylindrical coordinates are:

$$\begin{aligned} \epsilon_x &= \frac{\partial u}{\partial x} \\ \epsilon_\theta &= \frac{1}{r} \left( \frac{\partial v}{\partial \theta} + w \right) \\ \epsilon_r &= \frac{\partial w}{\partial r} \\ \gamma_{\theta r} &= \frac{1}{r} \left( \frac{\partial w}{\partial \theta} - v + r \frac{\partial v}{\partial r} \right) \\ \gamma_{xr} &= \frac{\partial u}{\partial r} - \frac{\partial w}{\partial x} \\ \gamma_{x\theta} &= \frac{\partial v}{\partial x} + \frac{1}{r} \frac{\partial u}{\partial \theta} \end{aligned} \quad (2)$$

In the material coordinate system, strains and stresses are related through the following form of Hooke's Law:

$$\begin{Bmatrix} \sigma_1 \\ \sigma_2 \\ \sigma_3 \\ \tau_{23} \\ \tau_{13} \\ \tau_{12} \end{Bmatrix} = \begin{bmatrix} C_{11} & C_{12} & C_{13} & 0 & 0 & 0 \\ C_{12} & C_{22} & C_{23} & 0 & 0 & 0 \\ C_{13} & C_{23} & C_{33} & 0 & 0 & 0 \\ 0 & 0 & 0 & C_{44} & 0 & 0 \\ 0 & 0 & 0 & 0 & C_{55} & 0 \\ 0 & 0 & 0 & 0 & 0 & C_{66} \end{bmatrix} \begin{Bmatrix} \epsilon_1 - \epsilon_1^T \\ \epsilon_2 - \epsilon_2^T \\ \epsilon_3 - \epsilon_3^T \\ \gamma_{23} \\ \gamma_{23} \\ \gamma_{23} \end{Bmatrix} \quad (3)$$

Where [C] is the stiffness matrix and  $\epsilon_i^T$  are the unconstrained thermal

deformations. The thermal expansion response is assumed to be a linear function of temperature as shown in eq. 4 where  $\alpha_i$  are the coefficients of thermal expansion (CTE).

$$\epsilon_i^T = \alpha_i \Delta T \quad (4)$$

The inverse of eq. 3 is shown below where [S] (compliance matrix) is the inverse of the stiffness matrix [C].

$$\begin{Bmatrix} \epsilon_1 - \epsilon_1^T \\ \epsilon_2 - \epsilon_2^T \\ \epsilon_3 - \epsilon_3^T \\ \gamma_{23} \\ \gamma_{23} \\ \gamma_{23} \end{Bmatrix} = \begin{bmatrix} S_{11} & S_{12} & S_{13} & 0 & 0 & 0 \\ S_{12} & S_{22} & S_{23} & 0 & 0 & 0 \\ S_{13} & S_{23} & S_{33} & 0 & 0 & 0 \\ 0 & 0 & 0 & S_{44} & 0 & 0 \\ 0 & 0 & 0 & 0 & S_{55} & 0 \\ 0 & 0 & 0 & 0 & 0 & S_{66} \end{bmatrix} \begin{Bmatrix} \sigma_1 \\ \sigma_2 \\ \sigma_3 \\ \tau_{23} \\ \tau_{13} \\ \tau_{12} \end{Bmatrix} \quad (5)$$

In the cylinder coordinate system the stress-strain relations are expressed in terms of the transformed stiffness and compliance matrices.

$$\begin{Bmatrix} \sigma_x \\ \sigma_\theta \\ \sigma_r \\ \tau_{\theta r} \\ \tau_{x\theta} \\ \tau_{x\theta} \end{Bmatrix} = \begin{bmatrix} \bar{C}_{11} & \bar{C}_{12} & \bar{C}_{13} & 0 & 0 & \bar{C}_{16} \\ \bar{C}_{12} & \bar{C}_{22} & \bar{C}_{23} & 0 & 0 & \bar{C}_{26} \\ \bar{C}_{13} & \bar{C}_{23} & \bar{C}_{33} & 0 & 0 & \bar{C}_{36} \\ 0 & 0 & 0 & \bar{C}_{44} & \bar{C}_{45} & 0 \\ 0 & 0 & 0 & \bar{C}_{45} & \bar{C}_{55} & 0 \\ \bar{C}_{16} & \bar{C}_{26} & \bar{C}_{36} & 0 & 0 & \bar{C}_{66} \end{bmatrix} \begin{Bmatrix} \epsilon_x - \epsilon_x^T \\ \epsilon_\theta - \epsilon_\theta^T \\ \epsilon_r - \epsilon_r^T \\ \gamma_{\theta r} \\ \gamma_{x\theta} \\ \gamma_{x\theta} \end{Bmatrix} \quad (6)$$

$$\begin{Bmatrix} \epsilon_x - \epsilon_x^T \\ \epsilon_\theta - \epsilon_\theta^T \\ \epsilon_r - \epsilon_r^T \\ \gamma_{\theta r} \\ \gamma_{xr} \\ \gamma_{x\theta} \end{Bmatrix} = \begin{bmatrix} \bar{S}_{11} & \bar{S}_{12} & \bar{S}_{13} & 0 & 0 & \bar{S}_{16} \\ \bar{S}_{12} & \bar{S}_{22} & \bar{S}_{23} & 0 & 0 & \bar{S}_{26} \\ \bar{S}_{13} & \bar{S}_{23} & \bar{S}_{33} & 0 & 0 & \bar{S}_{36} \\ 0 & 0 & 0 & \bar{S}_{44} & \bar{S}_{45} & 0 \\ 0 & 0 & 0 & \bar{S}_{45} & \bar{S}_{55} & 0 \\ \bar{S}_{16} & \bar{S}_{26} & \bar{S}_{36} & 0 & 0 & \bar{S}_{66} \end{bmatrix} \begin{Bmatrix} \sigma_x \\ \sigma_\theta \\ \sigma_r \\ \tau_{\theta r} \\ \tau_{xr} \\ \tau_{x\theta} \end{Bmatrix} \quad (7)$$

Again, the transformed compliance matrix is the inverse of the transformed stiffness matrix. The relations and transformations between the various [S] and [C] matrices and the engineering elastic constants can be found in Whitney [7] (Note the sign error in equations 1.43 and 1.45).

The cylindrical coordinate compatibility equations are:

$$\begin{aligned} \frac{\partial^2 \epsilon_r}{\partial x^2} + \frac{\partial^2 \epsilon_x}{\partial r^2} + \frac{\partial^2 \gamma_{x\theta}}{\partial x \partial r} &= 0 \\ \frac{\partial^2 \epsilon_\theta}{\partial x^2} - \frac{1}{r} \frac{\partial^2 \gamma_{x\theta}}{\partial x \partial r} + \frac{1}{r^2} \frac{\partial^2 \epsilon_x}{\partial \theta^2} + \frac{1}{r} \frac{\partial \epsilon_x}{\partial r} - \frac{1}{r} \frac{\partial \gamma_{xr}}{\partial x} &= 0 \\ \frac{\partial^2 \epsilon_r}{\partial \theta^2} - r \frac{\partial \epsilon_r}{\partial r} - \frac{\partial^2 (r \gamma_{\theta r})}{\partial \theta \partial r} + \frac{\partial}{\partial r} \left( r^2 \frac{\partial \epsilon_\theta}{\partial r} \right) &= 0 \\ \frac{\partial^2 \gamma_{\theta r}}{\partial x^2} - r \frac{\partial^2}{\partial x \partial r} \left( \frac{1}{r} \gamma_{x\theta} \right) - \frac{1}{r} \frac{\partial^2 \gamma_{xr}}{\partial x \partial \theta} + 2 \frac{\partial^2}{\partial \theta \partial r} \left( \frac{1}{r} \epsilon_x \right) &= 0 \\ \frac{2}{r} \frac{\partial^2 \epsilon_r}{\partial x^2} - \frac{\partial^2}{\partial \theta \partial r} \left( \frac{1}{r} \gamma_{xr} \right) + \frac{\partial}{\partial r} \left( \frac{1}{r} \frac{\partial}{\partial r} (r \gamma_{x\theta}) \right) - \frac{1}{r^2} \frac{\partial^2}{\partial x \partial r} (r^2 \gamma_{\theta r}) &= 0 \\ \frac{\partial \gamma_{xr}}{\partial \theta} - 2r \frac{\partial \epsilon_r}{\partial x} - \frac{\partial^2 (r \gamma_{x\theta})}{\partial \theta \partial r} + 2r \frac{\partial^2 (r \epsilon_\theta)}{\partial x \partial r} - \frac{\partial^2 (r \gamma_{\theta r})}{\partial x \partial \theta} &= 0 \end{aligned} \quad (8)$$

The cylindrical coordinate equilibrium equations are:

$$\begin{aligned}
\frac{\partial \sigma_r}{\partial r} + \frac{1}{r}(\sigma_r - \sigma_\theta) + \frac{1}{r} \frac{\partial \tau_{\theta r}}{\partial \theta} + \frac{\partial \tau_{xr}}{\partial x} + B_r &= 0 \\
\frac{\partial \tau_{\theta r}}{\partial r} + \frac{1}{r} \frac{\partial \sigma_\theta}{\partial \theta} + \frac{\partial \tau_{x\theta}}{\partial x} + \frac{2}{r} \tau_{\theta r} + B_\theta &= 0 \\
\frac{\partial \tau_{xr}}{\partial r} + \frac{1}{r} \frac{\partial \tau_{x\theta}}{\partial \theta} + \frac{\partial \sigma_x}{\partial x} + \frac{1}{r} \tau_{xr} + B_x &= 0
\end{aligned} \tag{9}$$

Where  $B_i$  are the body forces.

The thermal and pressure loading and the tube geometry are all assumed to be axisymmetric. Therefore, none of the components of displacement depend on the circumferential coordinate,  $\theta$ , and:

$$\frac{\partial(\quad)}{\partial \theta} = 0 \tag{10}$$

where  $(\quad)$  is any stress, strain or displacement. Also, by St. Venant's Principle, the stress (and therefore strain) do not vary with the axial coordinate,  $x$ , at points far from the cylinder ends. Therefore:

$$\begin{aligned}
\frac{\partial}{\partial x}(\text{STRESS}) &= 0 \\
\frac{\partial}{\partial x}(\text{STRAIN}) &= 0
\end{aligned} \tag{11}$$

This is the plane deformation assumption. The radial displacement is also not a function of  $x$  far from the ends. With these assumptions, the ply displacements now have the form:

$$\begin{aligned}
u &= u(x, r) \\
v &= v(x, r) \\
w &= w(r)
\end{aligned} \tag{12}$$

and the strain displacements simplify to:

$$\epsilon_x = \frac{\partial u}{\partial x} \quad (13a)$$

$$\epsilon_\theta = \frac{w}{r} \quad (13b)$$

$$\epsilon_r = \frac{dw}{dr} \quad (13c)$$

$$\gamma_{\theta r} = \frac{\partial v}{\partial r} - \frac{v}{r} \quad (13d)$$

$$\gamma_{xr} = \frac{\partial u}{\partial r} \quad (13e)$$

$$\gamma_{x\theta} = \frac{\partial v}{\partial x} \quad (13f)$$

Three of the compatibility equations are satisfied automatically. The remaining three simplify to the following:

$$\frac{d^2 \epsilon_x}{dr^2} = 0 \quad (14a)$$

$$\frac{1}{r} \frac{d^2 \epsilon_x}{dr^2} = 0 \quad (14b)$$

$$\frac{1}{2} \frac{d}{dr} \left( \frac{1}{r} \frac{d}{dr} (r \gamma_{x\theta}) \right) = 0 \quad (14c)$$

The equilibrium equations simplify to (neglecting body forces):

$$\frac{d\sigma_r}{dr} + \frac{1}{r}(\sigma_r - \sigma_\theta) = 0 \quad (15a)$$

$$\frac{d\tau_{\theta r}}{dr} + \frac{2}{r}\tau_{\theta r} = 0 \quad (15b)$$

$$\frac{d\tau_{xr}}{dr} + \frac{1}{r}\tau_{xr} = 0 \quad (15c)$$

Integrating eq. (14a) yields an equation for axial strain in terms of constants A and B:

$$\epsilon_x(r) = Ar + B \quad (16)$$

The constant A is clearly zero by eq (14b). The axial strain is now constant with respect to position and is redesignated  $\epsilon^\circ$ .

$$\epsilon(r) = \epsilon^\circ \quad (17)$$

Substitution of eq. (17) into eq. (13a) and integrating gives the expression for axial displacement:

$$u(x, r) = \epsilon^\circ r + f(r) \quad (18)$$

where  $f(r)$  is an arbitrary function of  $r$ .

Integrating eq. (14c) yields  $\gamma_{x\theta}$  in terms of constants C and D:

$$\gamma_{x\theta} = Cr + \frac{D}{r} \quad (19)$$

Substituting eq. (19) into eq. (13f) and integrating yields an equation for circumferential displacement:

$$v(x, r) = \left( Cr + \frac{D}{r} \right) x + g(r) \quad (20)$$

where  $g(r)$  is an arbitrary function of  $r$ .

Integrating the second and third equilibrium equations ((15b), (15c)) results in:

$$\tau_{\theta r} = \frac{E}{r^2} \quad (21)$$

$$\tau_{xr} = \frac{F}{r} \quad (22)$$

where E and F are constants.

Eq. (13e) can now be written in terms of f(r) (eq. (18)):

$$\gamma_{xr} = \frac{\partial u}{\partial r} = \frac{df(r)}{dr} \quad (23)$$

Using Hooke's Law (eq. (7), (54)) and eq. (21), (22),  $\gamma_{xr}$  can be written in terms of E and F:

$$\begin{aligned} \gamma_{xr} &= \frac{df(r)}{dr} = \bar{S}_{45} \tau_{\theta r} + \bar{S}_{55} \tau_{xr} \\ &= \bar{S}_{45} \left( \frac{E}{r^2} \right) + \bar{S}_{55} \left( \frac{F}{r} \right) \end{aligned} \quad (24)$$

Integrating, f(r) is found to be:

$$f(r) = -\bar{S}_{45} \left( \frac{E}{r} \right) + \bar{S}_{55} F \ln r + F_1 \quad (25)$$

Substitution of f(r) into u(x,r) reveals  $F_1$  to be rigid body motion.

g(r) can be obtained in a similar manner:

$$\begin{aligned} \gamma_{\theta r} &= \frac{\partial v}{\partial r} - \frac{v}{r} = \frac{dg(r)}{dr} - \frac{g(r)}{r} - \frac{2Dx}{r^2} \\ &= \bar{S}_{44} \tau_{\theta r} + \bar{S}_{45} \tau_{xr} \\ &= \bar{S}_{44} \frac{E}{r^2} + \bar{S}_{45} \frac{F}{r} \end{aligned} \quad (26)$$

or

$$\frac{dg(r)}{dr} - \frac{g(r)}{r} = \bar{S}_{44} \frac{E}{r^2} + \bar{S}_{45} \frac{F}{r} + \frac{2D}{r^2} \quad (27)$$

Because  $g(r)$  is not a function of  $x$ :

$$D = 0 \quad (28)$$

$g(r)$  can be obtained by integration:

$$g(r) = -\bar{S}_{44} \frac{E}{2r} - \bar{S}_{45} F + G_1 r \quad (29)$$

$G_1$  represents rigid body rotation. The in-plane deformations are now complete:

$$u(x, r) = \varepsilon^0 x - \bar{S}_{45} \frac{E}{r} - \bar{S}_{55} F \ln r + F_1 \quad (30)$$

$$v(x, r) = \gamma^0 x r - \bar{S}_{44} \frac{E}{2r} - \bar{S}_{45} F + G_1 r \quad (31)$$

The constant  $C$ , representing twist per unit length, has been redefined as  $\gamma^0$ .

The first equilibrium equation (eq. (14a)), in terms of displacements, is now:

$$\begin{aligned} \frac{d^2 w}{dr^2} + \frac{1}{r} \frac{dw}{dr} - \frac{\bar{C}_{22}}{\bar{C}_{33}} \frac{1}{r^2} w \\ = \frac{1}{\bar{C}_{33}} \left[ \frac{(\bar{C}_{12} - \bar{C}_{13}) \varepsilon^0 + \bar{Z}}{r} + (\bar{C}_{26} - 2\bar{C}_{26}) \gamma^0 \right] \end{aligned} \quad (32)$$

Equation 32 can now be solved for  $w(r)$ :

$$\begin{aligned}
 w(r) = & A_1 r^\lambda + A_2 r^{-\lambda} + \left( \frac{\bar{C}_{12} - \bar{C}_{13}}{\bar{C}_{33} - \bar{C}_{22}} \right) \epsilon^\circ r + \left( \frac{\bar{C}_{26} - 2 \bar{C}_{36}}{4 \bar{C}_{33} - \bar{C}_{22}} \right) \gamma^\circ r^2 \\
 & + \left( \frac{\bar{Z}}{\bar{C}_{33} - \bar{C}_{22}} \right) r
 \end{aligned} \tag{33}$$

$$\lambda = \sqrt{\frac{\bar{C}_{22}}{\bar{C}_{33}}}$$

$$\begin{aligned}
 \bar{Z} = & (\bar{C}_{13} - \bar{C}_{12}) \epsilon_x^T + (\bar{C}_{23} - \bar{C}_{22}) \epsilon_\theta^T \\
 & + (\bar{C}_{33} - \bar{C}_{23}) \epsilon_r^T + (\bar{C}_{36} - \bar{C}_{26}) \gamma_{x\theta}^T
 \end{aligned}$$

$A_1$  and  $A_2$  are additional constants.

The displacements, stresses and strains are now known for a single ply of arbitrary orientation in terms of 8 unknown constants ( $A_1$ ,  $A_2$ ,  $\epsilon^\circ$ ,  $\gamma^\circ$ ,  $E$ ,  $F$ ,  $G_1$ ,  $F_1$ ).

### 2.2.2 Multi-Ply Solution

For a general Laminate, each ply will have a different set of constants and a different stiffness matrix. For the  $k^{\text{th}}$  ply the displacements are of the form :

$$u^{(k)}(x, r) = \epsilon^{\circ(k)} x - \bar{S}_{45}^{(k)} \frac{E^{(k)}}{r} - \bar{S}_{55}^{(k)} F^{(k)} \ln r + F_1^{(k)} \quad (34a)$$

$$v^{(k)}(x, r) = \gamma^{\circ(k)} x r - \bar{S}_{44}^{(k)} \frac{E}{2r} - \bar{S}_{45}^{(k)} F^{(k)} + G_1^{(k)} r \quad (34b)$$

$$w^{(k)}(r) = A_1^{(k)} r^{\lambda^{(k)}} + A_2^{(k)} r^{-\lambda^{(k)}} + \left( \frac{\bar{C}_{12}^{(k)} - \bar{C}_{13}^{(k)}}{\bar{C}_{33}^{(k)} - \bar{C}_{22}^{(k)}} \right) \epsilon^{\circ(k)} r + \left( \frac{\bar{C}_{26}^{(k)} - 2 \bar{C}_{36}^{(k)}}{4 \bar{C}_{33}^{(k)} - \bar{C}_{22}^{(k)}} \right) \gamma^{\circ(k)} r^2 + \left( \frac{\bar{Z}^{(k)}}{\bar{C}_{33}^{(k)} - \bar{C}_{22}^{(k)}} \right) r \quad (34c)$$

$$\lambda^{(k)} = \sqrt{\frac{\bar{C}_{22}^{(k)}}{\bar{C}_{33}^{(k)}}}$$

$$\begin{aligned} \bar{Z}^{(k)} = & (\bar{C}_{13}^{(k)} - \bar{C}_{12}^{(k)}) \epsilon_x^{T^{(k)}} + (\bar{C}_{23}^{(k)} - \bar{C}_{22}^{(k)}) \epsilon_{\theta}^{T^{(k)}} \\ & + (\bar{C}_{33}^{(k)} - \bar{C}_{23}^{(k)}) \epsilon_r^{T^{(k)}} + (\bar{C}_{36}^{(k)} - \bar{C}_{26}^{(k)}) \gamma_{x\theta}^{T^{(k)}} \end{aligned}$$

There are now  $8N$  constants where  $N$  is the number of plies. These constants will be determined by:

- i. Boundary conditions on the inner and outer surfaces. [6]
- ii. Continuity of tractions at the ply interfaces. [3(N-1)]
- iii. Continuity of displacements at the ply interfaces. [3(N-1)]
- iv. Suppress rigid body motion. [2N]
- iv. Integrated boundary conditions over the cross-sectional area. [2]

i. The inner ( $k = 1$ ) and outer ( $k = N$ ) surfaces are subject to normal stresses (pressure) and sustain no surface shear tractions.

$$\sigma_r^{(i)}(r_i) = -P_i \quad (35a)$$

$$\tau_{\theta r}^{(i)}(r_i) = 0 \quad (35b)$$

$$\tau_{xr}^{(i)}(r_i) = 0 \quad (35c)$$

$$\sigma_r^{(o)}(r_o) = -P_o \quad (35d)$$

$$\tau_{\theta r}^{(o)}(r_o) = 0 \quad (35e)$$

$$\tau_{xr}^{(o)}(r_o) = 0 \quad (35f)$$

The shear stresses are:

$$\tau_{\theta r}^{(k)} = \frac{E}{r^2} \quad (36)$$

$$\tau_{xr}^{(k)} = \frac{F}{r} \quad (37)$$

By considering the boundary conditions 35b, 35c, 35e, 35f and equations 36, 37 the following assignments can be made:

$$E^{(1)} = E^{(N)} = 0 \quad (38)$$

$$F^{(1)} = F^{(N)} = 0 \quad (39)$$

reducing the unknowns to 8N-4.

**ii.** Continuity of interface tractions is expressed as:

$$\sigma_r^{(k)}(r_k) = \sigma_r^{(k+1)}(r_k) \quad (40a)$$

$$\tau_{\theta r}^{(k)}(r_k) = \tau_{\theta r}^{(k+1)}(r_k) \quad (40b)$$

$$\tau_{xz}^{(k)}(r_k) = \tau_{xz}^{(k+1)}(r_k) \quad (40c)$$

$$k = 1, 2, \dots, N-1$$

Combining equations 36-39 and 40b, 40c results in:

$$E^{(k)} = 0 \quad k = 1 \dots N \quad (41)$$

$$F^{(k)} = 0 \quad k = 1 \dots N \quad (42)$$

There are now 6N unknown constants.

**iii.** Continuity of interface displacements is expressed as:

$$u^{(k)}(x, r_k) = u^{(k+1)}(x, r_k) \quad (43a)$$

$$v^{(k)}(x, r_k) = v^{(k+1)}(x, r_k) \quad (43b)$$

$$w^{(k)}(r_k) = w^{(k+1)}(r_k) \quad (43c)$$

$$k = 1, 2, \dots, N-1$$

Substituting equation 34a into 43a gives:

$$\epsilon^{\circ(k)}x + F_1^{(k)} = \epsilon^{\circ(k+1)}x + F_1^{(k+1)} \quad k = 1 \dots N-1 \quad (44)$$

From this it follows that, in general, the constant axial strain for each ply is the same for all plies. The entire cylinder has a constant axial strain  $\epsilon^{\circ}$ .

$$\epsilon^{\circ(k)} = \epsilon^{\circ} \quad k = 1 \dots N \quad (45)$$

**iv.** Also, from equation 44, all  $F_1^{(k)}$  must be equal. Consequently, rigid body translation will be neglected.

$$F_1^{(k)} = 0 \quad k = 1 \dots N \quad (46)$$

This leaves  $3N + 1$  unknown constants.

Similarly, considering equations 34b and 43b:

$$\gamma^{(k)} x r + G_1^{(k)} r = \gamma^{(k+1)} x r + G_1^{(k+1)} r \quad k = 1 \dots N-1 \quad (47)$$

From this it follows that  $\gamma^{(k)}$ , the twist per unit length, and  $G_1^{(k)}$ , the rigid body rotation, must be the same for each ply. The rigid body rotation will be considered zero.

$$\gamma^{(k)} = \gamma^0 \quad k = 1 \dots N \quad (48)$$

$$G_1^{(k)} = 0 \quad k = 1 \dots N \quad (49)$$

At this point:

$$u^{(k)}(x, r) = \epsilon^0 x \quad (50)$$

$$v^{(k)}(x, r) = \gamma^0 x r \quad (51)$$

$$w^{(k)}(r) = A_1^{(k)} r^{\lambda^{(k)}} + A_2^{(k)} r^{-\lambda^{(k)}} + \left( \frac{\bar{C}_{12}^{(k)} - \bar{C}_{13}^{(k)}}{\bar{C}_{33}^{(k)} - \bar{C}_{22}^{(k)}} \right) \epsilon^0 r + \left( \frac{\bar{C}_{26}^{(k)} - 2 \bar{C}_{36}^{(k)}}{4 \bar{C}_{33}^{(k)} - \bar{C}_{22}^{(k)}} \right) \gamma^0 r^2 + \left( \frac{\bar{Z}^{(k)}}{\bar{C}_{33}^{(k)} - \bar{C}_{22}^{(k)}} \right) r \quad (52)$$

**V.** There are now  $2N + 2$  unknown constants ( $N A_1$ 's,  $N A_2$ 's,  $\epsilon^0$ ,  $\gamma^0$ ). There are currently  $2N$  equations available (40a, 43c, 35a, 35d). The last two equations come from the requirement that the integral over the cross-sectional area of the axial stress and the shear couple ( $\gamma_{x\theta} r$ ) must equal the axial load ( $F_x$ ) and the torsion load ( $T_x$ ) respectively.

$$\int_A \sigma_x r d\theta dr = F_x \quad (53)$$

$$\int_A \tau_{x\theta} r^2 d\theta dr = T_x$$

Where  $A$  is the annular area of the cylinder. These relations are used in a summation form:

$$2\pi \sum_{k=1}^N \int_A \sigma_x r dr = F_x \quad (54)$$

$$2\pi \sum_{k=1}^N \int_A \tau_{x\theta} r^2 dr = T_x$$

The  $2N + 2$  relations can now be solved simultaneously for the constants. The complete solution is now available for an arbitrary laminate of orthotropic plies.

This solution has been coded in BASIC (Microsoft QuickBASIC Compiler) and C (MIX Software PowerC). The source codes are listed in Appendix D. The accuracy of the formulated model was checked using data from Pagano [8] and Rousseau [6]. The elasticity solution was used independently and as a subroutine in the optimization routine discussed next.

## 2.3 Inverse Solution

### 2.3.1 Use of Optimization

The objective of this program is the calculation of the material elastic properties from the response of a mechanically and thermally loaded laminated cylinder. There are a total of ten elastic properties involved in the cylinder solution ( $E_1, E_2, E_3, G_{12}, \nu_{12}, \nu_{13}, \nu_{23}, \alpha_1, \alpha_2, \alpha_3$ ) and four loadings (axial, torsion, pressure, thermal). The surface strain state is determined by three strains ( $\epsilon_x, \epsilon_y, \gamma_{xy}$  etc.). The system is therefore over determined (12 relations, 10 unknowns) and an optimization method is suitable for the solution.

The optimization method is used to find a set of properties for which the elasticity solution predicts a response that is the closest possible to the measured response. The objective function should represent the N-spacial distance between the point representing the measured strains and the point determined by the elasticity solution using the current estimate of the properties.

### 2.3.2 Objective Function

The objective function chosen is the sum of the squares of the errors between the measured and calculated values of the surface strain response under various loads.

$$Y(x_n) = \sum_{i=1}^4 \sum_{j=1}^3 (\phi_{ij}(x_n))^2 \quad (1)$$

$$\phi_{ij}(x_n) = \epsilon_{mij} - \epsilon_{cij}(x_n)$$

$\epsilon_m$  : Measured strains

$\epsilon_c(x)$  : Calculated strains

$x_n$  : Elastic properties ( $E_1, E_2 \dots$  etc.)

$i$  : Loads (axial, torsion ... etc.)

$j$  : Strains ( $\epsilon_x, \epsilon_y, \gamma_{xy}$ )

For convenience the i and j subscripts will be combined and designated k.

$$Y(x_n) = \sum_{k=1}^{12} (\phi(x_n)_k)^2 \quad (2)$$

or, in vector notation:

$$Y(x_n) = \bar{\phi} \bar{\phi}^T \quad (3)$$

Parametric studies have shown that, in general, the surface strain response is a nonlinear function of the elastic properties, and that all of the elastic properties involved influence the surface strains for one or more loadings (Appendix A).

For this type of objective function the least squares method, as presented in Reference [9], offers an efficient solution. The derivation will be repeated below for completeness.

### 2.3.3 Derivation of Least Squares Method

As the objective function approaches an extrema (or inflection pt.) the gradient goes to zero. The gradient of Y is given by:

$$\nabla Y(x_n) = 2J \bar{\phi} \quad (4)$$

where J is the k by n Jacobean matrix.

$$J \equiv \nabla \bar{\phi} = \begin{bmatrix} \frac{\partial \phi_1}{\partial x_1} & \frac{\partial \phi_1}{\partial x_2} & \dots & \frac{\partial \phi_1}{\partial x_n} \\ \frac{\partial \phi_2}{\partial x_1} & \cdot & \dots & \cdot \\ \vdots & \cdot & \dots & \cdot \\ \frac{\partial \phi_k}{\partial x_1} & \cdot & \dots & \frac{\partial \phi_k}{\partial x_n} \end{bmatrix} \quad (5)$$

Gauss suggested that at a point  $\bar{x} + \Delta \bar{x}$  the gradient of Y can be approximated by:

$$\nabla Y(\bar{x} + \Delta \bar{x}) \approx 2J \bar{\phi}(\bar{x} + \Delta \bar{x}) \quad (6)$$

A first order Taylor series expansion of  $\phi$  about  $\bar{x}$  yields:

$$\begin{aligned}\bar{\phi}(\bar{x} + \Delta\bar{x}) &\approx \bar{\phi}(\bar{x}) + \frac{\partial \bar{\phi}(\bar{x})}{\partial \bar{x}} \Delta\bar{x} \\ &\approx \bar{\phi}(\bar{x}) + J^T \Delta\bar{x}\end{aligned}\tag{7}$$

Substituting into equation 6 yields:

$$\nabla Y(\bar{x} + \Delta\bar{x}) \approx 2(J\bar{\phi} + J J^T \Delta\bar{x})\tag{8}$$

Setting the gradient of  $Y = 0$  yields the increment in  $x$ :

$$\Delta\bar{x} = -(J J^T)^{-1} J \bar{\phi}\tag{9}$$

For the case where  $\phi$  is a linear function of  $x$  the minimum of  $Y(x_n)$  is reached in one step (linear regression). For non-linear  $\phi$  the process is iterative with each  $\Delta x$  improving the estimate of the property values until the objective function is sufficiently small.

For this problem, the Jacobean derivatives must be evaluated numerically. A two point formula is used in order to minimize the number of functional evaluations:

$$\frac{\partial \phi(\bar{x})}{\partial x_i} \approx \frac{\phi(H_i \bar{x}) - \phi(\bar{x})}{h x_i}\tag{10}$$

where  $H$  is the  $n$  by  $n$  identity matrix with the  $i^{\text{th}}$  non-zero position replaced by  $h = 1 + \xi$  ( $\xi = .00001$  was commonly used in the program).

Programs were also developed to implement this method and are listed in Appendix D. Note that this solution requires  $(L + 2(L \circ NP))$  evaluations of the elasticity solution (where  $L$  is the number of loads employed and  $NP$  is the number of active properties). Considering that the elasticity solution must solve a  $2N + 2$  matrix equation for each evaluation this method can quickly cost a lot of computer time, especially for large  $N$ . However, the modest applications applied run well on an i486DX 33 mhz PC.

## 3.0 Method Verification

This chapter shows sample inversions of analytically generated data sets verifying the concept and coding of the inversion program.

### 3.1 *Sample Geometry and Properties*

Three cases will be examined. Case I uses geometry and properties representative of the ceramic matrix composites tubes examined experimentally. Case II uses the same properties and geometry but with the more limited load set available at this time (axial and torsional loads only). Case III also uses the same properties and laminate but with a thin-wall cylinder ( $R/h = 50$ ).

#### 3.1.1 *CASE I*

The following properties are representative of the properties of an aluminum oxide/aluminum oxide ("oxide/oxide") continuous fiber ceramic matrix composite (CFCC) manufactured by the sol-gel process and having a total porosity of approximately 15%. The geometry is typical of the tubes examined experimentally in Chapter 4. The properties are intentionally chosen to be non-transversely isotropic for generality.

**Table 3.1 Case I Properties and Geometry**

$E_1 = 20 \times 10^6 \text{ psi.}$	$\nu_{12} = 0.12$
$E_2 = 6 \times 10^6 \text{ psi.}$	$\nu_{12} = 0.09$
$E_3 = 5 \times 10^6 \text{ psi.}$	$\nu_{12} = 0.15$
$G_{12} = 3 \times 10^6 \text{ psi}$	
$\alpha_1 = 9.0 \times 10^{-6} \text{ in/in/}^\circ\text{F}$	
$\alpha_2 = 8.2 \times 10^{-6} \text{ in/in/}^\circ\text{F}$	
$\alpha_3 = 8.1 \times 10^{-6} \text{ in/in/}^\circ\text{F}$	
$R_o = 0.7 \text{ in.}$	$R_i = 0.6125 \text{ in.}]$
$R/h = 7.5$	
$[-45 / 45]_3$	

Note that the demonstration values of  $E_2$ ,  $E_3$  and the Poisson ratios are chosen to demonstrate the methods ability to resolve each property independently. The values of  $E_2$  relative to  $E_3$  and the relations between Poisson ratios are not necessarily characteristic of the material.

The strain response (Table 3.2) is calculated using the BASIC version of the forward (elasticity) solution listed in Appendix D for each of the loads.

**Table 3.2 Case I Strain Response**

<b>Axial Load</b>		<b>Torsional Load</b>	
$\epsilon_x(R_o) / Fx =$	$3.315063 \times 10^{-7}$	$\epsilon_1(R_o) / Tx =$	$3.608430 \times 10^{-7}$
$\epsilon_y(R_o) / Fx =$	$-1.234481 \times 10^{-7}$	$\epsilon_2(R_o) / Tx =$	$-3.665945 \times 10^{-7}$
$\gamma_{xy}(R_o) / Fx =$	$-3.435782 \times 10^{-9}$	$\gamma_{12}(R_o) / Tx =$	$4.064973 \times 10^{-9}$
<b>Internal Pressure Load</b>		<b>Thermal Load</b>	
$\epsilon_1(R_o) / P_i =$	$2.270987 \times 10^{-7}$	$\epsilon_1(R_o) / dT =$	$8.789824 \times 10^{-6}$
$\epsilon_2(R_o) / P_i =$	$2.275619 \times 10^{-7}$	$\epsilon_2(R_o) / dT =$	$8.771486 \times 10^{-6}$
$\gamma_{12}(R_o) / P_i =$	$1.104973 \times 10^{-6}$	$\gamma_{12}(R_o) / dT =$	$-4.745028 \times 10^{-7}$

This data were read into the BASIC version of the least-squares program (Appendix

D) from a data file. The specimen geometry (Table 3.1) is coded in the Elasticity solution subroutine (pg. ). The program prompts the user for an initial estimate of the properties as well as several other parameters (number of data points., number of parameters etc.). The following figures show the convergence of the program. The properties are non-dimensionalized by dividing by the actual properties given in Table 3.1 and are plotted relative to the left axis.

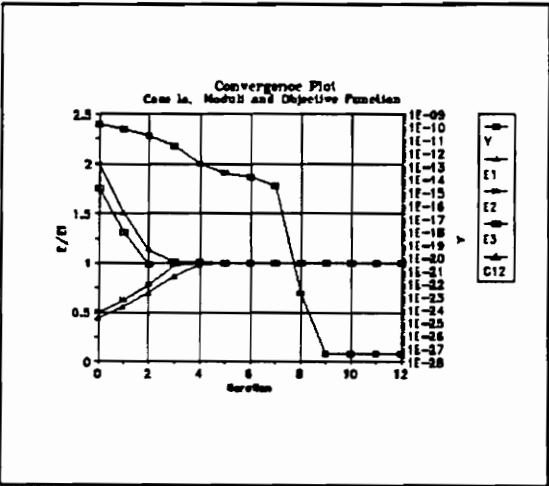


**Figure 3.1** Case Ia, Moduli and Objective Function vs. Iterations

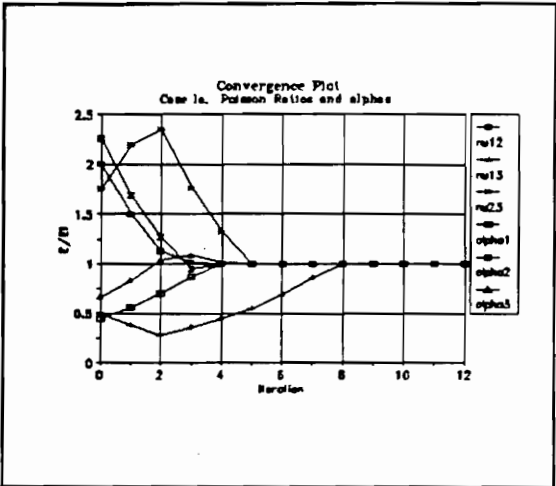


**Figure 3.2** Case Ia, Poisson Ratios and CTE's vs. Iterations

A different initial estimate is used for Case Ib. Note that the initial estimate for  $E_2$  is *greater* than the estimate of  $E_1$  for this trial.

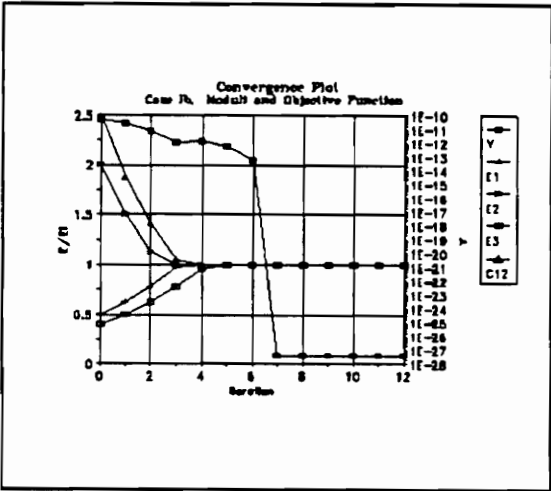


**Figure 3.3** Case Ib, Moduli and Objective Function vs. Iterations

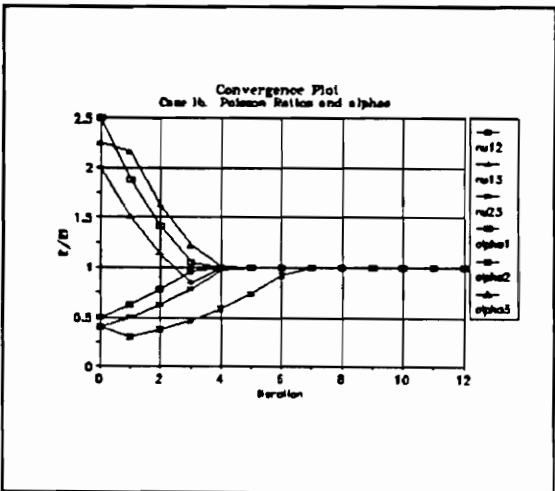


**Figure 3.4** Case Ib, Poisson Ratios and CTE's vs. Iterations

The convergence is generally rapid and well behaved. Many other initial estimates have been successfully run. The codes always converge to the same solution for well posed problems. There is no evidence that this is only a local minima or that there are local minima within the set of properties where convergence occurs (no attempt has been made to define this region). It is necessary to limit the step size of the correction or the first corrections will often result in a property set which creates a singular or complex **A** matrix in the elasticity subroutine. Limiting the step size to 25% of the current property value is generally successful and was used for these trials.

For trials Ia and Ib six significant figures were kept in the strain data set. This implies shear strains accurate to approximately  $(10^{-15} \times \text{load})$  for the axial and torsional loads. This is clearly not realistic even for ideal specimens. A simple effort was therefore made to determine, qualitatively, the effect of inaccuracies in the strain measurements. This was done by running the Least-Squares programs for Case I several times. Additional significant figures were carried for the larger strains so that all of the load normalized strains were accurate to 15 decimal places. The first run was done with this accuracy. For each succeeding run one significant figure was truncated from the strain measurements as shown for the axial load strains in Table 3.3. Figures 3.5 and 3.6 show the influence of the data truncation on the converged properties. The in-plane properties are influenced to a much smaller degree than the out-of-plane properties. Also notice, in Fig. 3.6, that the objective function increases significantly as more places are truncated. This indicates that the data set resulting from truncation is becoming increasingly unrealistic. The optimization code can no longer find a set of properties to duplicate the input strains even after many iterations. The program generally does converge (Objective function remains constant) indicating that this is the best possible solution. This phenomena becomes critical in the interpretation of the experimental results and will be discussed in detail in Ch. 6.

Table 3.3 Truncation of Strains for Error Analysis

Round-Off #	$(\epsilon_x(R_o) / Fx) \times 10^6$	$(\epsilon_y(R_o) / Fx) \times 10^6$	$(\gamma_{xy}(R_o) / Fx) \times 10^6$
0	0.331506343	-0.123448121	-0.003435782
1	0.33150634	-0.12344812	-0.00343578
2	0.3315063	-0.1234481	-0.0034357
3	0.331506	-0.123448	-0.003435
4	0.33150	-0.12344	-0.00343
5	0.3315	-0.1234	-0.0034
6	0.331	-0.123	-0.003

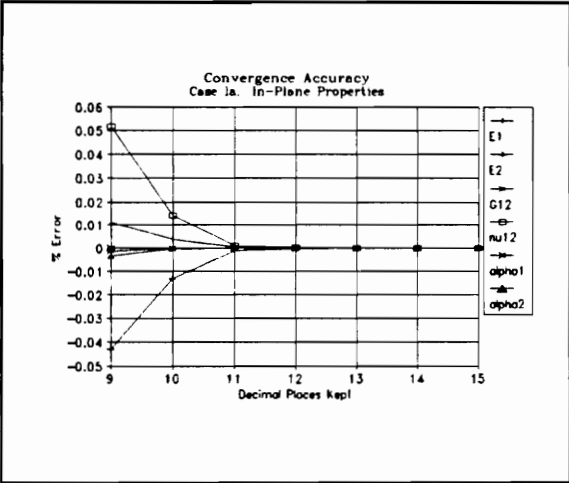


Figure 3.5 Case I, Error in In-Plane Properties due to Data Truncation.

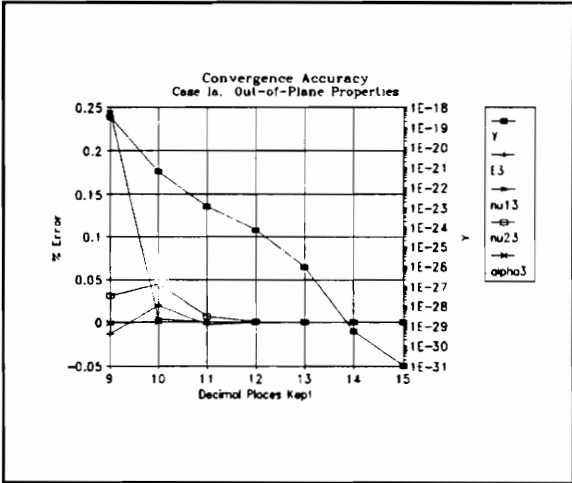


Figure 3.6 Case I, Objective Function and Error in Out-Of-Plane Properties due to Data Truncation

3.1.2 CASE II

The experimental data obtained do not include pressure or thermal loading. In this case there are only six data points, but still seven properties (CTE's are not involved). The system is under-defined and an infinite number of solutions exists. Therefore, the number of properties must be reduced. This is done by assuming that the out-of-plane Poisson ratios ( $\nu_{13}$ ,  $\nu_{23}$ ) are both equal to the in-plane Poisson ratio ( $\nu_{12}$ ). The values of the out-of-plane Poisson ratios do not *directly* affect the converged values (Jacobean elements are not computed for  $\nu_{13}$  and  $\nu_{23}$ ). This approximation is reasonable for  $\nu_{13}$  because the physical situation is similar (transverse isotropy) but is questionable for  $\nu_{23}$ . However, the out-of-plane Poisson ratios have a weak influence on the computed strains for these loads (Appendix A). Attempts to solve for six properties using these six data points are not generally successful, especially if  $\nu_{23}$  is considered the additional active variable.

Case II examines the convergence and error for this situation. The properties and geometry of Case I (Table 3.1) are used. Figures 3.7 and 3.8 show the convergence characteristics for this example. Note that the objective function is now the sum of only six errors and is not directly comparable to the objective function of case I.

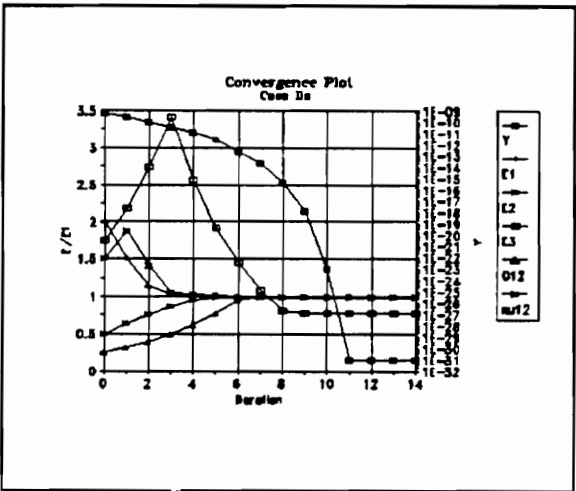


Figure 3.7 Case IIa, Properties and Objective Function vs. Iterations

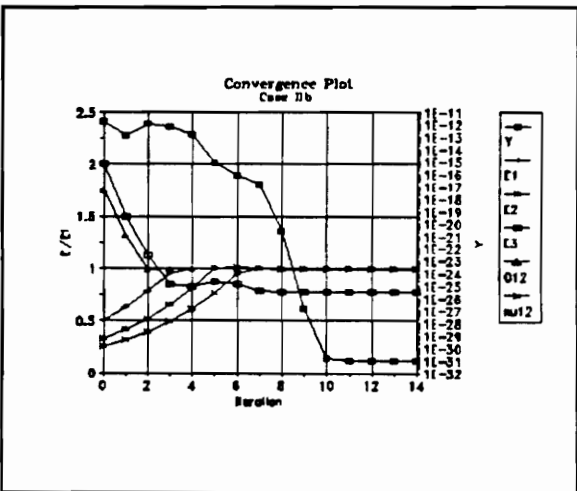
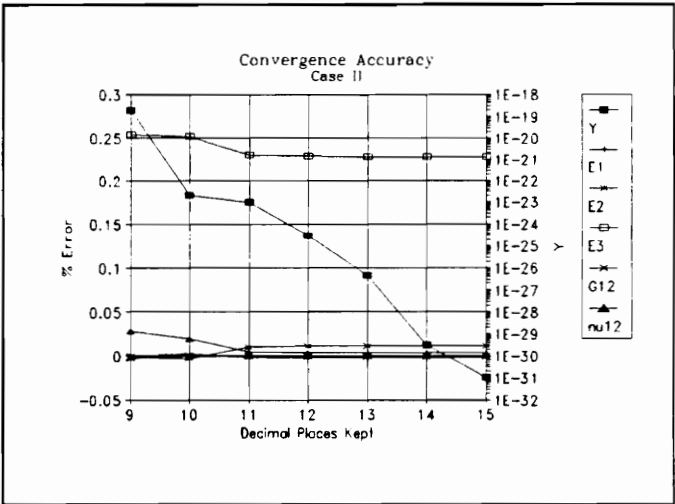


Figure 3.8 Case IIb, Properties and Objective Function vs. Iterations

Note that, except for  $E_3$ , the convergence is still very accurate. The difficulty in obtaining the out-of-plane properties is due to the available loadings. The out-of-

The error with data truncation (fig 3.9) is also reasonable, but again, the objective function gets relatively large indicating that the input strains do not represent the response of a real material.



**Figure 3.9** Case II, Objective function and Property Error due to Data Truncation.

### 3.1.3 CASE III

Case III examines the response of the inversion method for a thin wall cylinder. For thin wall cylinders, the elasticity response approaches the response predicted by Donnell Shell theory. Donnell theory does not consider out-of-plane effects or properties therefore the inversion should not be able to consistently resolve out-of-plane properties. The Case I properties were again used, however, the geometry was changed to a thin wall cylinder (Table 3.4)

**Table 3.4** Case III Properties and Geometry

$R_o = 1.0 \text{ in.}$	$R_i = 0.9802 \text{ in.}]$
$R/h = 50.0$	
$[-45 / 45]_3$	

The calculated strain response is given in Table 3.5.

**Table 3.5 Case III Strain Response**

Axial Load		Torsional Load	
$\epsilon_x(R_o) / Fx = 9.711248 \times 10^{-7}$		$\epsilon_1(R_o) / Tx = 6.706167 \times 10^{-7}$	
$\epsilon_y(R_o) / Fx = -3.787917 \times 10^{-7}$		$\epsilon_2(R_o) / Tx = -6.722326 \times 10^{-7}$	
$\gamma_{xy}(R_o) / Fx = -1.435921 \times 10^{-9}$		$\gamma_{12}(R_o) / Tx = 1.255958 \times 10^{-9}$	
Internal Pressure Load		Thermal Load	
$\epsilon_1(R_o) / P_i = 1.768084 \times 10^{-6}$		$\epsilon_1(R_o) / dT = 8.801730 \times 10^{-6}$	
$\epsilon_2(R_o) / P_i = 1.769022 \times 10^{-6}$		$\epsilon_2(R_o) / dT = 8.799113 \times 10^{-6}$	
$\gamma_{12}(R_o) / P_i = 8.187393 \times 10^{-6}$		$\gamma_{12}(R_o) / dT = -7.334097 \times 10^{-9}$	

The convergence plots are again given for two different initial estimates (fig. 3.10-3.13).

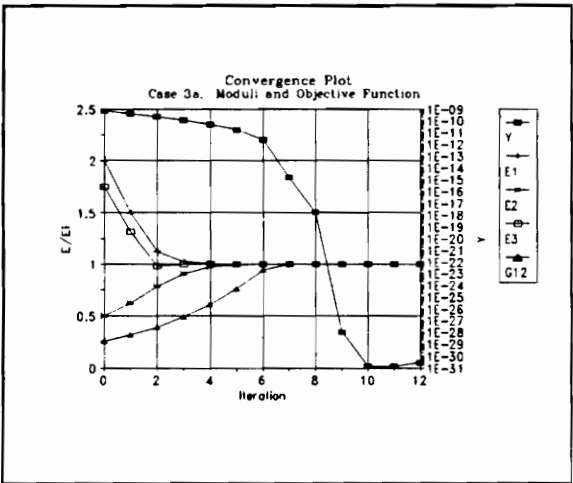


**Figure 3.10 Case IIIa, Moduli and Objective Function vs. Iterations**

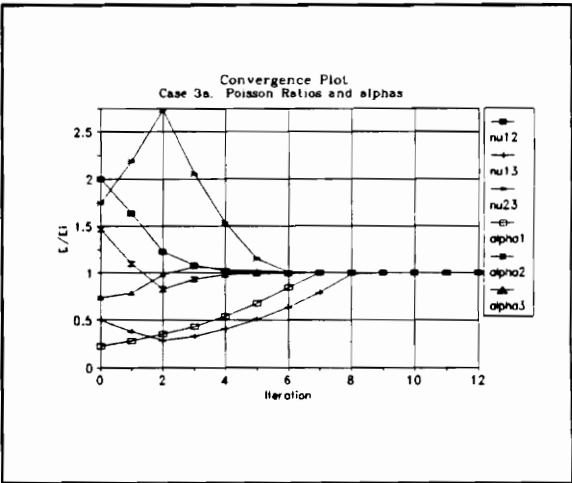


**Figure 3.11 Case IIIa, Poisson Ratios and CTE's vs. Iterations**

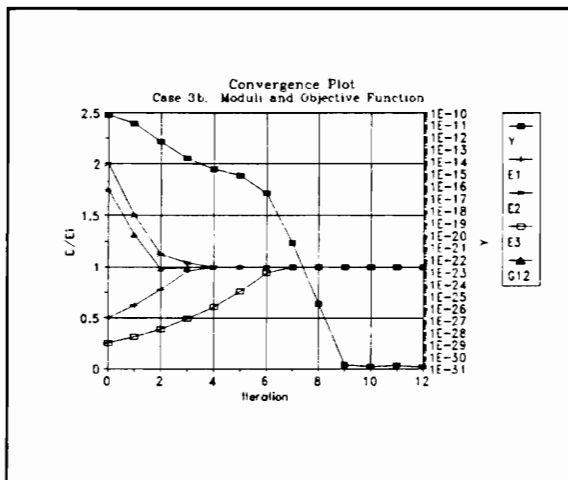


**Figure 3.12** Case IIIb, Moduli and Objective Function vs. Iterations

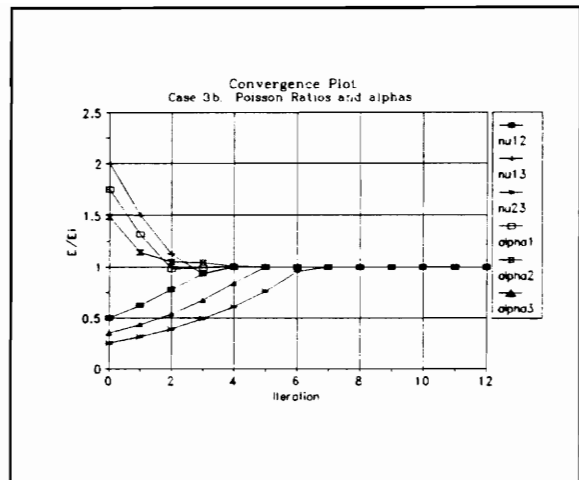


**Figure 3.13** Case IIIb, Poisson Ratios and CTE's vs. Iterations

For these cases 15 decimal places were kept. The convergence is once again accurate and well behaved. The effect of experimental error is now examined (fig 3.14, 3.15) through data truncation in the same manner as in cases I and II.

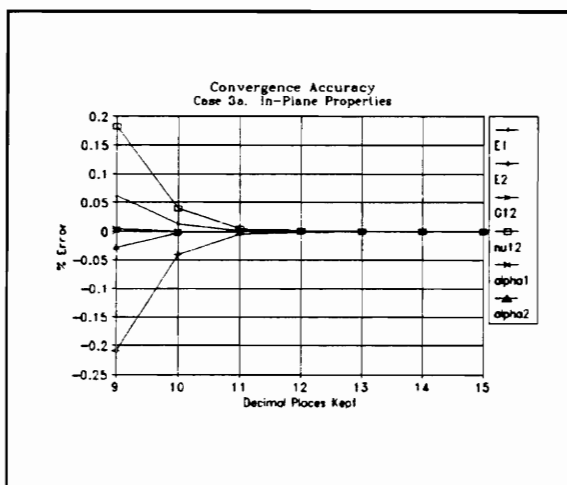


**Figure 3.14** Case III, Error in In-Plane Properties Due to Data Truncation

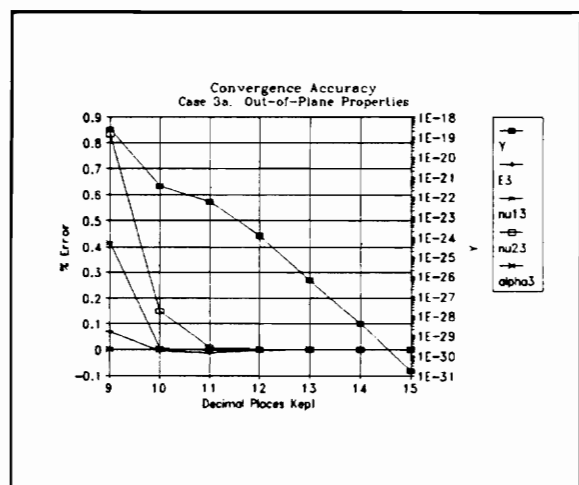


**Figure 3.15** Case III, Error in Out-of-Plane Properties Due to Data Truncation

Notice that the errors are much larger for this case and that there are significant errors in the in-plane properties as well.

For thin specimens a different model should be used in place of the elasticity solution (Donnell Shell Theory). However, care must be taken in the design of the specimen lay-up or the problem will be under-determined. For example; a balanced, symmetric

symmetric laminate will have  $\gamma_{x\theta} = 0$  regardless of the material properties (the partial of  $\gamma_{x\theta}$  with respect to the elastic properties is zero), and thus, cannot be used in the inversion. Unsymmetric, unbalanced laminates will probably work best. Note that attempts to use the elasticity-based method for 0/90 laminates (actually  $[(0 \pm \xi)/(90 \pm \xi)]$  where  $\xi \ll 1$ , as the elasticity solution breaks down at  $0^\circ$  and  $90^\circ$ ) was unsuccessful even for thick laminates. This is because some of the strains are identically zero (eg.  $\gamma_{x\theta}(F_x) = 0$ ) and thus cannot contribute any information to the solution making the problem under-defined in a manner similar to the CLT case.

### 3.4 Conclusions

For analytical data the coded inversion scheme converges rapidly and consistently to an apparent global minimum from a wide range of initial estimates for well posed problems. Well posed, in this case, means thick, angle-ply (not 0/90) cylinders.

Case I examined the most general loading case (axial, torsion, internal pressure and thermal loads). Case II examined the same geometry with the more limited load set available experimentally (axial and torsion loads). Accurate in-plane properties could again be determined but the out-of-plane Poisson ratios had to be approximated as equal to  $\nu_{12}$  and  $E_3$  suffered in accuracy.

Case III examined a thin wall cylinder. The convergence was still accurate, though slower, for high accuracy data but the convergence accuracy dropped significantly as the data accuracy was reduced.

To simulate experimental error, the inversion was examined with truncated data. It was found that, for cases I and II, good in-plane properties could still be obtained with large truncations of the data. It was noted that, for all three cases, as the data were truncated the converged value of the objective function increased substantially. This means that the inversion could not find properties that could reproduce the truncated data as well as the untruncated data. In effect, this means that the truncated (or inaccurate) data represent an unreal physical situation. This phenomena is critical to the interpretation of the experimental results in Ch. 6.

## ***4.0 Experimental Specimens and Apparatus***

### ***4.1 Experimental Specimens***

The experimental specimens used in this study are continuous fiber, ceramic matrix composite tubes produced by Babcock & Wilcox<sup>1</sup>. The material system consists of aluminum oxide fibers in an aluminum oxide matrix ("oxide/oxide").

#### ***4.1.1 Manufacturing, Porosity and Voids***

The cylinder is constructed by sol-gel infiltrations of an aluminum oxide precursor into a filament wound aluminum oxide fiber preform. The preform is dried and fired after each infiltration. Typically fifteen such infiltration cycles are required to achieve a total density of 82% - 88%.

The fiber volume fraction is approximately 43%. Assuming that the porosity of the fibers is negligible, the matrix porosity is approximately 20% - 30%. Because the Young and shear moduli of aluminum oxide decrease exponentially with increasing porosity (ch. 6), this measurement is critical to the performance of the material.

---

<sup>1</sup>Research and Development Division, Lynchburg Research Center, Lynchburg, Va.

The material also contains large voids, especially in the inter-ply region (fig. 4.1). The effect of this inter-ply region is discussed in ch. 6.

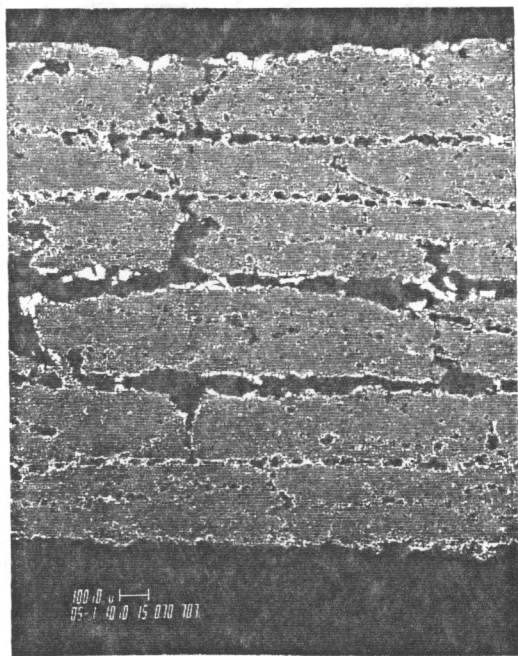


Figure 3.16 Photomicrograph

4.1.2 Gross Geometry

Specimen # 67A was used for the experimental characterization. The relevant dimensions are given in Table 4.1, where again, the plies are numbered from inner to outer.

$R_o = 0.72 \text{ in.}$	$R_i = 0.624 \text{ in.}$
$h = .096 \text{ in.}$	
$t_i = .016 \text{ in.}$	
$R/h = 7$	
$N = 6$	
$[-45.37 / 46.08 / -46.78 / 47.46 / -48.12 / 48.77]_T$	
Length = 8 in.	
Gauge Length = 5 in.	

Table 3.6 Specimen 67A Geometry

The ply thickness is simply the laminate thickness divided by the number of plies. The outer radius is the average of several measurements taken at the center of the tube at points away from the ply crossovers regions.

The unusual ply angle sequence is due to the filament winding process. It was observed that the outer ply angles did not appear to be the nominal  $\pm 45^\circ$ . A pencil rubbing of the tube surface (fig. 4.3) confirms this. Average measurements from the rubbing give an outer ply angle of approximately  $\pm 49.15^\circ$ .

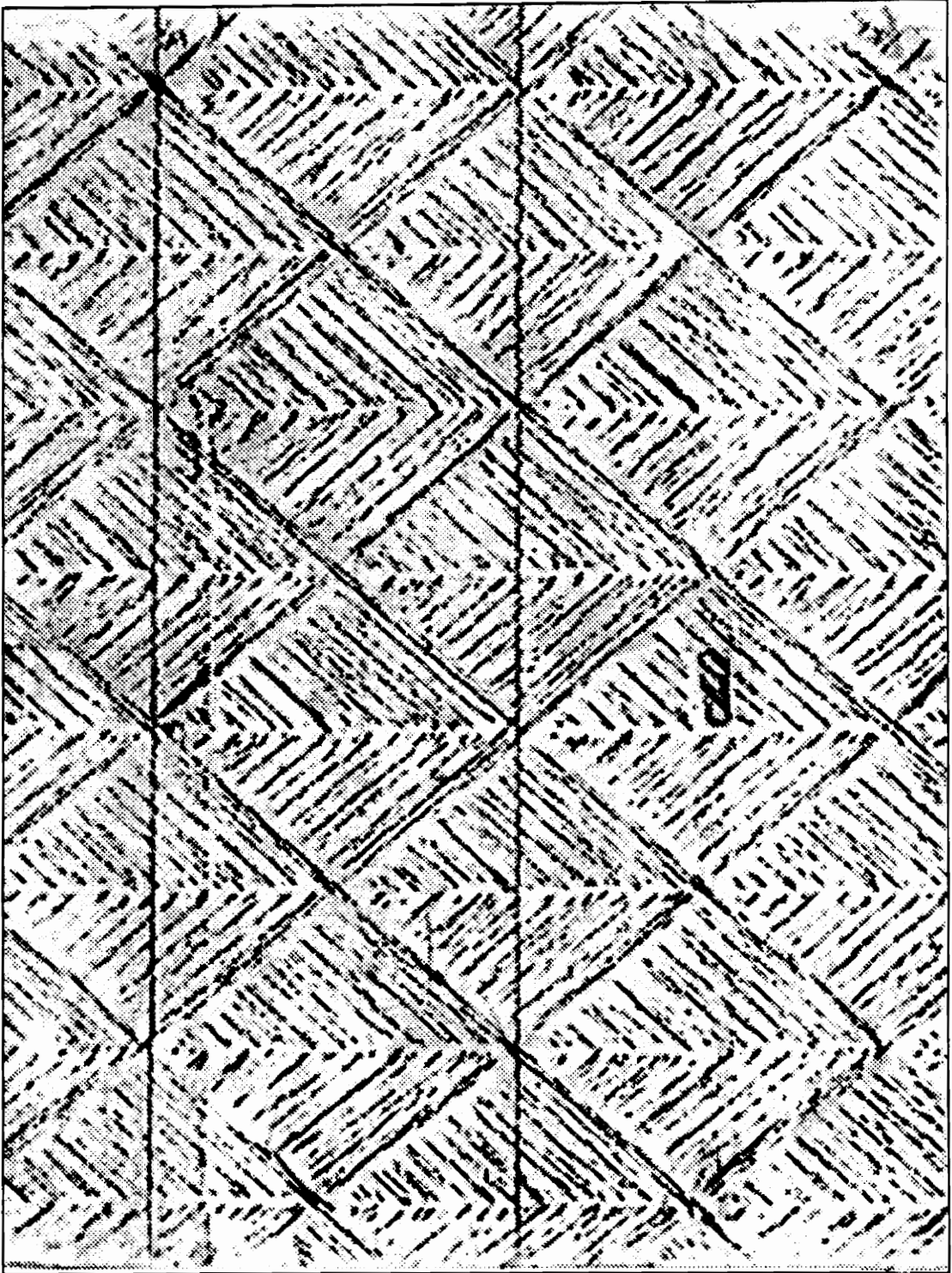


**Figure 4.2** Graphite Rubbing of Cylinder Surface (Full Scale, 2 Diamonds = 1 Circumference)

The inner ply angles are more difficult to measure but appear to be approximately  $\pm 45^\circ$ . Therefore the ply angle changes through the thickness. Consulting the supplier, it was discovered that the cylinders were wound using constant winding parameters throughout the thickness. However, the thickness change is appreciable for these specimens, causing an increase in the ply angle through the thickness as shown below.

The relevant winding parameters are the traverse speed,  $x'$ , and the mandrel rotation speed,  $\theta'$ . By considering a flat projection of the tube surface with the axial direction along the ordinate and the circumferential direction along the abscissa (fig. 4.3) it can be seen that the ply angle,  $\phi$ , is given by:

$$\phi = \tan^{-1} \left( \frac{R \theta'}{x'} \right) \tag{4.1}$$

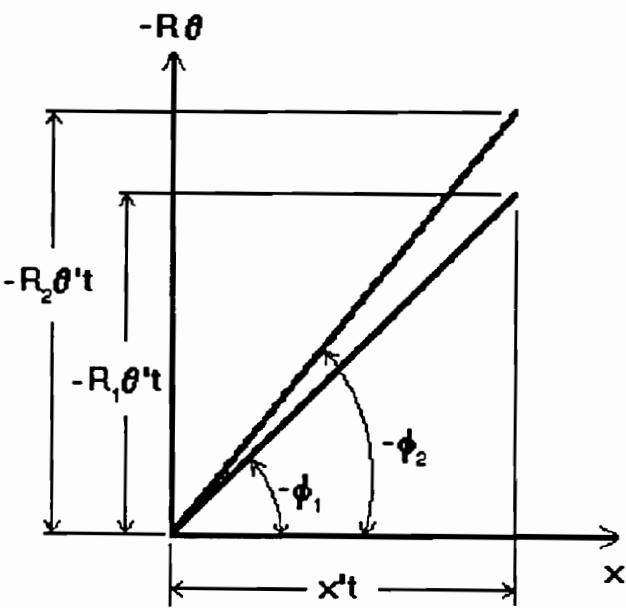


**Figure 4.3** Relationship between radius and ply angle for constant winding parameters

Assuming the inner ply angle is  $45^\circ$  and  $R_i = 0.624$ , the winding parameters are related by eq. 4.1 as follows:

$$x' = 0.624\theta' \quad (4.2)$$

$\phi$  is now given by:

$$\phi = \tan^{-1}\left(\frac{R}{0.624}\right) \quad (4.3)$$

Equation 4.3 is plotted below:

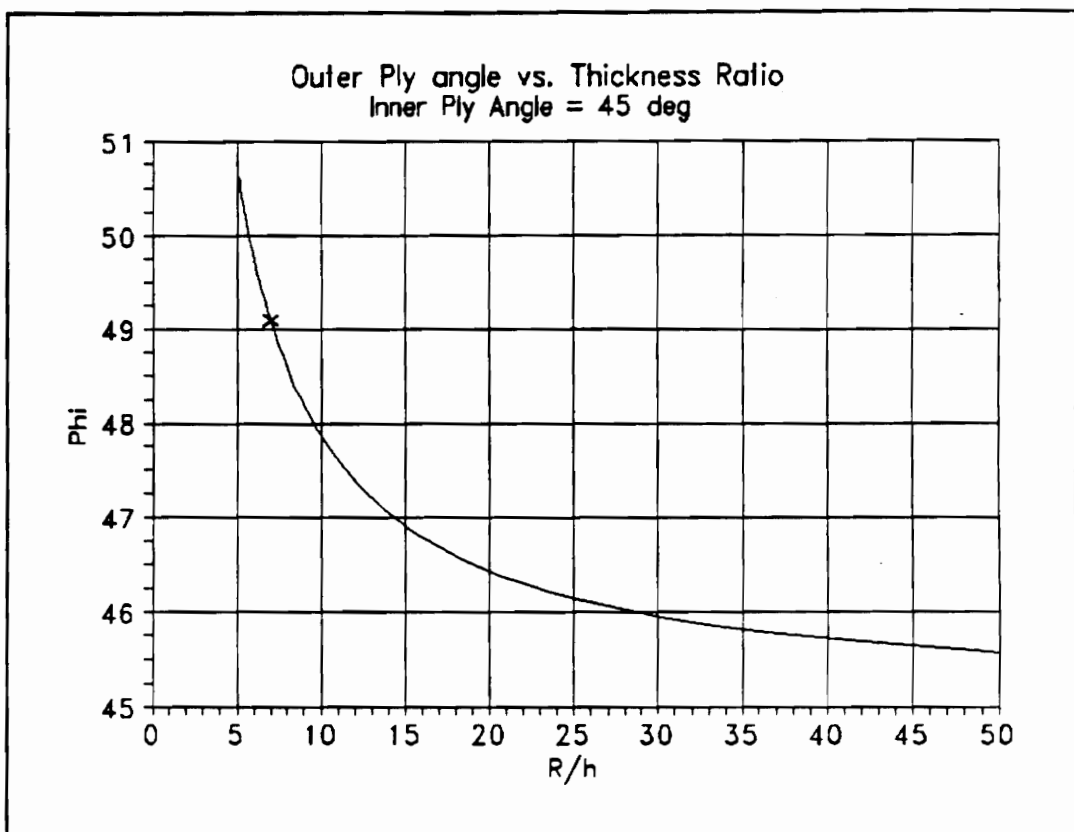
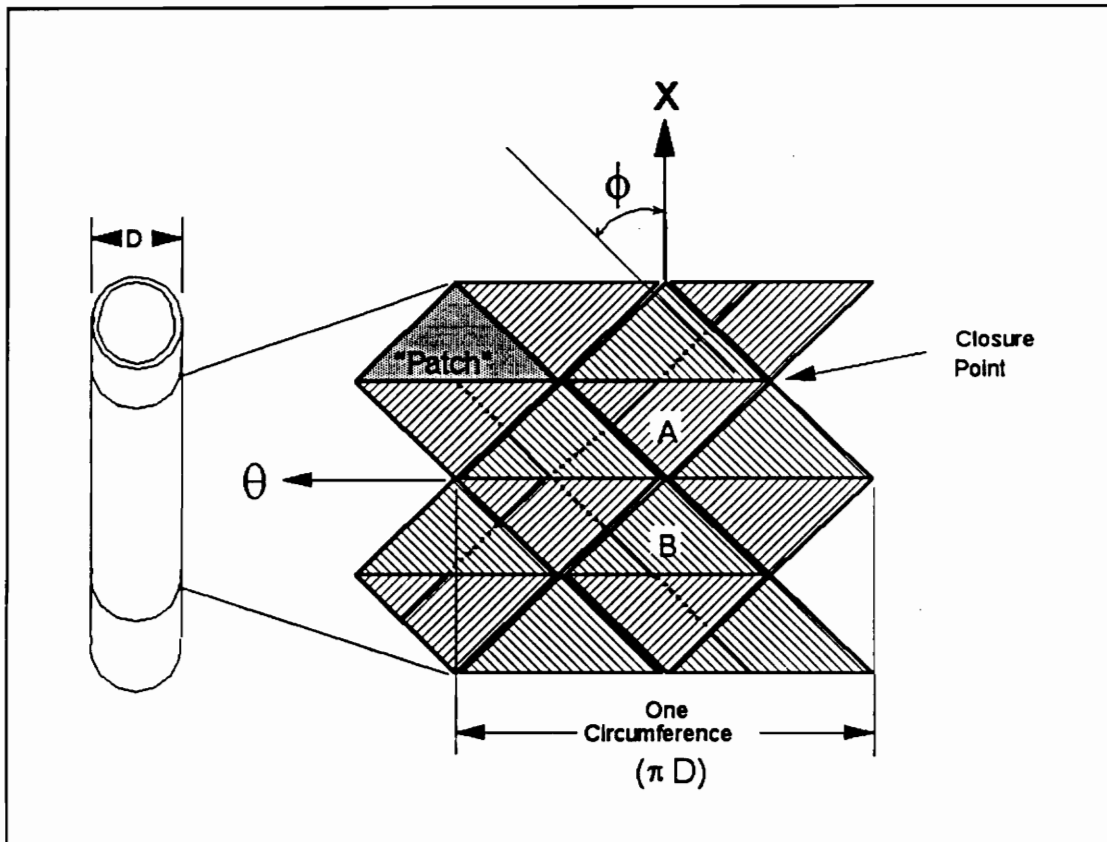


Figure 4.4 Ply Angle vs. Thickness Ratio

Note that the calculated ply angle ( $\phi = 49.09^\circ$ ) is very close to that measured from the pencil rubbing. The angles used in Table 4.1 were calculated using eq. 4.4 and the mid-ply radius of the ply considered.

Another characteristic of the cylinders is the ply crossover pattern created by the filament winding process. The fiber direction ( $\phi$ ) varies from point to point over the

tube (fig. 4.2, fig. 4.5) in a regular pattern. The laminate at any point, away from the actual crossover region, is anti-symmetric (ignoring the variation with thickness discussed) and consists of one or more "closures" of two inter-woven  $\pm \phi$  plies. If the laminate of "patch" B (fig. 4.5) is  $[-\phi / \phi / -\phi / \phi]$  then the (+) patches all have that stacking sequence while the (-) patches have the reverse;  $[\phi / -\phi / \phi / -\phi]$ . In general the sign of a patch corresponds to the sign of the outer ply angle and will be given when relevant.



**Figure 4.5** Filament Winding Geometry

Note that the elasticity solution cannot account for this crossover pattern. The cylinders are not axisymmetric, a prime assumption in the development of the elastic cylinder solution. However, no analytic solution for this type of cylinder could be found in the literature and a finite element model would be too costly (time and computer power) to use in the Least Squares method.

## 4.2 Specimen Preparation and Instrumentation

The experimental work; specimen preparation, instrumentation and data collection, etc., was done by Kin Liao and Jack Lesko<sup>2</sup>. The details of this work are presented in reference [10] (Liao, Lesko, Stinchcomb, Reifsneider, Dunyak). The following is a brief summary of this work.

The first step in preparing the specimens is to bond aluminum plugs into the ends of the tubes to prevent crushing of the specimens by the grips. Specimen 67A was only tested at room temperature so epoxy was used for the bonding. A ceramic cement is used for high temperature tests. Figures 4.6, 4.7 shows a schematic of the end-plug bonding procedure.

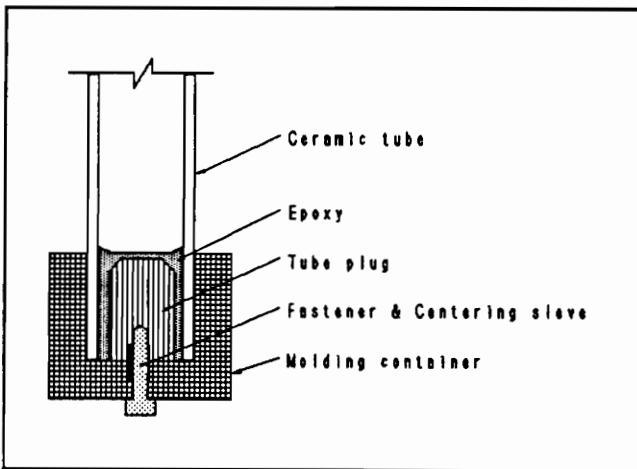


Figure 4.6 End Plug Alignment Detail

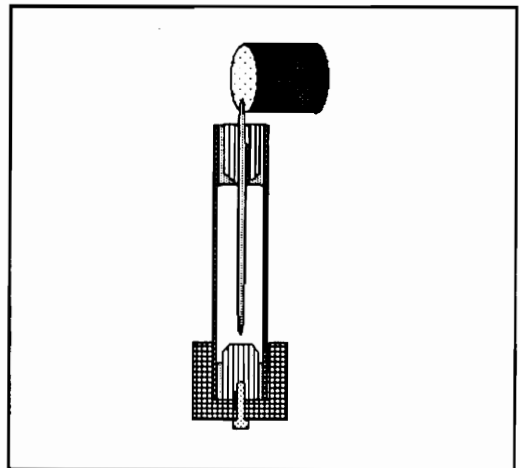


Figure 4.7 Procedure for Second Plug

In addition to internal plugs, the specimen ends must be shimmed with sandpaper or aluminum C rings in order to accommodate the testing machine grips and reduce slipping. This is complicated by a significant variation in diameter along the length of the cylinder.

---

<sup>2</sup> Ph.D Candidates, Virginia Tech

The next step is to prepare the surface for the strain gauges. As can be seen from the pencil rubbing of tube 67A (fig. 4.2), the tube surface is very coarse making installation of strain gauges difficult and unreliable. A thin layer of epoxy was applied to the gauge section to create a smoother surface.

The strain gauges are then installed. Large strain gauges would generally be used for such a rough surface in order to obtain an average surface strain. However, previous attempts suggested that it is important to measure all three strain components on a single patch and as close to a single point as possible due to the strain variation over the patch (Appendix C). Therefore, smaller gauges are desirable for closer packing. This is in conflict with the larger gauges desired to reduce the effect of the surface roughness.

A three-gauge (-45/ 0 /45) rosette was used. The individual gauges on the rosette are approximately in. by in.. Four of these rosettes (A, B, C, D) were placed on the specimen; two on (+) patches and two on (-) patches. The 0° gauge is aligned with the tube axis. The same-sign gauges were placed on directly opposite sides of the tube at the same axial location as shown in fig. 4.9 which also shows the notation used.

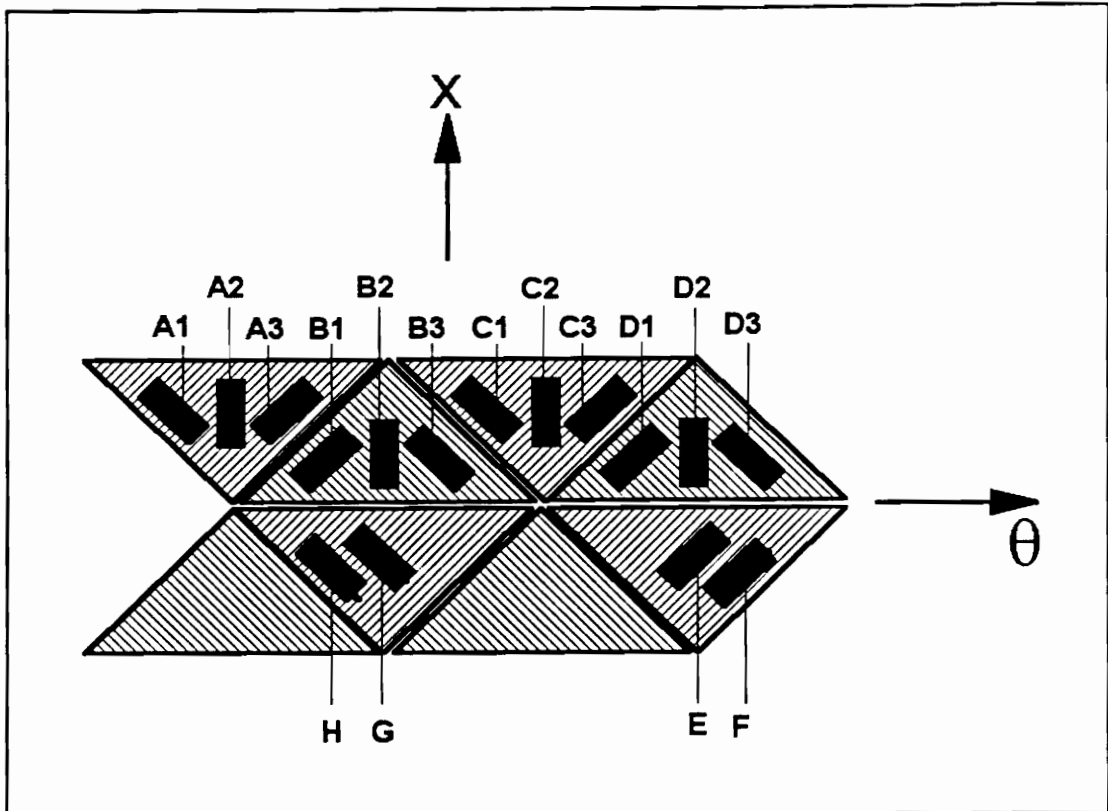


**Figure 4.8** Strain Gauge Placement, Specimen 67A

In addition to the four rosettes, four individual gauges (E, F, G, H) were placed on the specimen to quantify the strain variation between the center and the edge of the patches under axial and torsional loads.

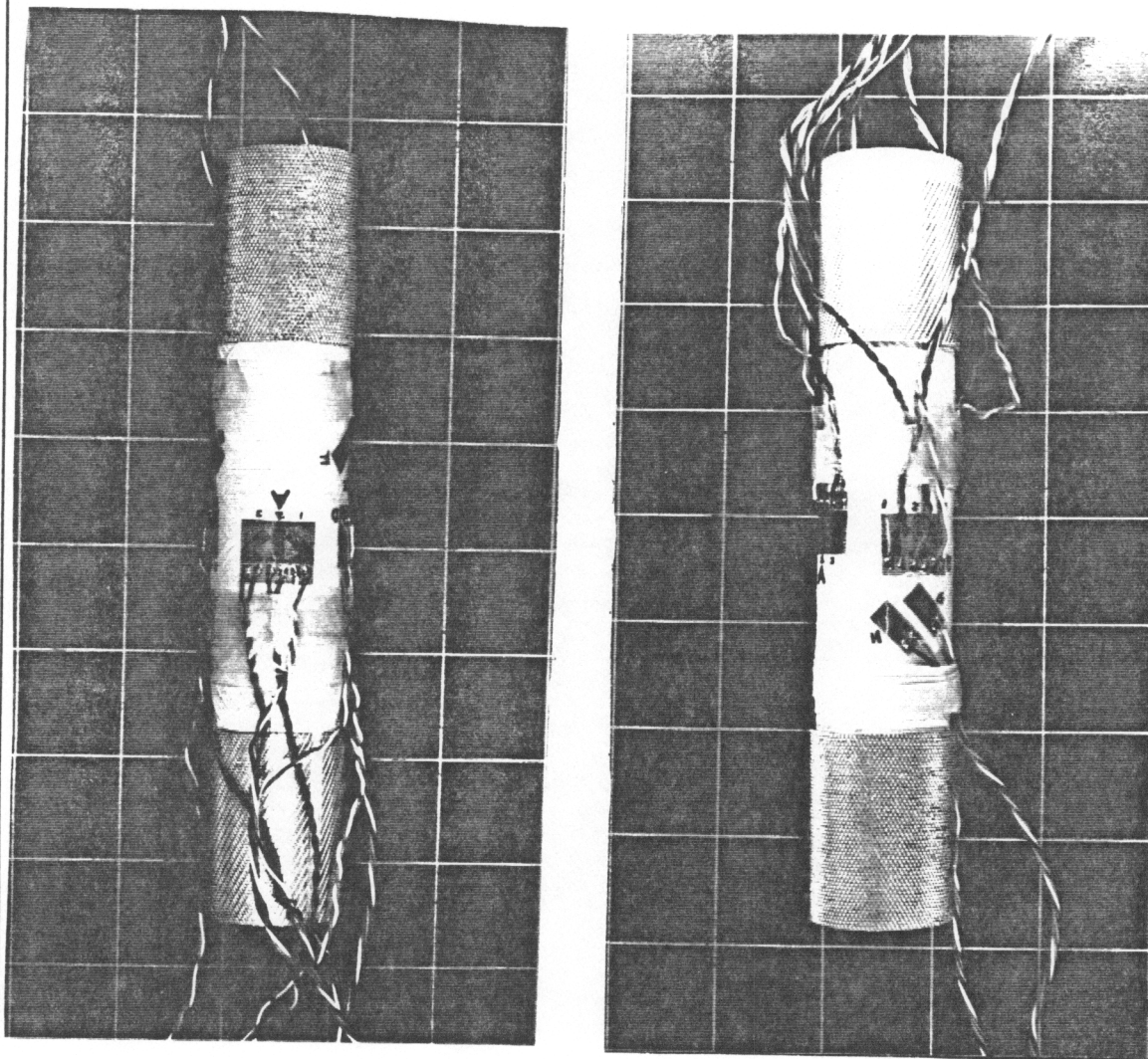


Figure 4.9 Photo of Specimen 67A

## **5.0 *Experimental Results***

The Instrumentation of specimen 67A was discussed in ch. 4. The present chapter details the loads applied and the reduction of the large quantities of data to a form fit for interpretation using the Least Squares method.

### **5.1 *Applied Loads***

The specimen was loaded three times for each of four loadings ( $\pm$  axial,  $\pm$  torsion). The nominal maximum load applied was  $\pm 400$  lbs. axial and  $\pm 100$  in.-lbs. torsion. The data were collected continuously as the cylinder was loaded and unloaded. All twelve rosette data channels were collected independently (no balancing) and simultaneously for each loading. The resulting strain-load curves are presented in Appendix B.

### **5.2 *Data Reduction***

Examination of the strain-load curves reveals generally linear behavior for all gauges over the load ranges examined. The data were therefore first reduced by taking the linear regression of each gauge under each load. The low values ( $|T_x| < 10$  in.-lbs.,  $|F_x| < 20$  lbs.) of each load trial were discarded prior to finding the linear regression. A two degree of freedom regression was used resulting in an equation for the data of the form:

$$y = mx + b \quad (5.1)$$

where  $y$  is the strain,  $x$  is the load,  $m$  is the slope and  $b$  is the  $y$  axis intercept.

The y intercept should, of course, be zero but it was often significant. The two degree-of-freedom regression was generally a better fit then a one degree-of-freedom fit (forced through the origin); therefore, the two degree of freedom fit was used and the offset was subsequently neglected. This effectively shifts all of the curves to the origin. This procedure also improved the consistency of the data. Tables 5.1-5.12 show the regressions of the data at this point. The data reduction and linear regressions were done using Borland's *Quattro Pro 4.0*. The Standard Errors are the curve fitting errors reported by Quattro and can be interpreted as  $m \pm E_m$  and  $b \pm E_b$  (Quattro Pro User's Guide [11]). Note that the error in the y intercept is generally about the same magnitude or larger then the intercept itself.

**Table 5.1 Tension Trial #1**

<b>67A Tension Trial #1</b>			<b>Standard Error (<math>E_m</math>)</b>	<b>Standard Error (<math>E_b</math>)</b>
<b>Gauge</b>	<b>m</b>	<b>b</b>		
<b>A1</b>	1.21862e-07	1.32460e-07	3.20767e-10	2.16209e-07
<b>A2</b>	3.25017e-07	2.38196e-06	1.02425e-09	6.90383e-07
<b>A3</b>	9.80045e-08	-1.56351e-06	2.10420e-09	1.41831e-06
<b>B1</b>	1.07601e-07	2.91251e-06	1.17587e-09	7.92578e-07
<b>B2</b>	2.82721e-07	-1.24291e-07	3.72596e-09	2.51144e-06
<b>B3</b>	1.02034e-07	-5.25906e-07	1.74024e-09	1.17299e-06
<b>C1</b>	1.07184e-07	-3.08941e-06	2.42340e-09	1.63346e-06
<b>C2</b>	3.22047e-07	-3.97993e-06	7.08205e-09	4.77357e-06
<b>C3</b>	1.06350e-07	-7.89990e-07	2.10020e-09	1.41562e-06
<b>D1</b>	9.80369e-08	1.94178e-08	2.01138e-09	1.35575e-06
<b>D2</b>	2.81854e-07	8.99271e-08	5.81034e-09	3.91639e-06
<b>D3</b>	1.13434e-07	-5.94437e-07	2.65208e-09	1.78760e-06

Table 5.2 Tension Trial #2

67A Tension Trial #2			Standard Error (m)	Standard Error (b)
Gauge	m	b		
A1	1.20094e-07	-6.86297e-07	3.49817e-10	2.31790e-07
A2	3.22131e-07	3.59285e-06	1.60008e-09	1.06022e-06
A3	1.00300e-07	-2.00559e-06	2.41075e-09	1.59737e-06
B1	1.06420e-07	4.45697e-06	9.75379e-10	6.46290e-07
B2	2.81577e-07	3.07930e-06	3.68066e-09	2.43882e-06
B3	1.01500e-07	1.91173e-06	1.60191e-09	1.06143e-06
C1	1.07357e-07	-7.48991e-07	2.02793e-09	1.34371e-06
C2	3.22127e-07	-1.93816e-06	6.41656e-09	4.25163e-06
C3	1.05560e-07	-3.04507e-07	2.08695e-09	1.38282e-06
D1	9.66155e-08	8.88661e-10	2.31744e-09	1.53555e-06
D2	2.78587e-07	3.63728e-07	6.24846e-09	4.14025e-06
D3	1.12019e-07	-3.33519e-07	2.86151e-09	1.89605e-06

**Table 5.3** Tension Trial #3

<b>67A Tension Trial #3</b>			<b>Standard Error (m)</b>	<b>Standard Error (b)</b>
<b>Gauge</b>	<b>m</b>	<b>b</b>		
<b>A1</b>	1.27131e-07	-2.61028e-07	3.25304e-10	2.18051e-07
<b>A2</b>	3.27605e-07	1.82050e-06	2.49986e-09	1.67565e-06
<b>A3</b>	9.42364e-08	-9.13201e-07	1.38766e-09	9.30143e-07
<b>B1</b>	1.02915e-07	1.22053e-06	1.36043e-09	9.11892e-07
<b>B2</b>	2.75233e-07	1.69261e-06	4.16952e-09	2.79482e-06
<b>B3</b>	9.80769e-08	-9.28220e-07	1.86374e-09	1.24926e-06
<b>C1</b>	1.07322e-07	-2.49793e-06	2.01088e-09	1.34789e-06
<b>C2</b>	3.17651e-07	-2.79871e-06	5.72235e-09	3.83568e-06
<b>C3</b>	1.09767e-07	1.59386e-06	1.32594e-09	8.88776e-07
<b>D1</b>	1.06467e-07	2.41137e-07	1.71154e-09	1.14724e-06
<b>D2</b>	2.92086e-07	2.36364e-07	5.27435e-09	3.53539e-06
<b>D3</b>	1.11276e-07	1.81136e-07	2.59572e-09	1.73990e-06

**Table 5.4** Compression Trial #1

<b>67A Compression Trial #1</b>			<b>Standard Error (m)</b>	<b>Standard Error (b)</b>
<b>Gauge</b>	<b>m</b>	<b>b</b>		
<b>A1</b>	1.22551e-07	-8.51846e-07	5.38153e-10	3.53121e-07
<b>A2</b>	3.26596e-07	-4.57775e-07	1.04546e-09	6.86002e-07
<b>A3</b>	9.93998e-08	1.19472e-06	2.46688e-09	1.61870e-06
<b>B1</b>	1.06909e-07	2.96972e-06	8.08313e-10	5.30393e-07
<b>B2</b>	2.82246e-07	2.24507e-06	3.37536e-09	2.21482e-06
<b>B3</b>	1.01030e-07	1.95774e-06	1.63221e-09	1.07101e-06
<b>C1</b>	1.06886e-07	-1.17498e-06	1.85827e-09	1.21935e-06
<b>C2</b>	3.16921e-07	-2.47493e-06	6.97565e-09	4.57723e-06
<b>C3</b>	1.03663e-07	7.59658e-07	2.04249e-09	1.34023e-06
<b>D1</b>	9.50401e-08	-1.94094e-07	2.15767e-09	1.41580e-06
<b>D2</b>	2.78047e-07	-7.33726e-07	6.23300e-09	4.08993e-06
<b>D3</b>	1.14388e-07	-7.07644e-07	2.62297e-09	1.72112e-06

Table 5.5    Compression Trial #2

<u>67A Compression Trial #2</u>			Standard Error (m)	Standard Error (b)
Gauge	m	b		
A1	1.20402e-07	-9.19270e-07	3.74253e-10	2.42173e-07
A2	3.24530e-07	1.41224e-06	1.37226e-09	8.87964e-07
A3	1.02330e-07	9.82200e-07	2.31588e-09	1.49856e-06
B1	1.07859e-07	2.60941e-06	1.35144e-09	8.74495e-07
B2	2.79960e-07	2.10351e-06	3.52075e-09	2.27821e-06
B3	1.00082e-07	1.88560e-06	1.69797e-09	1.09873e-06
C1	1.05911e-07	-1.45304e-06	1.73714e-09	1.12407e-06
C2	3.17634e-07	-1.86839e-06	6.81711e-09	4.41123e-06
C3	1.02986e-07	8.71021e-07	2.43443e-09	1.57528e-06
D1	9.47011e-08	-6.71437e-08	2.44215e-09	1.58027e-06
D2	2.76655e-07	-8.11089e-07	6.47983e-09	4.19298e-06
D3	1.12675e-07	-1.72743e-08	2.67654e-09	1.73194e-06

Table 5.6 Compression Trial #3

67A Compression Trial #3			Standard Error (m)	Standard Error (b)
Gauge	m	b		
A1	1.31652e-07	-7.42186e-07	5.89869e-10	3.95402e-07
A2	3.34663e-07	1.02789e-06	9.06396e-10	6.07576e-07
A3	9.89185e-08	-1.14566e-06	1.37979e-09	9.24906e-07
B1	1.06709e-07	1.93833e-06	1.05021e-09	7.03975e-07
B2	2.77016e-07	7.27052e-07	2.69673e-09	1.80767e-06
B3	9.68266e-08	-1.00385e-06	1.19106e-09	7.98391e-07
C1	1.06745e-07	-2.24490e-06	1.84145e-09	1.23437e-06
C2	3.11389e-07	-2.49271e-06	7.29717e-09	4.89145e-06
C3	1.05425e-07	4.96719e-07	2.32454e-09	1.55819e-06
D1	1.01533e-07	2.85772e-08	2.57282e-09	1.72462e-06
D2	2.86535e-07	-6.88019e-07	6.47704e-09	4.34170e-06
D3	1.13596e-07	-9.96219e-08	2.61172e-09	1.75069e-06

**Table 5.7** Positive Torsion Trial #1

<b>67A Positive Torsion Trial #1</b>			<b>Standard Error (m)</b>	<b>Standard Error (b)</b>
<b>Gauge</b>	<b>m</b>	<b>b</b>		
<b>A1</b>	-3.15958e-07	-3.04415e-07	2.08716e-09	3.13325e-07
<b>A2</b>	-1.08381e-08	3.82201e-06	1.54808e-09	2.32399e-07
<b>A3</b>	3.05582e-07	-3.28600e-06	1.22353e-08	1.83677e-06
<b>B1</b>	3.21725e-07	1.74771e-06	3.87005e-09	5.80974e-07
<b>B2</b>	-1.92701e-08	1.87116e-06	1.42953e-09	2.14602e-07
<b>B3</b>	-3.40434e-07	3.34050e-06	6.46157e-09	9.70015e-07
<b>C1</b>	-3.46967e-07	-3.53772e-07	6.81495e-09	1.02306e-06
<b>C2</b>	7.38009e-09	-1.26220e-06	1.38363e-09	2.07712e-07
<b>C3</b>	3.30874e-07	-2.55949e-07	9.36929e-09	1.40652e-06
<b>D1</b>	3.11126e-07	-9.56094e-07	9.52034e-09	1.42920e-06
<b>D2</b>	1.38176e-08	-1.67059e-07	6.43007e-10	9.65286e-08
<b>D3</b>	-3.30760e-07	4.91284e-07	1.19153e-08	1.78874e-06

**Table 5.8** Positive Torsion Trial #2

<b>67A Positive Torsion Trial #2</b>			<b>Standard Error (m)</b>	<b>Standard Error (b)</b>
<b>Gauge</b>	<b>m</b>	<b>b</b>		
<b>A1</b>	-3.18592e-07	5.31941e-07	1.41283e-09	2.11396e-07
<b>A2</b>	-6.50695e-09	3.02488e-06	1.65160e-09	2.47123e-07
<b>A3</b>	3.00009e-07	1.31355e-06	1.09303e-08	1.63547e-06
<b>B1</b>	3.11501e-07	6.47532e-07	3.81158e-09	5.70314e-07
<b>B2</b>	-2.17838e-08	3.16492e-06	1.69841e-09	2.54127e-07
<b>B3</b>	-3.36778e-07	1.57947e-06	5.41220e-09	8.09808e-07
<b>C1</b>	-3.46469e-07	8.76893e-08	5.91866e-09	8.85587e-07
<b>C2</b>	1.05933e-08	-1.17909e-06	1.82138e-09	2.72526e-07
<b>C3</b>	3.36113e-07	-1.23964e-07	9.72845e-09	1.45563e-06
<b>D1</b>	3.14261e-07	-1.10988e-06	8.67868e-09	1.29856e-06
<b>D2</b>	1.65226e-08	1.60657e-07	1.62195e-09	2.42686e-07
<b>D3</b>	-3.30757e-07	1.69773e-06	1.03634e-08	1.55063e-06

**Table 5.9** Positive Torsion Trial #3

<b>67A Positive Torsion Trial #3</b>			<b>Standard Error (m)</b>	<b>Standard Error (b)</b>
<b>Gauge</b>	<b>m</b>	<b>b</b>		
<b>A1</b>	-3.33157e-07	6.61998e-07	1.83163e-09	2.75091e-07
<b>A2</b>	-1.45633e-08	2.16370e-06	1.78101e-09	2.67488e-07
<b>A3</b>	3.01758e-07	-1.77776e-06	6.65355e-09	9.99292e-07
<b>B1</b>	3.25570e-07	2.47371e-06	4.26943e-09	6.41223e-07
<b>B2</b>	-1.19210e-08	3.57938e-06	1.46652e-09	2.20255e-07
<b>B3</b>	-3.41011e-07	4.84053e-07	5.46909e-09	8.21399e-07
<b>C1</b>	-3.45931e-07	-1.47553e-06	6.20292e-09	9.31612e-07
<b>C2</b>	1.69810e-08	-2.79689e-06	3.05928e-09	4.59472e-07
<b>C3</b>	3.36916e-07	5.93021e-07	7.72444e-09	1.16013e-06
<b>D1</b>	3.12875e-07	-2.42400e-07	8.73086e-09	1.31128e-06
<b>D2</b>	1.16983e-08	4.35309e-07	8.00758e-10	1.20265e-07
<b>D3</b>	-3.34692e-07	-3.14013e-07	1.11887e-08	1.68043e-06

**Table 5.10** Negative Torsion Trial #1

<b>67A Negative Torsion Trial #1</b>			<b>Standard Error (m)</b>	<b>Standard Error (b)</b>
<b>Gauge</b>	<b>m</b>	<b>b</b>		
<b>A1</b>	-3.21708e-07	1.82839e-07	1.82245e-09	2.54950e-07
<b>A2</b>	-1.62553e-08	2.81802e-06	2.25039e-09	3.14816e-07
<b>A3</b>	2.91720e-07	-5.00955e-07	1.01349e-08	1.41781e-06
<b>B1</b>	3.24227e-07	2.96347e-06	3.72868e-09	5.21621e-07
<b>B2</b>	-1.56793e-08	3.14170e-06	1.68408e-09	2.35593e-07
<b>B3</b>	-3.42551e-07	1.45475e-06	6.28645e-09	8.79439e-07
<b>C1</b>	-3.50173e-07	-9.89687e-07	6.30273e-09	8.81716e-07
<b>C2</b>	3.90892e-09	-2.31388e-06	1.46519e-09	2.04971e-07
<b>C3</b>	3.35434e-07	-1.89452e-07	9.26745e-09	1.29646e-06
<b>D1</b>	3.11042e-07	-1.28893e-06	8.64948e-09	1.21001e-06
<b>D2</b>	1.45037e-08	3.96482e-08	9.69782e-10	1.35667e-07
<b>D3</b>	-3.28369e-07	1.71830e-06	1.15630e-08	1.61760e-06

**Table 5.11** Negative Torsion Trial #2

<b>67A Negative Torsion Trial #2</b>			<b>Standard Error (m)</b>	<b>Standard Error (b)</b>
<b>Gauge</b>	<b>m</b>	<b>b</b>		
<b>A1</b>	-3.16552e-07	2.26227e-07	1.77463e-09	2.91497e-07
<b>A2</b>	-7.74721e-09	3.10411e-06	1.52448e-09	2.50407e-07
<b>A3</b>	2.82577e-07	-3.10771e-06	6.74460e-09	1.10785e-06
<b>B1</b>	3.27508e-07	2.83828e-06	2.59404e-09	4.26091e-07
<b>B2</b>	-1.67333e-08	2.63498e-06	9.93333e-10	1.63162e-07
<b>B3</b>	-3.36735e-07	5.95394e-07	5.82563e-09	9.56904e-07
<b>C1</b>	-3.45290e-07	-7.74415e-07	5.92362e-09	9.72999e-07
<b>C2</b>	4.72789e-09	-2.39923e-06	2.03910e-09	3.34937e-07
<b>C3</b>	3.33242e-07	-1.07967e-06	6.81360e-09	1.11919e-06
<b>D1</b>	3.13917e-07	-1.02484e-06	6.98570e-09	1.14745e-06
<b>D2</b>	1.52385e-08	-3.92302e-07	7.76272e-10	1.27509e-07
<b>D3</b>	-3.29990e-07	6.07616e-07	9.33217e-09	1.53288e-06

**Table 5.12 Negative Torsion Trial #3**

<b>67A Negative Torsion Trial #3</b>			<b>Standard Error (m)</b>	<b>Standard Error (b)</b>
<b>Gauge</b>	<b>m</b>	<b>b</b>		
<b>A1</b>	-3.33447e-07	7.75273e-07	2.16551e-09	3.17832e-07
<b>A2</b>	-1.40732e-08	2.22595e-06	1.94158e-09	2.84965e-07
<b>A3</b>	3.14340e-07	-1.91642e-06	8.07293e-09	1.18486e-06
<b>B1</b>	3.20088e-07	2.81403e-06	6.57642e-09	9.65220e-07
<b>B2</b>	-1.40741e-08	1.72086e-06	1.25753e-09	1.84567e-07
<b>B3</b>	-3.34347e-07	-2.08670e-08	5.04029e-09	7.39762e-07
<b>C1</b>	-3.44478e-07	-1.55217e-06	6.64230e-09	9.74889e-07
<b>C2</b>	1.05982e-08	-4.26856e-06	1.73704e-09	2.54945e-07
<b>C3</b>	3.29060e-07	4.80812e-07	7.69604e-09	1.12955e-06
<b>D1</b>	3.09376e-07	-2.01180e-08	8.26863e-09	1.21358e-06
<b>D2</b>	9.32684e-09	6.30513e-07	2.32536e-09	3.41293e-07
<b>D3</b>	-3.30379e-07	1.99628e-07	1.08950e-08	1.59905e-06

All of the individual load trials were then averaged. The intercept values (b) are discarded at this point.

**Table 5.13** Average Gauge Strains

<b>67A Average Gauge Strains</b>				
	<u>Axial Load</u>		<u>Torsional Load</u>	
	m	±error	m	±error
<b>A1</b>	1.23949e-07	1.75492e-10	-3.23236e-07	7.61345e-10
<b>A2</b>	3.26757e-07	6.15907e-10	-1.16640e-08	7.35118e-10
<b>A3</b>	9.88648e-08	8.41916e-10	2.99331e-07	3.82544e-09
<b>B1</b>	1.06402e-07	4.64504e-10	3.21770e-07	1.76080e-09
<b>B2</b>	2.79792e-07	1.45178e-09	-1.65769e-08	5.88856e-10
<b>B3</b>	9.99249e-08	6.67372e-10	-3.38643e-07	2.35594e-09
<b>C1</b>	1.06901e-07	8.14637e-10	-3.46551e-07	2.57598e-09
<b>C2</b>	3.17962e-07	2.75103e-09	9.03157e-09	8.15016e-10
<b>C3</b>	1.05625e-07	8.50262e-10	3.33606e-07	3.47064e-09
<b>D1</b>	9.87323e-08	9.06528e-10	3.12100e-07	3.47278e-09
<b>D2</b>	2.82294e-07	2.49117e-09	1.35179e-08	5.43542e-10
<b>D3</b>	1.12898e-07	1.09067e-09	-3.30824e-07	4.45363e-09

The error throughout the data reduction is calculated according to the formula:

$$\delta_R = \sqrt{\sum_{i=1}^n \left(\frac{\partial R}{\partial X_i} \delta_i\right)^2} \tag{5.2}$$

$$R = f(X_1, X_2, ..., X_n)$$

where  $\delta_R$  is the error of the value R which is a function of the constants  $X_i$  each with

error  $\delta_i$  ( $R \pm \delta_R = f(X_1 \pm \delta_i, X_2 \pm \delta_{2,...}, X_n \pm \delta_n)$ ).

The data were then averaged according to the sign of the patch as shown below in Table C.13. Because the same-sign patches are on opposite sides of the cylinder this operation eliminates the influence of bending in the same manner as balancing the gauges would have.

**Table 5.14** Gauge Balancing Formulas

<u>Formulas</u>		m
<b>(+) Patch</b>	$\epsilon_I$	(B1+D1)/2
	$\epsilon_{II}$	(B2+D2)/2
	$\epsilon_{III}$	(B3+D3)/2
<b>(-) Patch</b>	$\epsilon_I$	(A1+C1)/2
	$\epsilon_{II}$	(A2+C2)/2
	$\epsilon_{III}$	(A3+C3)/2

The results at this point are given in Tables 5.15 - 5.16.

**Table 5.15** Balanced Average Gauge Strain Values, Axial Load

<b>67A Axial Load</b>		<b>m</b>	<b>±error</b>
<b>(+) Patch</b>	$\epsilon_I$	1.02567e-07	5.09303e-10
	$\epsilon_{II}$	2.81043e-07	1.44166e-09
	$\epsilon_{III}$	1.06411e-07	6.39327e-10
<b>(-) Patch</b>	$\epsilon_I$	1.15425e-07	4.16663e-10
	$\epsilon_{II}$	3.22359e-07	1.40957e-09
	$\epsilon_{III}$	1.02245e-07	5.98283e-10

**Table 5.16** Balanced Average Gauge Strain Values, Torsional Load

<b>67A Torsional Load</b>		<b>m</b>	<b>±error</b>
<b>(+) Patch</b>	$\epsilon_I$	3.16935e-07	1.94683e-09
	$\epsilon_{II}$	-1.52950e-09	4.00684e-10
	$\epsilon_{III}$	-3.34734e-07	2.51919e-09
<b>(-) Patch</b>	$\epsilon_I$	-3.34893e-07	1.34307e-09
	$\epsilon_{II}$	-1.31621e-09	5.48783e-10
	$\epsilon_{III}$	3.16469e-07	2.58260e-09

The strains for each load are now rotated to their respective "principle" strain coordinates. "Principle" strain direction in this case refers to the coordinate system for which an quasi-isotropic,  $\pm 45^\circ$  laminate would have true principal stresses (zero shear stresses). These are the cylinder coordinates for axial loads ( $\epsilon_x$ ,  $\epsilon_\theta$ ,  $\gamma_{x\theta}$ ) and the material coordinates for the torsional loads ( $\epsilon_1$ ,  $\epsilon_2$ ,  $\gamma_{12}$ ). Note that

the shear stresses will not be zero in this case because; the laminates are *anti*-symmetric, thick wall cylinder, ply-angle variation through thickness. Despite these effects, these choices of axes generally have large extensional strains and smaller (less accurate) shear strains. This means there are only two measurements with high error as opposed to four if coordinates were chosen to maximize the shear components. This choice is somewhat arbitrary but seems to work well.

The data from Tables 5.15 and 5.16 are now rotated to the proper coordinate system through the strain transformation equations ((+) Patch):

$$\begin{Bmatrix} \epsilon_I \\ \epsilon_J \\ \frac{\gamma_{IJ}}{2} \end{Bmatrix} = \begin{bmatrix} \cos^2 \beta & \sin^2 \beta & 2 \sin \beta \cos \beta \\ \sin^2 \beta & \cos^2 \beta & -2 \sin \beta \cos \beta \\ -\sin \beta \cos \beta & \sin \beta \cos \beta & (\cos^2 \beta - \sin^2 \beta) \end{bmatrix} \begin{Bmatrix} \epsilon_I \\ \epsilon_{III} \\ \frac{\gamma_{I-III}}{2} \end{Bmatrix} \quad (5.3)$$

$$\gamma_{I-III} = 2\epsilon_{II} - (\epsilon_I + \epsilon_{III})$$

where, for axial loads:

$$\begin{aligned} \{\epsilon_I, \epsilon_J, \gamma_{IJ}\} &= \{\epsilon_x, \epsilon_\theta, \gamma_{x\theta}\} \\ \beta &= 45^\circ \end{aligned} \quad (5.4)$$

and for torsional loads:

$$\begin{aligned} \{\epsilon_I, \epsilon_J, \gamma_{IJ}\} &= \{\epsilon_1, \epsilon_2, \gamma_{12}\} \\ \beta &= 94.15^\circ \quad ((+)Patch) \\ \beta &= -4.15^\circ \quad ((-)Patch) \end{aligned} \quad (5.5)$$

Because of the the numbering convention used  $\epsilon_I$  and  $\epsilon_{III}$  must be switched in the right hand side of eq. 5.3 for a (-) Patch. The geometry of the measured and calculated strains is shown below for a (+) oriented patch.

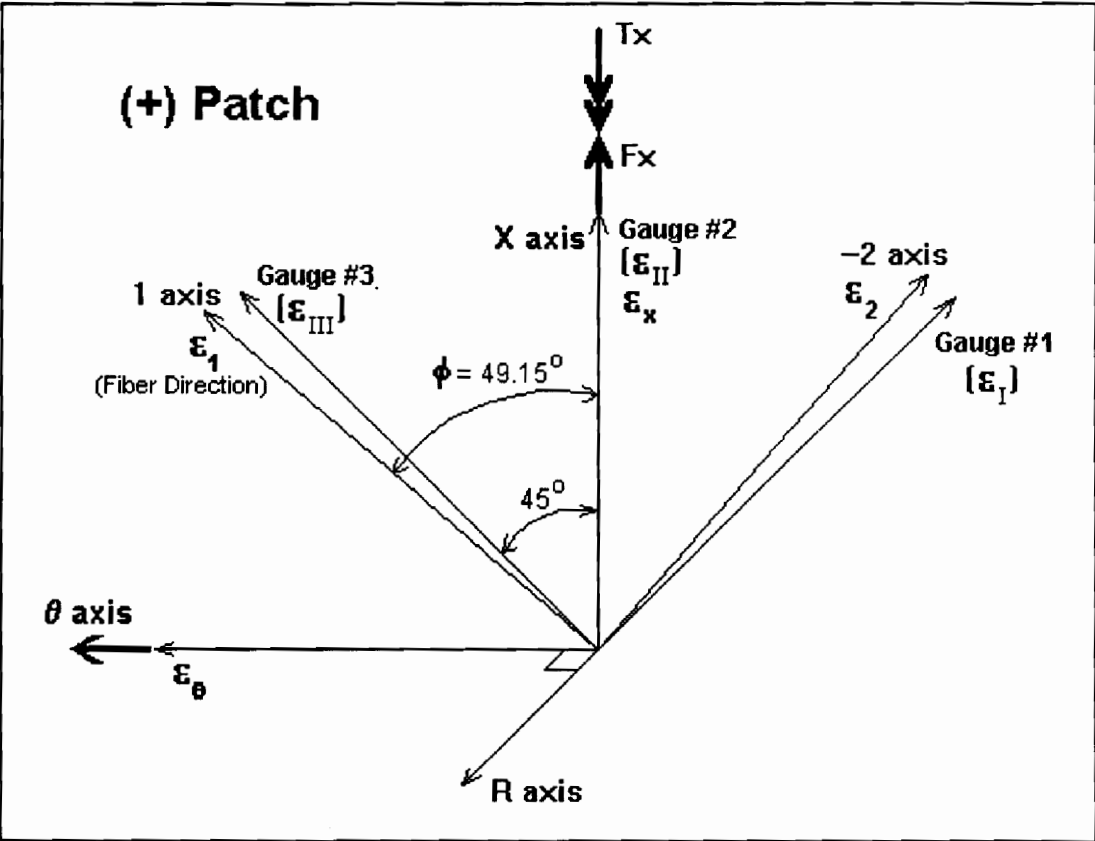


Figure 5.1 Coordinate Systems, Specimen 67A

The results of these rotations are given below.

Table 5.17 Axial Load Strains, Cylinder Coordinates

67A Axial Load		m	±error
(+) Patch	$\epsilon_x$	2.81043e-07	1.55321e-09
	$\epsilon_\theta$	-7.20644e-08	1.55321e-09
	$\gamma_{x\theta}$	3.84419e-09	8.17391e-10
(-) Patch	$\epsilon_x$	3.22359e-07	1.50088e-09
	$\epsilon_\theta$	-1.04690e-07	1.50088e-09
	$\gamma_{x\theta}$	1.31797e-08	7.29075e-10

**Table 5.18** Torsional Load Strains, Material Coordinates

<b>67A Torsional Load</b>		<b>m</b>	<b>±error</b>
<b>(+) Patch</b>	$\epsilon_1$	-3.32385e-07	2.51720e-09
	$\epsilon_2$	3.14586e-07	1.95113e-09
	$\gamma_{12}$	7.94868e-08	3.28105e-09
<b>(-) Patch</b>	$\epsilon_1$	3.11918e-07	2.57888e-09
	$\epsilon_2$	-3.30342e-07	1.35484e-09
	$\gamma_{12}$	1.09655e-07	3.10696e-09

**5.3 Final Data**

The final measurements used in the inversion are listed below and plotted on the following page. The strains from the (-) oriented patch were chosen over the (+) patch measurements because the linear regression errors were generally smaller. The data were not averaged together because the data from the patches of the same sign were generally self-consistent but not consistent with the patches of opposite sign. In other words, patches A and C ((-) patches) have very similar values while patches B and D ((+) patches) also have very consistent data but the (+) patch data is significantly different from the (-) patch data. The cause of this discrepancy is unknown and may be related to gripping or end effects.

A secondary effort was made to characterize the effect of strain gauge position on the measured strains using gauges E, F, G, and H. These results are contained in Appendix C.

The following chapter details the application of the inversion method to the data presented in this section.

**Table 5.30** Final Strain Measurements for Speciman 67A

<b><u>67A Final Strains</u></b>				
<b><u>Axial Load</u></b>		<b>m</b>	<b>error</b>	<b>% error</b>
<b>(-) Patch</b>	$\epsilon_x$	3.22359e-07	1.50088e-09	0.47
	$\epsilon_\theta$	-1.04690e-07	1.50088e-09	1.43
	$\gamma_{x\theta}$	1.31797e-08	7.29075e-10	5.53
<b><u>Torsional Load</u></b>		<b>m</b>	<b>error</b>	<b>% error</b>
<b>(-) Patch</b>	$\epsilon_1$	3.11918e-07	2.57888e-09	0.83
	$\epsilon_2$	-3.30342e-07	1.35484e-09	0.41
	$\gamma_{12}$	1.09655e-07	3.10696e-09	2.83

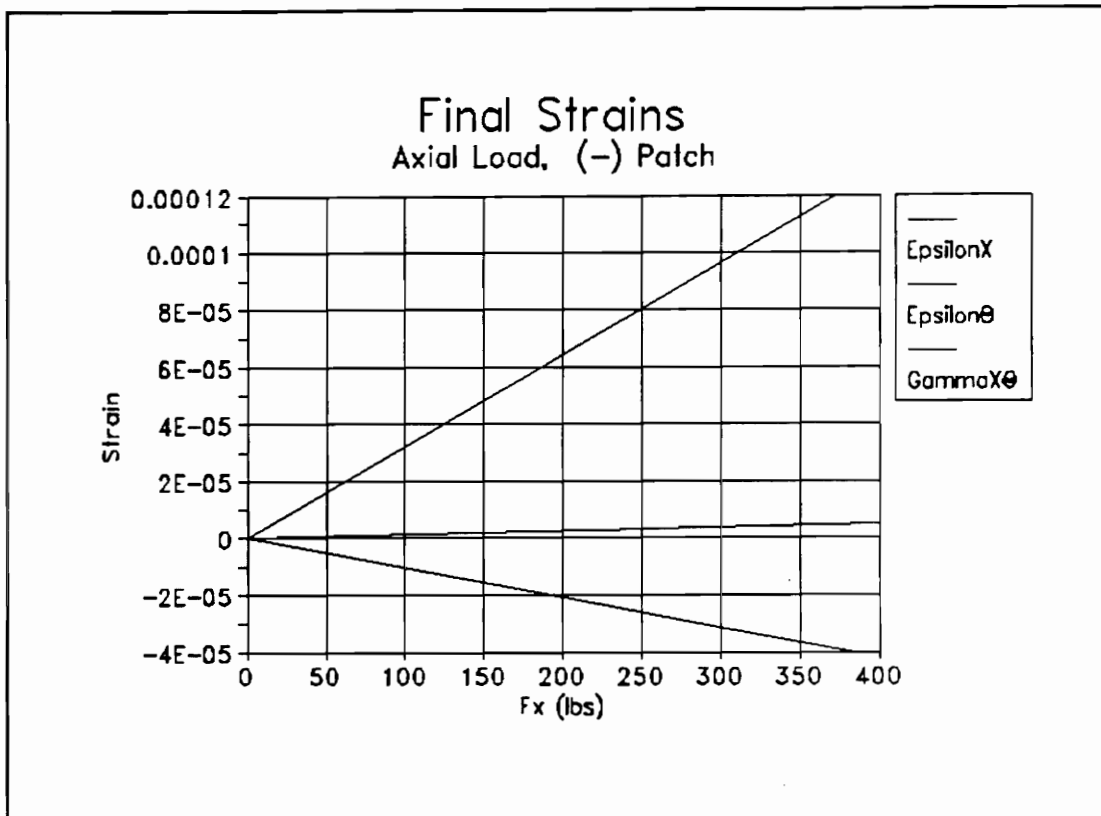


Figure 5.2 Final Strains, (-) Patch, Axial Load

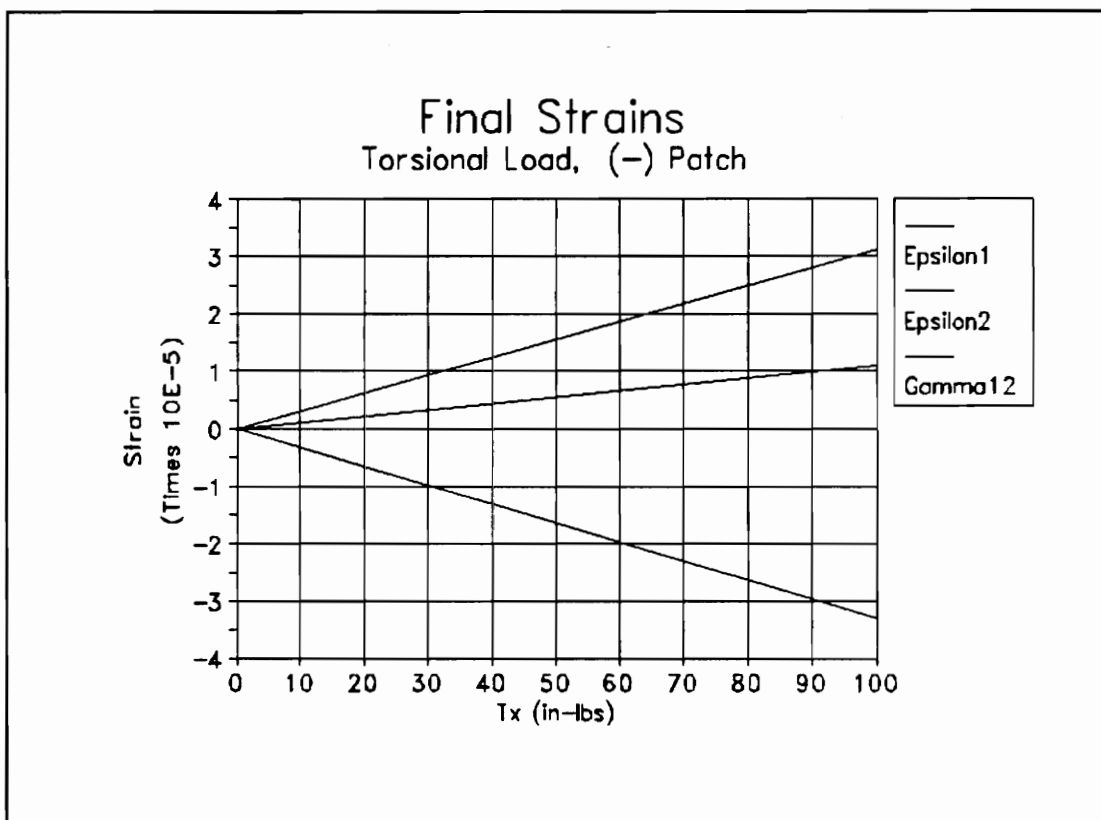


Figure 5.3 Final Strains, (-) Patch, Torsional Load

## **6.0 *Inversion of Experimental Data***

### **6.1 *Introduction***

This chapter discusses the inversion of the experimental data presented in ch. 5. The problems encountered and solutions employed are discussed. Final results are presented and discussed for specimen 67A.

### **6.2 *Initial Estimate***

The least squares inversion method requires a reasonable initial estimate of the elastic properties from which to work. As shown in the sample inversion shown in ch. 3, this initial estimate does not have to be very accurate for convergence to occur. However, an accurate initial estimate can greatly reduce the number of iterations required. For this study, a rule-of-mixtures approach is employed.

#### **6.2.1 *Effect of Porosity***

In ch. 4 porosity was discussed as a major factor influencing the properties of aluminum oxide. The matrix material was determined to have a porosity of approximately 20 to 30 percent. A middle value of 25% will be used for the estimate. The effect of porosity on the Young's modulus, shear modulus, and

Poisson's ratio of aluminum oxide are give empirically by Spriggs[12][13]. The equations are exponentials of the following form:

$$E = E_o e^{-bP} \quad (6.1)$$

where:

$E$  = Young's modulus of porous material

$E_o$  = Young's modulus of non-porous material

$b$  = an empirical constant

$P$  = volume fraction porosity

A similar expression is used for the shear modulus:

$$G = G_o e^{-dP} \quad (6.2)$$

where:

$G$  = Shear modulus of porous material

$G_o$  = Shear modulus of non-porous material

$d$  = an empirical constant

$P$  = volume fraction porosity

The Poisson Ratio is given by the isotropic relation:

$$\nu = \frac{E}{2G} - 1 \quad (6.3)$$

The zero porosity moduli are approximately:

$$E_o = 59 \text{ msi}$$

$$G_o = 23.5 \text{ msi}$$

The empirical constants for slip-cast and sintered aluminum oxide were used because this fabrication method was the only one reported with porosities in the range of the sol-gel experimental specimens used. The empirical constants are:  $b = 2.73$ ,  $d = 2.91$ . The resulting variation in properties with porosity is shown in fig. 6.1. Using equations 6.1-6.3 the matrix properties are calculated as:

$$E = 29.8 \text{ msi}$$

$$G = 11.4 \text{ msi}$$

$$\nu = .31$$

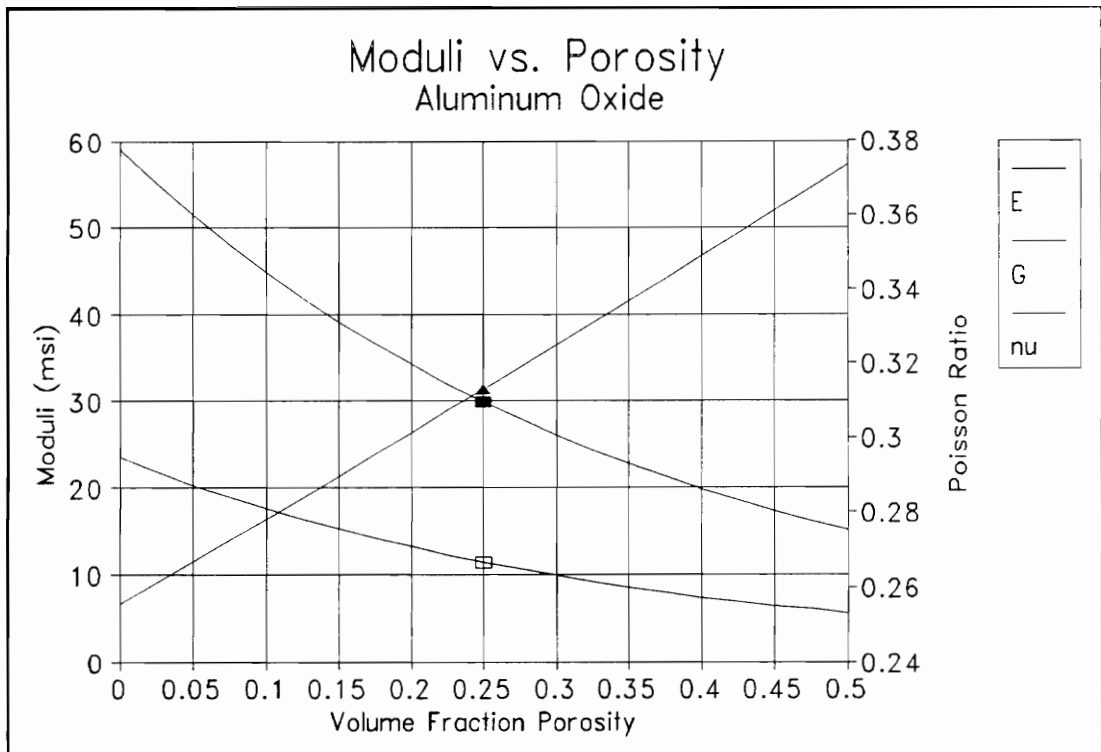


**Figure 6.1** Variation of Elastic Properties with Porosity

### 6.2.2 Rule-of-Mixtures

Rule-of-Mixtures calculations are now performed based on the properties given in Table 6.1. Fiber properties are based on information received from the manufacturer (Babcock & Wilcox).

**Table 6.1** Estimated Constituent Properties

<b>Estimated Constituent Properties</b>		
<b><math>V_{\text{fiber}} \approx 43\%</math></b>	<b>Matrix</b>	<b>Fibers</b>
<b>E</b>	29.8 msi	43 msi
<b>G</b>	11.4 msi	17.1 msi
<b><math>\nu</math></b>	0.31	0.26

The rule-of-mixtures equations are [17]:

$$E_1 = E_f V_f + E_m (1 - V_f) \tag{6.4}$$

$$E_2 = \frac{E_f E_m}{E_m V_f + E_f (1 - V_f)} \tag{6.5}$$

$$G_{12} = \frac{G_f G_m}{G_m V_f + G_f (1 - V_f)} \tag{6.6}$$

$$\nu_1 = \nu_f V_f + \nu_m (1 - V_f) \tag{6.7}$$

Application of these equations with the properties in Table 6.1 yields the following estimate for lamina properties (out-of-plane properties are estimated from in-plane properties):

**Table 6.2** Estimated Lamina Properties

Estimated Lamina Properties			
E <sub>1</sub>	35.5 ksi	ν <sub>12</sub>	0.29
E <sub>2</sub>	34.3 ksi	ν <sub>13</sub>	0.29
E <sub>3</sub>	34.3 ksi	ν <sub>23</sub>	0.29
G <sub>12</sub>	13.3 ksi		

### 6.3 Initial Inversion Attempt

The specimen geometry (Table 4.1) and the final reduction of the experimental data (Table 5.30) were input and an inversion attempt was made using the BASIC version of the Least Squares program. Because only axial and torsional load data are available ν<sub>13</sub> and ν<sub>23</sub> are set equal to ν<sub>12</sub> in order to have an over-defined system (see section 3.2).

The rule-of-mixtures initial estimate (Table 6.2, designated #1) was used in addition to two additional, more conservative, estimates (Table 6.3).

**Table 6.3** Additional Initial Estimates

<b><u>Additional Initial Estimates</u></b>			
<b>#2</b>		<b>#3</b>	
<b>E<sub>1</sub></b>	18 msi	<b>E<sub>1</sub></b>	20 msi
<b>E<sub>2</sub></b>	8 msi	<b>E<sub>2</sub></b>	6 msi
<b>E<sub>3</sub></b>	7 msi	<b>E<sub>3</sub></b>	5 msi
<b>G<sub>12</sub></b>	4 msi	<b>G<sub>12</sub></b>	3 msi
<b>ν<sub>12</sub></b>	0.1	<b>ν<sub>12</sub></b>	0.1

These inversion attempts were not successful. The rule-of-mixtures estimate attempt developed properties which led to an imaginary eigenvalue (  $\lambda$  ) in the elasticity solution after only five iterations. The additional estimates did not "crash" the program but they gave no sign of converging for over 125 iterations.

**6.3.1 Initial Adjustment to  $\gamma_{x0}(F_x)$**

The least squares program outputs "trace" files containing the values of the error function, elastic properties and calculated strains for each iteration. These trace files were examined in order to gain some insight into the failure to converge. It was discovered that the largest term in the error function was the  $\gamma_{x0}(F_x)$  term. Specifically, property values could not be found that produce shear strains as large as those measured. The possibility of a large error in this measurement is not surprising considering the typical magnitude of this strain (Appendix A, Ch. 3) and the testing situation (surface roughness, voids, strain variation over patch, etc.).

A preliminary attempt to obtain convergence was made by changing the value of  $\gamma_{x0}(F_x)$  to  $1 \times 10^{-9}$  in the data file. This change did produce convergence for estimates #2 and #3 (the rule-of-mixtures estimate again failed and was discarded) indicating that this component was part the problem. However, the error function is still relatively large indicating that the converged solution is not very good.

### **6.3.2 Discussion of Convergence Problem**

A failure of the method to converge, or convergence with large values of the error function, indicates that there is no feasible region of material properties that can reproduce the input strains for the given geometry and loads. This means that, either the model used does not accurately represent the strain response of the cylinder, or that the experimental error in the measurements is so large that the measurements are physically inconsistent. The latter problem was observed in ch. 3 with the inversions of the truncated analytical data.

A combination of these problems is most likely considering the specimen geometry and characteristics. However, there is no method available to better model the actual cylinder. Therefore, attempts will be made to find and correct inconsistencies in the data. The adjustment of  $\gamma_{x0}(F_x)$  in the previous section is an example of this. This adjustment made the data consistent enough for some convergence, however, the size of the error function indicates that there are still some significant inconsistencies. The following trace plots from the initial inversion attempts can provide some insight into the nature of the problem.

Table 6.4 Legend Key, Figures 6.2-6.12

Legend Key	
#1	Rule-of-Mixtures Initial Estimate
#2	Initial Estimate #1
#3	Initial Estimate #2
#4	Initial Estimate #1, $\gamma_{x\theta}(F_x)$ set to $1 \times 10^{-9}$
#5	Initial Estimate #2, $\gamma_{x\theta}(F_x)$ set to $1 \times 10^{-9}$

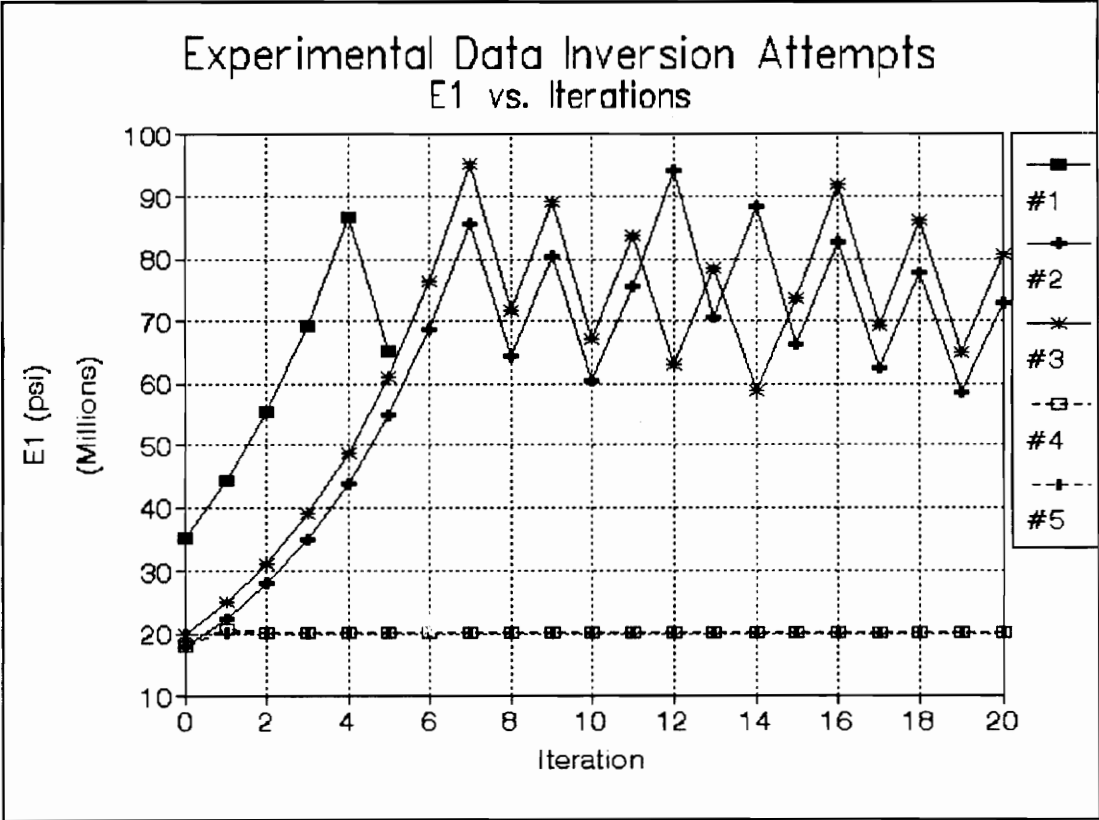
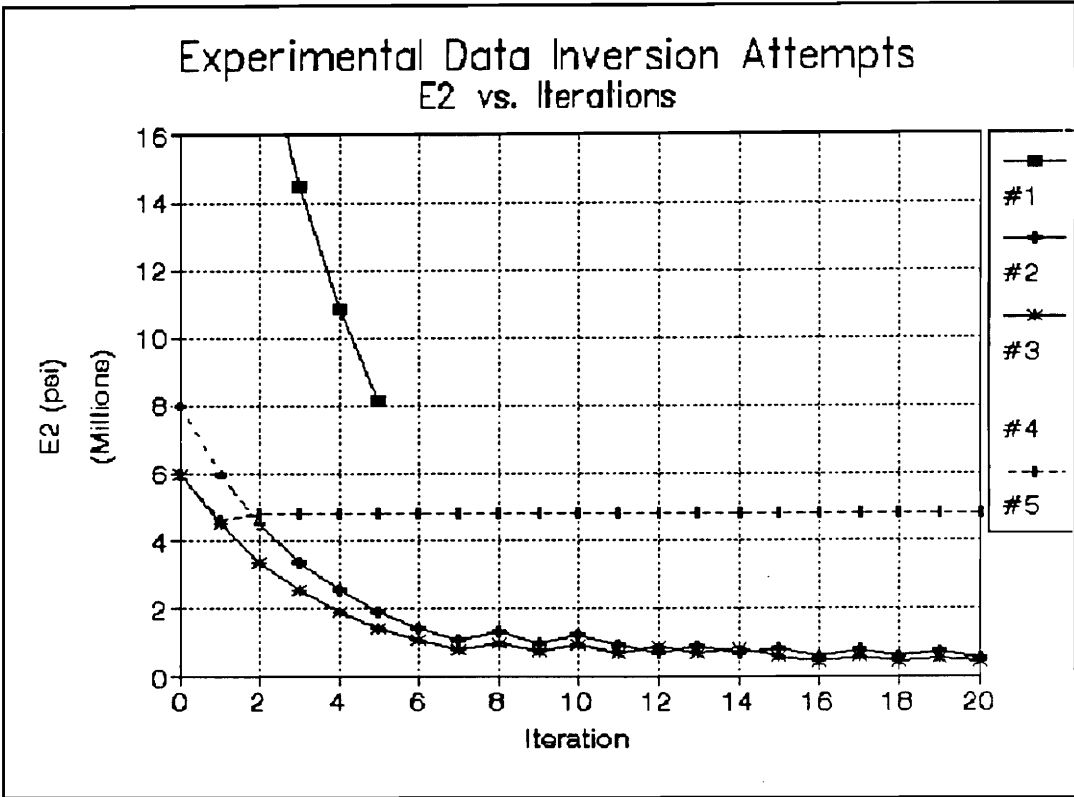
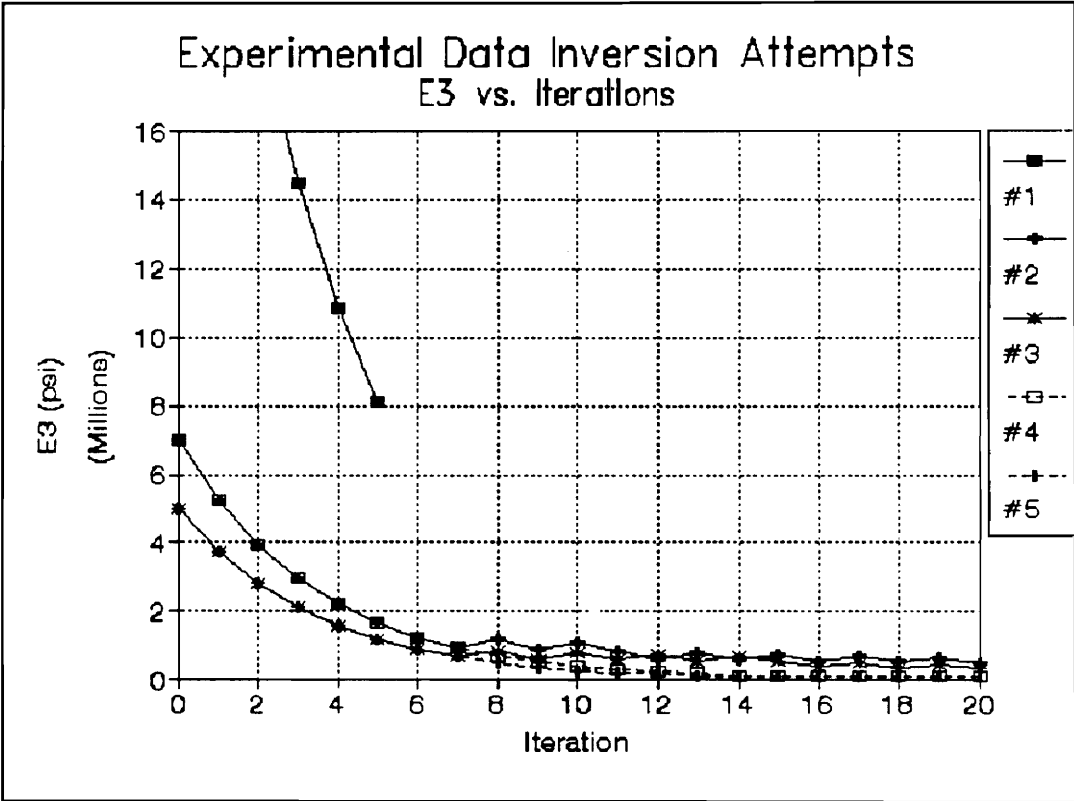


Figure 6.2 Initial Inversion Attempts, Fiber Direction Modulus (E<sub>1</sub>) vs. Iterations



**Figure 6.3** Initial Inversions Attempts, Transverse Direction Modulus ( $E_2$ ) vs. Iterations



**Figure 6.4** Initial Inversions Attempts, Out-of-Plane Modulus ( $E_3$ ) vs. Iterations

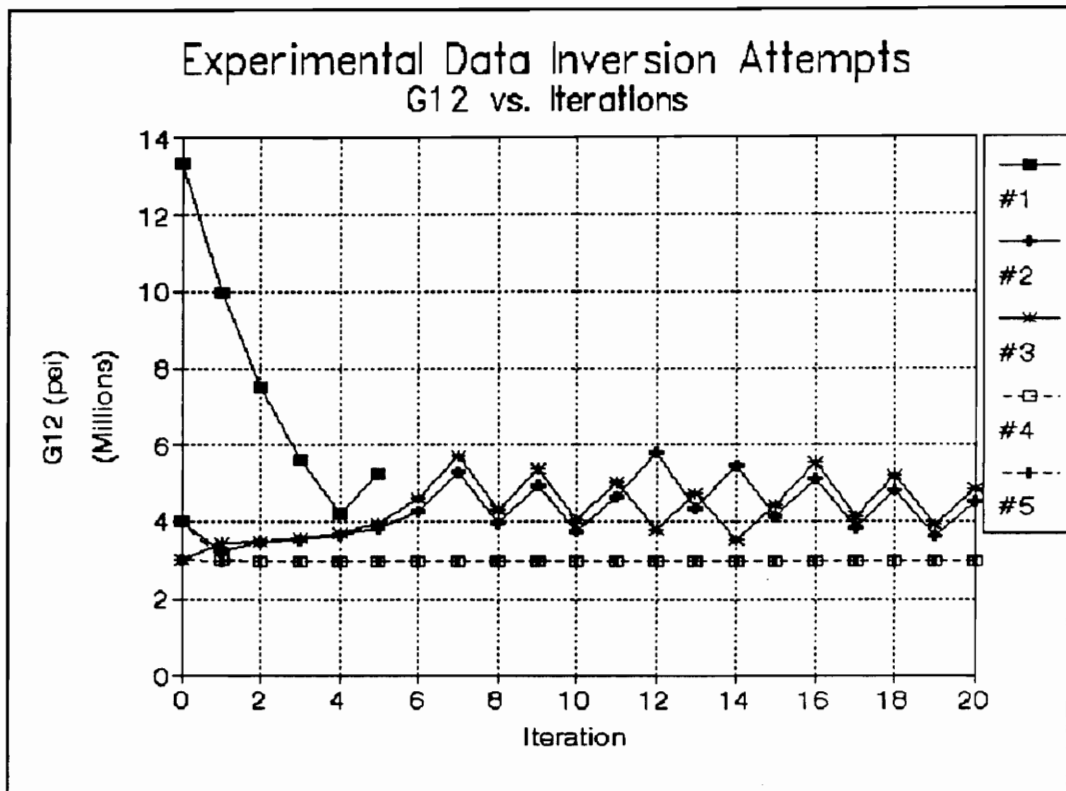


Figure 6.5 Initial Inversion Attempts, In-Plane Shear Modulus ( $G_{12}$ ) vs. Iterations

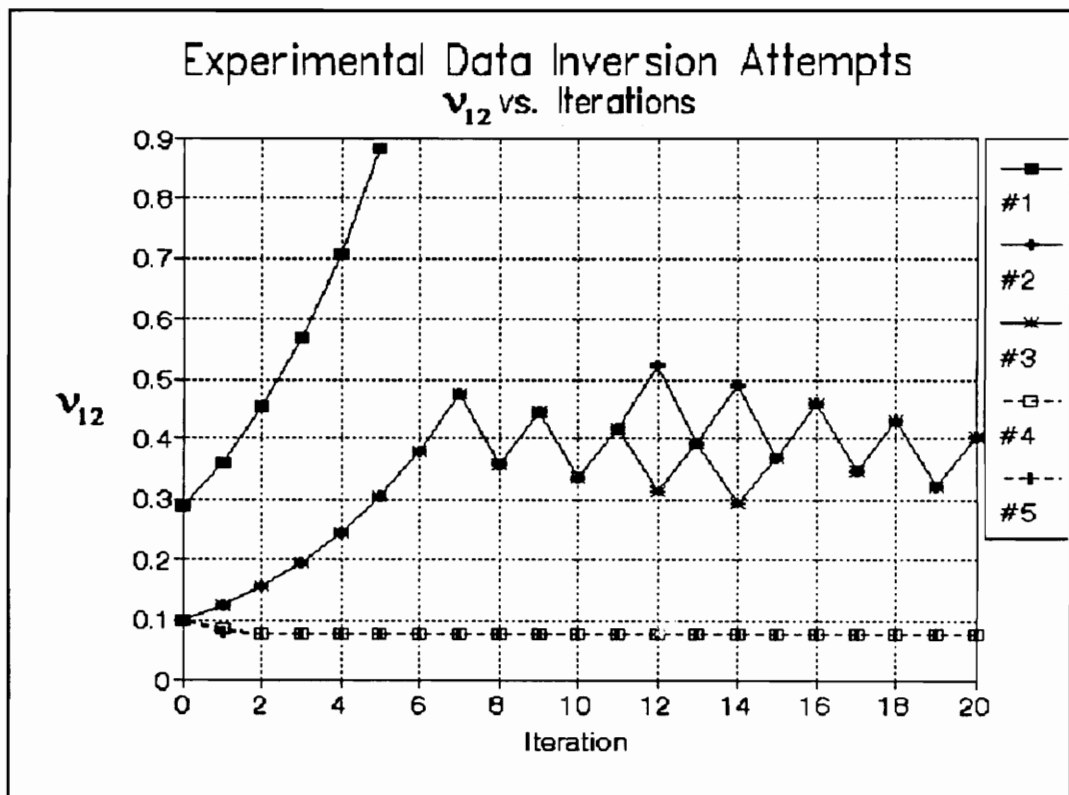


Figure 6.6 Initial Inversion Attempts, In-Plane Poisson's Ratio ( $\nu_{12}$ ) vs. Iterations

Recall that the out-of-plane Poisson Ratios were set equal to the in-plane ratio in order to achieve an over defined system.

The next plots show the calculated strains vs. iterations. The values are normalized by the experimental value used ( $\epsilon_i^*$ ). Therefore  $\gamma_{x\theta}(F_x)$  is normalized by  $1 \times 10^{-9}$  for trials #4 and #5 rather than the values given in Table 5.30 which were used for the rest of the lines.

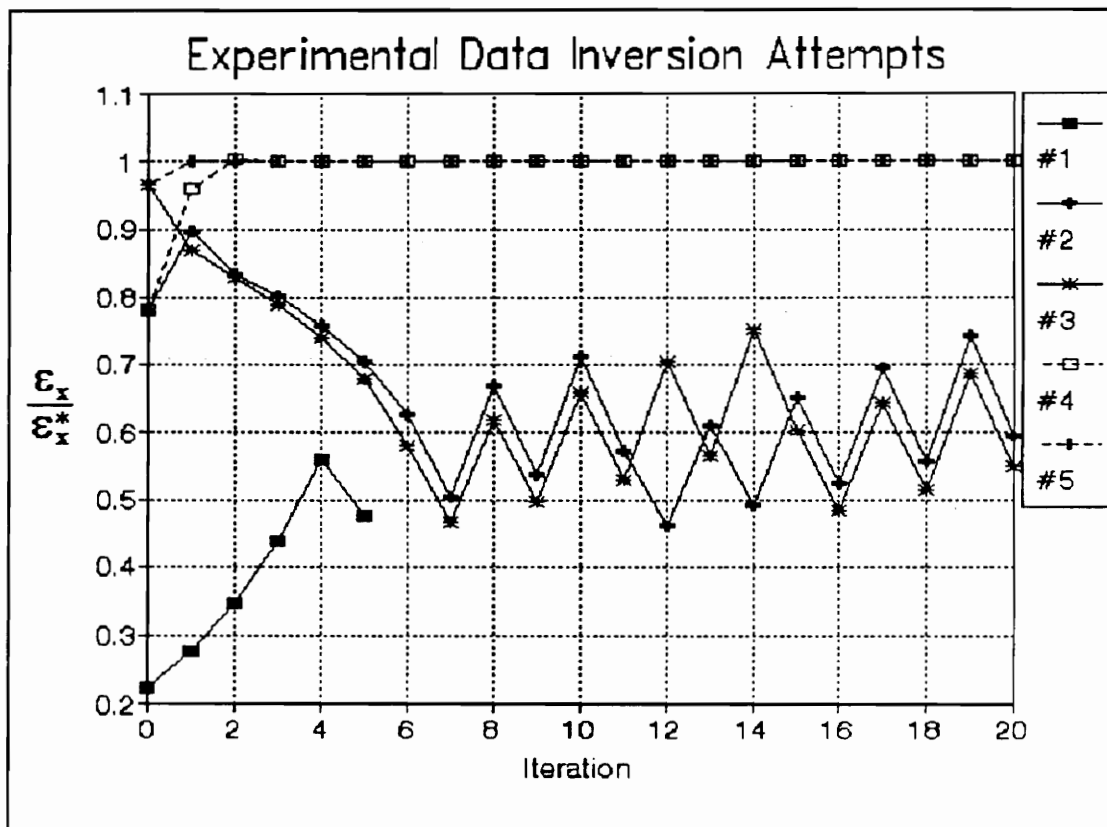


Figure 6.7 Initial Inversion Attempts,  $\epsilon_x(F_x)$  vs. Iterations

Note the rapid convergence for the trials with the adjusted shear modulus.

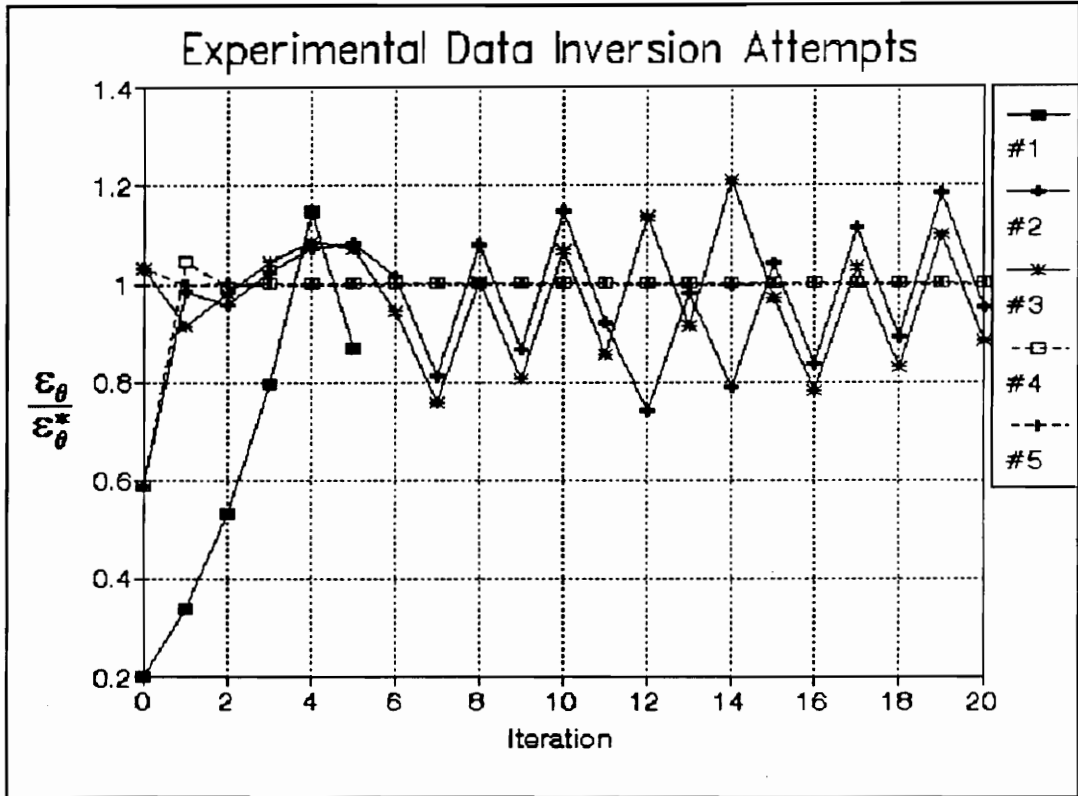


Figure 6.8 Initial Inversion Attempts,  $\epsilon_{\theta}(F_X)$  vs. Iterations

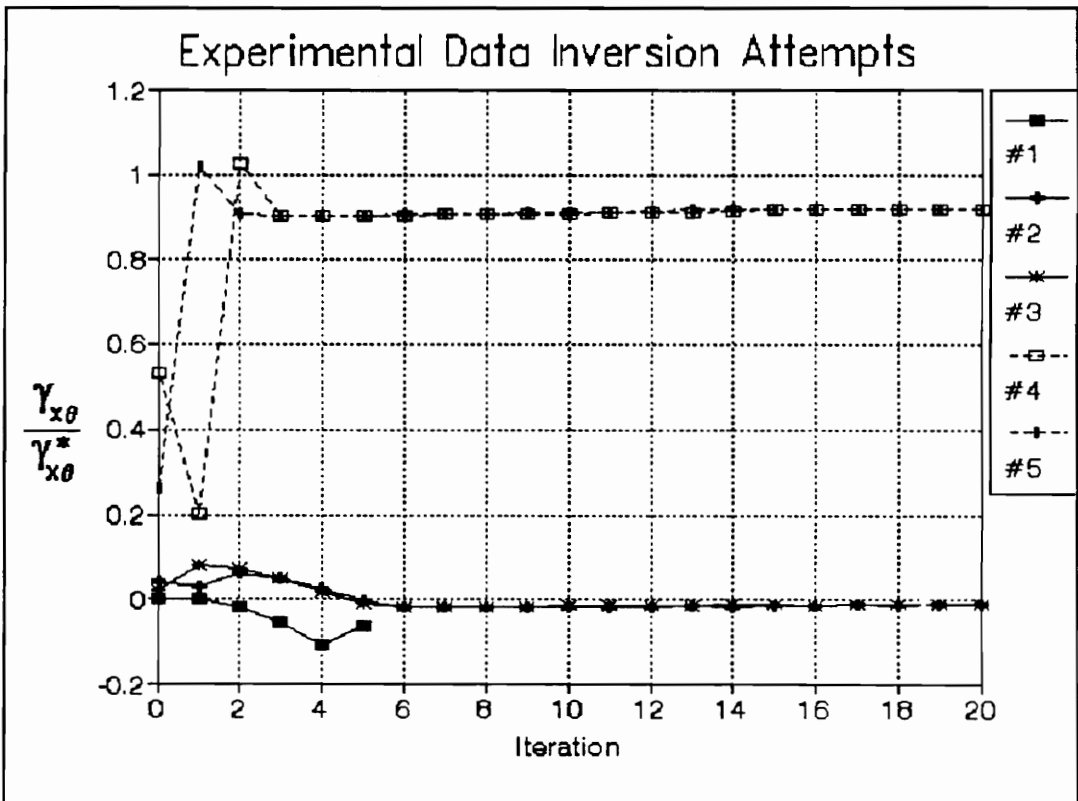


Figure 6.9 Initial Inversion Attempts,  $\gamma_{x\theta}(F_X)$  vs. Iterations

Note that, for fig. 6.9, the convergence to the adjusted shear value (trials #4, #5) is still not complete.

The plots for  $\epsilon_1(T_x)$  and  $\epsilon_2(T_x)$  use a different format in order to emphasize an important effect discussed in the next section.

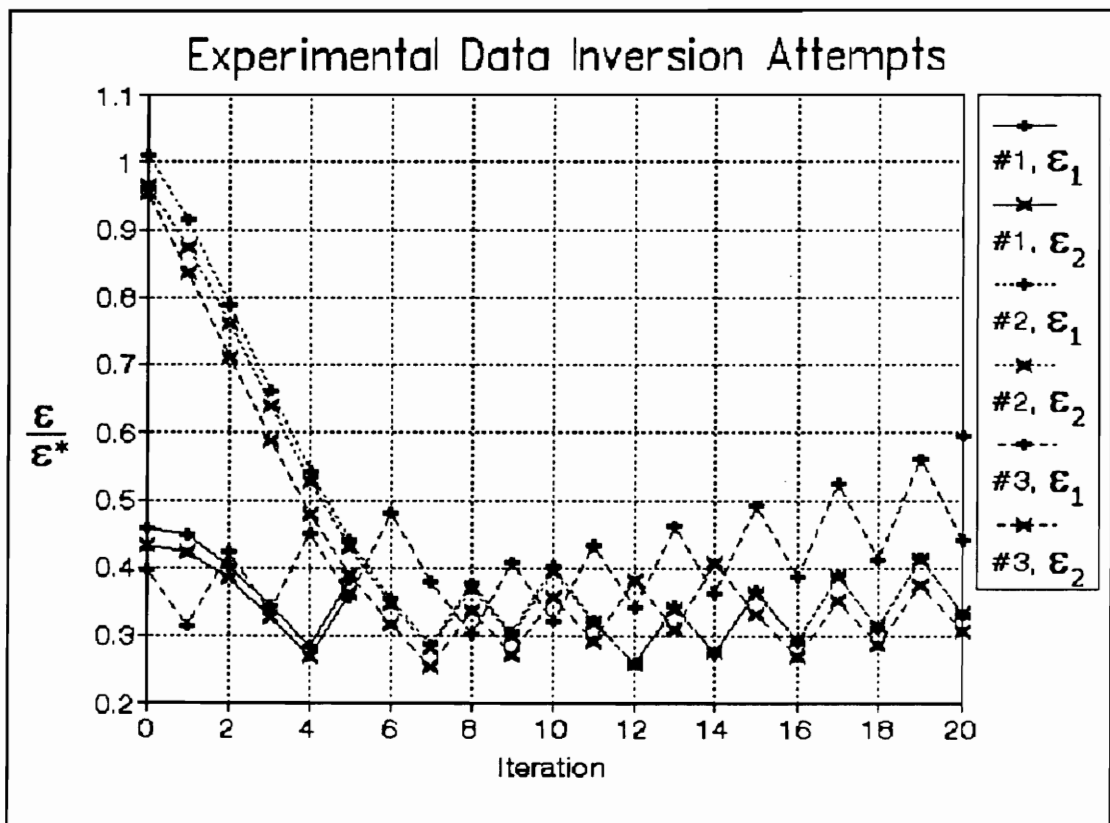


Figure 6.10 Initial Inversion Attempts,  $\epsilon_1(T_x)$ ,  $\epsilon_2(T_x)$  vs Iterations, Original Data

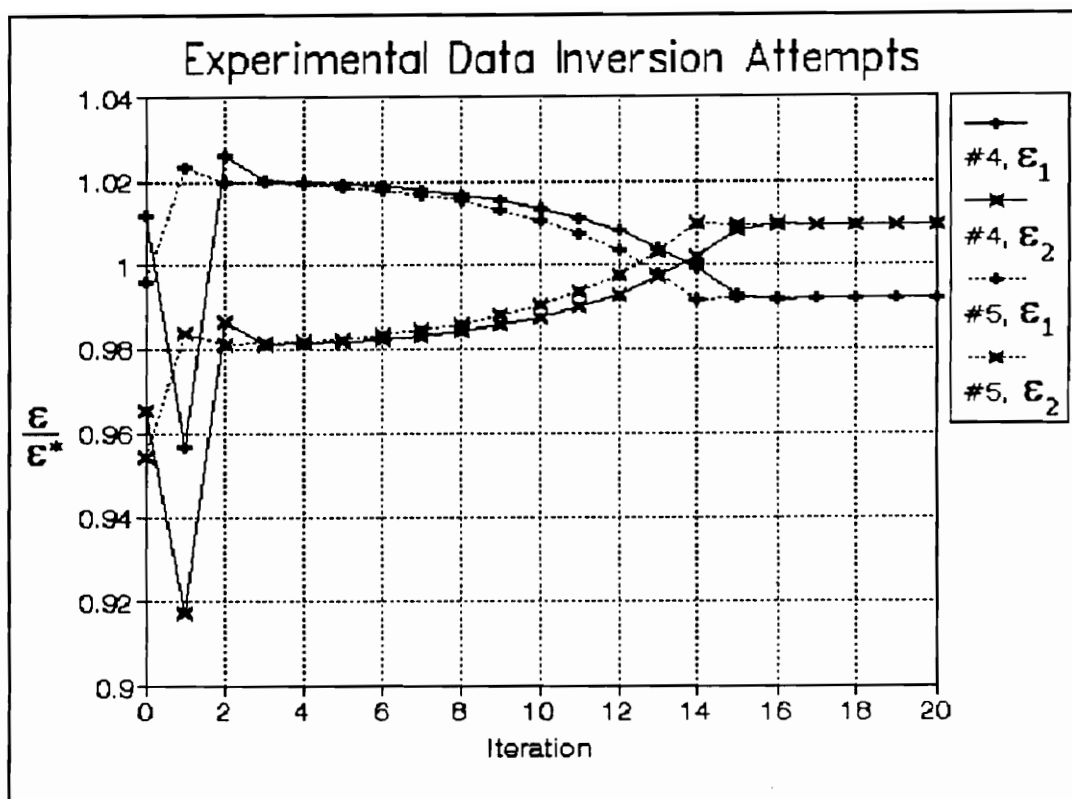


Figure 6.11 Initial Inversion Attempts,  $\epsilon_1(T_x)$ ,  $\epsilon_2(T_x)$  vs Iterations, Adjusted Data

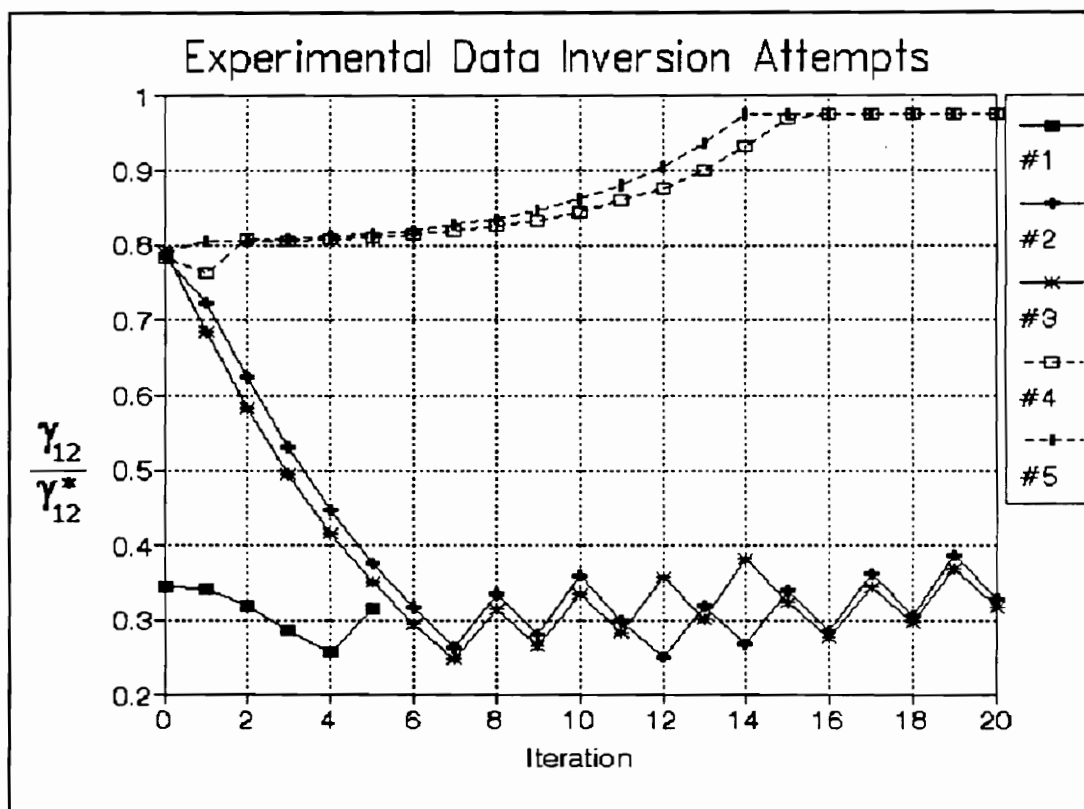


Figure 6.12 Initial Inversion Attempts,  $\gamma_{12}(T_x)$  vs Iterations

### 6.3.1 Initial Adjustment to $\epsilon_1(T_x)$ and $\epsilon_2(T_x)$

The trace plots show that, with the adjustment to  $\gamma_{x\theta}(F_x)$ , there are still significant errors in the converged values for  $\gamma_{x\theta}(F_x)$ ,  $\epsilon_1(T_x)$ ,  $\epsilon_2(T_x)$ , and  $\gamma_{12}(T_x)$ . In particular, consider fig. 6.11. This plot shows the convergence of the extensional strains under torsional loading. Note that the error in the convergence (vertical distance from 1.0) after a few iterations appears to be always equal and opposite for the two strains. This tends to indicate that the problem is not with converging to the measured value of  $\epsilon_1(T_x)$  or  $\epsilon_2(T_x)$  but rather converging to the measured value of  $\epsilon_1$  *relative to* the measured value of  $\epsilon_2$ .

Note that, for a thin wall cylinder with a balanced, symmetric laminate, the absolute values of  $\epsilon_1(T_x)$  and  $\epsilon_2(T_x)$  are identical. The difference seen is a thickness effect (ply-angle variation and anti-symmetry of laminate also contribute). Therefore, the problem is similar to that considered for  $\gamma_{x\theta}(F_x)$  earlier, which was also largely a thickness effect. The approach taken will also be similar. The values will be adjusted until a region of good convergence is found. However, in this case, the two values will be adjusted relative to a central value; the average of the absolute values of the strains:

$$AVG = \frac{|\epsilon_1(T_x)| + |\epsilon_2(T_x)|}{2} \quad (6.8)$$

$$DIFF = \left| \frac{|\epsilon_1(T_x)| - |\epsilon_2(T_x)|}{2} \right| \quad (6.9)$$

$$\epsilon_1(T_x) = AVG - DIFF \quad (6.10)$$

$$\epsilon_2(T_x) = -AVG - DIFF$$

The average value (**AVG**) is calculated from the experimental data and does not change. For the (-) patch  $\text{AVG} / T_x = 3.2113 \times 10^{-7}$  and the initial value of the difference is  $\text{DIFF} / T_x = 9.212 \times 10^{-9}$ . Note that attempts to adjust the values of **AVG** or  $\gamma_{12}(T_x)$  instead of **DIFF** did not significantly improve the convergence characteristics of  $\epsilon_1(T_x)$  and  $\epsilon_2(T_x)$ .

## 6.4 Inversion within "Convergence Zones"

There are now two parameters ( $\gamma_{x\theta}(F_x)$ , **DIFF**) which can be varied in order to obtain "good" (or any) convergence. These parameters will be taken as representing perpendicular axis, thus defining a plane with coordinates ( $\gamma_{x\theta}(F_x)$ , **DIFF**). Areas containing points for which the least squares inversion converges will be called "convergence zones". No attempt will be made to completely map these zones, instead a rough mapping will be performed and then another optimization method will be used to find the best values within the zones.

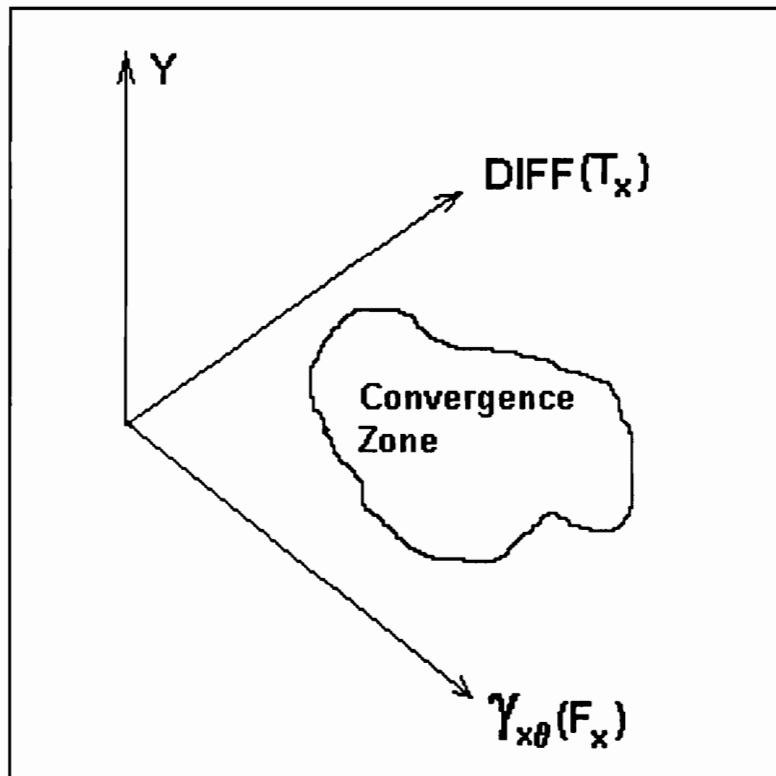
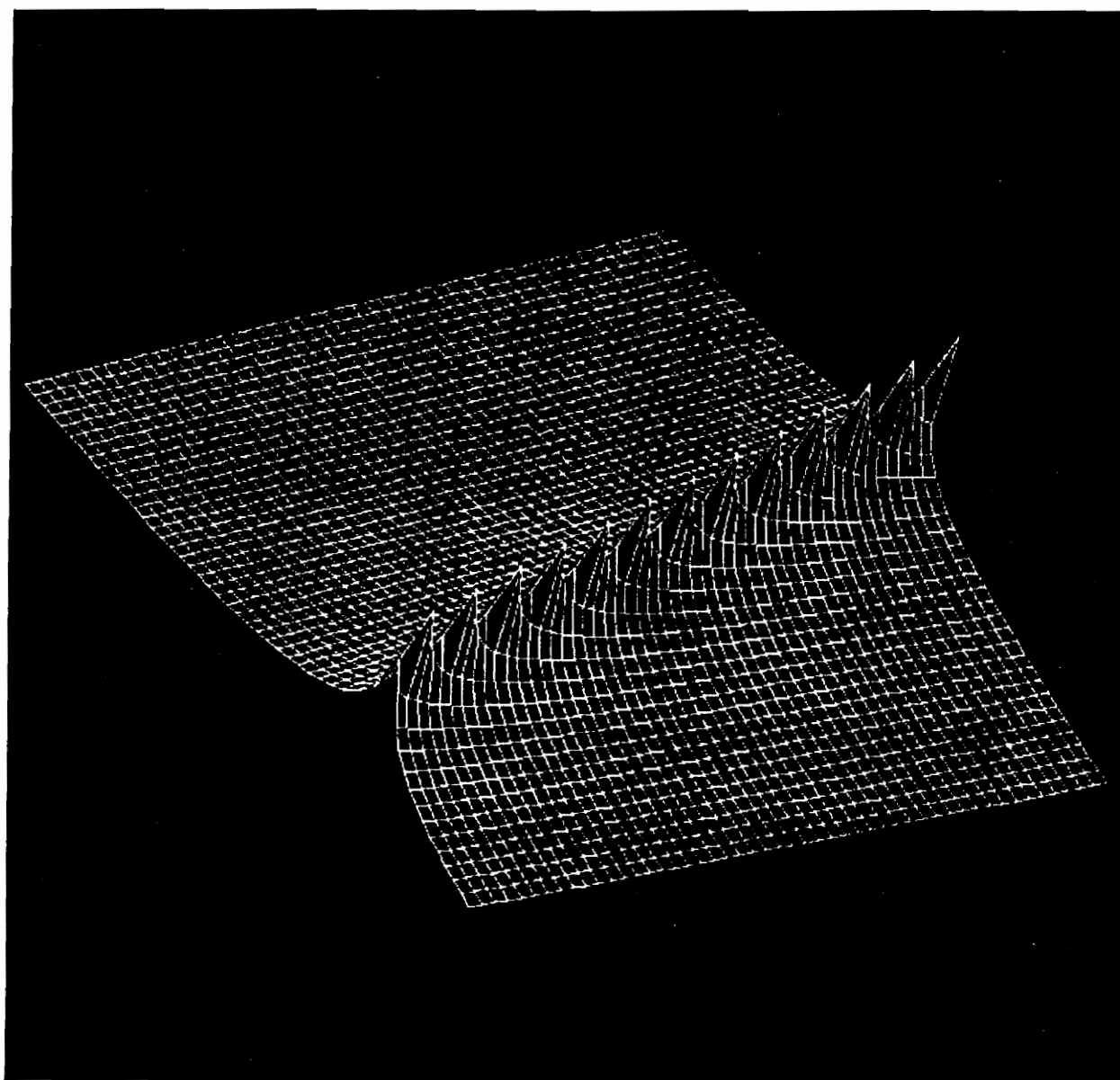


Figure 6.13 Convergence Zone Geometry

The first step in identifying the convergence zones is to find reasonable values for the parameters by observing their values as given by the elasticity program using realistic estimates of the properties. This approach leads to estimates on the order of  $10^{-11}$  for  $\gamma_{x\theta}(F_x)/F_x$  and  $10^{-8}$  for  $\text{DIFF}/T_x$ . At this point the least squares program is used to "map" the area by calculating the converged value of the error function (Y) in a region around the estimates. A wire-frame surface of part of a convergence zone is shown below. A faster C language version of the code was used due to the large number of inversions involved.



**Figure 6.14** Convergence Zone Mapping

Inversion of Experimental Data

In this figure GAMMAxy(Fx) is plotted along the x axis, DIFF along the y axis and Y is the surface height. Note the linear ridge of high convergence. The spikes along this ridge are an artifact of the resolution of the mapping. From this plot a rough estimate of a linear relation between  $\gamma_{x0}(F_x)$  and **DIFF** can be found. A "Pattern Search" optimization algorithm[4] (see listing and algorithm, Appendix D) was then used to identify points on the line to obtain a better relation. Note that the pattern search algorithm tends to find and accelerate along ridges. In applying it to this problem it was not observed to move along the ridge indicating that any peaks or slope seen in fig. 6.14 are artifacts of the grid size used to calculate the mapping and not properties of the ridge. The pattern search was used to find six points for the data set which were then used to find a linear relation for the convergence line:

$\gamma_{x0}(F_x)$	Diff	Error Function (Y)
9.60500e-12	1.22400e-08	1.9e-30
2.25650e-11	1.22580e-08	1.9e-30
3.98463e-11	1.22820e-08	4.5e-31
6.50460e-11	1.23170e-08	4.2e-32
8.16060e-11	1.23400e-08	3.4e-32
9.99660e-11	1.23655e-08	4.2e-32
Linear Regression		
DIFF = $\gamma_{x0}(F_x)$ m + b		±error
m	1.388873	7.88e-06
b	1.222666e-08	6.18e-16

**Table 6.5** Convergence Line Points and Properties

A graph of the data and equation shown above is presented on the following page.

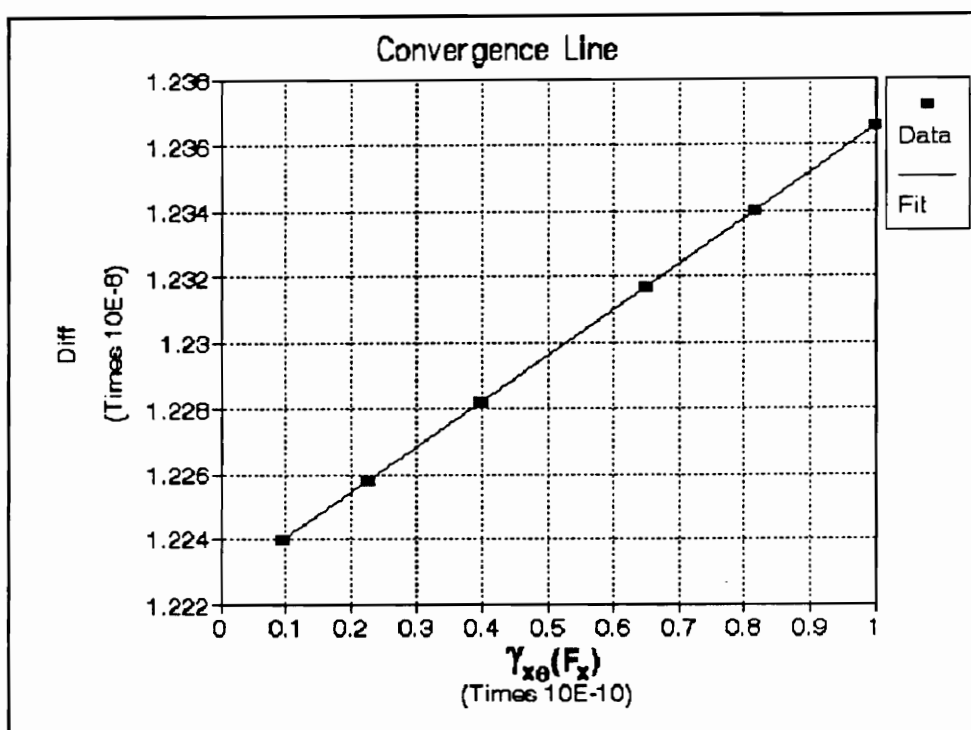


Figure 6.15 A Section of the "Convergence Line"

### 6.3.1 Properties Along "Convergence Line"

Because a line of "best convergence" was found rather than a point, the properties must be found all along the line. It will be useful in presenting these results to define a coordinate,  $X$ , along this line. The origin ( $X = 0$ ) will be taken as the DIFF axis intercept ( $\gamma_{x0}(F_x) = 0$ ) and the position along the line will be given by the value of  $\gamma_{x0}(F_x)$  at that point:

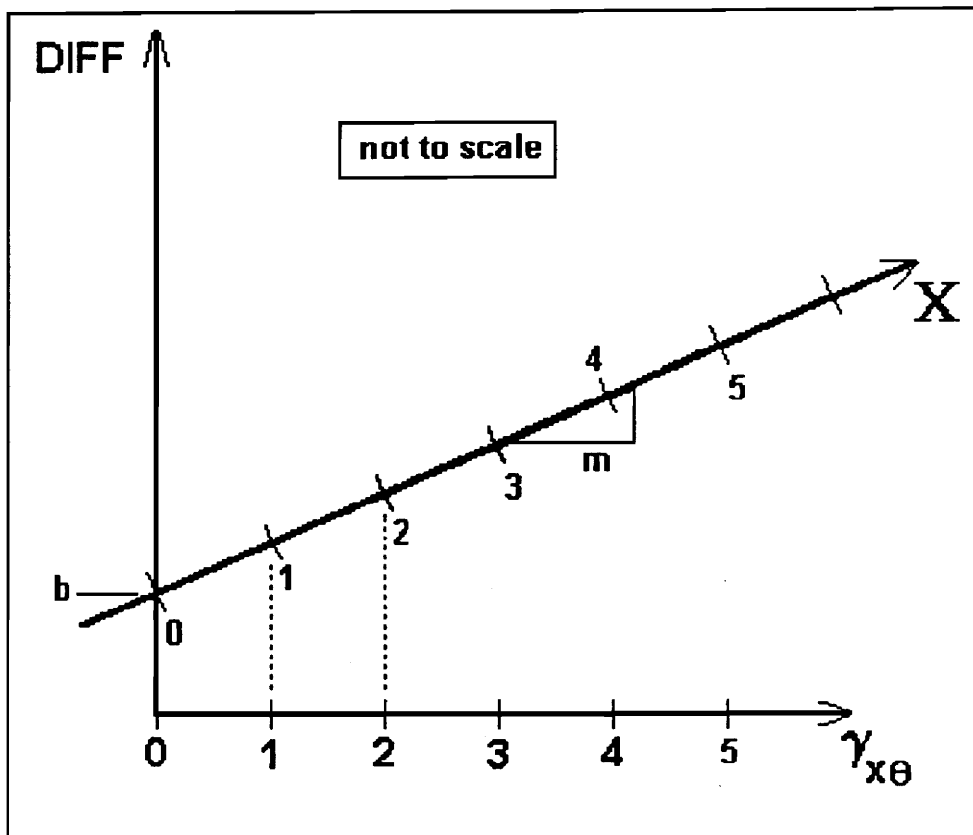
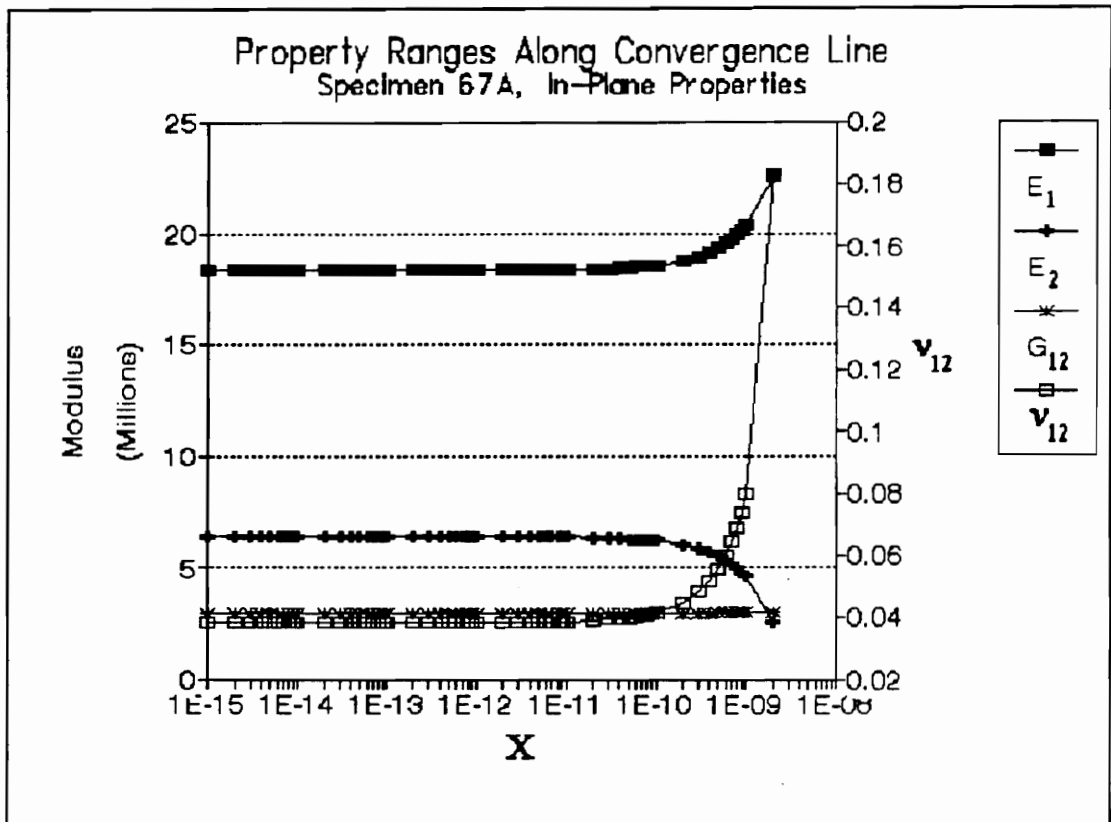


Figure 6.16 Convergence Line Coordinate Geometry

The error function and elastic properties will now be presented as a function of position along the convergence line (X).



**Figure 6.17** Final In-Plane Property Ranges, Specimen 67A

Note that, for values of  $X$  ( $\gamma_{x0}(F_x)$ ) below  $1 \times 10^{-10}$  there is virtually no change in the property values. It is very likely that  $\gamma_{x0}(F_x)$  lies in this range, the initial rough estimate for  $\gamma_{x0}(F_x)$  was  $\approx 1 \times 10^{-11}$ . The consistency of the data over five orders of magnitude variation in the shear strain suggests a limiting value that may be the correct value. However the surest way to find the correct values would be to measure one of the properties by some other method (ultrasonics, etc.) and correlate that value to a horizontal position on the above graph. The remaining properties could then be obtained from the graph. The following page displays  $E_3$  and the error function along the convergence line.

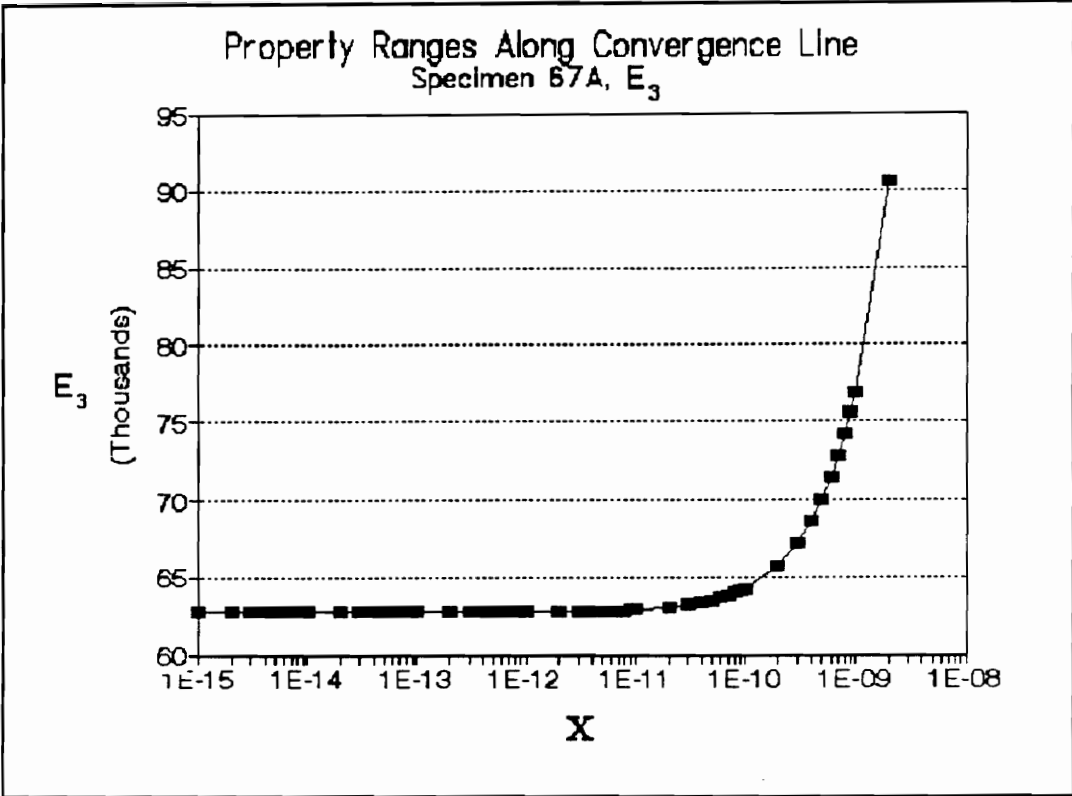


Figure 6.18 Final Out-of-Plane Modulus ( $E_3$ ) Range, Specimen 67A

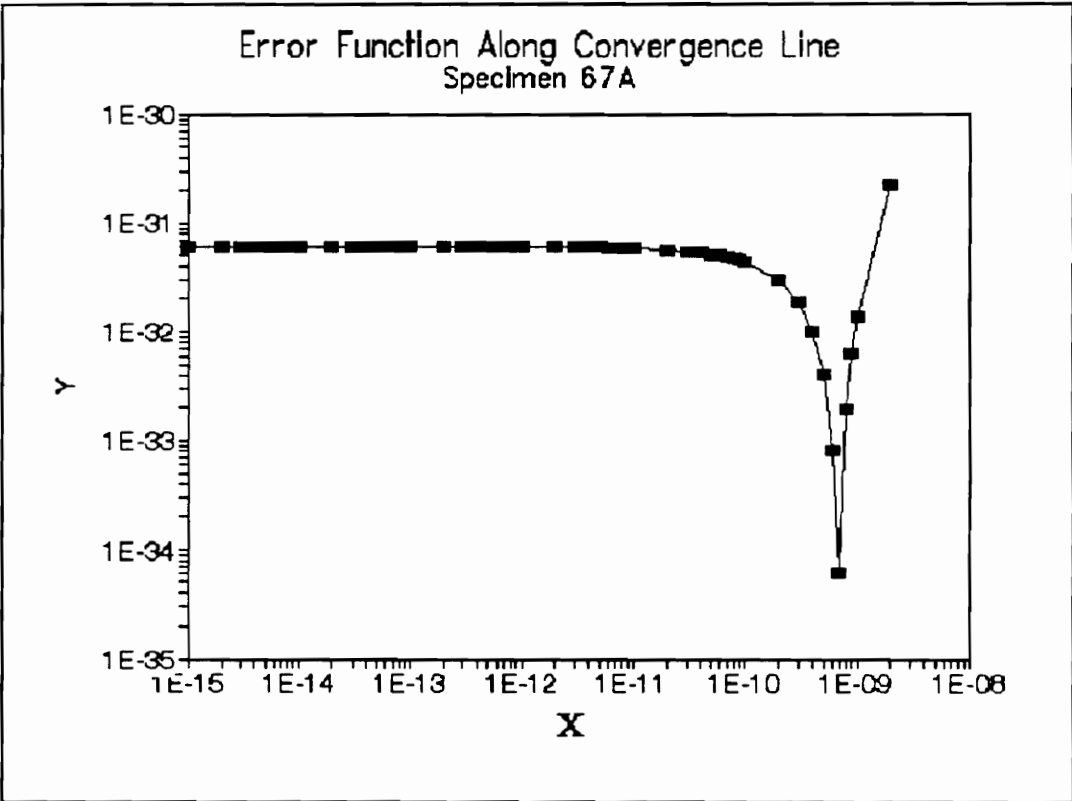


Figure 6.19 Error Function Along Convergence Line

Note the extremely low values of  $E_3$  found. This may be a relatively true estimate considering the large voids in the material which tend to be concentrated along the ply interfaces. A cursory examination of a model of a cylinder with very compliant inter-ply regions lends some credence to this idea. The effect of the out-of-plane Poisson's ratios was also investigated parametrically but were found to have an insignificant influence on  $E_3$ . Recall also, from ch. 3, that inaccuracy in the experimental data most strongly effects the out-of-plane properties. This, in conjunction with the large voids is the most likely explanation for this phenomena. Internal pressure loading of the cylinder may aid in the accurate calculation of this value.

When considering the error function plot the large spike on the right should be considered an artifact of; the accuracy to which the equation of the convergence line is obtained, the interval between data points. I believe that this spike represents the point at which the equation of the convergence line (Table 6.5) crosses the actual convergence line. The pattern search algorithm can generally obtain convergence to  $Y \leq 10^{-35}$  for any point along the convergence line.

A partial tabulation of the data from figures 6.17 - 6.19 is included below. Further discussions and recommendations follow in ch. 7.

<b><u>Final Property Ranges</u></b>						
$\gamma_{x\theta}(F_x)$	Y	E <sub>1</sub>	E <sub>2</sub>	E <sub>3</sub>	G <sub>12</sub>	U <sub>12</sub>
1e-15	6.0e-32	18356767	6362590	62754.7	2931634	0.0382
5e-15	6.0e-32	18356775	6362583	62754.8	2931634	0.0382
1e-14	6.0e-32	18356785	6362575	62754.8	2931634	0.0382
5e-14	6.0e-32	18356864	6362507	62755.4	2931635	0.0382
1e-13	6.0e-32	18356963	6362422	62756.2	2931637	0.0382
5e-13	6.0e-32	18357754	6361742	62762.2	2931651	0.0382
1e-12	6.0e-32	18358744	6360892	62769.7	2931668	0.0382
5e-12	5.9e-32	18366659	6354092	62829.7	2931808	0.0384
1e-11	5.8e-32	18376555	6345591	62904.8	2931982	0.0385
5e-11	5.2e-32	18455757	6277526	63503.1	2933381	0.0397
1e-10	4.4e-32	18554861	6192295	64246.6	2935138	0.0413
5e-10	4.2e-33	19352644	5503390	70027.6	2949573	0.0557
1e-09	1.4e-32	20368792	4616831	76904.8	2968884	0.0795
2e-09	2.3e-31	22606007	2587459	90578.9	3019318	0.1833
3e-09	6.0e-15	27337949	238957	87513.2	3342418	0.4742

## ***7.0 Summary, Conclusions and Recommendations***

### ***7.1 Summary and Conclusions***

The objectives of this research were:

1. Development of a method by which the ply level, elastic properties of a thick, axisymmetric, laminated angle-ply cylinder can be determined from the strain response of the tube subject to axisymmetric thermal and mechanical loading.
2. To use the analysis to calculate the ply level mechanical properties of experimental specimens from measured surface strains.

Objective 1 was met by the development of a numerical inversion of an elasticity based strain response model. The strain response model and the Least-Squares optimization routine used for the inversion were derived ch. 2. This inversion method was verified using analytical data for several geometries in ch. 3. The inversion convergence was found to be very rapid and robust for thick angle-ply cylinders with very high accuracy data. However the out-of-plane properties suffered greatly with reductions in the input data accuracy although the in-plane properties were not affected tremendously for the error magnitudes simulated. It

was also shown that the inversion is very intolerant of data inaccuracy for thin wall cylinders. Problems encountered with analytical data inversions for cross-ply ([0/90]) laminates and CLT based methods were also mentioned.

Ch. 4 detailed the geometry of the CFCC characterization specimen used for objective 2. In addition to the general geometry many important but obscure characteristics of the specimen were detailed such as the ply-angle variation through the thickness, the filament winding "patch" geometry, and the large voids present in the material. The specimen preparation and strain gauge geometry was also covered.

The reduction of the experimental data to a form convenient for use in the inversion attempts was detailed in ch. 5. While the errors involved in the linear regressions of the experimental data were determined and carried through the reduction no effort was made to quantify the error produced by the many other factors involved (surface roughness, gauge alignment and position, voids, thickness variation, etc.). A small side effort regarding the effect of strain gauge position on the recorded strains was briefly considered in Appendix D.

The inversion of the experimental data was covered in ch. 6. It was found that the Least-Squares method would not converge for the experimental data. The problem is considered to be an inconsistency among the measured strain values for which a feasible region of properties cannot be found.

The probable cause was traced to the value of  $\gamma_{x\theta}(F_x)$  and difference between the absolute values of  $\epsilon_1(T_x)$  and  $\epsilon_2(T_x)$  (defined DIFF). Both of these measurements are very small and are primarily due to thickness effects. In an effort to extract some useful property information from the remaining data, these two measurements were varied in order to find a more consistent data set. The measure of the consistency is the error function, Y. A pattern search optimization program (Appendix D) was constructed to find the best values of the parameters within some feasible region. It was found that there is a linear relation between  $\gamma_{x\theta}(F_x)$  and DIFF for which very good convergence is possible.

The Least-Squares method was then run for points along this line. The result are the ranges of properties displayed in figures 6.17 - 6.19. It was noted that the properties seem to have a limiting value for values of  $\gamma_{x\theta}(F_x) < 10^{-10}$  and suggested that limiting values may be the correct property values although the rest of the curve should be considered as well.

The property range for  $E_3$  was observed to be extremely low, two orders of magnitude lower than  $E_2$ . The exact cause of this phenomena is unknown. It is known that the out-of-plane properties are effected by experimental error much more then the in-plane properties, especially if out-of-plane loading (internal pressure) is not available. Also, the effective out-of-plane modulus may actually be much lower then the in-plane transverse modulus due to the large voids concentrated in the inter-ply region.

## ***7.2 Recommendations***

Many problems were encountered with the application of the method to experimental data. The following are recommendations for more effective use of the method as well as areas for further research.

### ***7.2.1 Specimen Geometry and Characteristics***

If possible, filament wound cylinders should not be used for material characterization unless a model is developed which can account for the non-axisymmetric nature of these specimens. If they are to be used, a more fundamental analytical or experimental understanding of the strain variation with position on a patch should be developed. A longer gauge section is also desirable to reduce end and gripping effects.

The effect of surface roughness on the accuracy of strain gauge data should be investigated with the aim of determining the size of gauges to be necessary for accurate measurements on various surfaces. Due to the strain variation over a patch very small gauges are desirable in order to improve the assumption of a point

strain state. This conflicts with the need for large gauges to reduce the effect of the rough surface. This information is of course unnecessary if the surface can be manufactured smoother or filament wound cylinders are not used.

The effect of the lamination sequence and angles on the inversion method should be investigated with regard to the sensitivity of the determined properties to experimental error. There is some evidence to suggest that a balanced  $\pm 45^\circ$  laminate may be a relatively degenerate case. An unbalanced laminate may be a better choice.

The possibility of non-tubular specimens might be examined. A thick, unsymmetric, angle-ply beam subject to bending and extension may be a good specimen. The problem of edge effects is again present but the specimen will most likely be easier to manufacture and test and may be closer to the desired component geometry than a cylinder. The inversion method developed is, in general, applicable for any over-determined system. Finite element models could easily be used in place of the elasticity solution employed although the computer power required would probably be prohibitive at this time.

### **7.2.2 *Experimental Data***

The addition of pressure loading data is essential to obtaining out-of-plane properties and would improve the accuracy of the in-plane properties as well. Free thermal expansion data should also improve the accuracy of the elastic properties in addition to providing the thermal expansion coefficients.

A thermal gradient loading would also provide additional data points and might make determination of the out-of-plane shear moduli possible. The current elasticity solution model does not include this capability.

### **7.2.3 *Inversion Method***

A better understanding of the effect of experimental error on the inversion procedure should be developed. Of interest is the failure of the model to converge for certain combinations of data. A better definition of what constitutes "inconsistent" data is needed.

Extensions of this method to strength characterization have been mentioned and should be feasible. This specimen is especially suited to strength studies due to the multi-axial stress states possible.

## References

1. K. L. Reifsneider, Personal communication, 14 JUL 1992
2. J.M. Whitney, J.C. Halpin, "Analysis of Laminated Anisotropic Tubes under Combined Loading," *J. Composite Materials*, Vol. 2 (1968), p. 360
3. N.J. Pagano, J.M. Whitney, "Geometric Design of Composite Characterization Specimens," *J. Composite Materials*, Vol. 4 (1970), p. 360
4. G.E. Foley, M.E. Roylance, W.W. Houghton, "Use of torsion tubes to measure In-Plane Shear Properties of Filament Wound Composites," *Test Methods for Design Allowables for Fibrous Composites: 2nd Volume*, ASTM STP 1003, C.C. Chamis, Ed., American Society for Testing and Materials, Philadelphia, 1989, p. 208
5. E. K. Bartkus, W. D. Humphrey, "Determination of Fiber-Reinforced Composite Material Properties Using Internal Pressurization of Filament Wound Cylinders", International SAMPE Symposium and Exhibition, volume 36 part 1, SAMPE, Covina, Ca., 1991, pg. 827-839
6. S. R. Swanson, A. P. Christoforou and G. E. Colvin Jr., "Biaxial Testing of Fiber Composites Using Tubular Specimens", *J. of Experimental Mechanics*, Sept 1988, pg. 238-243
7. S. R. Swanson, B. C. Trask, "Strength of Quasi-Isotropic Laminates under Off-Axis Loading", *Composites Science and Technology*, 1989, pg. 19-34
8. S. R. Swanson, Y. Qian, "Multiaxial Characterization of T800/3900-2 Carbon Epoxy Composites", *Composites Science and Technology*, 1992, pg. 197-203
9. C.Q. Rousseau, "Stresses and Deformations in Angle-Ply Composite Tubes", M.S. Thesis, Department of Engineering Mechanics, Virginia Polytechnic Institute and State University, Feb 1987.
10. J.M. Whitney, Structural Analysis of Laminated Anisotropic Plates, Technomic Publishing Company, Inc., 1987, pg. 6-13

11. N.J. Pagano, "Stress Gradients in Laminated Composite Cylinders", *J. Composite Materials*, Vol. 5 (1971), pg. 260
12. C.S. Beightler, D.T. Phillips, D.J. Wilde, Foundations Of Optimization, 2<sup>nd</sup> Ed., Prentice Hall Inc., 1979, pg 228-233.
13. K. Liao, J.J. Lesko, W.W. Stinchcomb, K.L. Reifsneider, T.J. Donyak, "An Axial/Torsional Test Method For Ceramic Matrix Composite Tubular Specimens", Ceramic Engineering & Science Proceedings, 17<sup>th</sup> Annual Conference on Composites and Advanced Ceramic Materials, Part 1, The American Ceramics Society, 1993
14. Quattro Pro User's Guide, Borland International, 1992, pg. 546-547
15. R.M. Spriggs, "Expression for Effect of Porosity on Elastic Modulus of Polycrystalline Refractory Materials, Particularly Aluminum Oxide", *Journal of the American Ceramics Society*, December, 1961, pg. 628-629
16. R.M. Spriggs, L.A. Brissette, "Expressions for Shear Modulus and Poisson's Ratio of Porous Refractory Oxides", *Journal of the American Ceramics Society*, April, 1962, pg. 198-199
17. R.M. Jones, "Mechanics of Composite Materials", Hemisphere Publishing Corporation, 1975, pg. 90-96
18. C.S. Beightler, D.T. Phillips, D.J. Wilde, Foundations of Optimization, 2<sup>nd</sup> Ed., Prentice Hall Inc., 1979, pg 236-242

# ***Appendix A.***

## **Strain-Property Influence Plots**

In order for the inversion method to work each property desired must show a significant influence on some measurable strain under some available load.

This Appendix presents graphs showing the nonlinear influence of the pertinent elastic parameters ( $E_1, E_2, E_3, G_{12}, \nu_{12}, \nu_{13}, \nu_{23}, \alpha_1, \alpha_2, \alpha_3$ ) (denoted  $x$ ) on the calculated surface strains ( $\epsilon_1, \epsilon_2, \gamma_{12}$  or  $\epsilon_x, \epsilon_\theta, \gamma_{x\theta}$ ) for axial, torsional, pressure, and thermal loads as calculated with the elasticity solution. Close examination of these plots can show which elastic properties can be found with a given combination of loadings. If a certain elastic property shows no influence under a combination of loadings then that combination cannot be used to obtain the property in question.

The plots shown here are not general, they will change with changes in geometry or properties. For example, the influence of the out-of-plane properties will generally decrease with increasing  $R/h$  as the tube approaches a thin wall geometry. The geometry and properties shown in Table 1 below are roughly representative of the experimental specimens examined.

**Table A.1** Sample Properties and Geometry

$E_1 = 20 \times 10^6$	$\nu_{12} = .1$
$E_2 = 5 \times 10^6$	$\nu_{13} = .1$
$E_3 = 5 \times 10^6$	$\nu_{23} = .1$
$G_{12} = 3 \times 10^6$	
$\alpha_1 = 9 \times 10^{-6}$	
$\alpha_2 = 8 \times 10^{-6}$	
$\alpha_3 = 8 \times 10^{-6}$	
$R/h = 10.304$	
$[-45/45]_3$	

The abscissa of the plots corresponds to the elastic properties given in the legend to the right of the plot. The properties are nondimensionalized by dividing by the corresponding initial property ( $x_0$ ) given in Table 1. The ordinate is also a percentage scale where  $K = \varepsilon_i / \varepsilon_i^0$  where  $i$  denotes the strain component and  $\varepsilon_i^0$  is the strain component found using the initial properties ( $x_0$ ). All strains are at the outer surface ( $r = R_0$ ).  $\varepsilon_i^0$  for this example are given in Table 2.

In constructing the plots and in the application of the final program, the material coordinate strains are generally used for torsion, thermal and pressure loads while the tube coordinate strains are generally used for the axial loading case. This is done to minimize the number of very small strains and to have as much uniformity in magnitudes as possible.

**Table A.2** Calculated Surface Strains

<u>Axial Load (Fx)</u>	
Cylinder Coordinates	Material Coordinates
$\epsilon_x^o / Fx = 1.8067 \times 10^{-7}$	$\epsilon_1^o / Fx = 5.7494 \times 10^{-8}$
$\epsilon_y^o / Fx = -6.4188 \times 10^{-8}$	$\epsilon_2^o / Fx = 5.8988 \times 10^{-8}$
$\gamma_{xy}^o / Fx = -1.4933 \times 10^{-9}$	$\gamma_{12}^o / Fx = -2.4486 \times 10^{-7}$
<u>Torsion Load (Tx)</u>	
Cylinder Coordinates	Material Coordinates
$\epsilon_x^o / Tx = -1.3551 \times 10^{-9}$	$\epsilon_1^o / Tx = 1.2205 \times 10^{-7}$
$\epsilon_y^o / Tx = -2.2581 \times 10^{-10}$	$\epsilon_2^o / Tx = -1.2363 \times 10^{-7}$
$\gamma_{xy}^o / Tx = -2.4568 \times 10^{-7}$	$\gamma_{12}^o / Tx = 1.1293 \times 10^{-9}$
<u>Internal Pressure Load (q)</u>	
Cylinder Coordinates	Material Coordinates
$\epsilon_x^o / q = -4.3662 \times 10^{-7}$	$\epsilon_1^o / q = 3.4827 \times 10^{-7}$
$\epsilon_y^o / q = 1.1340 \times 10^{-6}$	$\epsilon_2^o / q = 3.4911 \times 10^{-7}$
$\gamma_{xy}^o / q = -8.4057 \times 10^{-10}$	$\gamma_{12}^o / q = 1.5706 \times 10^{-6}$
<u>Thermal Load (dT)</u>	
Cylinder Coordinates	Material Coordinates
$\epsilon_x^o / dT = 8.7886 \times 10^{-6}$	$\epsilon_1^o / dT = 8.7763 \times 10^{-6}$
$\epsilon_y^o / dT = 8.7486 \times 10^{-6}$	$\epsilon_2^o / dT = 8.7610 \times 10^{-6}$
$\gamma_{xy}^o / dT = 1.5289 \times 10^{-8}$	$\gamma_{12}^o / dT = -3.9980 \times 10^{-8}$

All of the properties involved can be obtained using the inversion scheme developed. Examination of the influence plots reveals that, although all of the properties cause some variation for one or more loadings, the experimental accuracy required may be prohibitive. This is especially true for the out-of-plane Poisson ratios.

When considering these plots make careful note of the magnitude of the ordinate. For some cases the scale is large (0→3, Figure 3) and may obscure the smaller but important effect of other properties. In other cases there appears to be a significant influence but the scale is very small (.9994→1.0006, Figure 18) and the data portrayed is actually insignificant.

Figures 1 and 2 are now considered in detail to demonstrate the type of the information contained in these plots. Figure 1 shows the influence of the Young's moduli and shear modulus on the value of axial strain on the outer surface under axial load ( $\epsilon_x(R_o, F_x)$ ). For this case, the in-plane properties show significant slopes indicating that these properties have a large influence on the axial strain under axial load, or conversely, that measured values of  $\epsilon_x(R_o, F_x)$  can be used to obtain these in-plane moduli. Note that these curves are also non-linear and therefore a non-linear optimization method must be used. For the out-of-plane modulus however, the curve is essentially flat (at this scale). This means that any value of  $E_3$ , within the abscissa's range, will produce essentially the same value of  $\epsilon_x(R_o, F_x)$ .  $E_3$  has virtually no influence on this response, and therefore, measured values of  $\epsilon_x(R_o, F_x)$  cannot be used to obtain this property. Figure 3 shows the influence of the Poisson ratios on  $\epsilon_x(R_o, F_x)$ . Only the in-plane ratio ( $\nu_{12}$ ) shows any influence at this scale. Note that the scale is small enough that this influence has very little value.

A more quantitative understanding of the property influences can be obtained by considering the partial derivatives of the strains with respect to the elastic properties. This is the Jacobean matrix of Chapter 2. A visual representation of the Jacobean for the initial properties is given at the end of the appendix. Note that these derivatives are only valid at the defined point and does not reflect the nonlinear nature of the influence.

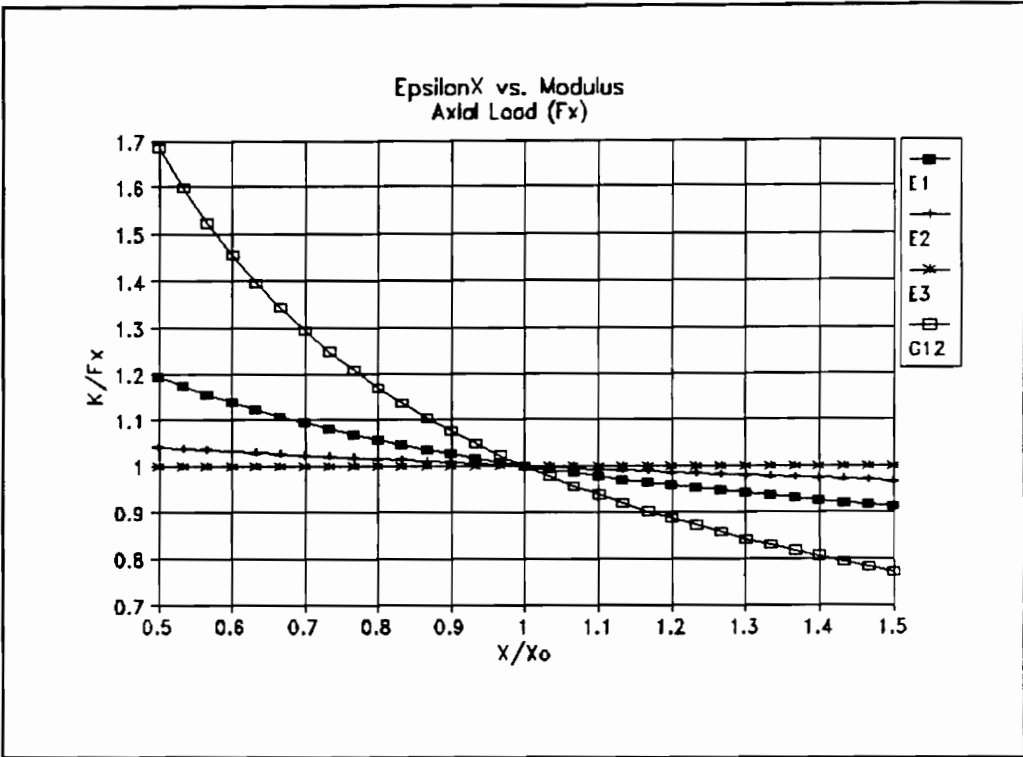


Figure A.1  $\epsilon_x$  vs. Moduli (Axial Load)

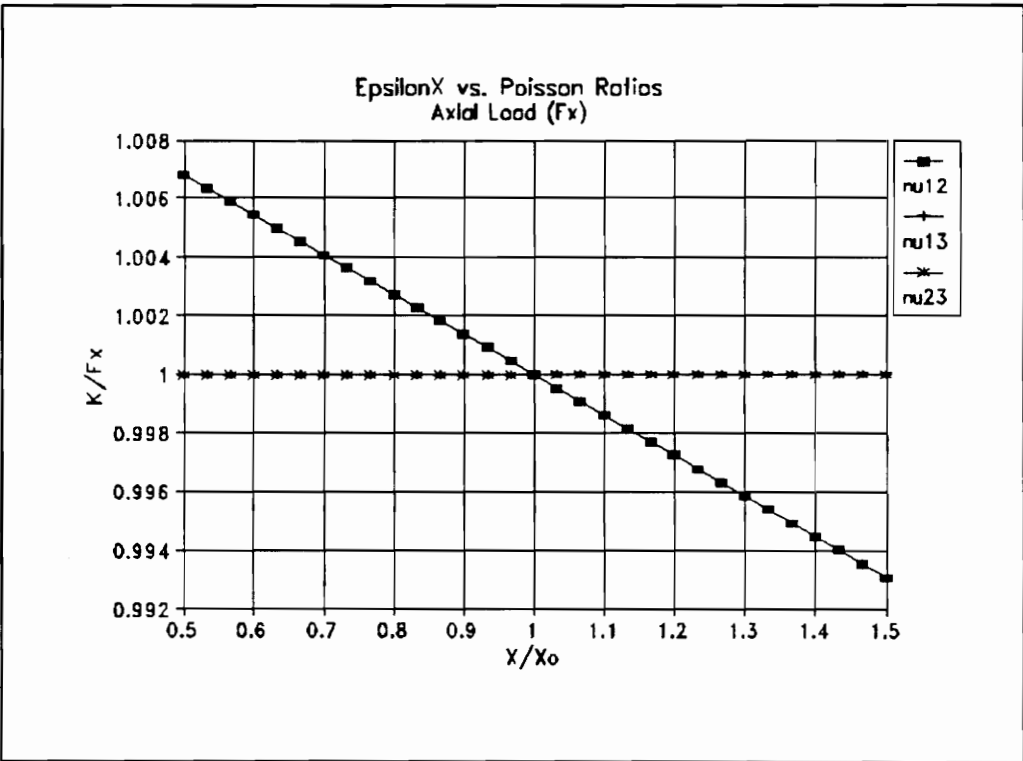


Figure A.2  $\epsilon_x$  vs. Poisson Ratios (Axial Load)

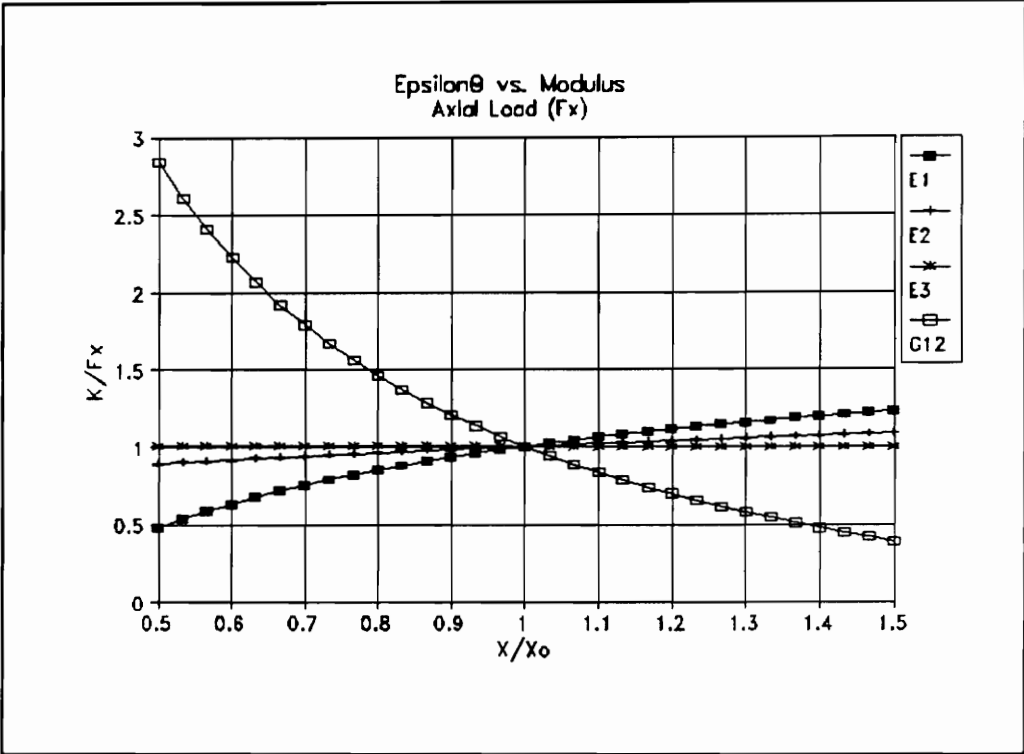


Figure A.3  $\epsilon_{\theta}$  vs. Moduli (Axial Load)

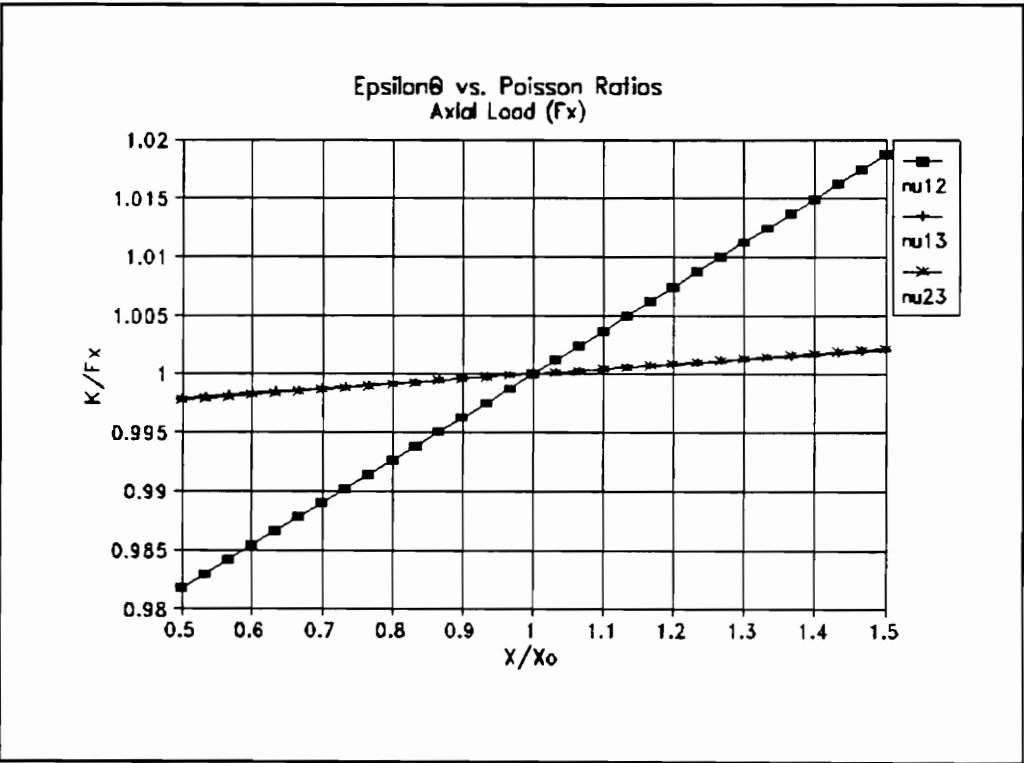
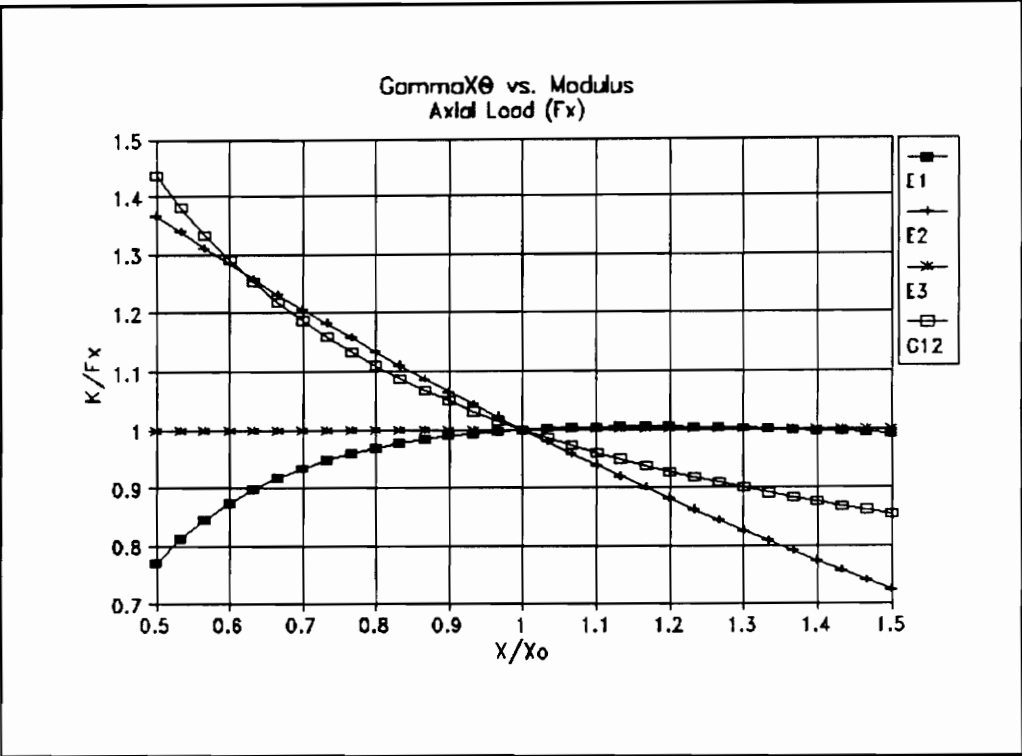
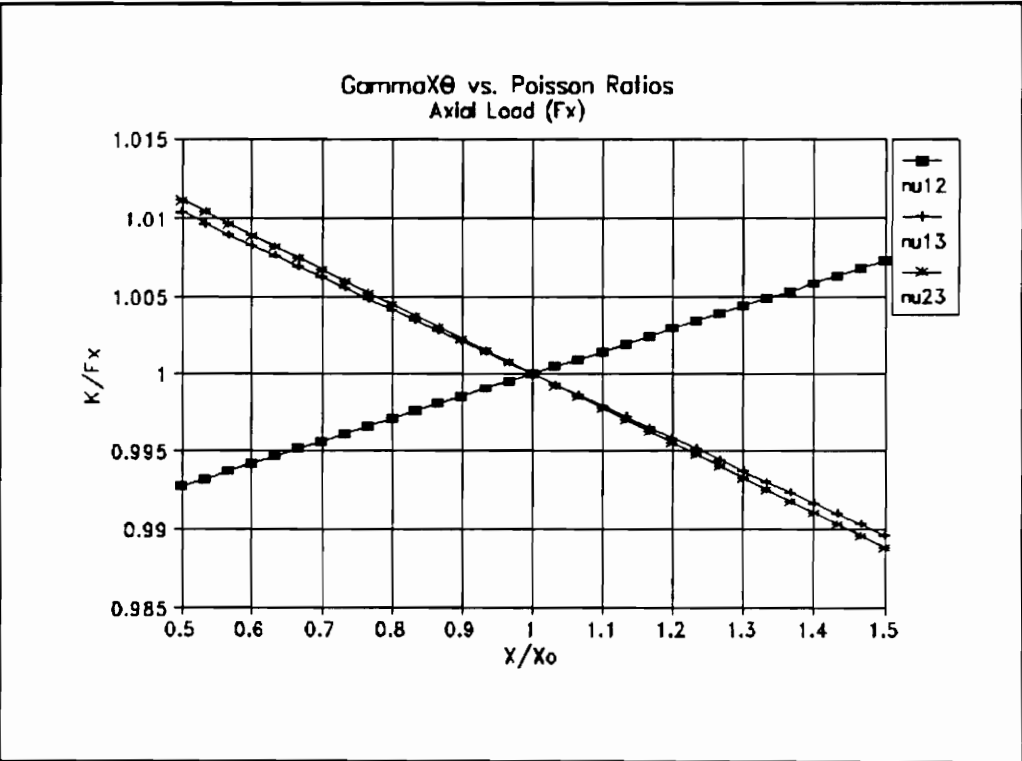


Figure A.4  $\epsilon_{\theta}$  vs. Poisson Ratios (Axial Load)



**Figure A.5**  $\gamma_{x\theta}$  vs. Moduli (Axial Load)



**Figure A.6**  $\gamma_{x\theta}$  vs. Poisson Ratios (Axial Load)

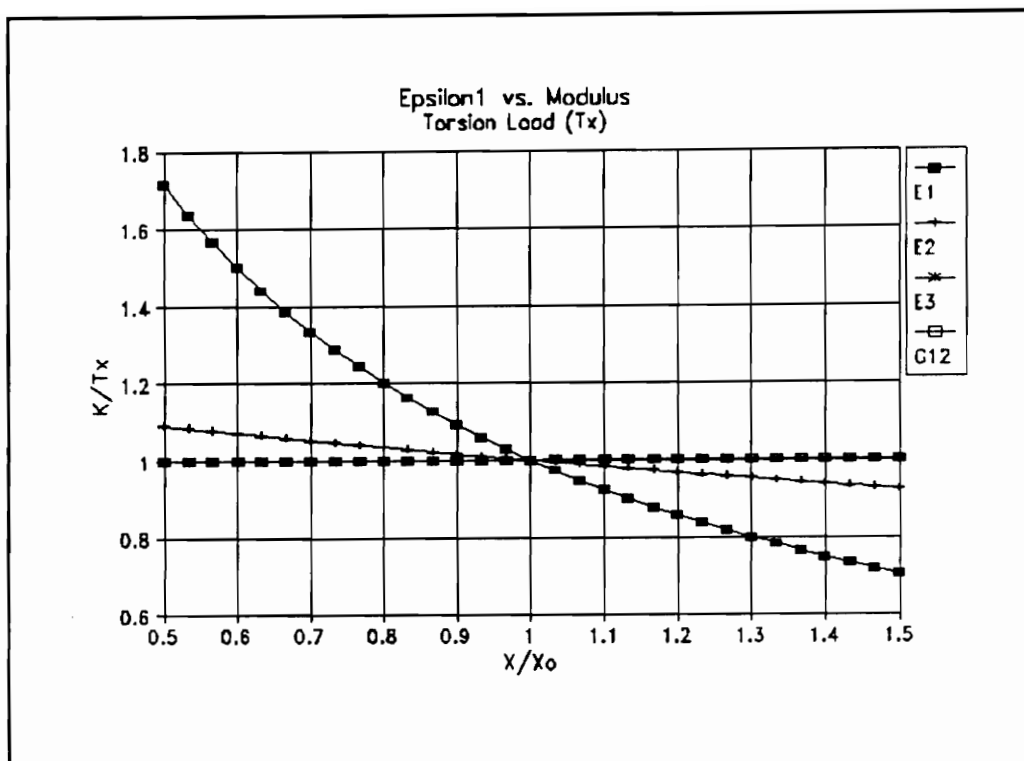


Figure A.7  $\epsilon_1$  vs. Moduli (Torsion Load)

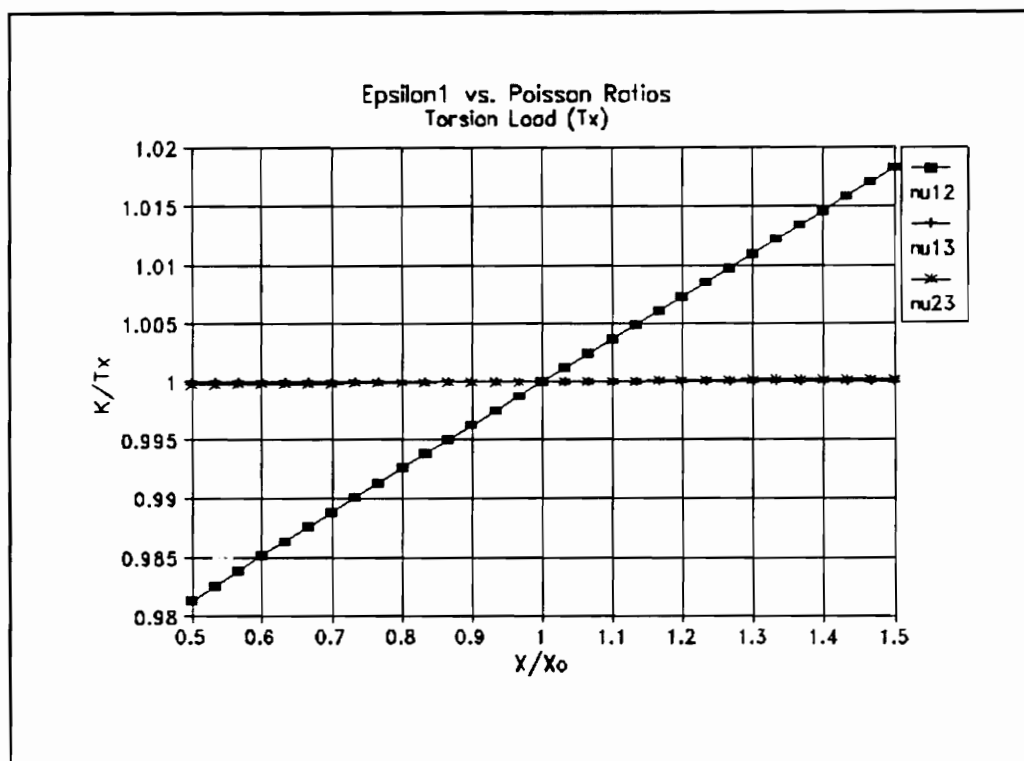


Figure A.8  $\epsilon_1$  vs. Poisson Ratios (Torsion Load)

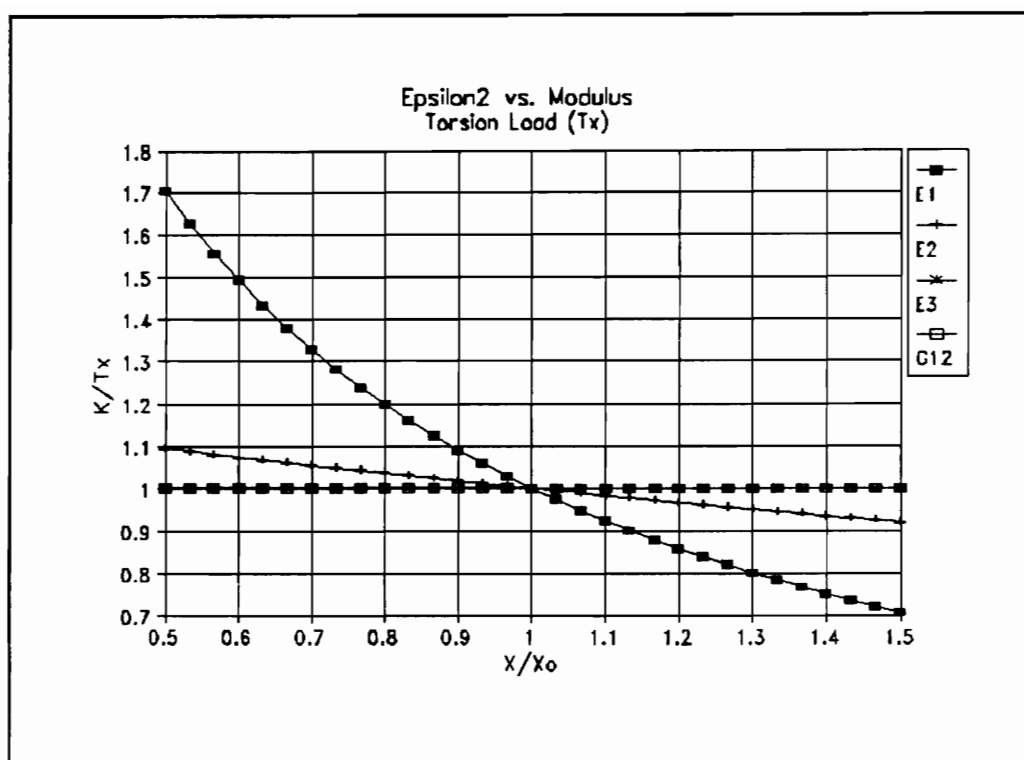


Figure A.9  $\epsilon_2$  vs. Moduli (Torsion Load)

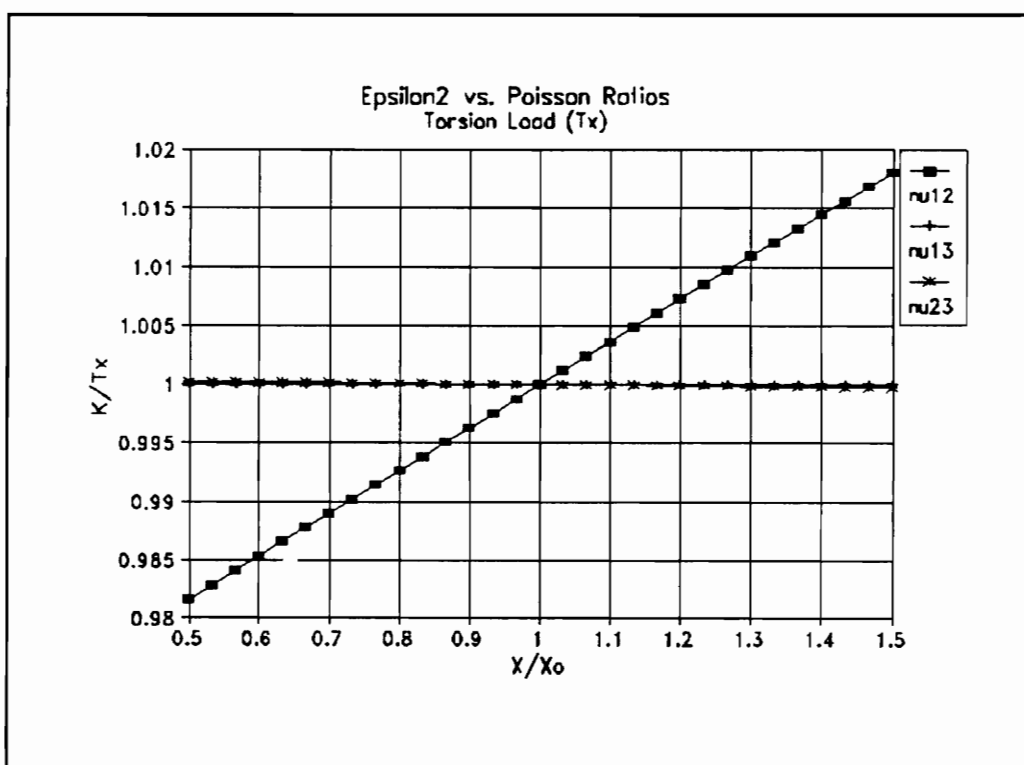


Figure A.10  $\epsilon_2$  vs. Poisson Ratios (Torsion Load)

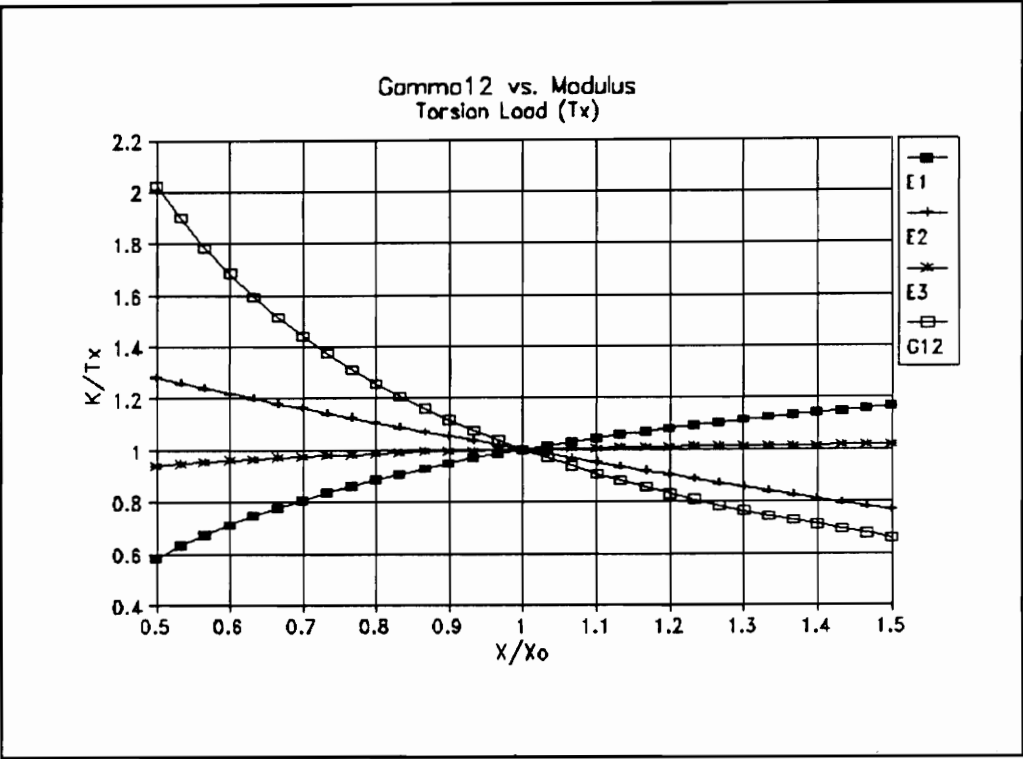


Figure A.11  $\gamma_{12}$  vs. Moduli (Torsion Load)

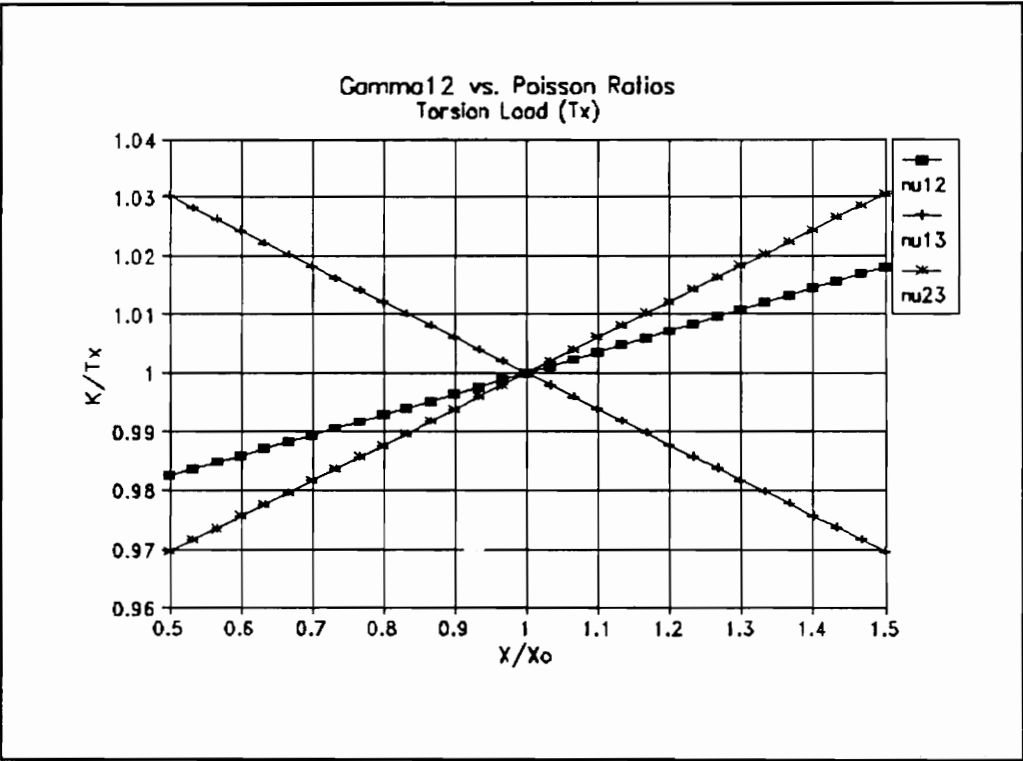


Figure A.12  $\gamma_{12}$  vs. Poisson Ratios (Torsion Load)

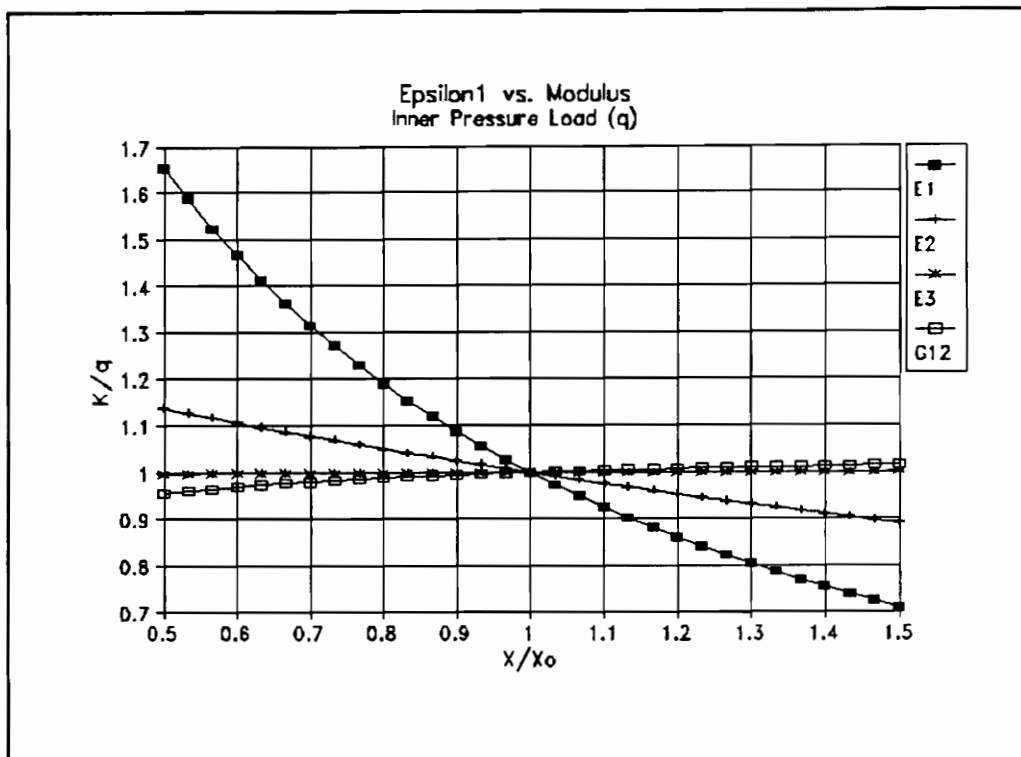


Figure A.13  $\epsilon_1$  vs. Moduli (Inner Pressure Load)

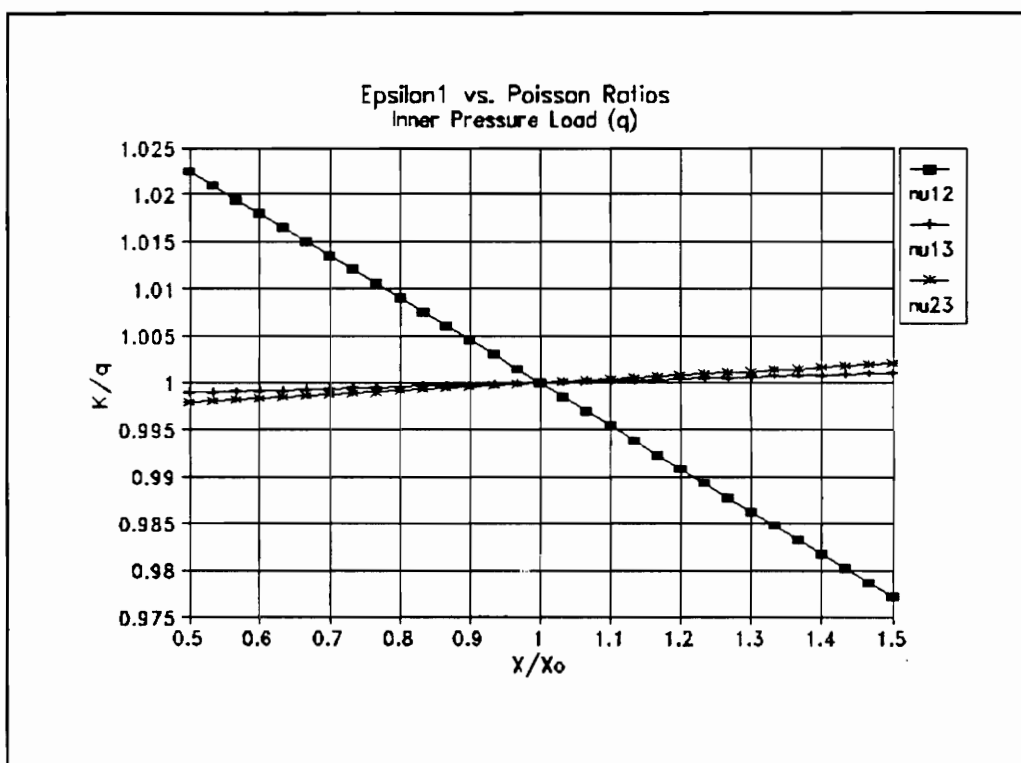


Figure A.14  $\epsilon_1$  vs. Poisson Ratios (Inner Pressure Load)

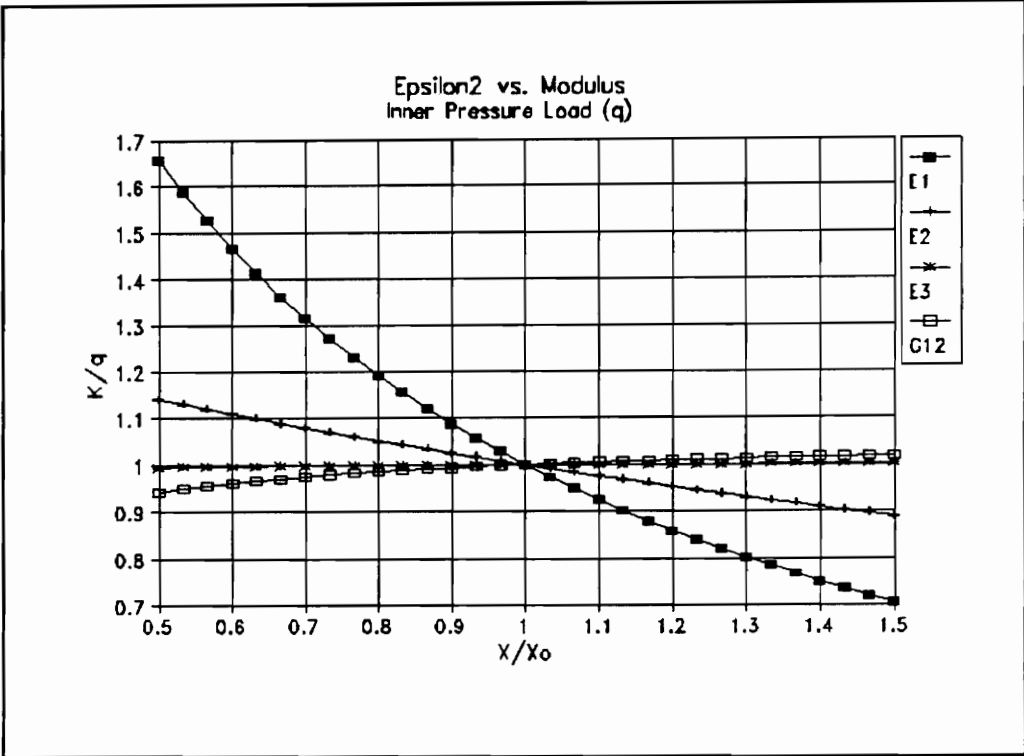


Figure A.15  $\epsilon_2$  vs. Moduli (Inner Pressure Load)

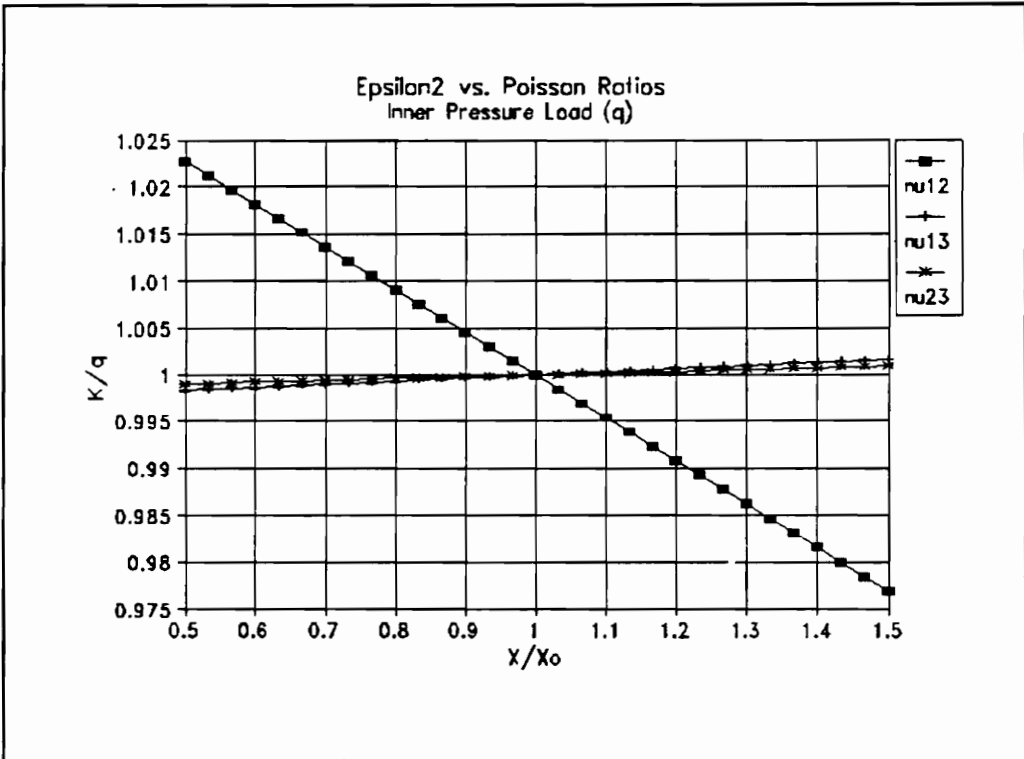


Figure A.16  $\epsilon_2$  vs. Poisson Ratios (Inner Pressure Load)

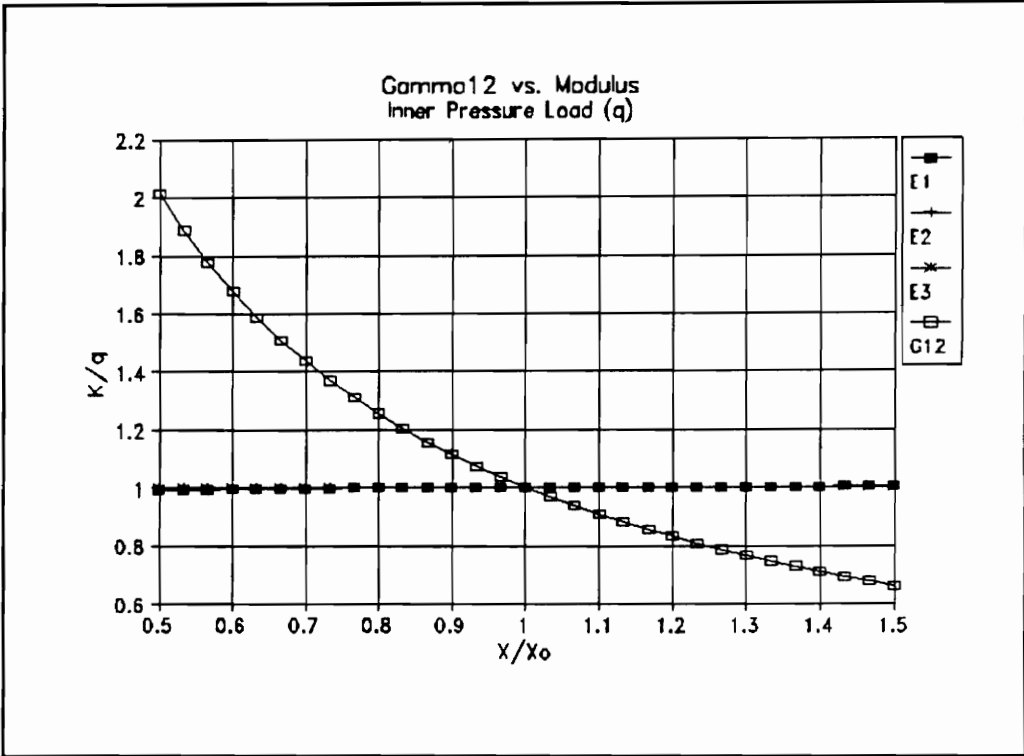


Figure A.17  $\gamma_{12}$  vs. Moduli (Inner Pressure Load)

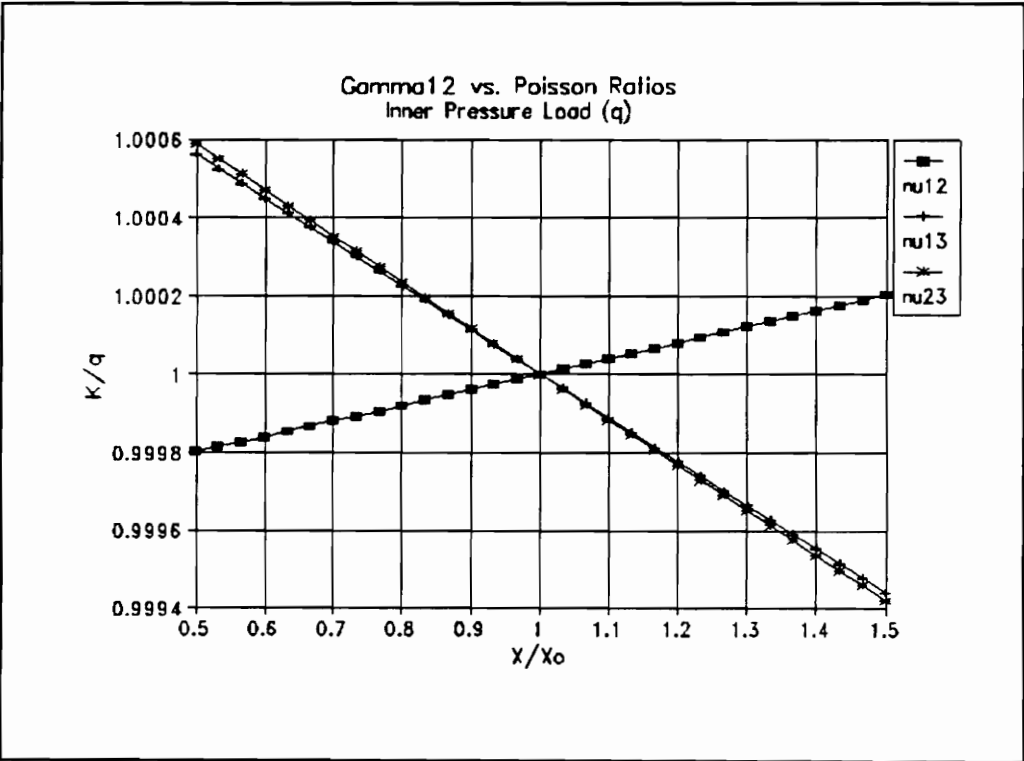


Figure A.18  $\gamma_{12}$  vs. Poisson Ratio (Inner Pressure Load)

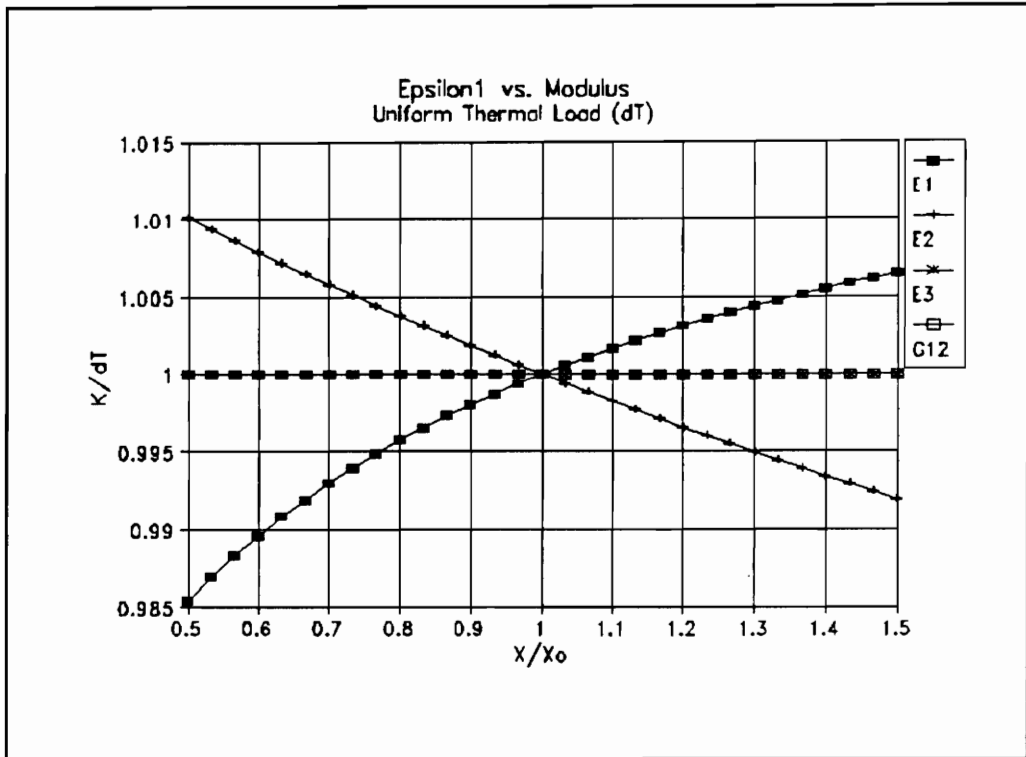


Figure A.19  $\epsilon_1$  vs. Moduli (Thermal Load)

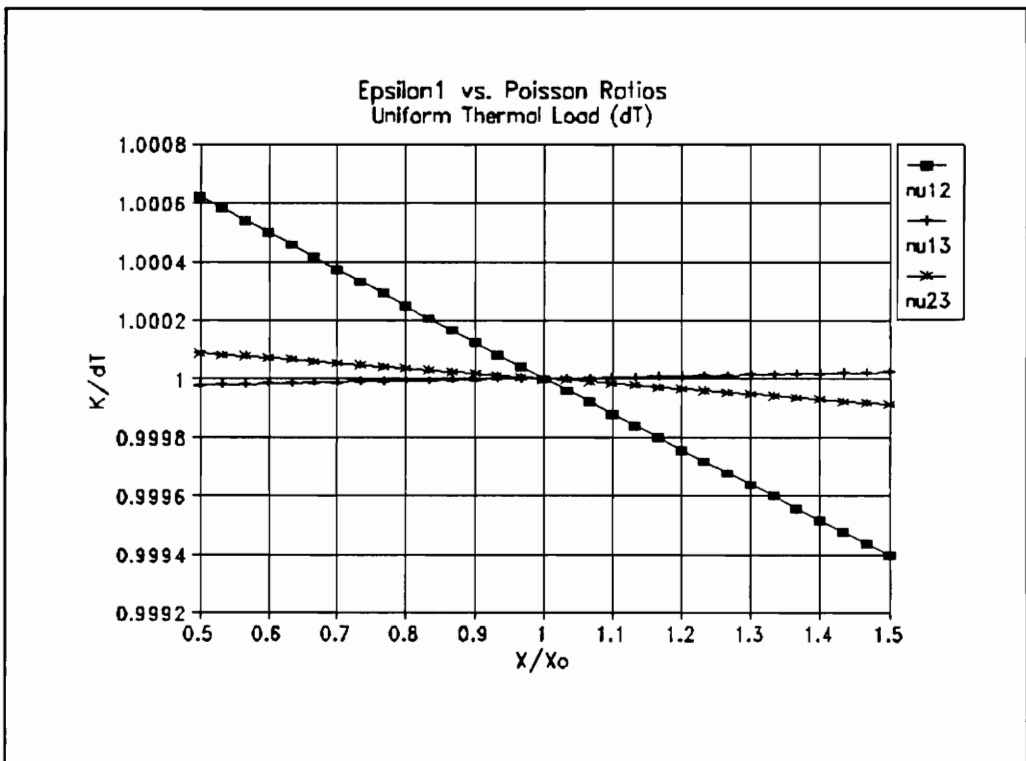


Figure A.20  $\epsilon_1$  vs. Poisson Ratios (Thermal Load)

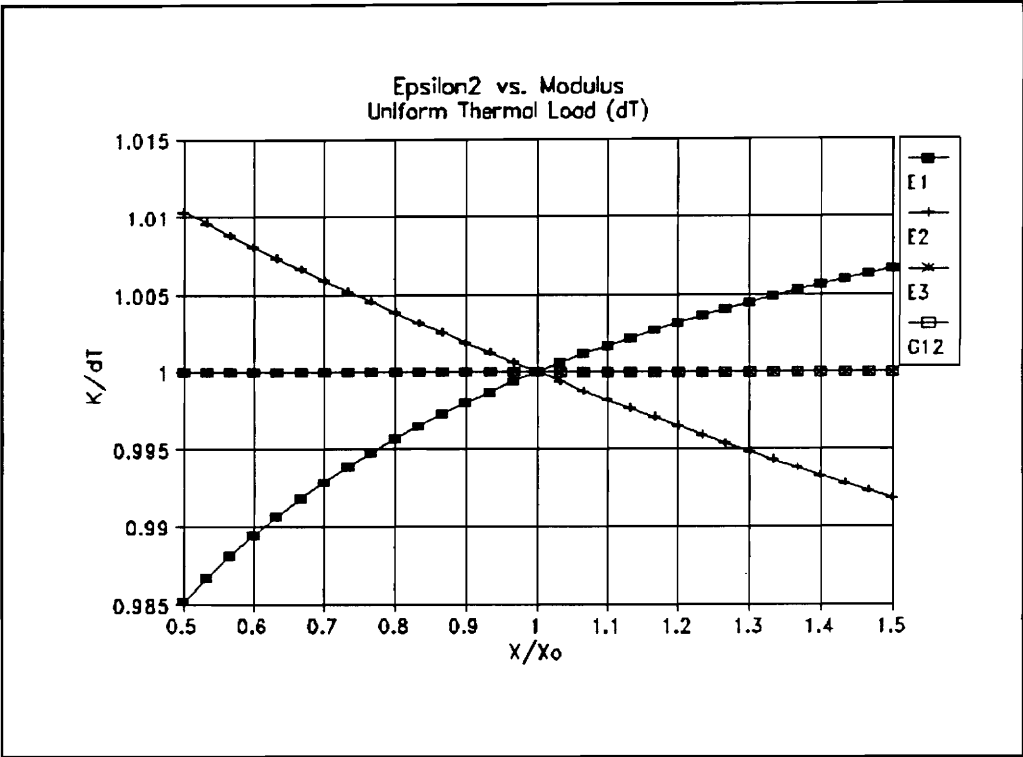


Figure A.21  $\epsilon_2$  vs. Moduli (Thermal Load)

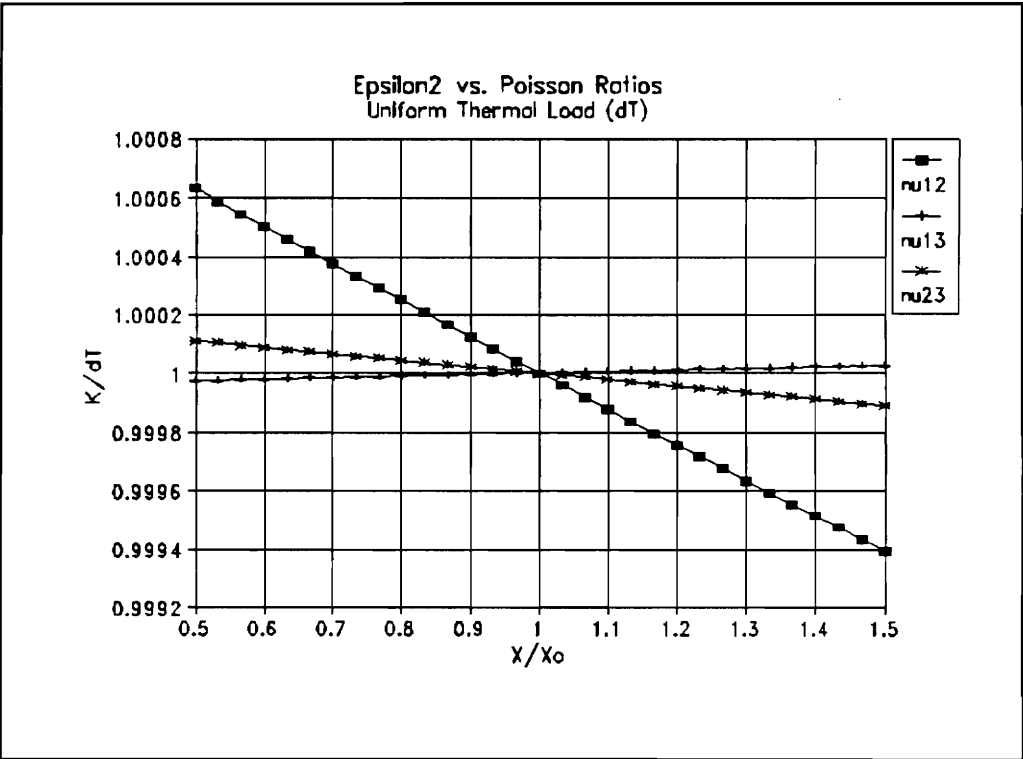


Figure A.22  $\epsilon_2$  vs. Poisson Ratio (Thermal Load)

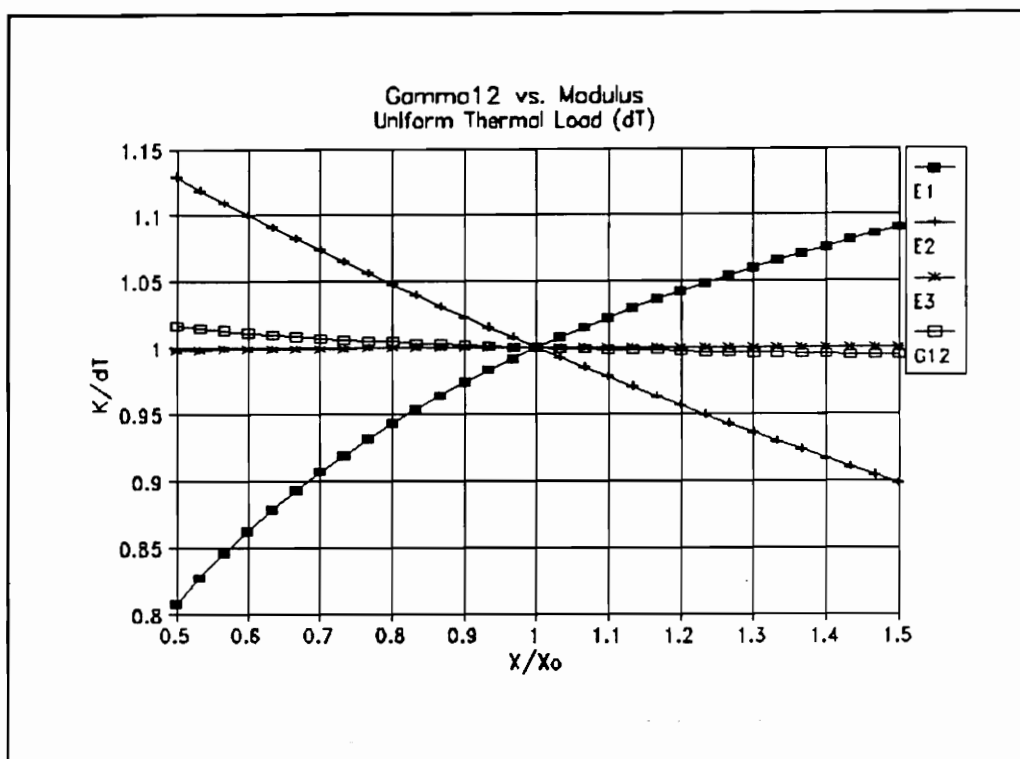


Figure A.23  $\gamma_{12}$  vs. Moduli (Thermal Load)

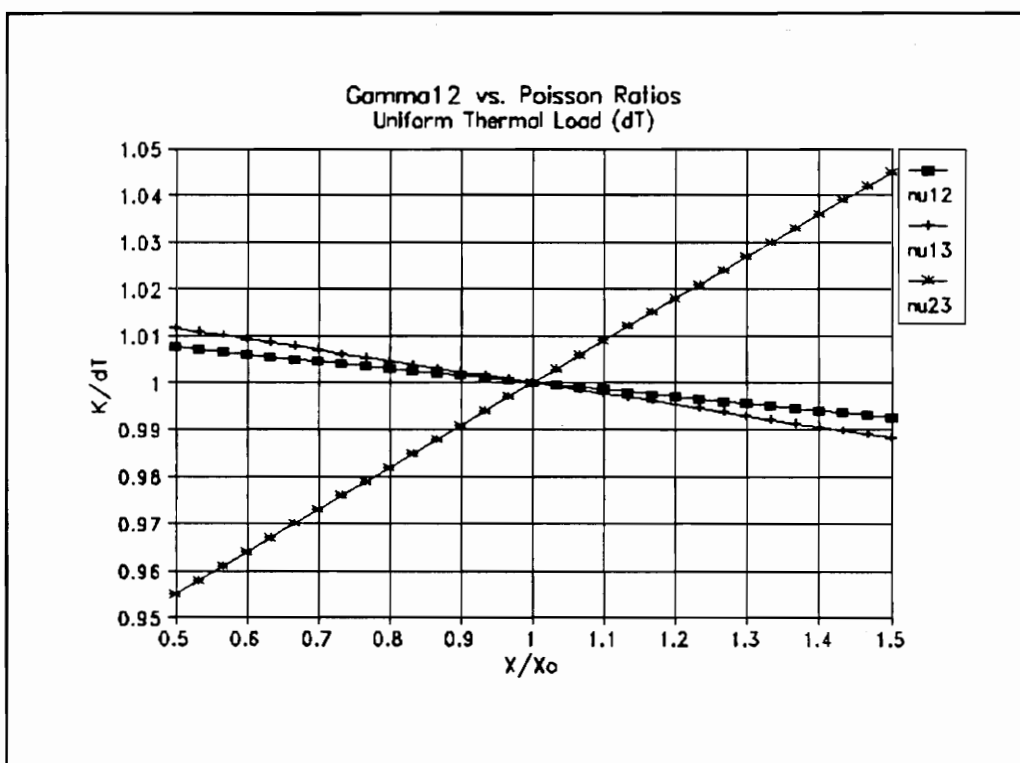


Figure A.24  $\gamma_{12}$  vs. Poisson Ratios (Thermal Load)

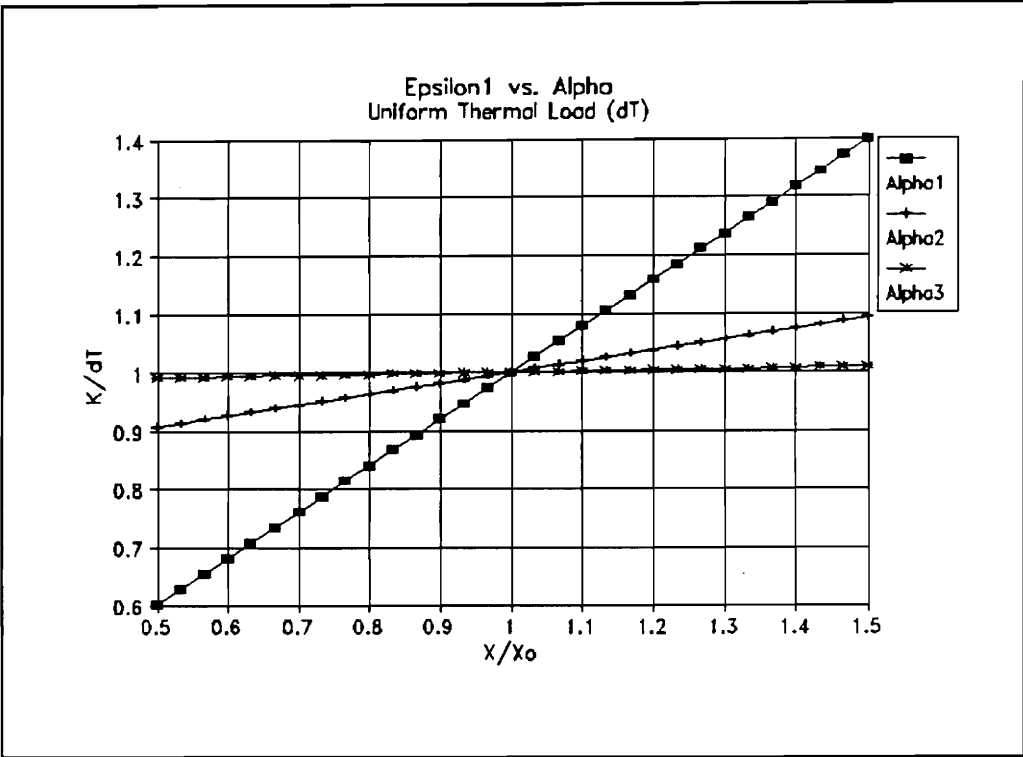


Figure A.25  $\epsilon_1$  vs.  $\alpha$  (Thermal Load)

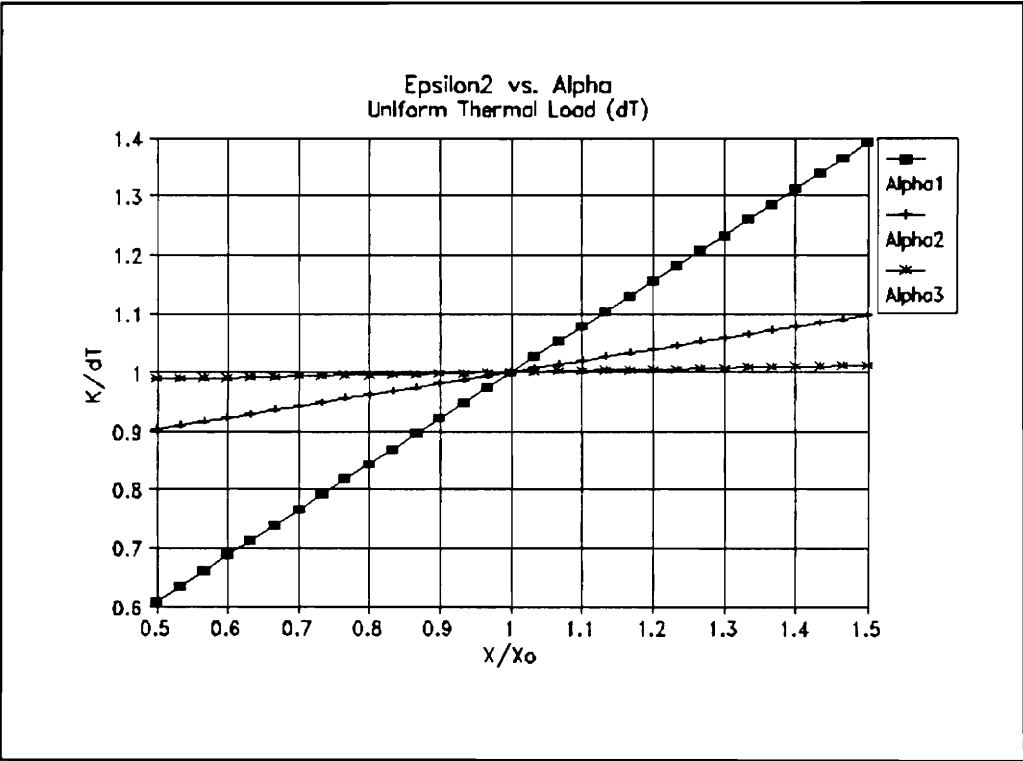


Figure A.26  $\epsilon_2$  vs.  $\alpha$  (Thermal Load)

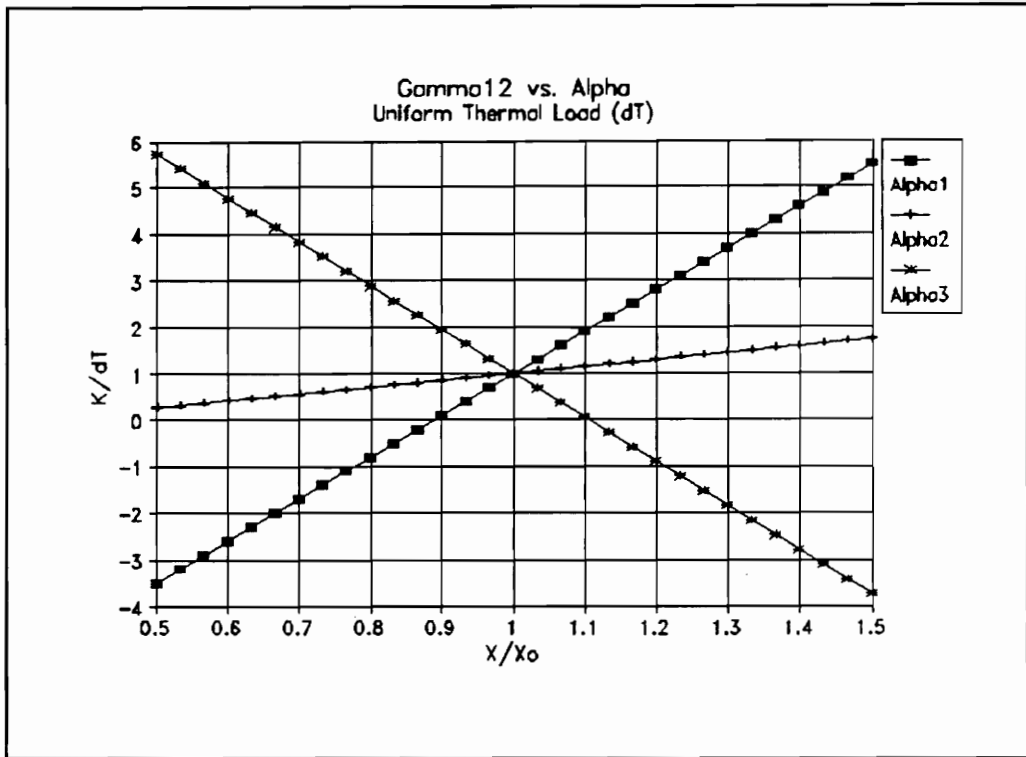
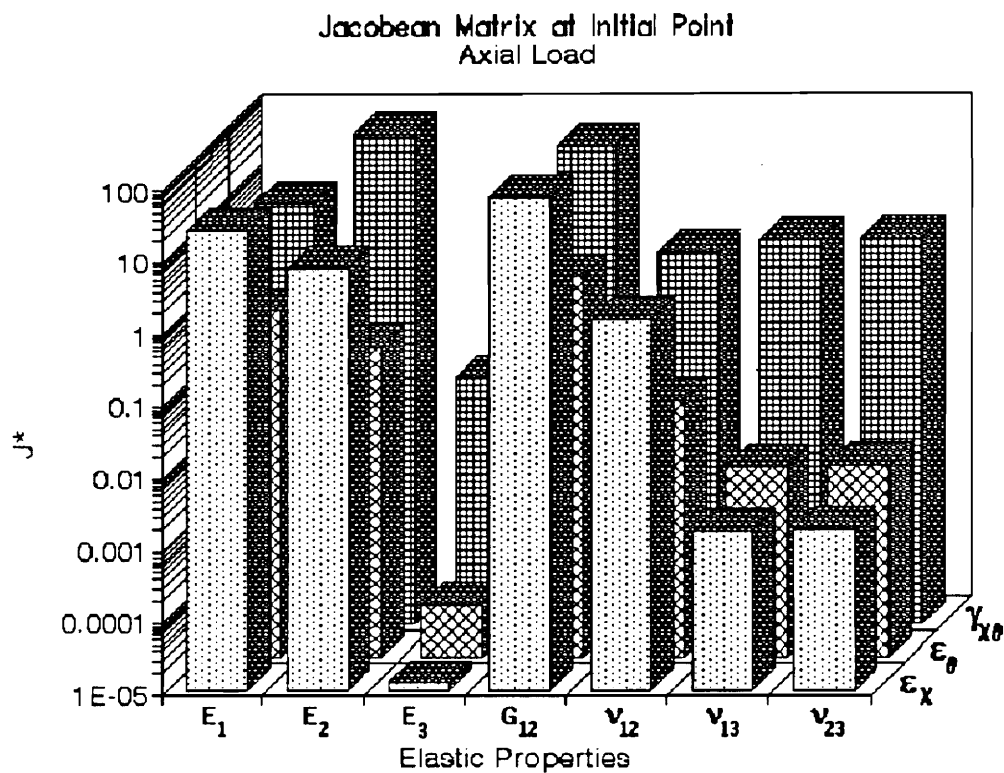


Figure A.27  $\gamma_{12}$  vs.  $\alpha$  (Thermal Load)

The following plots show the magnitude of the elements of the Jacobean matrix (Chap. 2). The elements are scaled as follows:

$$\hat{j}_{ij} = \frac{(J_{ij} \cdot E_i^{\circ})}{(\epsilon_j / \text{load})}$$

where  $E^{\circ}$  are the initial properties given in Table 1 and the denominators are the strains per unit load given in Table 2.



**Figure A.28** Components of Jacobean Matrix Under Axial Load

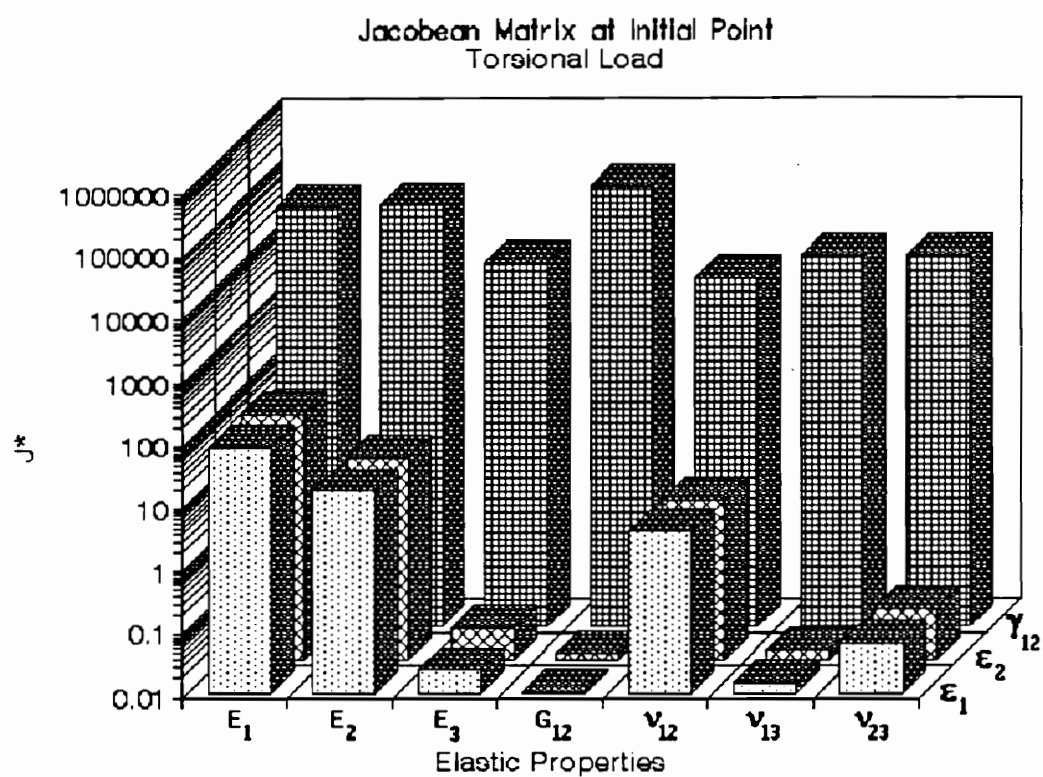


**Figure A.29** Components of Jacobean Matrix Under Torsional Load

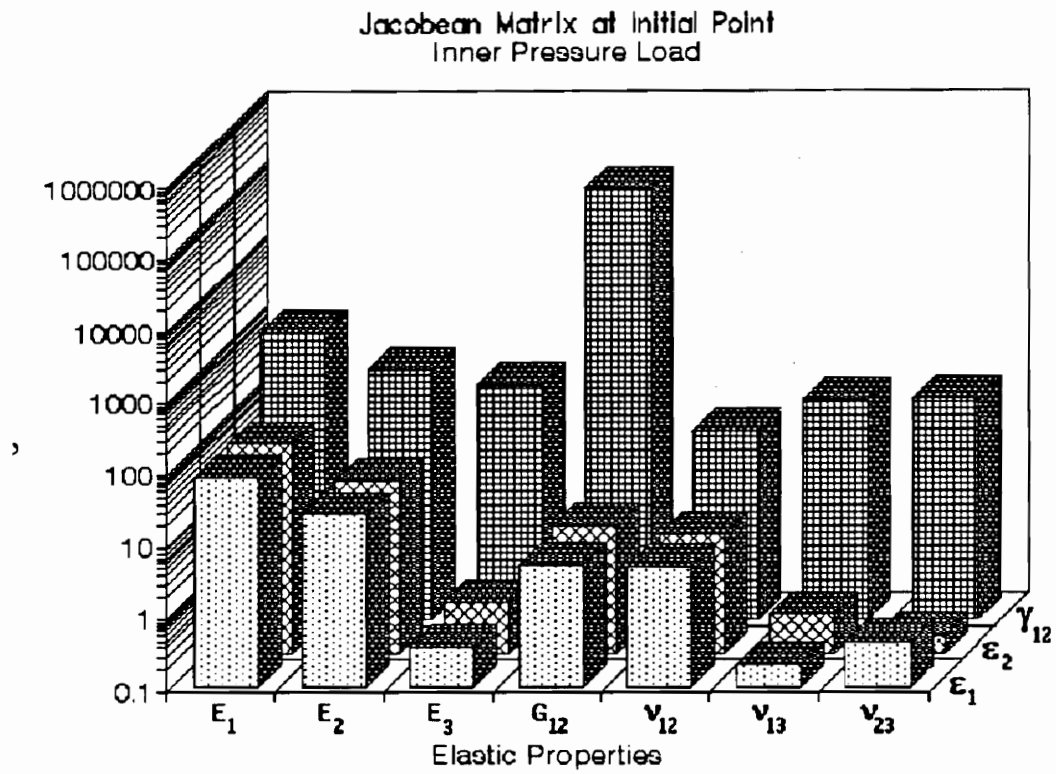


**Figure A.30** Components of Jacobean Matrix Under Inner Pressure Load

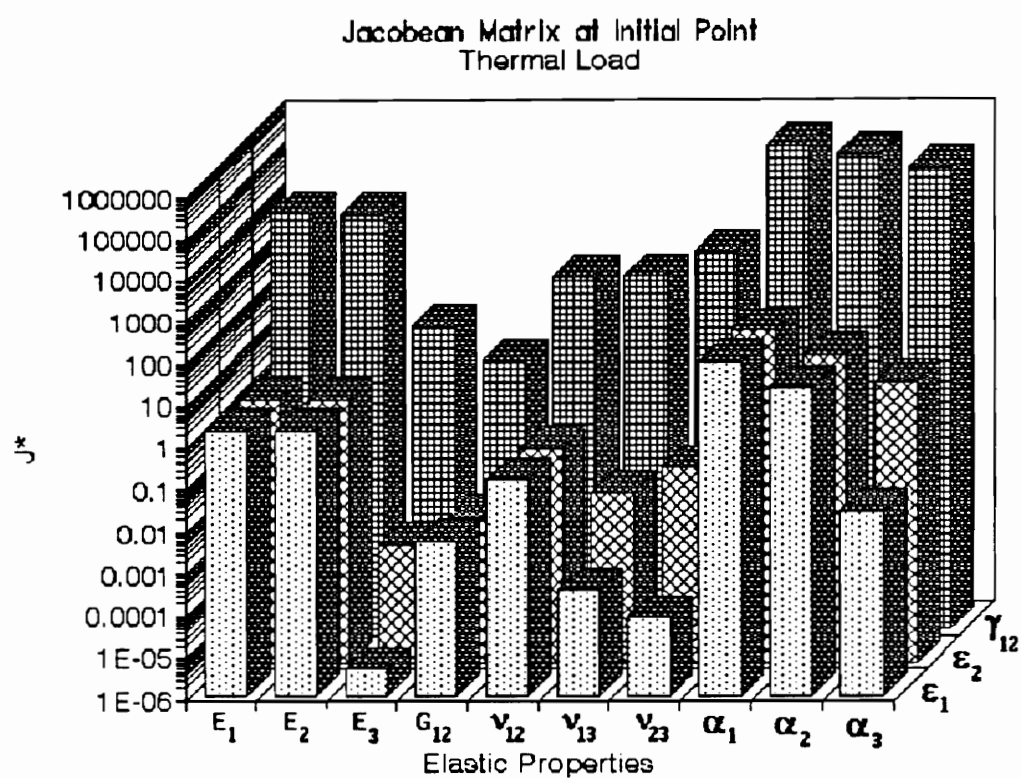


**Figure A.31** Components of Jacobean Matrix Under Thermal Load

# Appendix B

## Experimental Data

This Appendix contains plots of the experimental data obtained for B&W Speciman 67A. Each plot shows the data from one rosette under one load trial. The Appendix is organized as follows:

- Tension Trials
  - Rosette A
    - Trial 1, 2, 3
  - Rosette B
    - Trial 1, 2, 3
  - Rosette C
    - Trial 1, 2, 3
  - Rosette D
    - Trial 1, 2, 3
- Compression Trials
  - Rosette A
    - Trial 1, 2, 3
  - :
    - :
- Positive Torsion Trials
  - :
- Negative Torsion Trials

Fig. 4.9 is repeated below for reference.

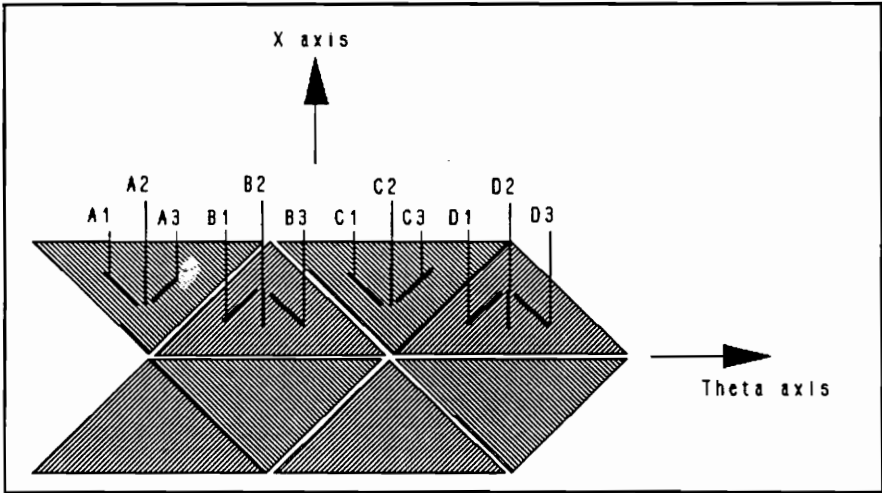


Figure 1 Strain Gauge Locations

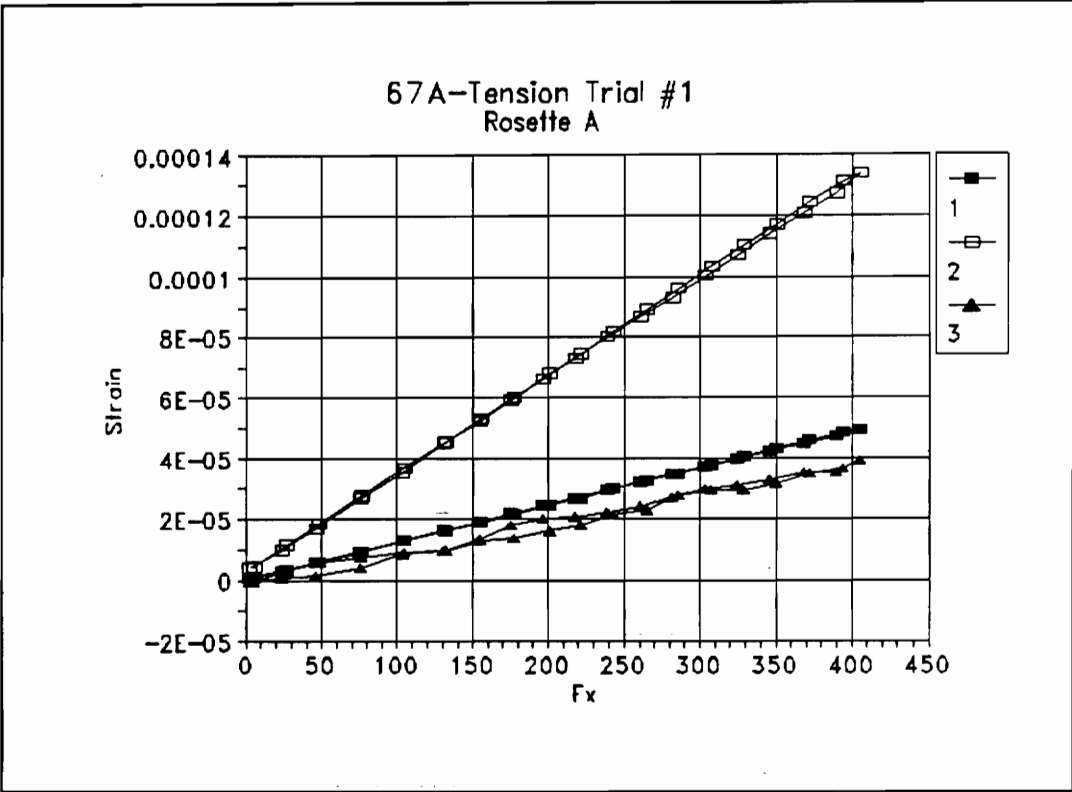


Figure B.1 Rosette A, Tension Load Trial #1

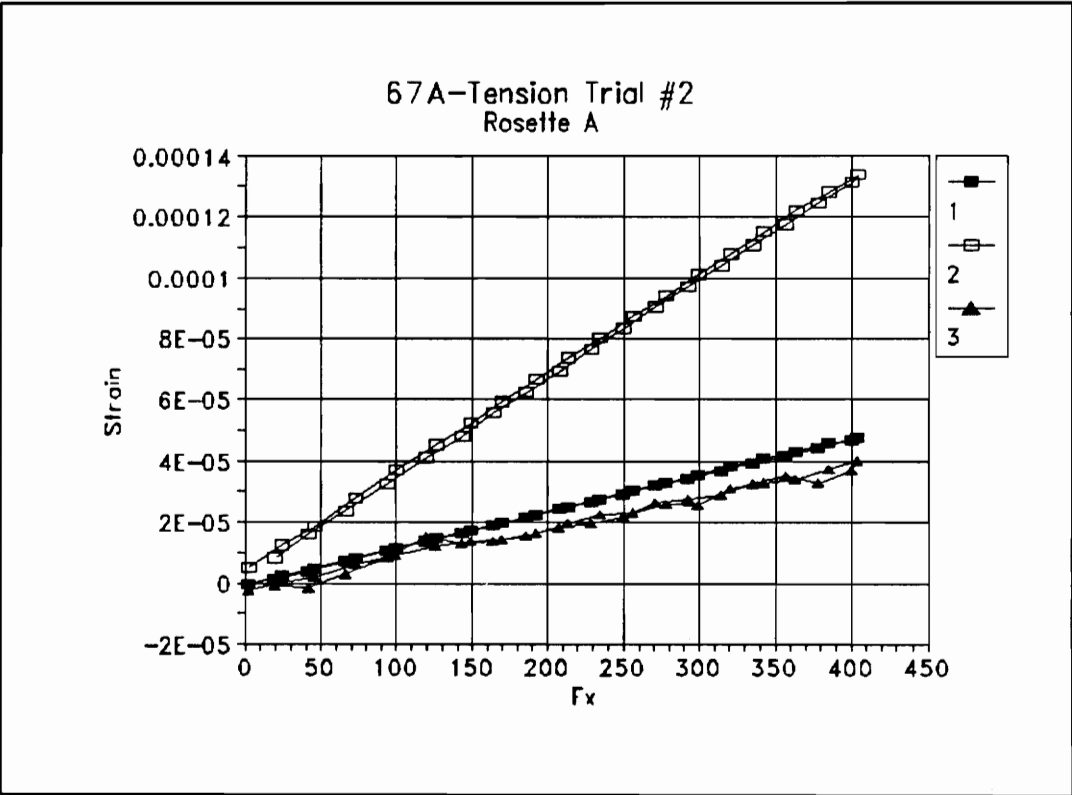


Figure B.2 Rosette A, Tension Load Trial #2

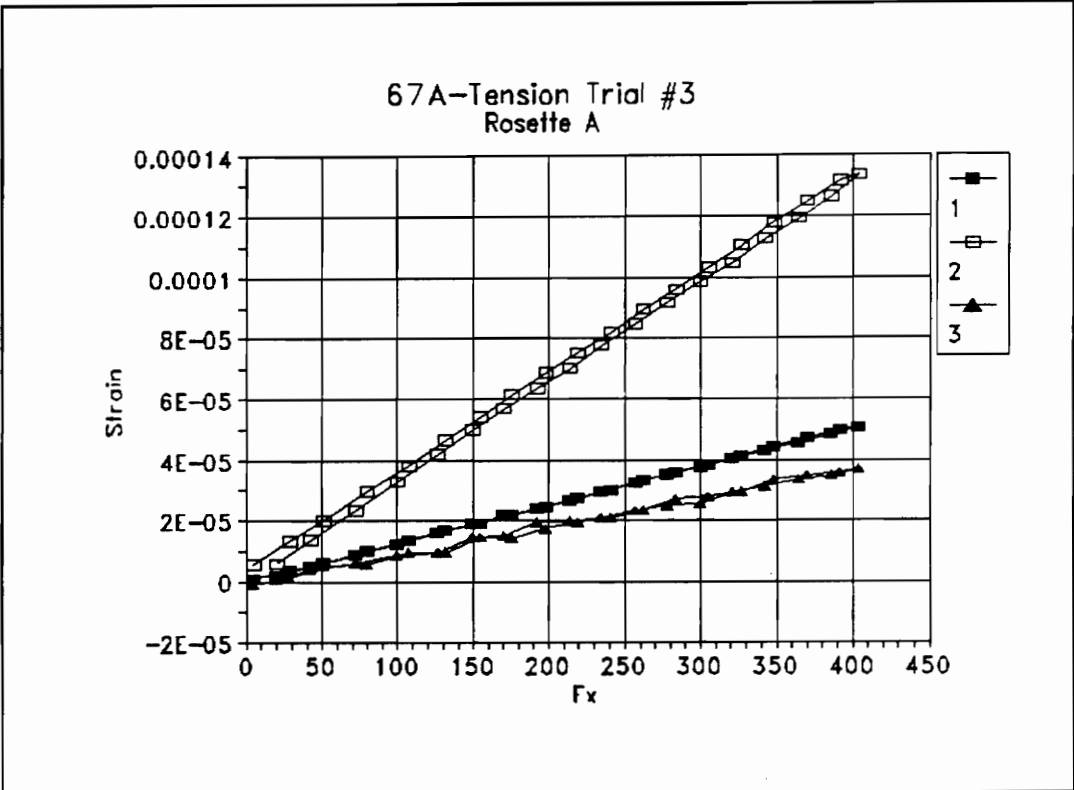


Figure B.3 Rosette A, Tension Load Trial #3

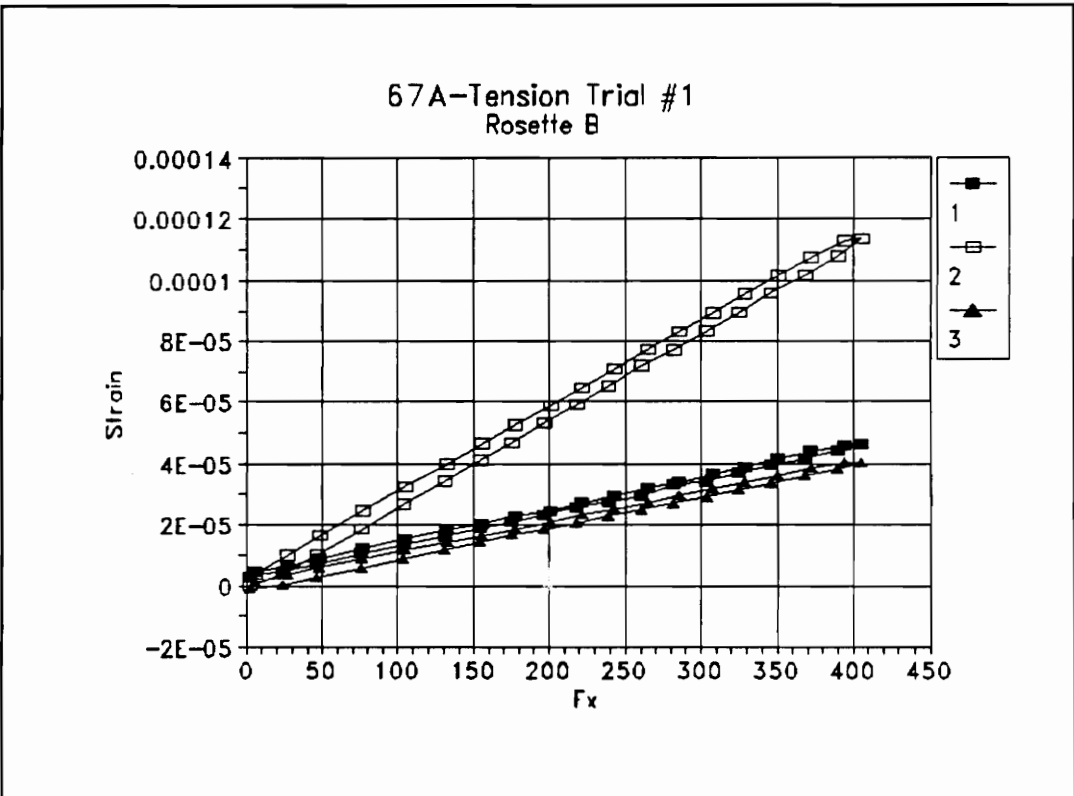


Figure B.4 Rosette B, Tension Load Trial #1

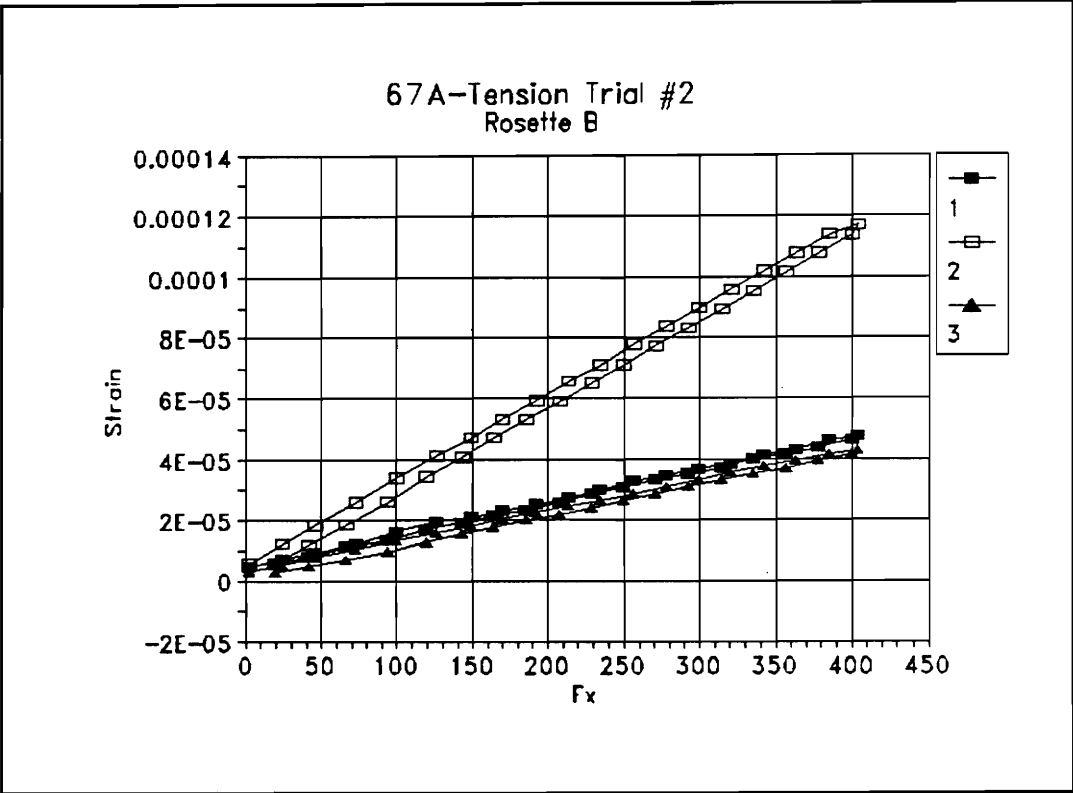


Figure B.5 Rosette B, Tension Load Trial #2

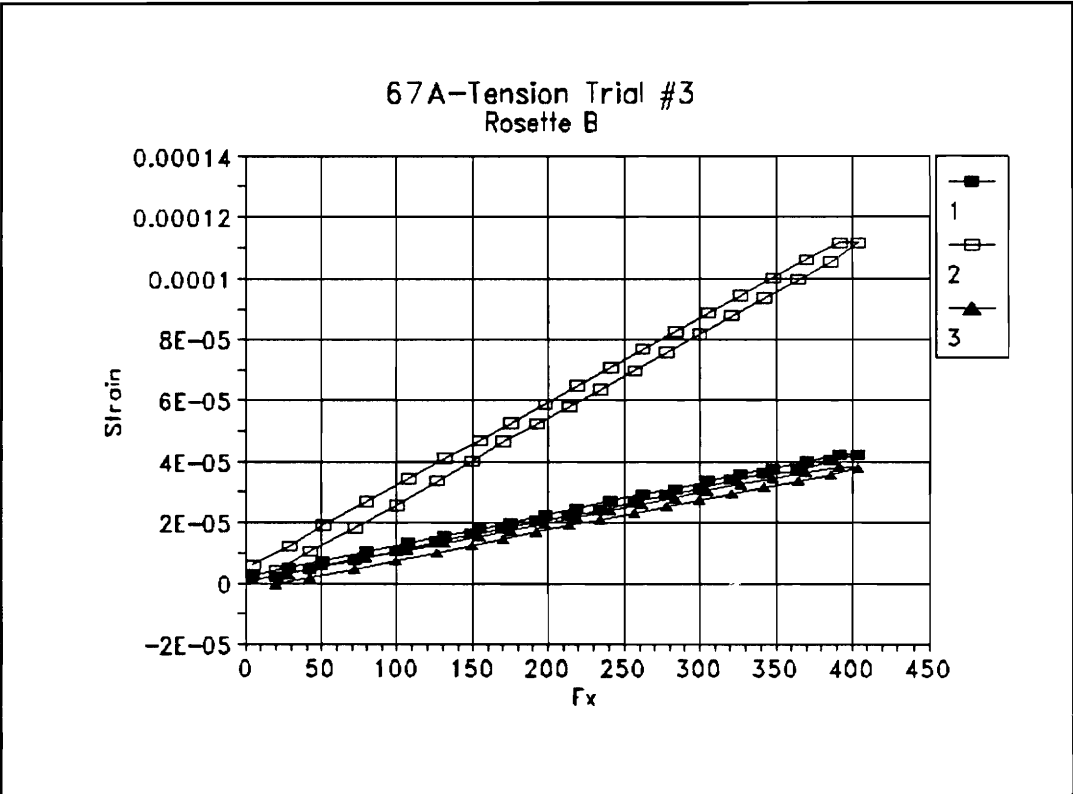


Figure B.6 Rosette B, Tension Load Trial #3

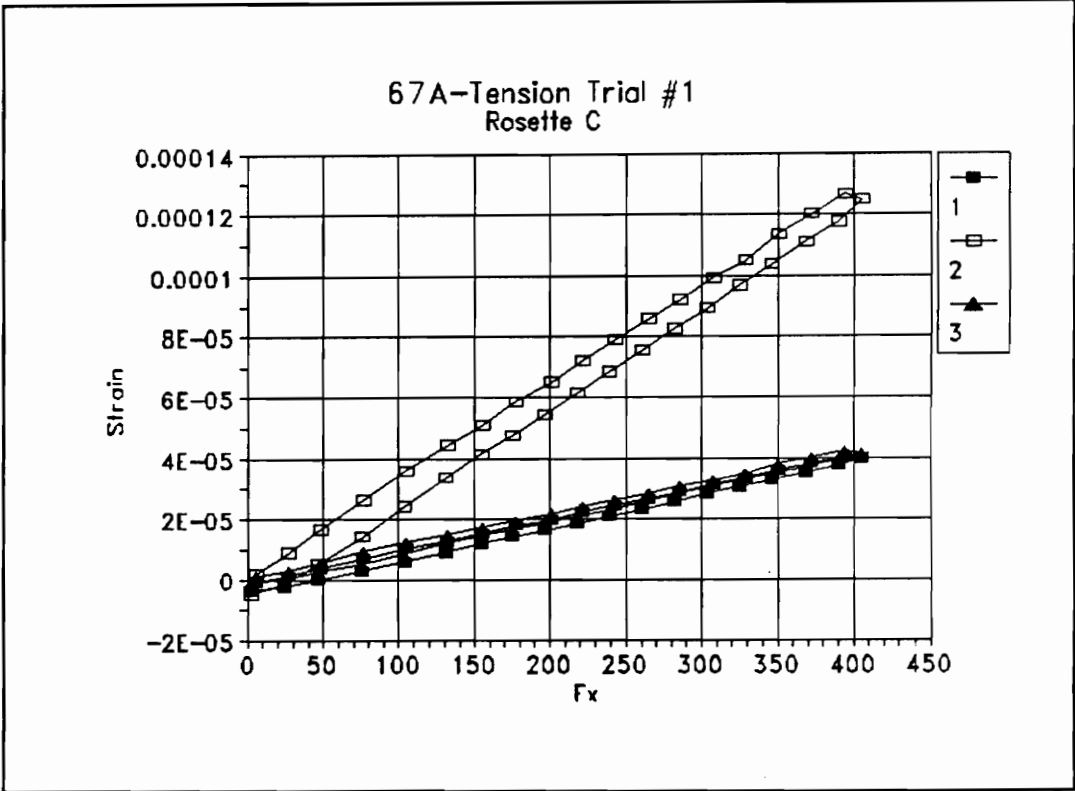


Figure B.7 Rosette C, Tension Load Trial #1

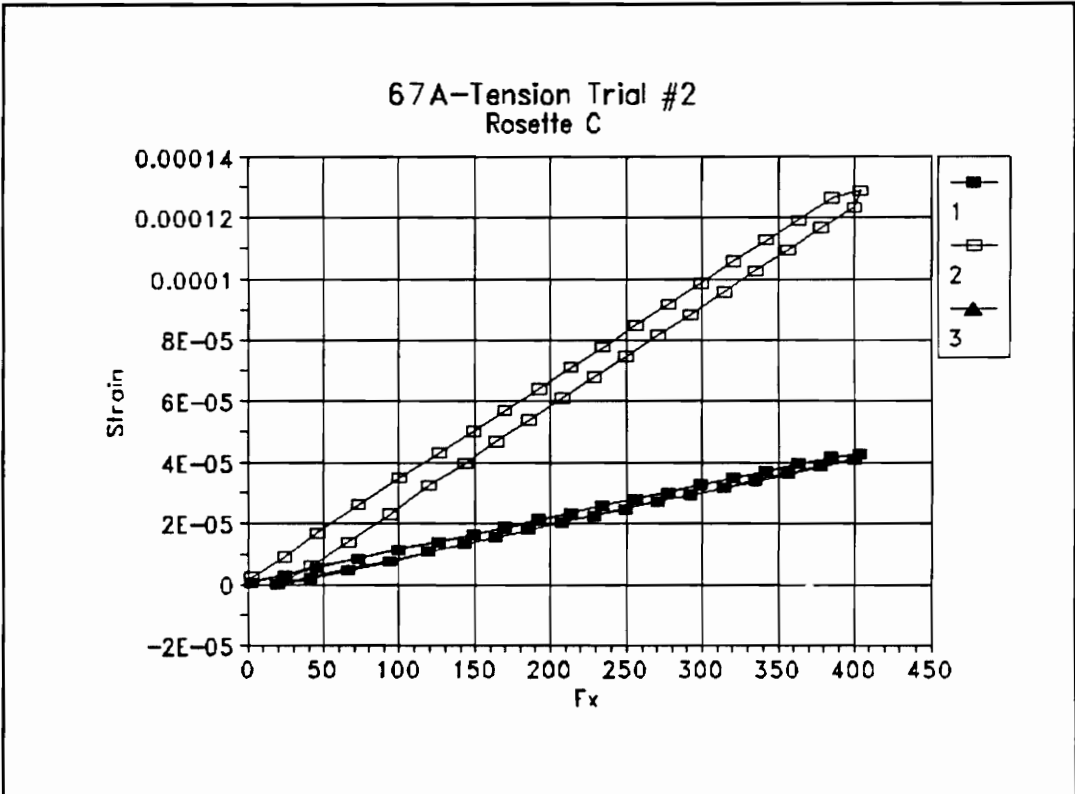


Figure B.8 Rosette C, Tension Load Trial #2

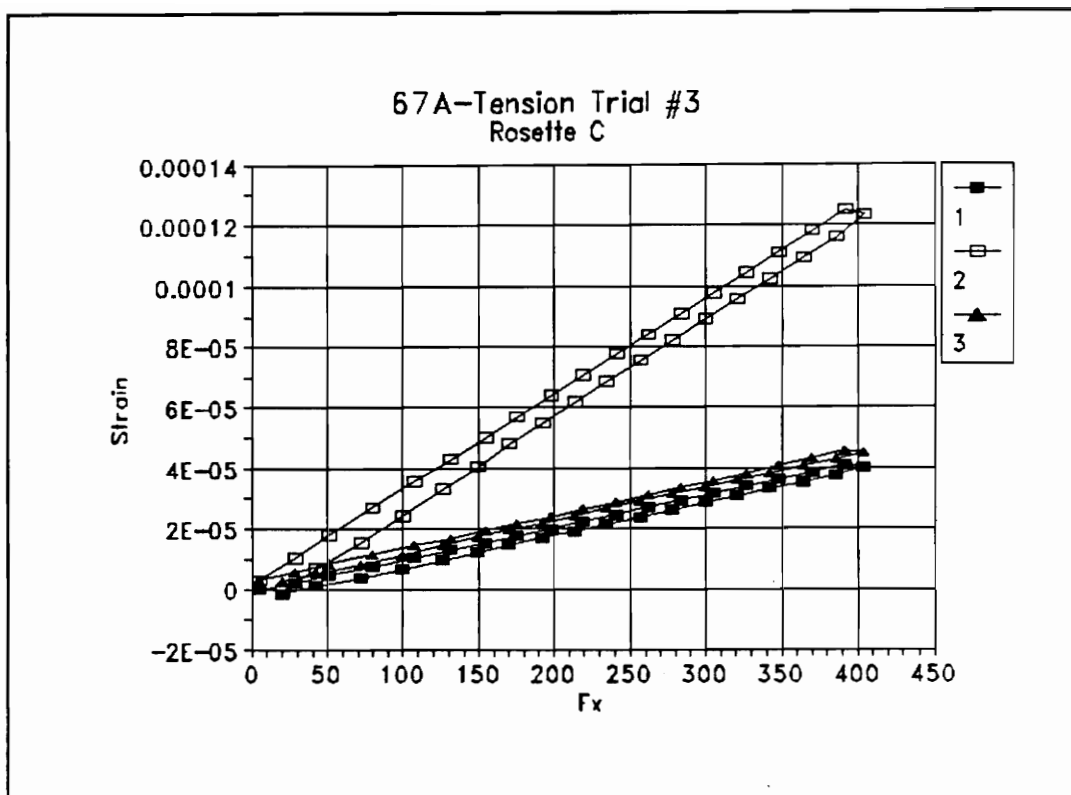


Figure B.9 Rosette C, Tension Load Trial #3

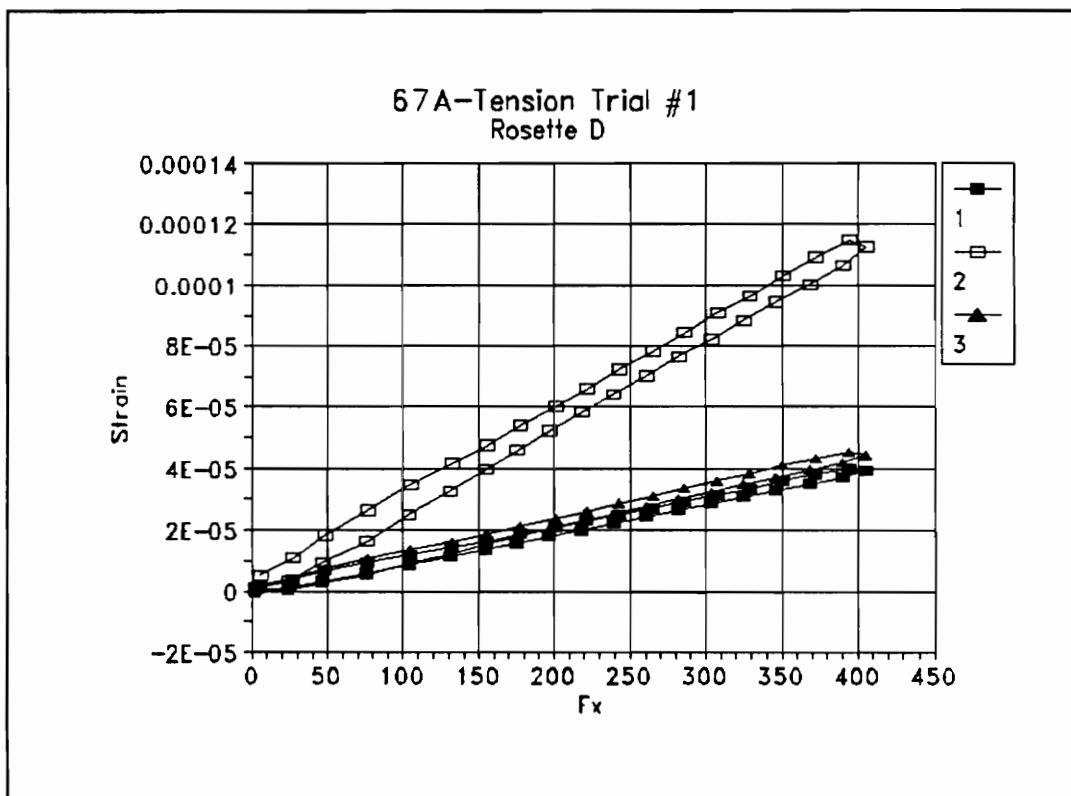


Figure B.10 Rosette D, Tension Load Trial #1

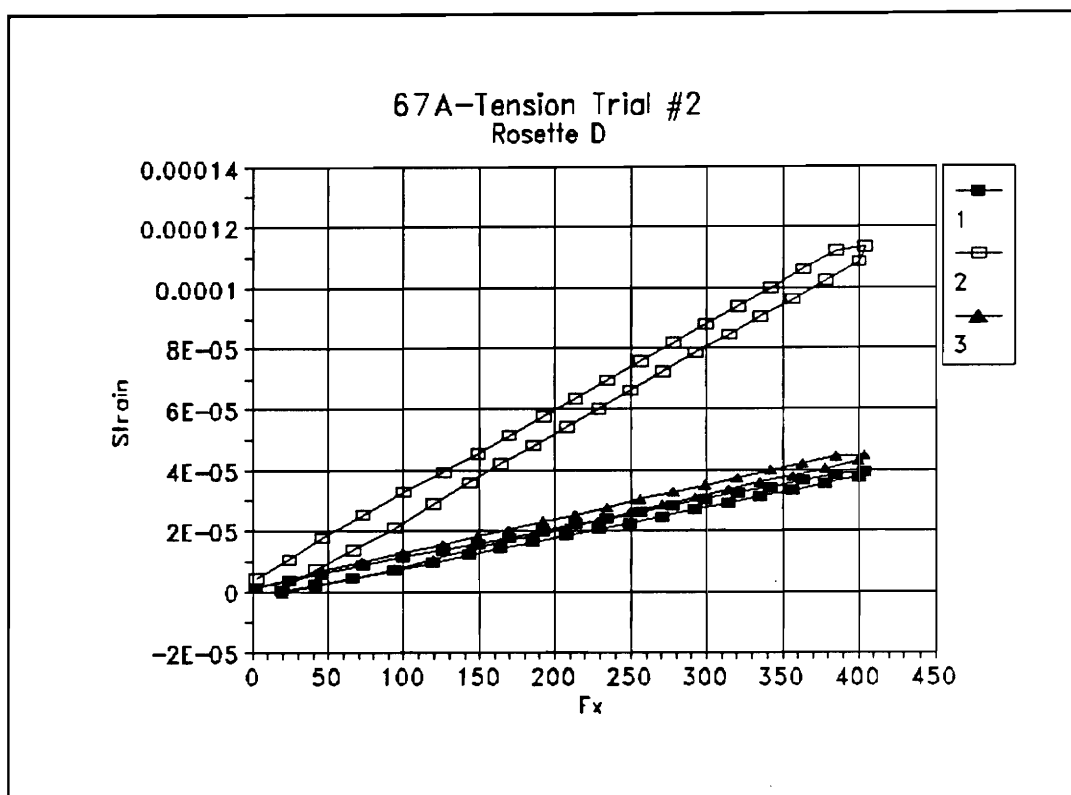


Figure B.11 Rosette D, Tension Load Trial #2

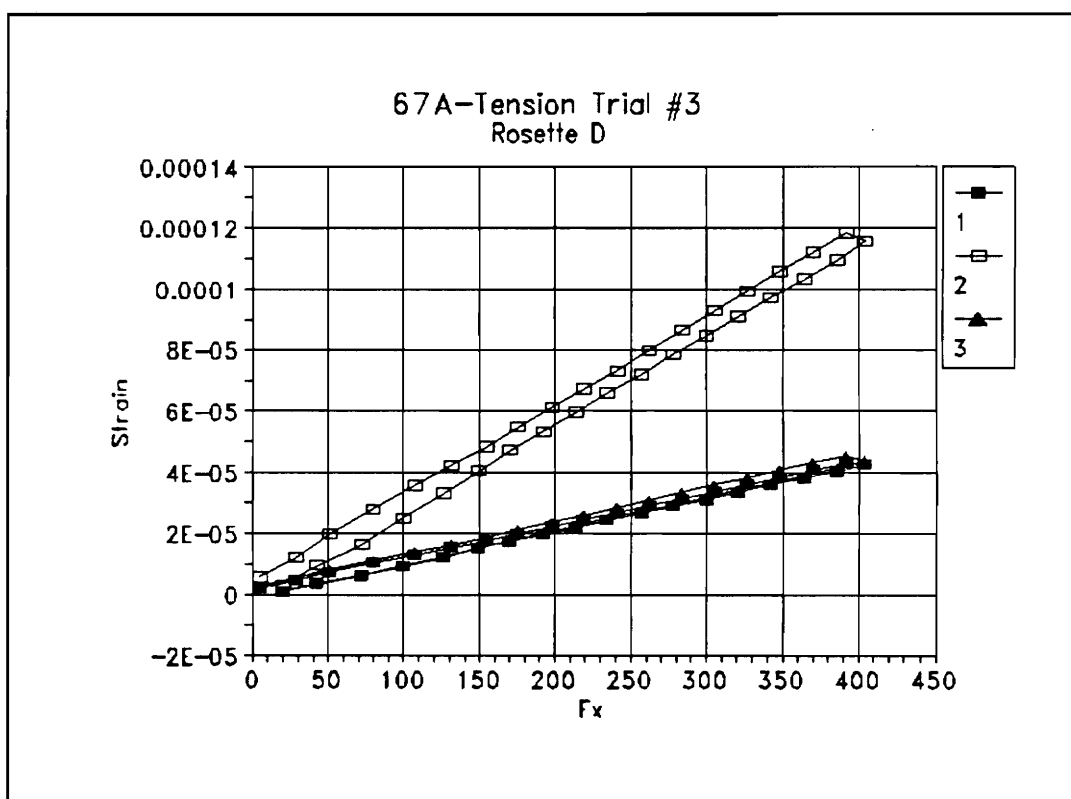


Figure B.12 Rosette D, Tension Load Trial #3

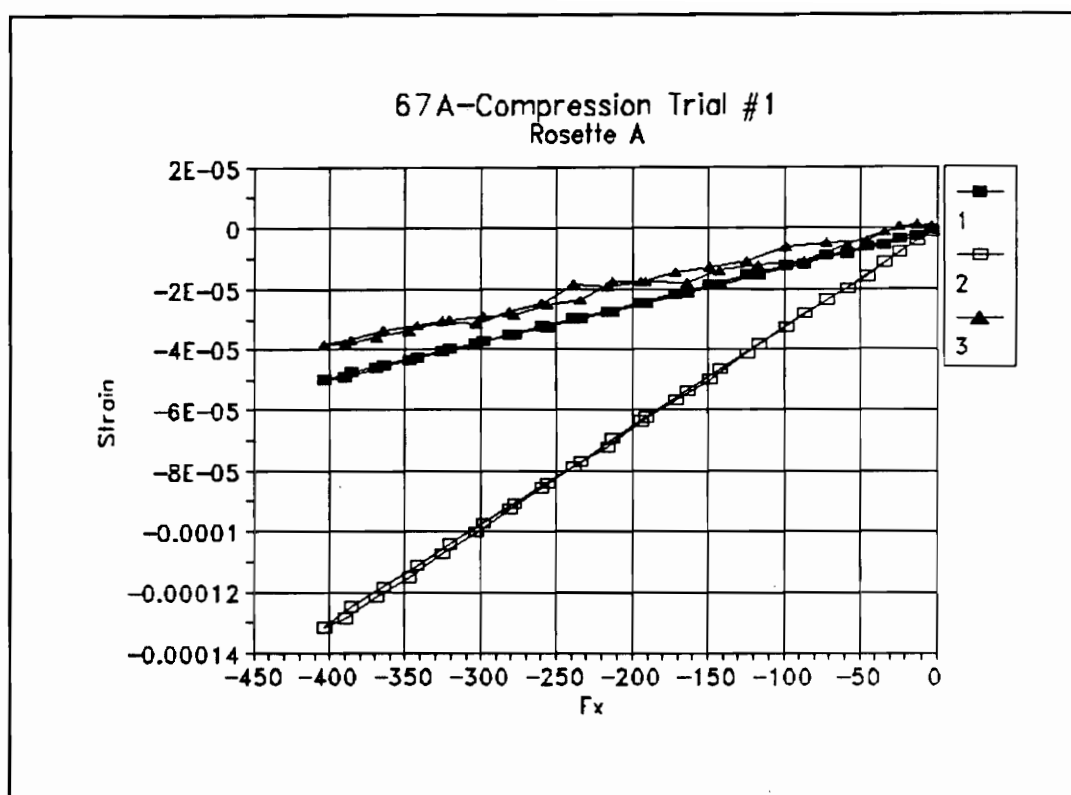


Figure B.13 Rosette A, Compression Load Trial #1

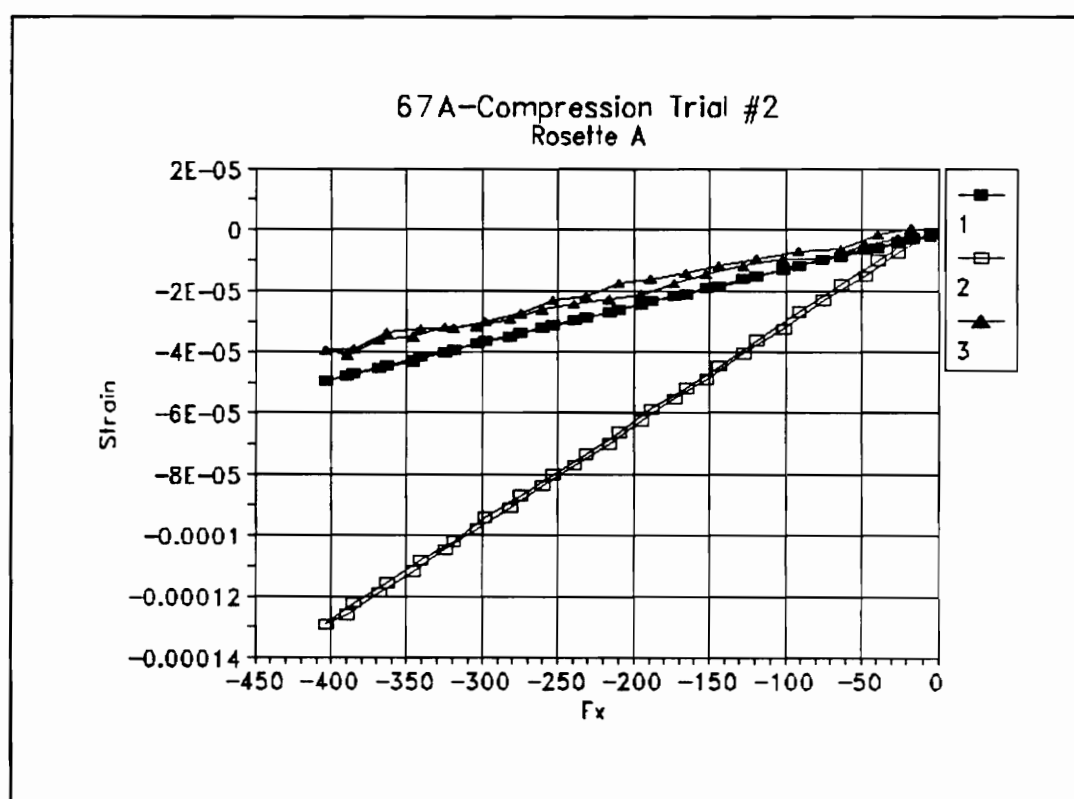


Figure B.14 Rosette A, Compression Load Trial #2

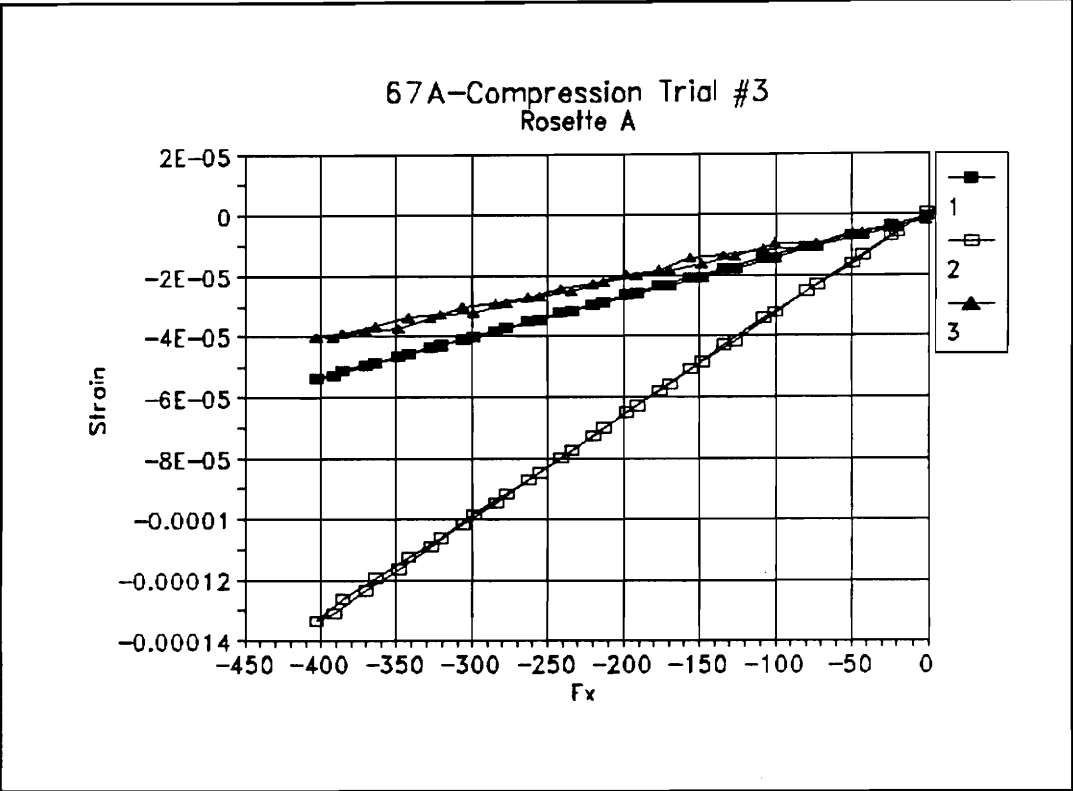


Figure B.15 Rosette A, Compression Load Trial #3

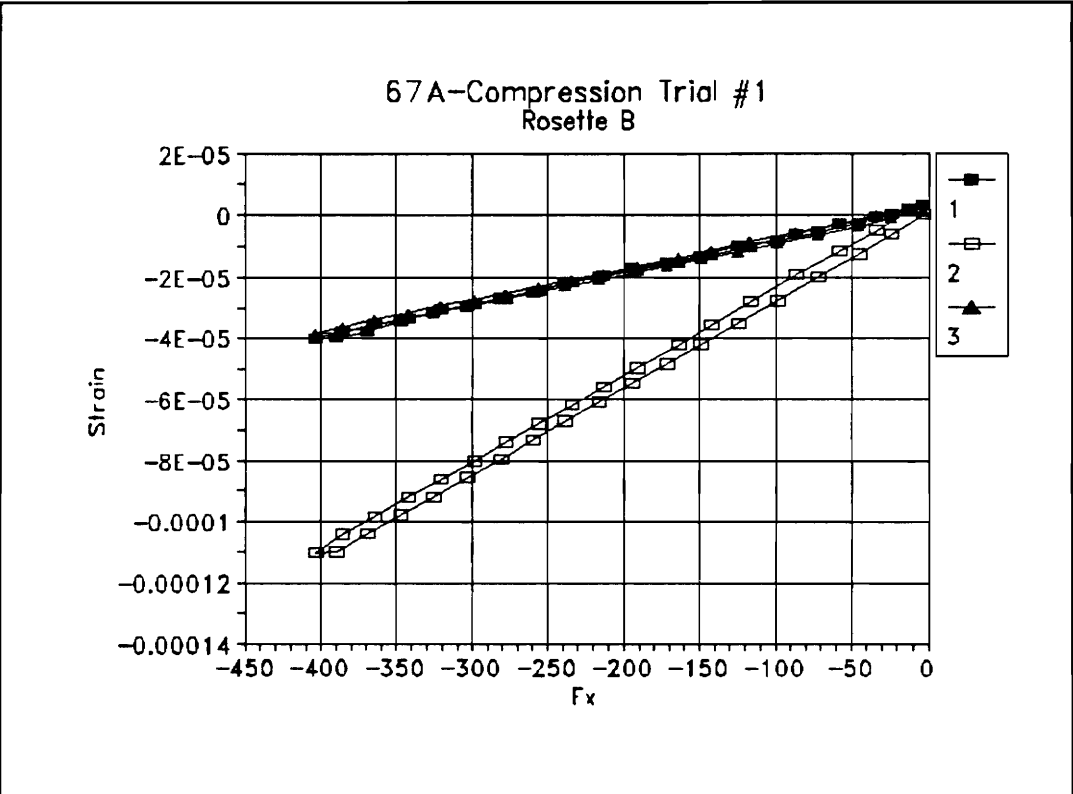


Figure B.16 Rosette B, Compression Load Trial #1

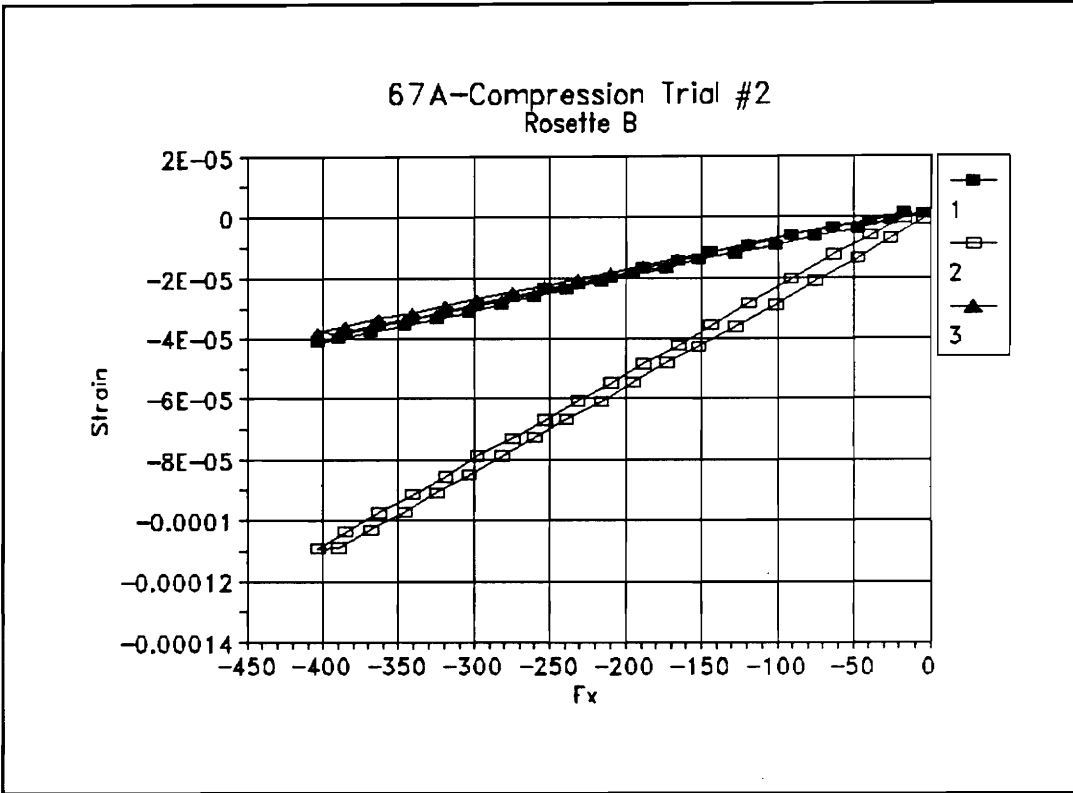


Figure B.17 Rosette B, Compression Load Trial #2

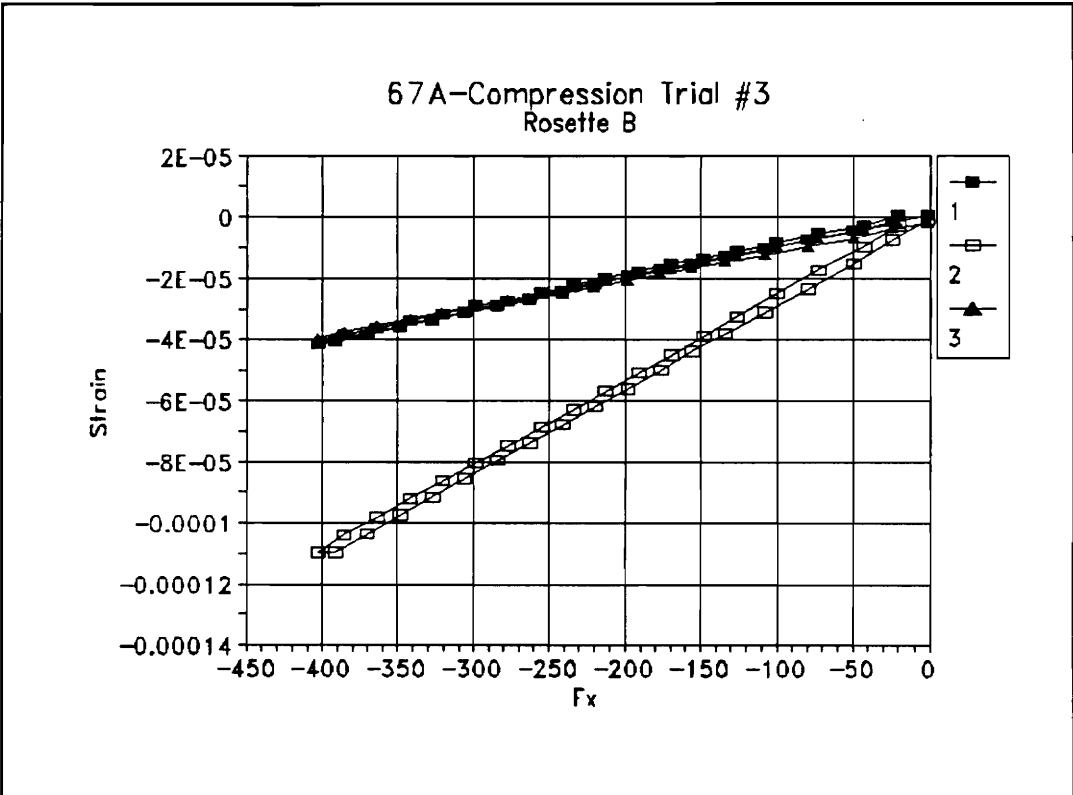


Figure B.18 Rosette B, Compression Load Trial #3

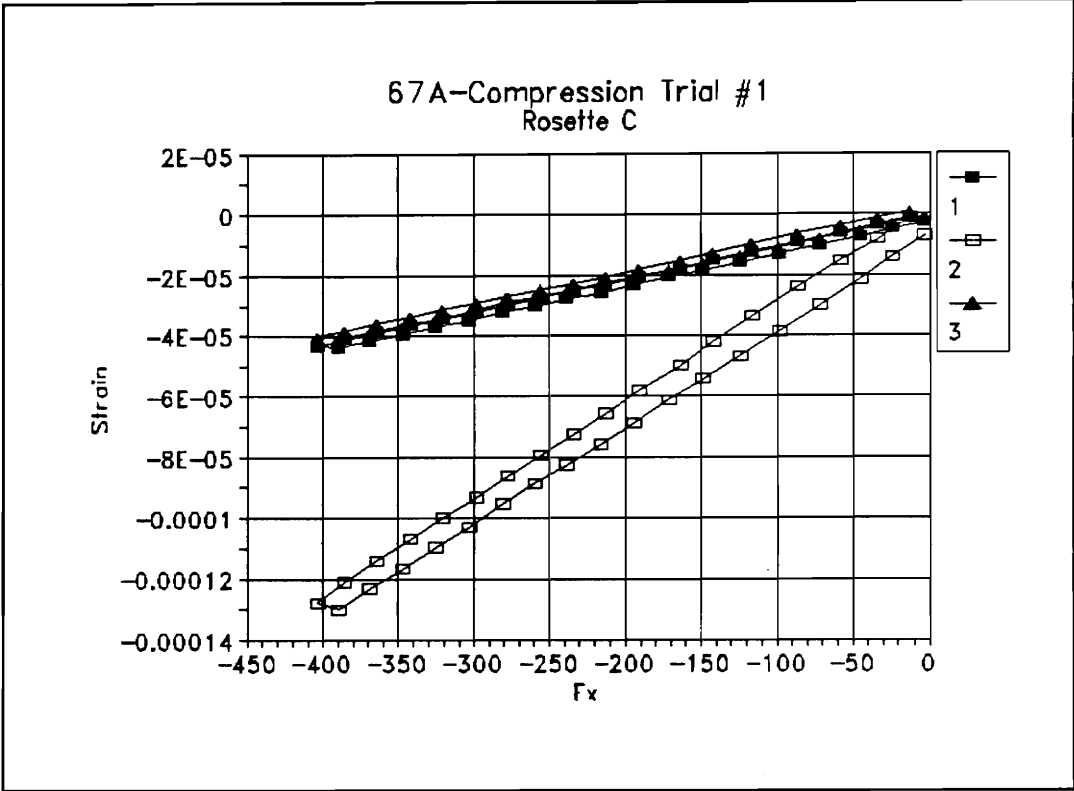


Figure B.19 Rosette C, Compression Load Trial #1

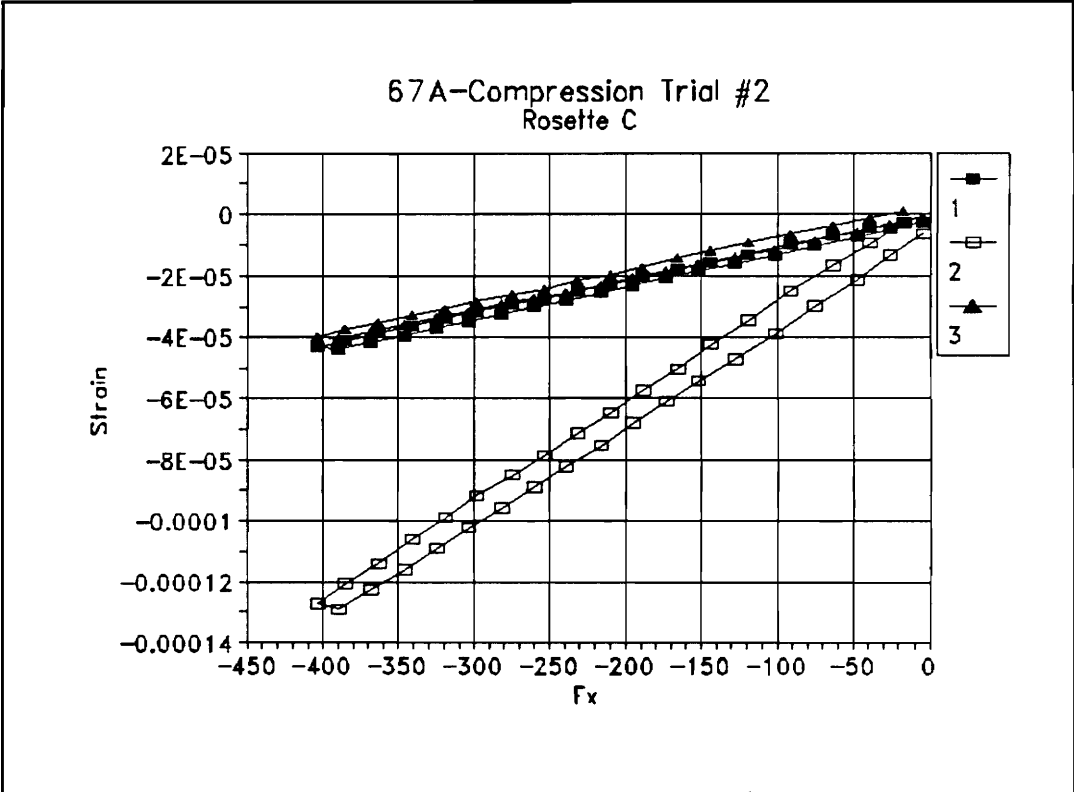


Figure B.20 Rosette C, Compression Load Trial #2

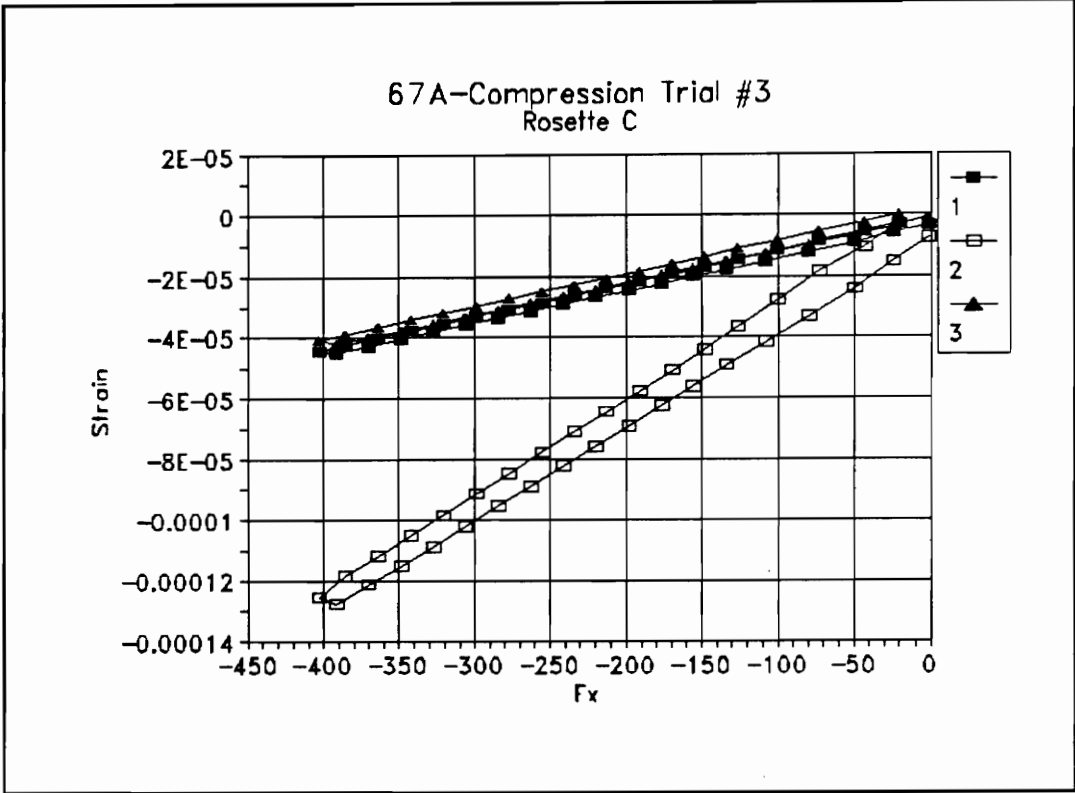


Figure B.21 Rosette C, Compression Load Trial #3

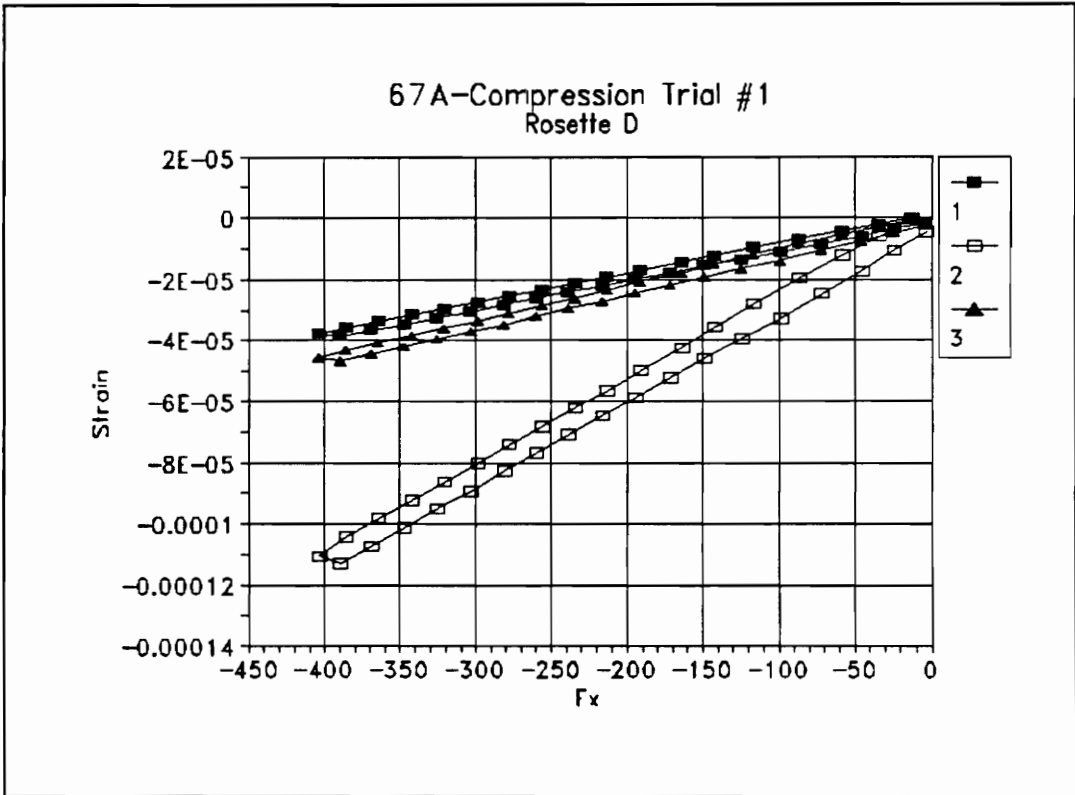


Figure B.22 Rosette D, Compression Load Trial #1

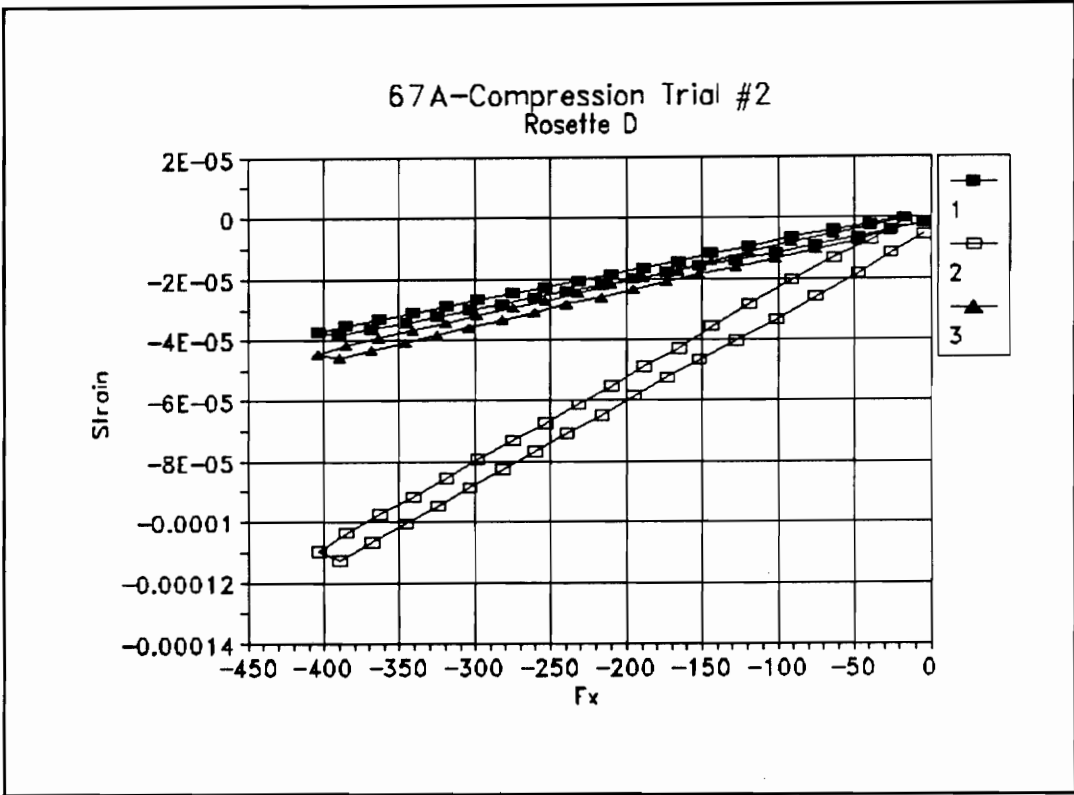


Figure B.23 Rosette D, Compression Load Trial #2

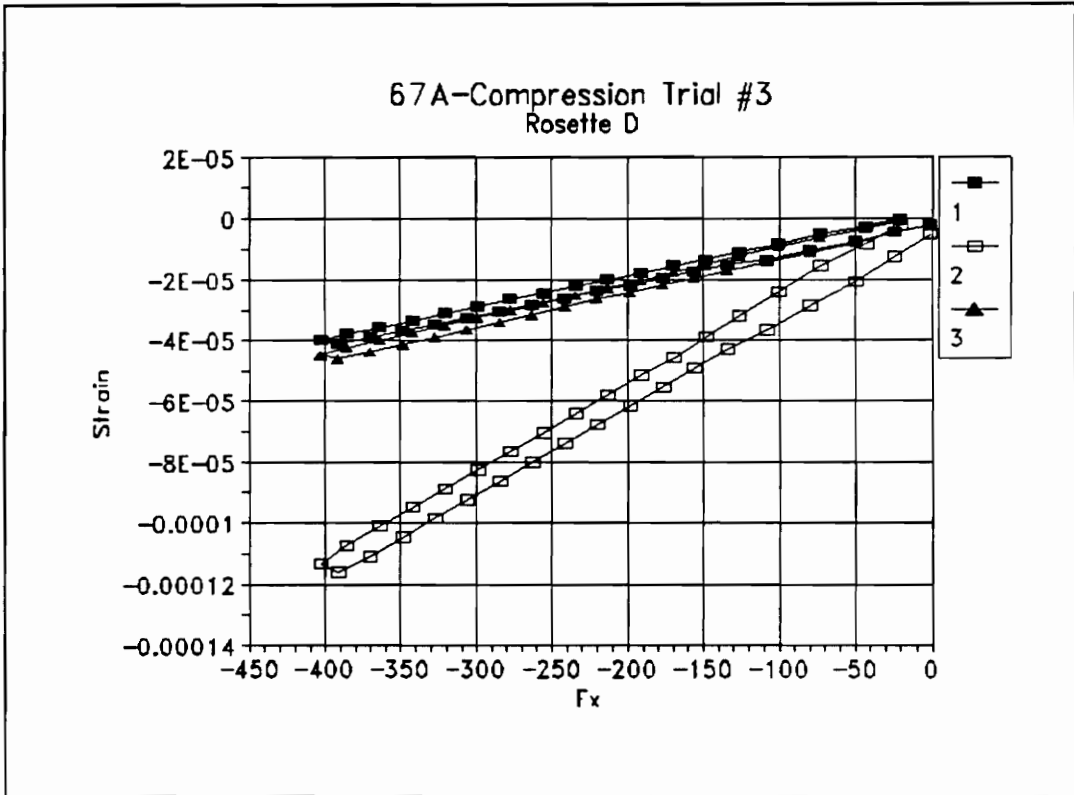


Figure B.24 Rosette D, Compression Load Trial #3

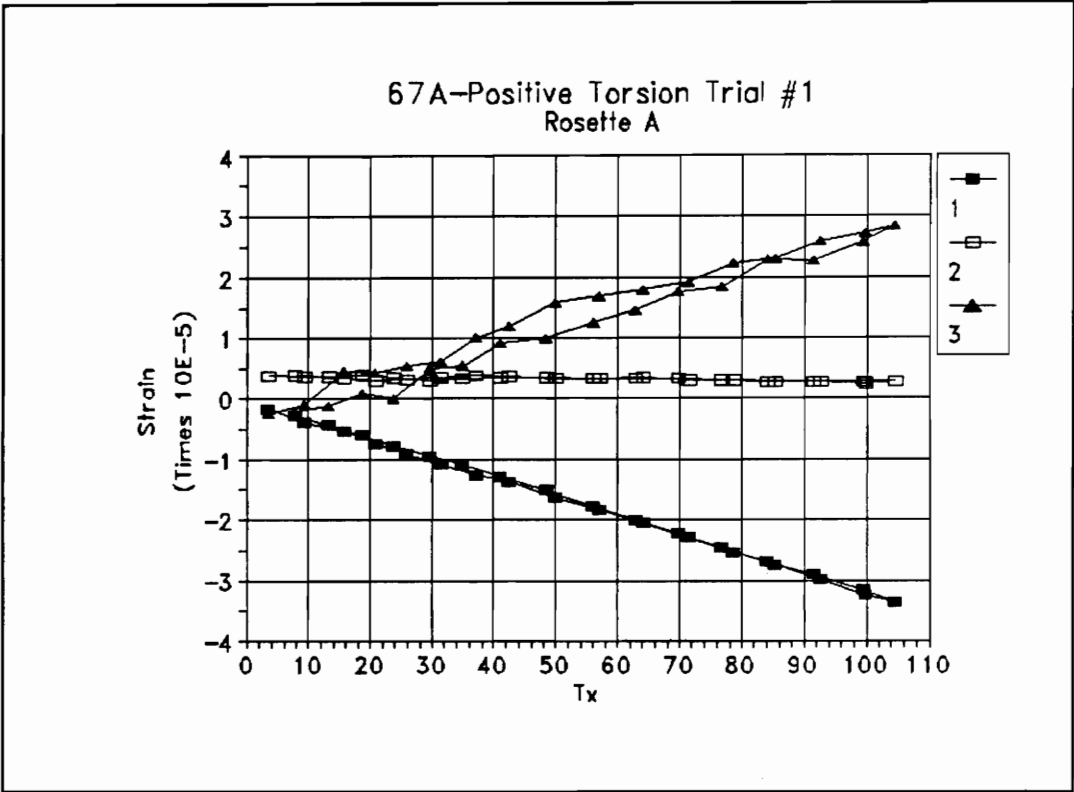


Figure B.25 Rosette A, Positive Torsion Load Trial #1

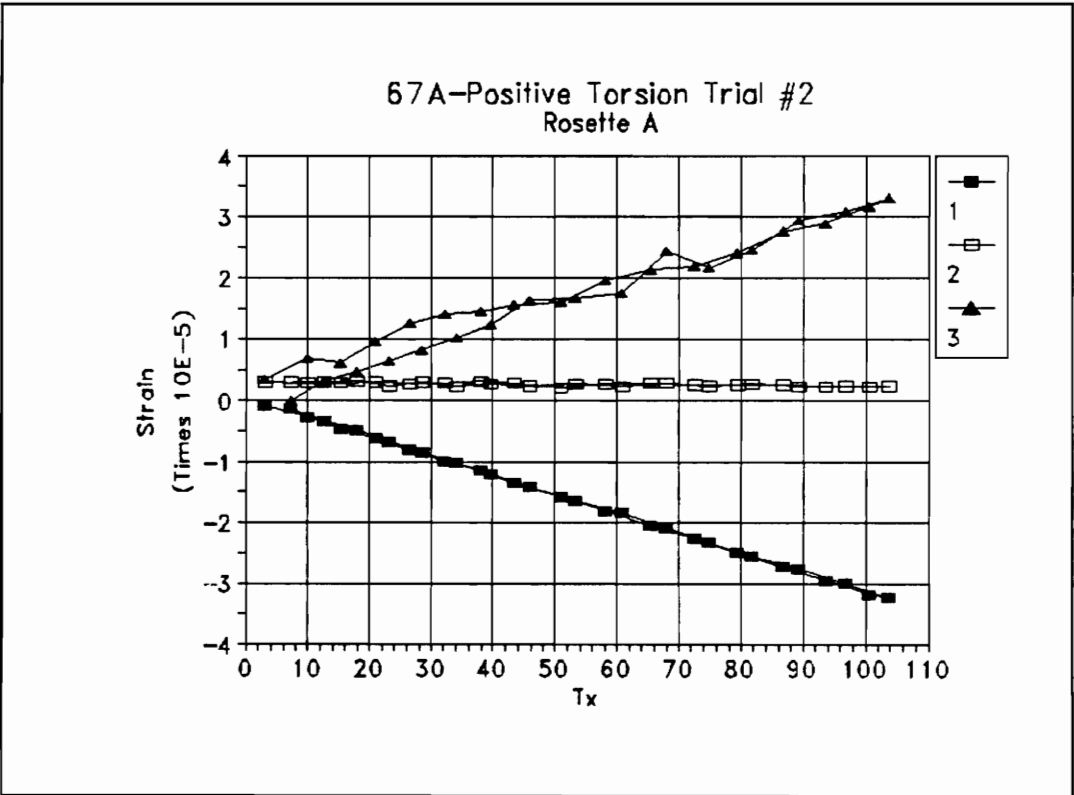


Figure B.26 Rosette A, Positive Torsion Load Trial #2

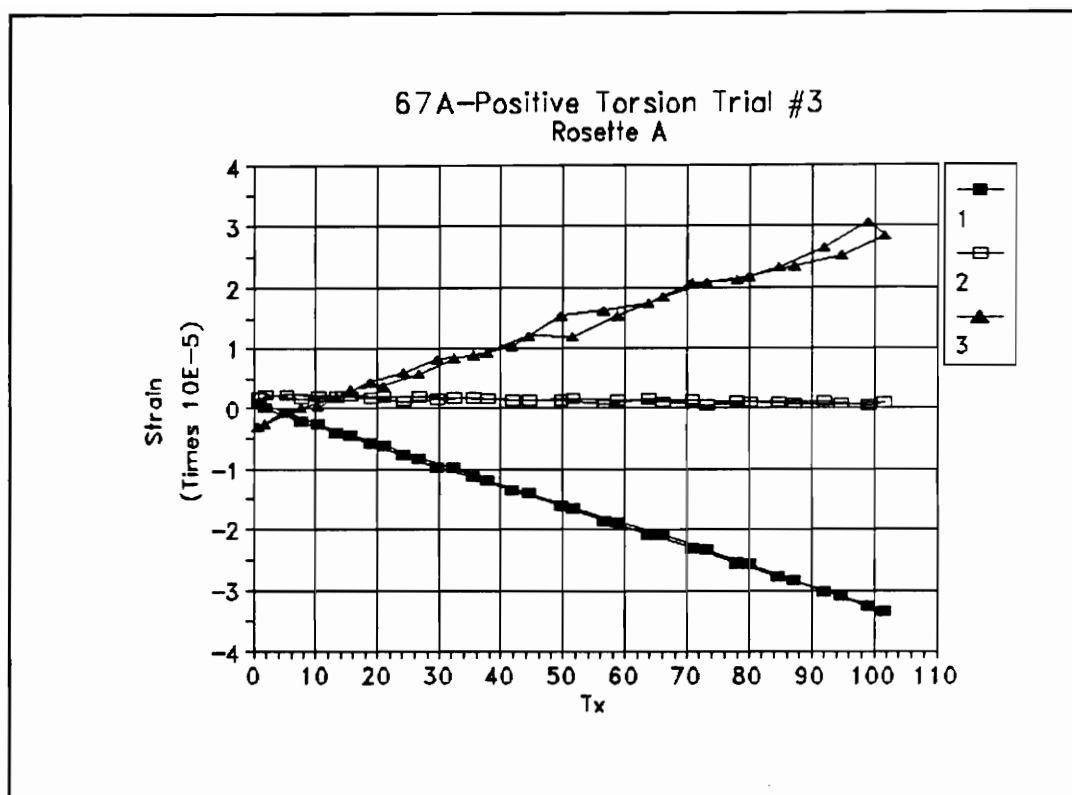


Figure B.27 Rosette A, Positive Torsion Load Trial #3

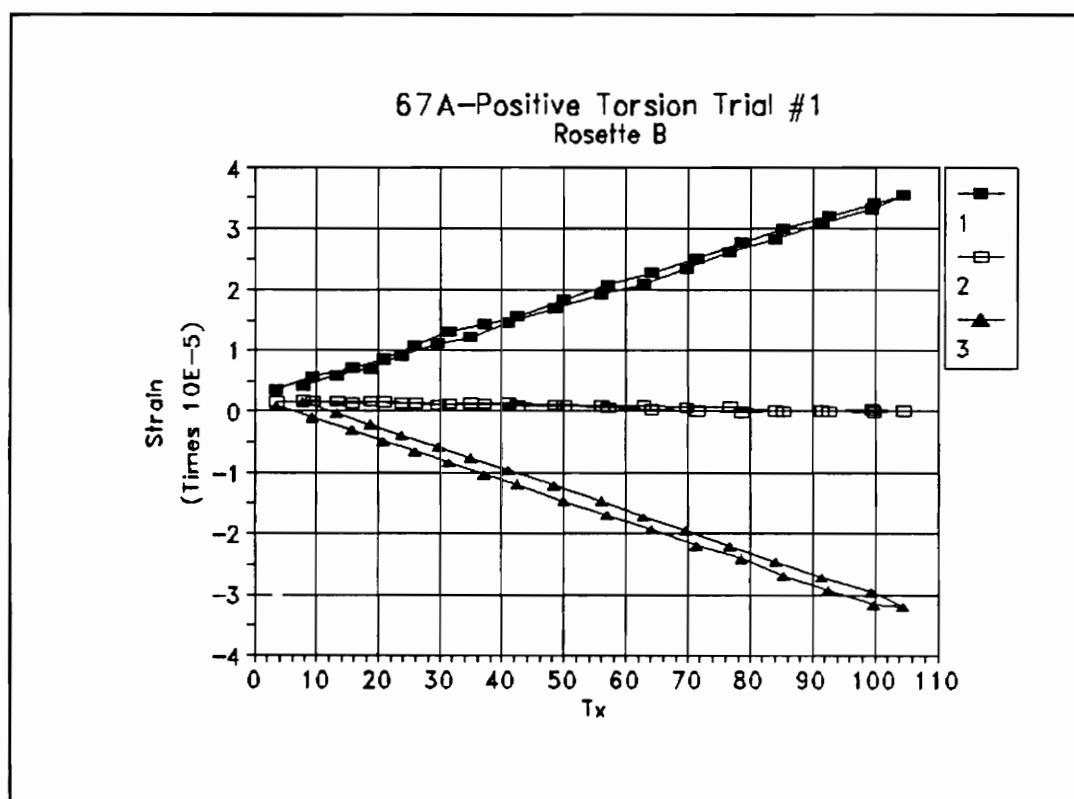


Figure B.28 Rosette B, Positive Torsion Load Trial #1

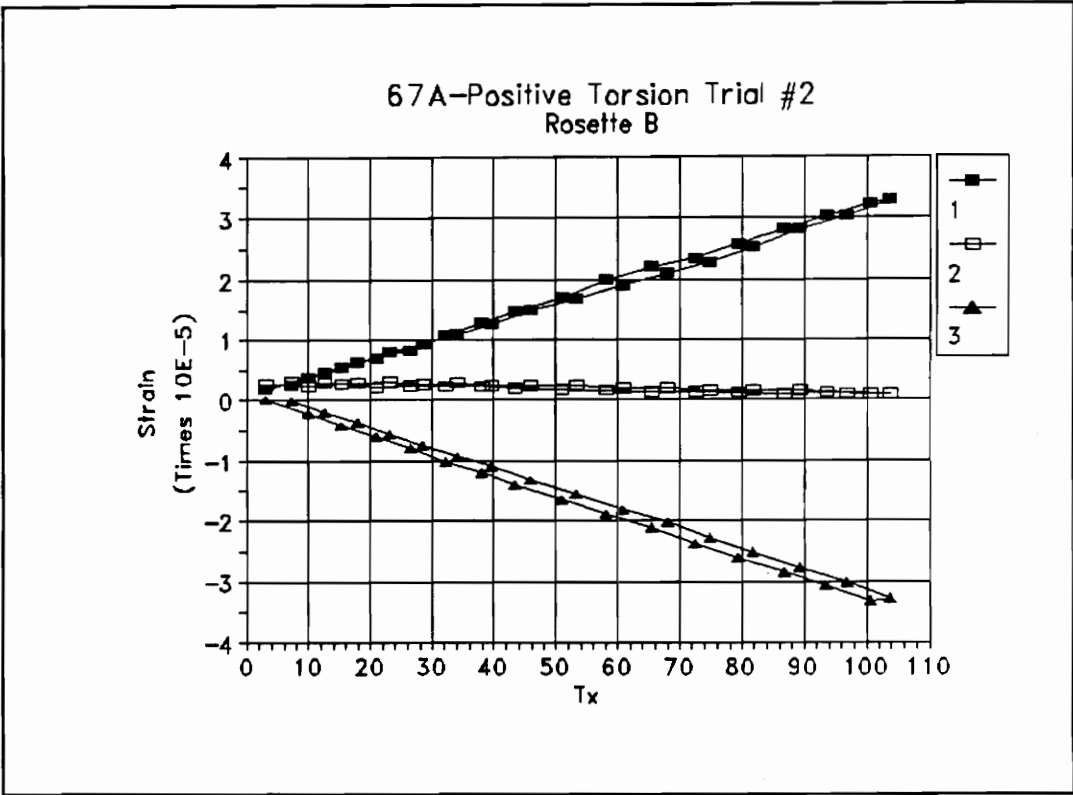


Figure B.29 Rosette B, Positive Torsion Load Trial #2

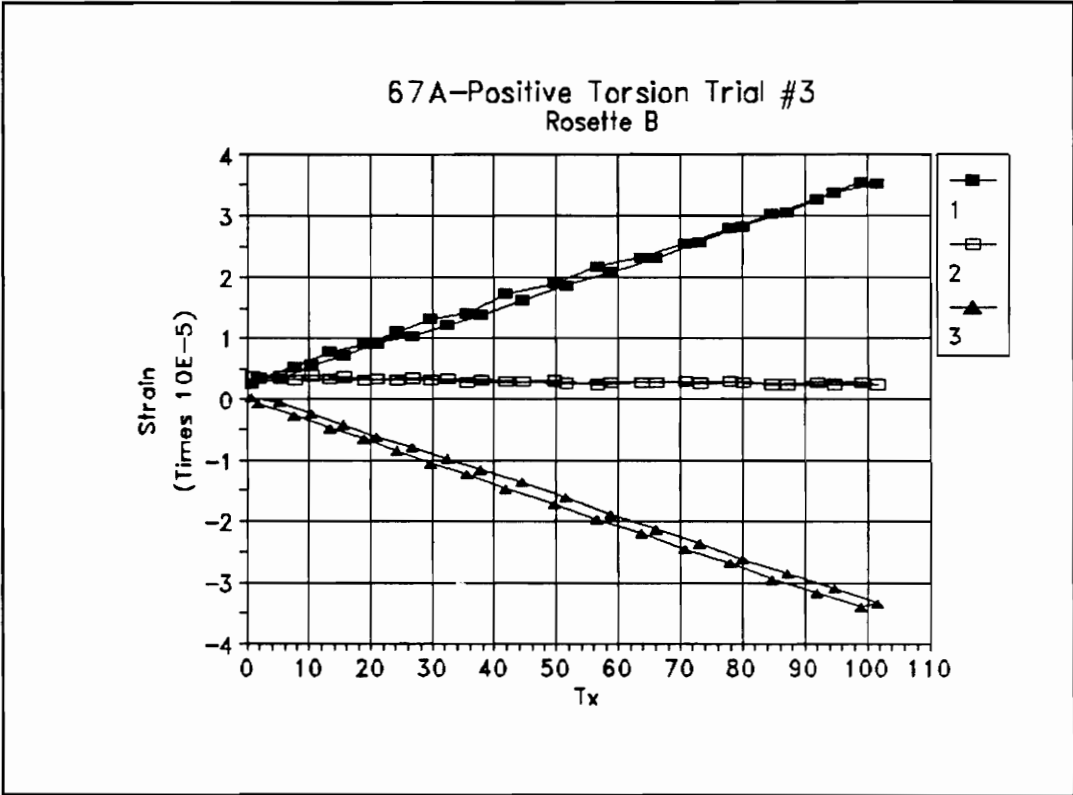


Figure B.30 Rosette B, Positive Torsion Load Trial #3

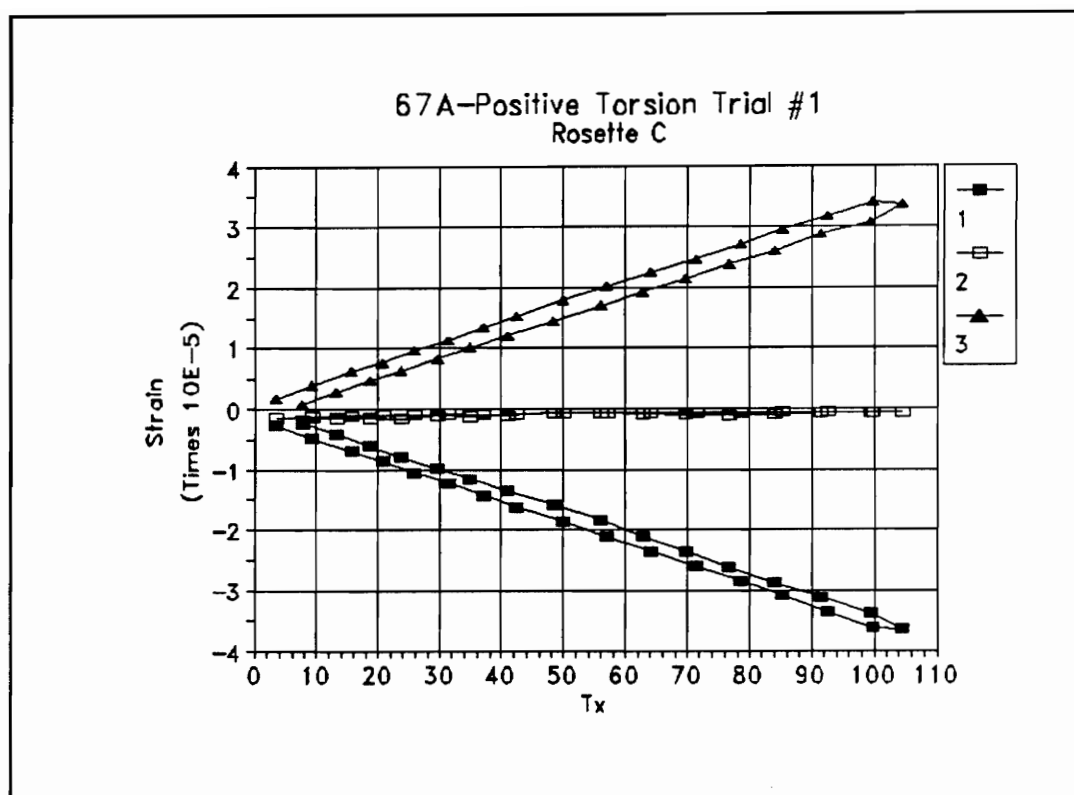


Figure B.31 Rosette C, Positive Torsion Load Trial #1

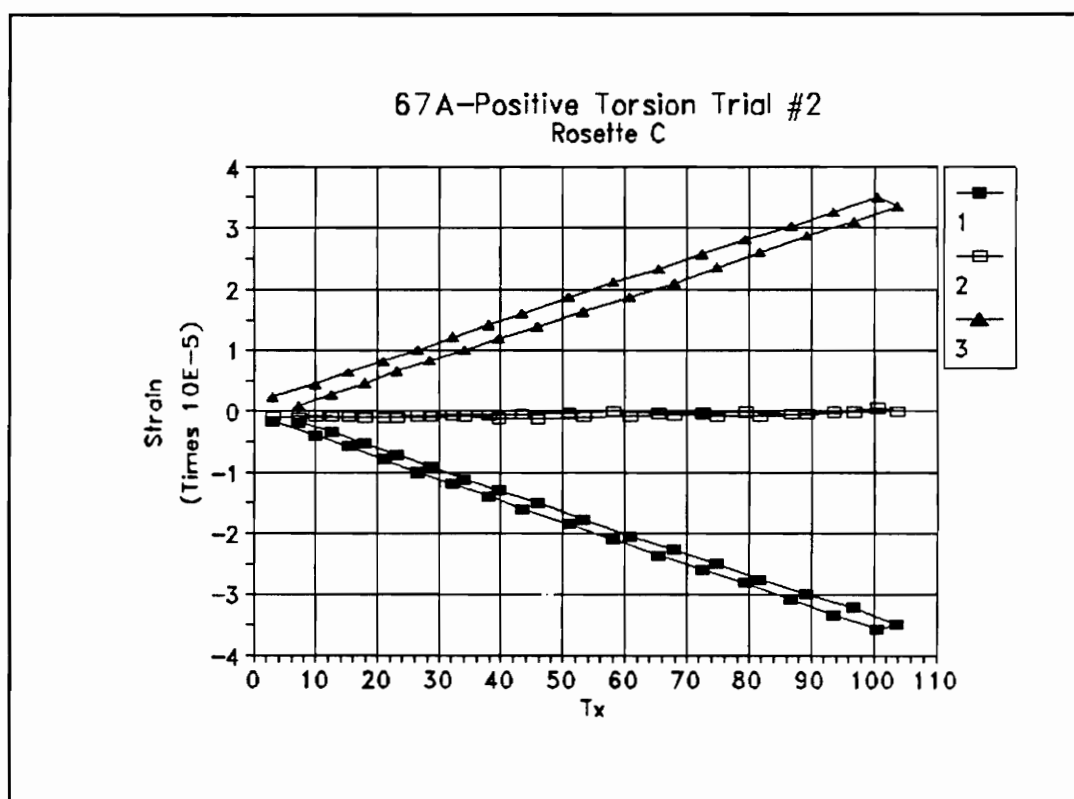


Figure B.32 Rosette C, Positive Torsion Load Trial #2

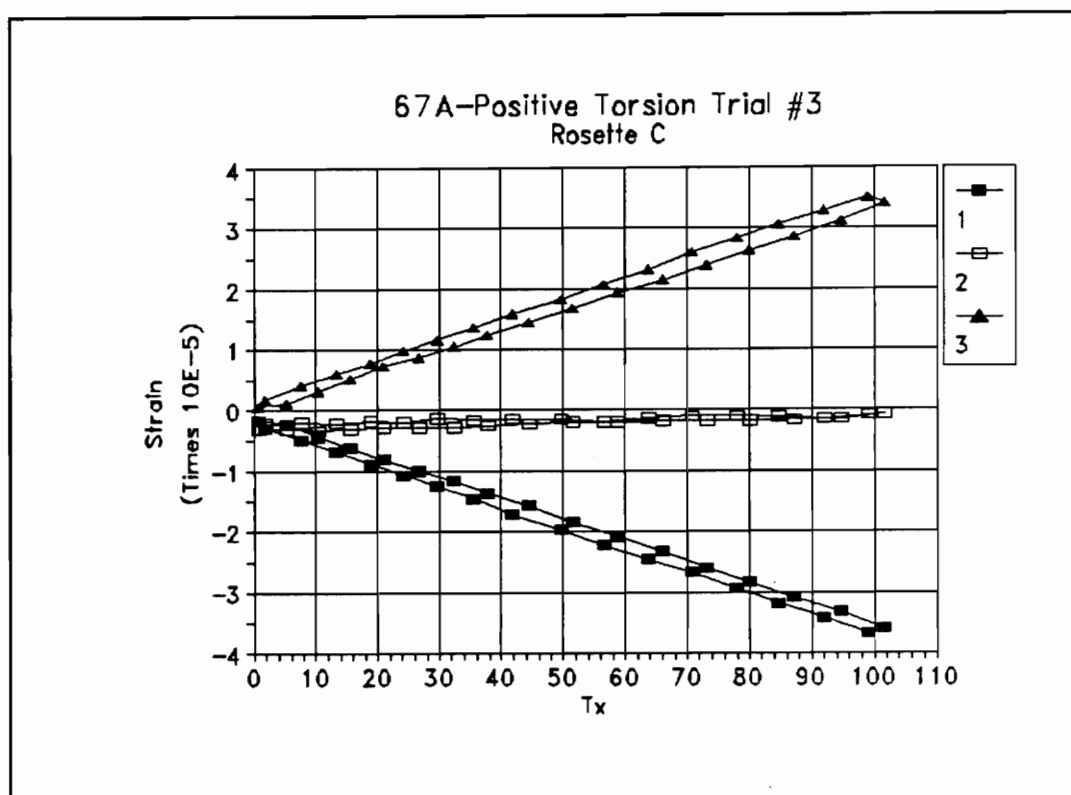


Figure B.33 Rosette C, Positive Torsion Load Trial #3

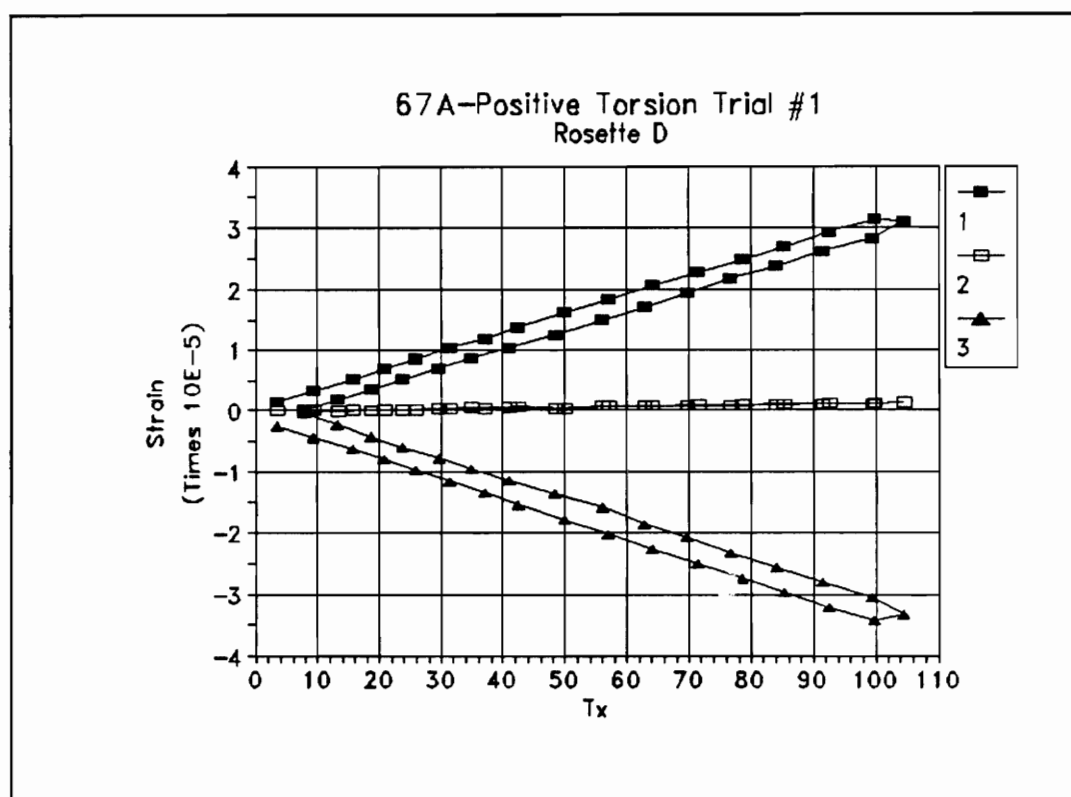


Figure B.34 Rosette D, Positive Torsion Load Trial #1

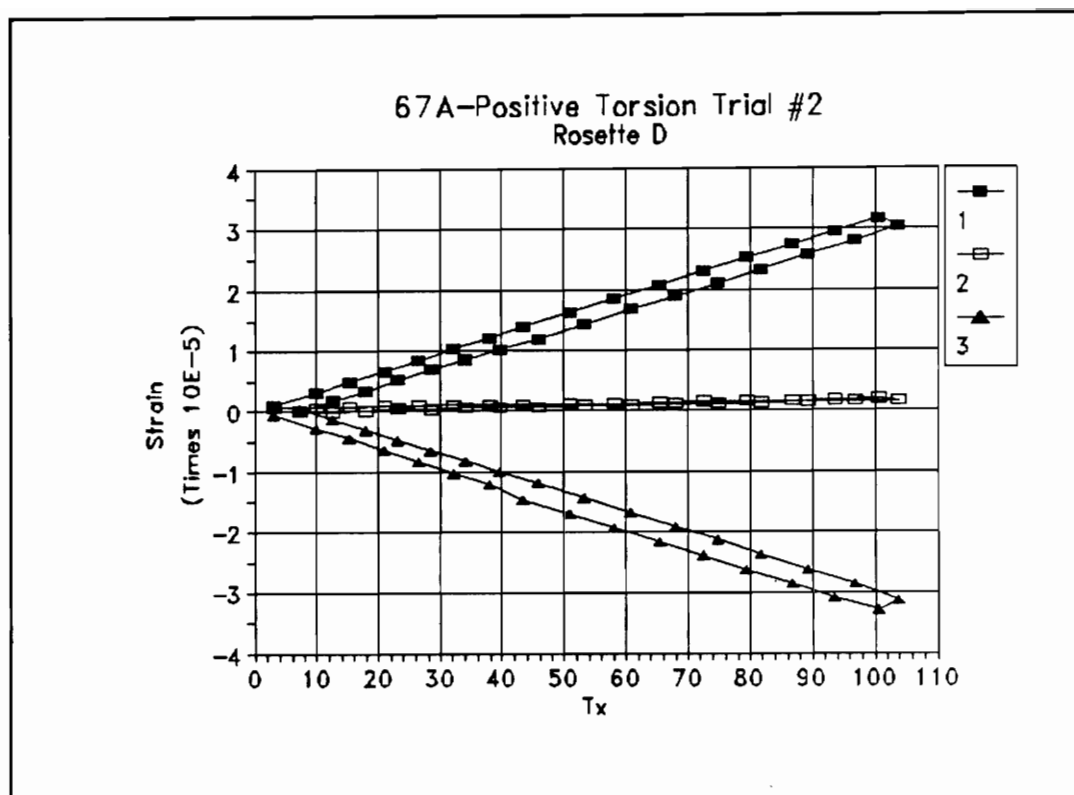


Figure B.35 Rosette D, Positive Torsion Load Trial #2

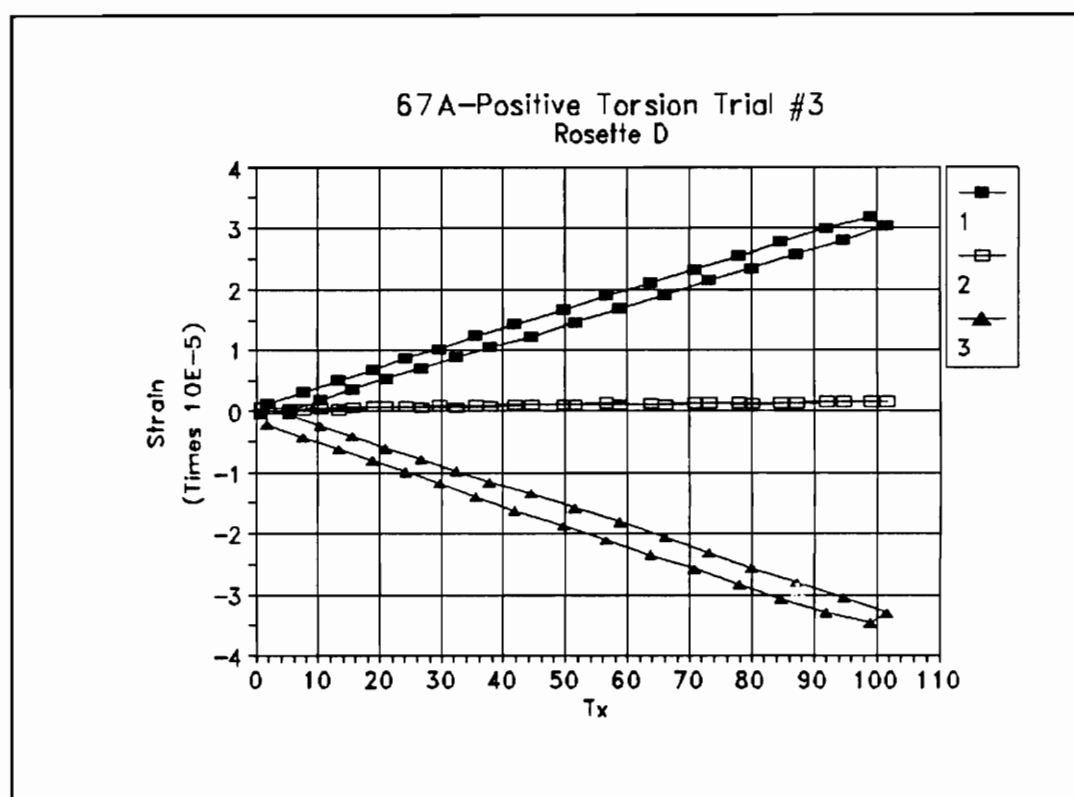


Figure B.36 Rosette D, Positive Torsion Load Trial #3

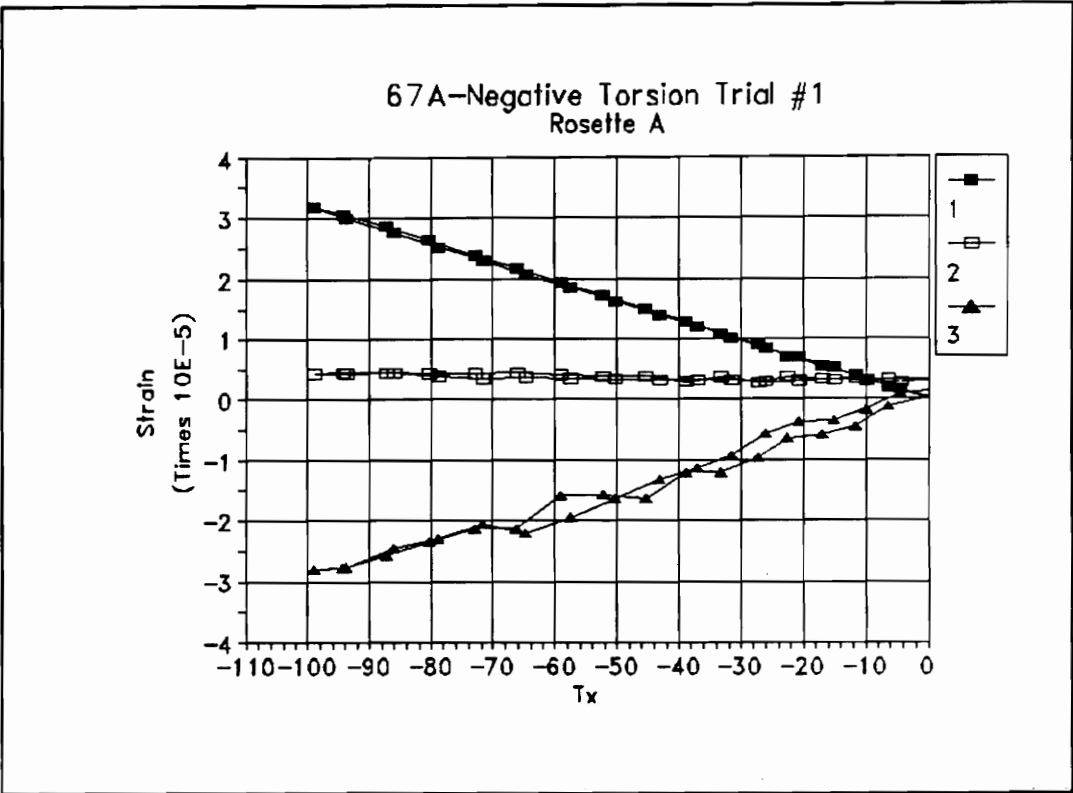


Figure B.37 Rosette A, Negative Torsion Load Trial #1

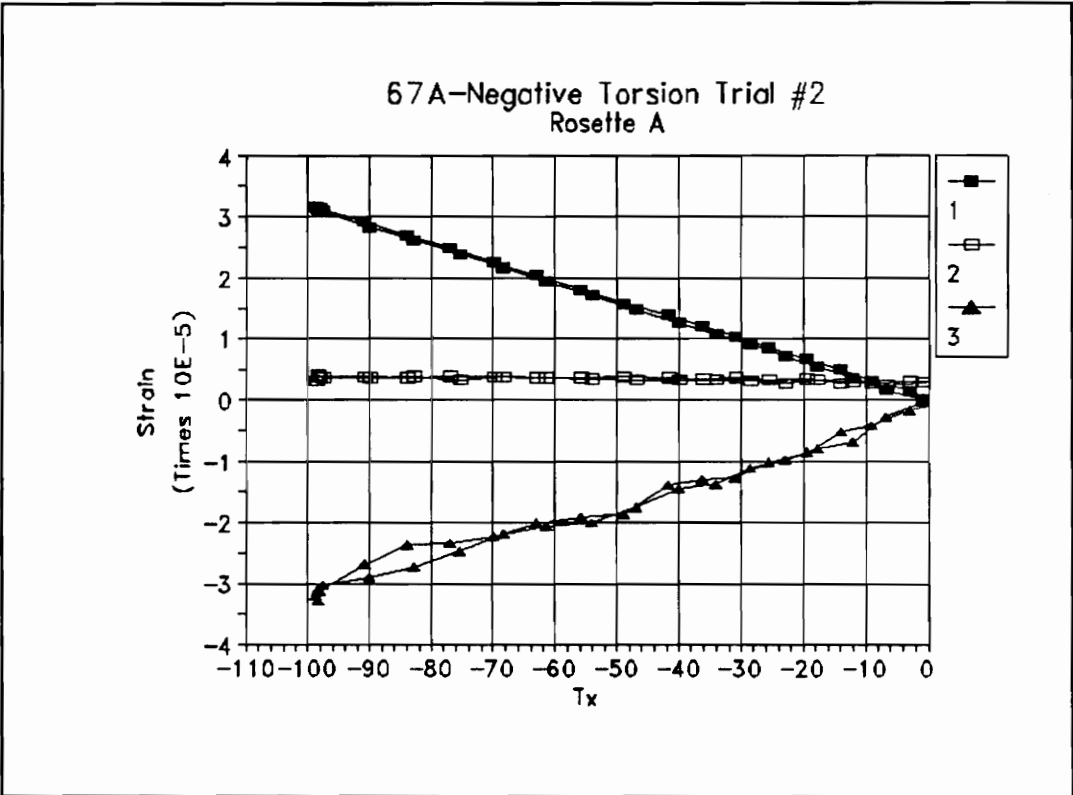


Figure B.38 Rosette A, Negative Torsion Load Trial #2

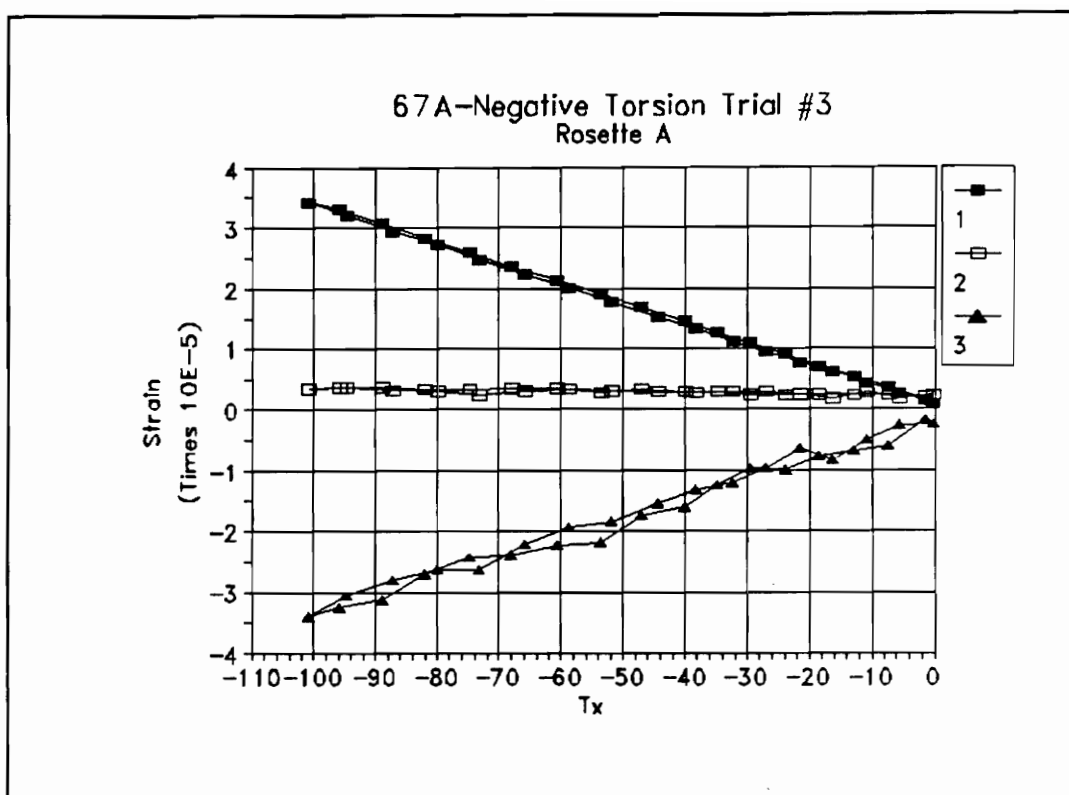


Figure B.39 Rosette A, Negative Torsion Load Trial #3

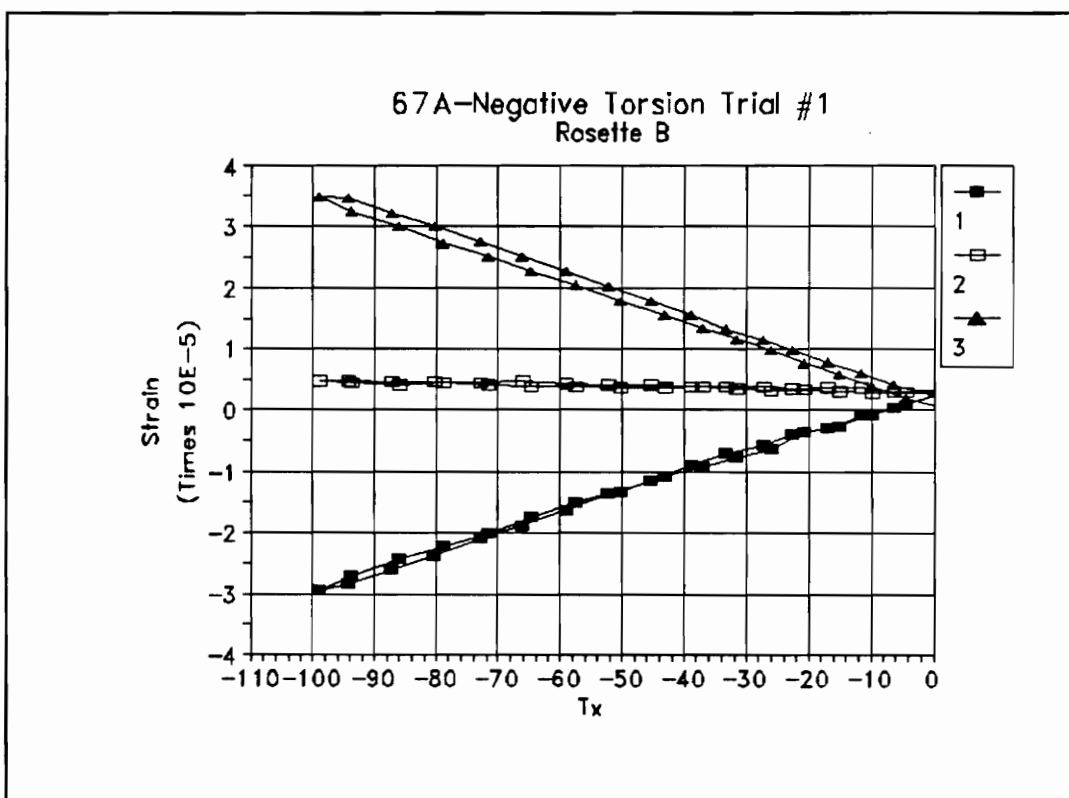


Figure B.40 Rosette B, Negative Torsion Load Trial #1

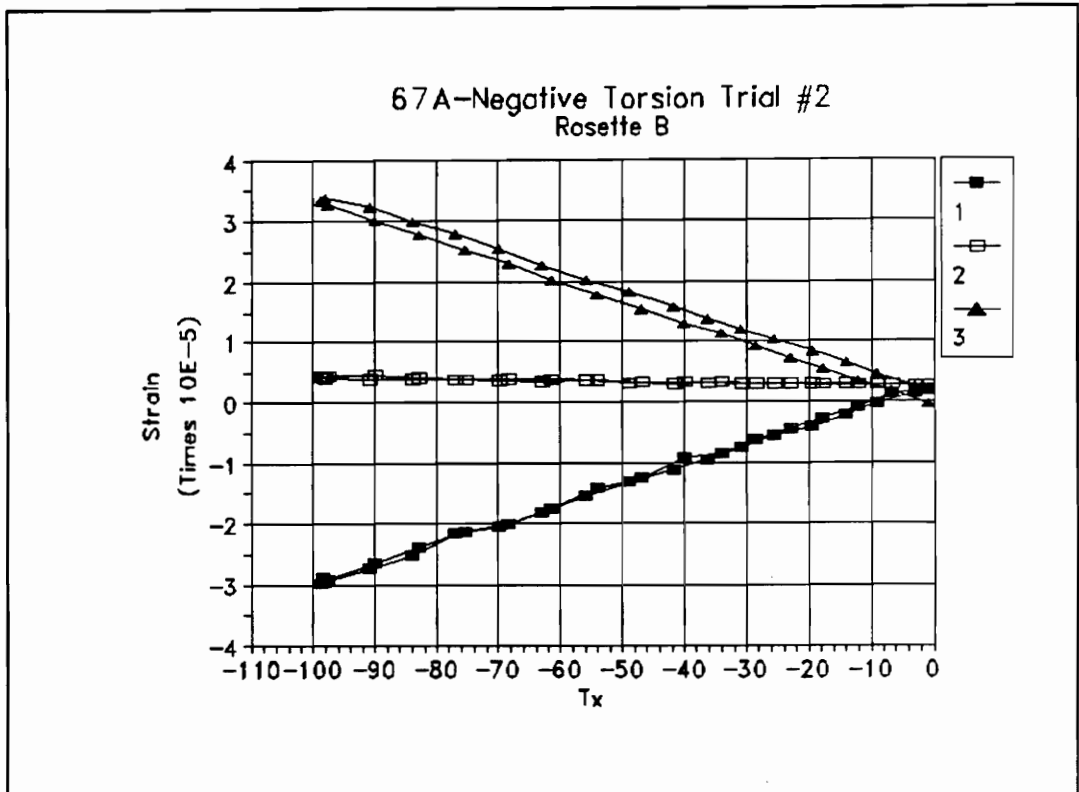


Figure B.41 Rosette B, Negative Torsion Load Trial #2

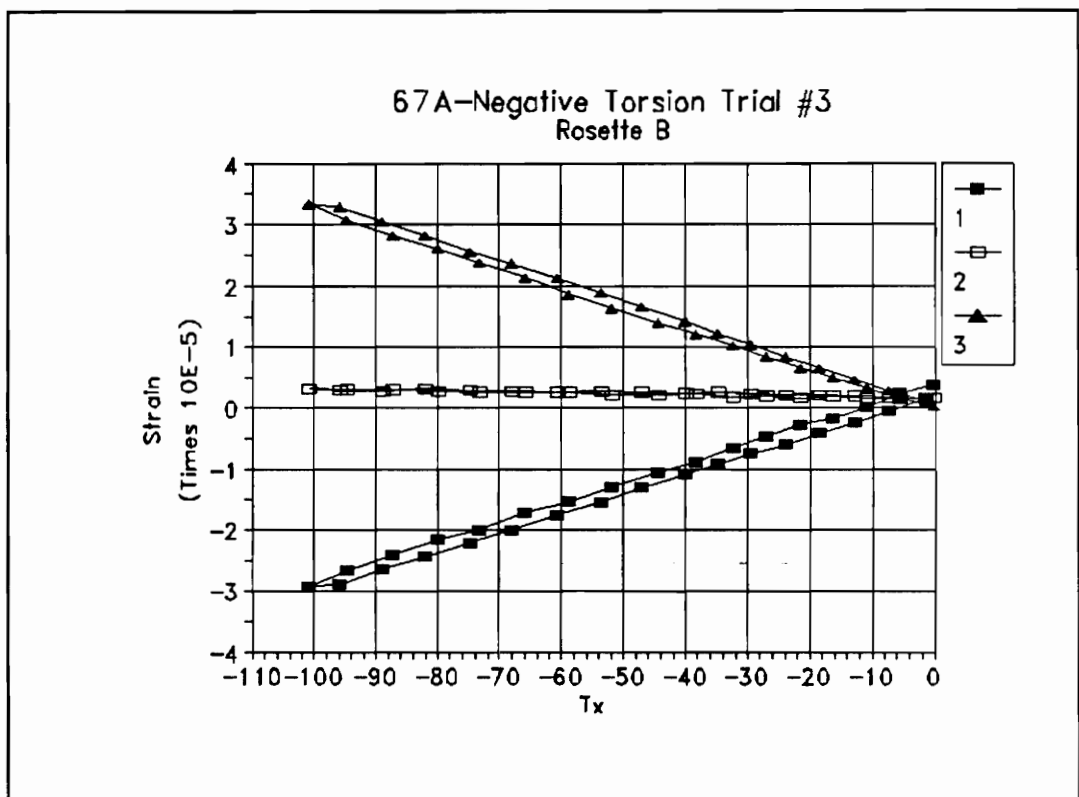


Figure B.42 Rosette B, Negative Torsion Load Trial #3

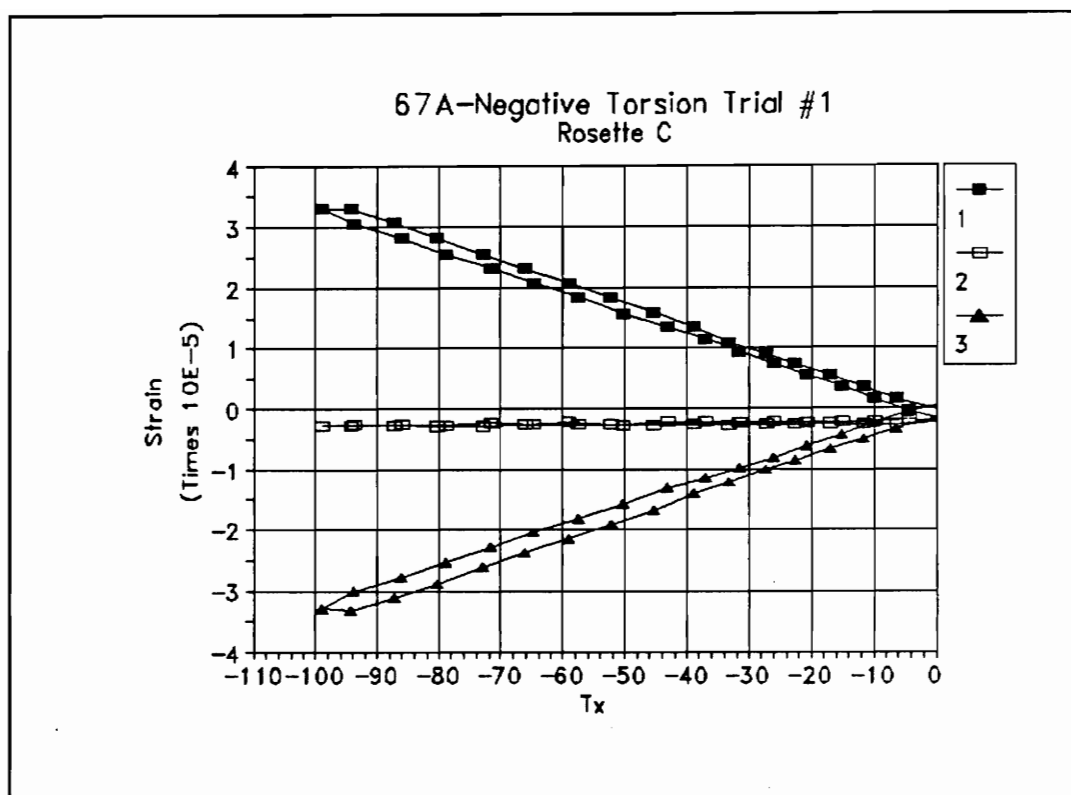


Figure B.43 Rosette C, Negative Torsion Load Trial #1

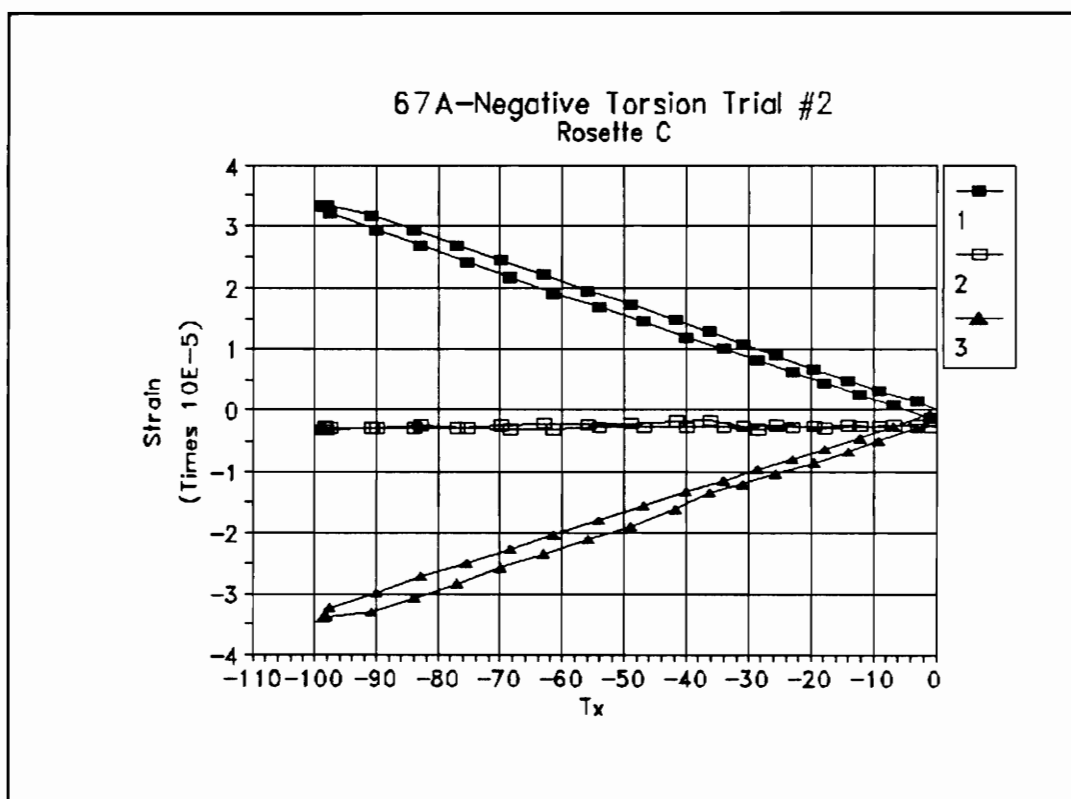


Figure B.44 Rosette C, Negative Torsion Load Trial #2

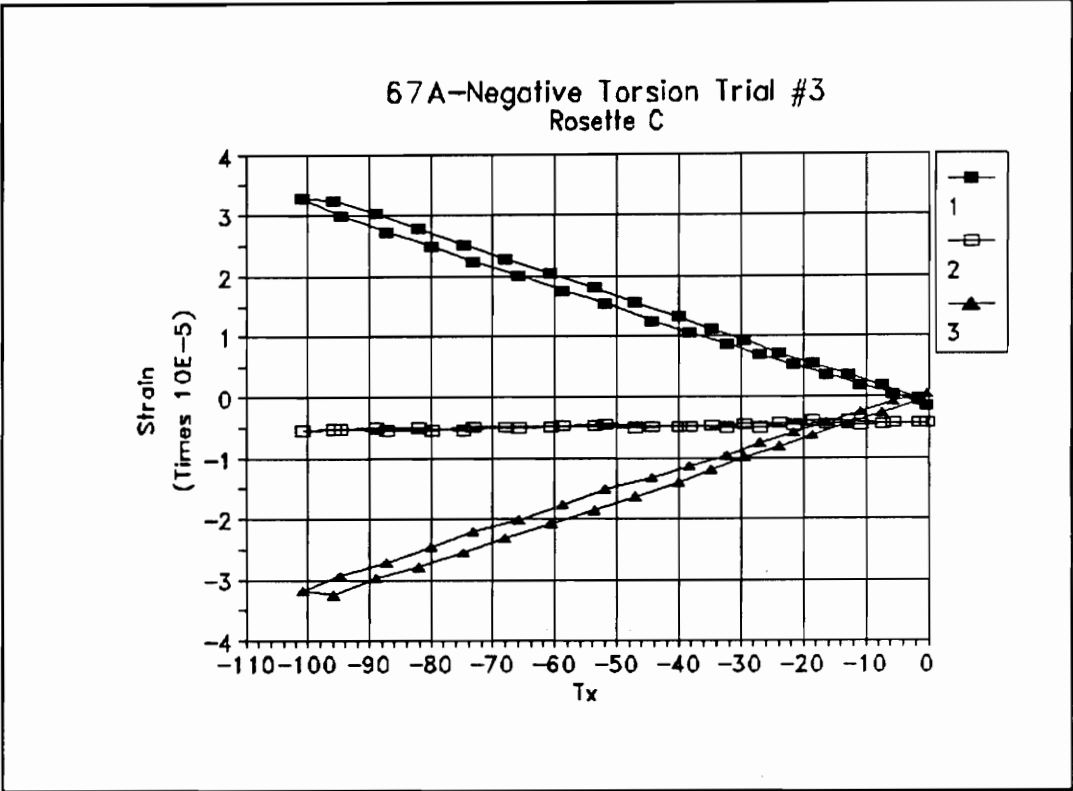


Figure B.45 Rosette C, Negative Torsion Load Trial #3

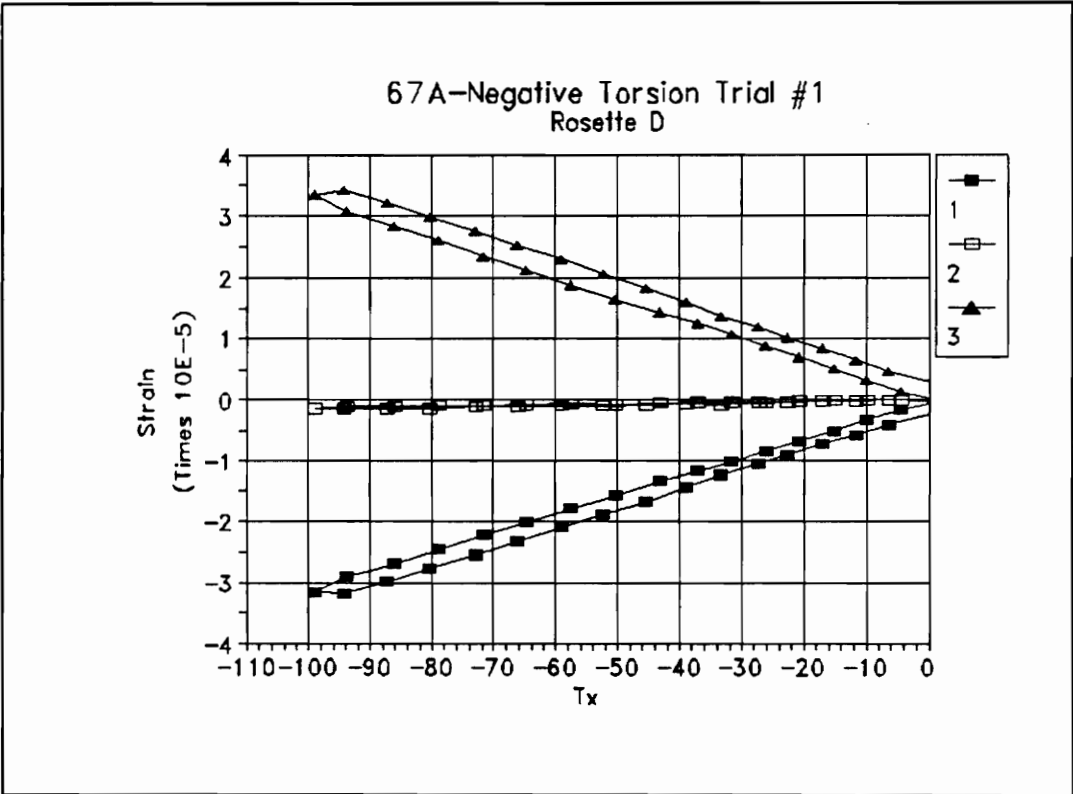


Figure B.46 Rosette D, Negative Torsion Load Trial #1

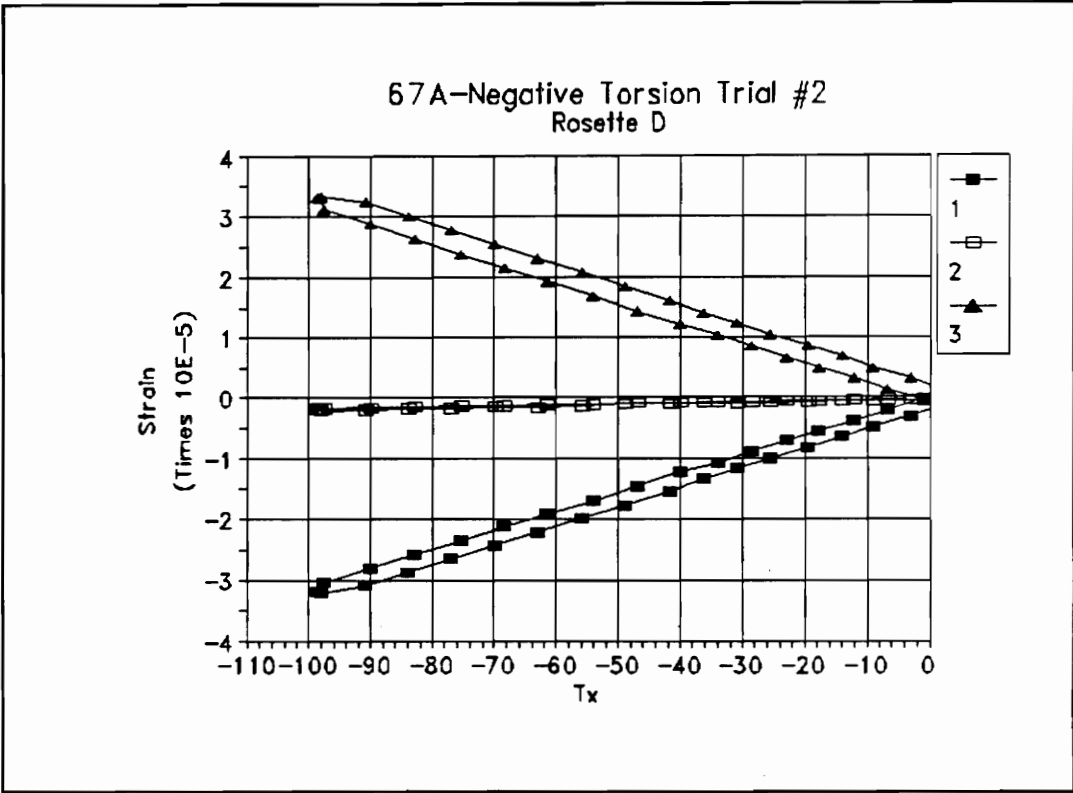


Figure B.47 Rosette D, Negative Torsion Load Trial #2

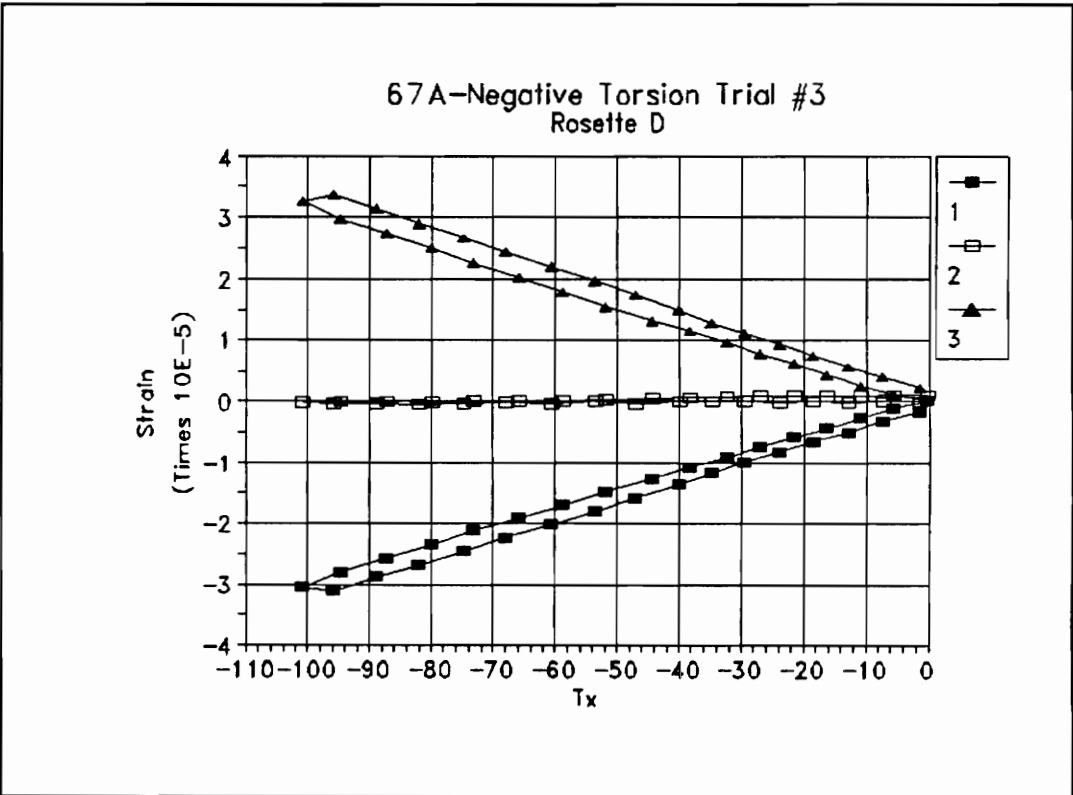


Figure B.48 Rosette D, Negative Torsion Load Trial #3

# Appendix C

## Effect of Gauge Position

The effect of the surface "patch" pattern on the surface strains is a prime concern for the filament wound specimens available. Specifically, how does the strain state vary over a given patch. A strain gauge rosette does not measure the entire strain state at a point. It measures three separate extensional strains at three separate points. If the strain state varies significantly within this region the measurement is inherently flawed. This effect can be reduced by using smaller gauges which can be placed closer together but, in this case, larger gauges are desired to reduce the effect of the surface roughness on the measurements.

A secondary effort was made to obtain qualitative information regarding the effect of strain gauge position on measured strain response for axial and torsional loads. This was done by collecting data from gauges E, F, G, and H (Fig. C.1) on specimen 67A under axial and torsional loads.

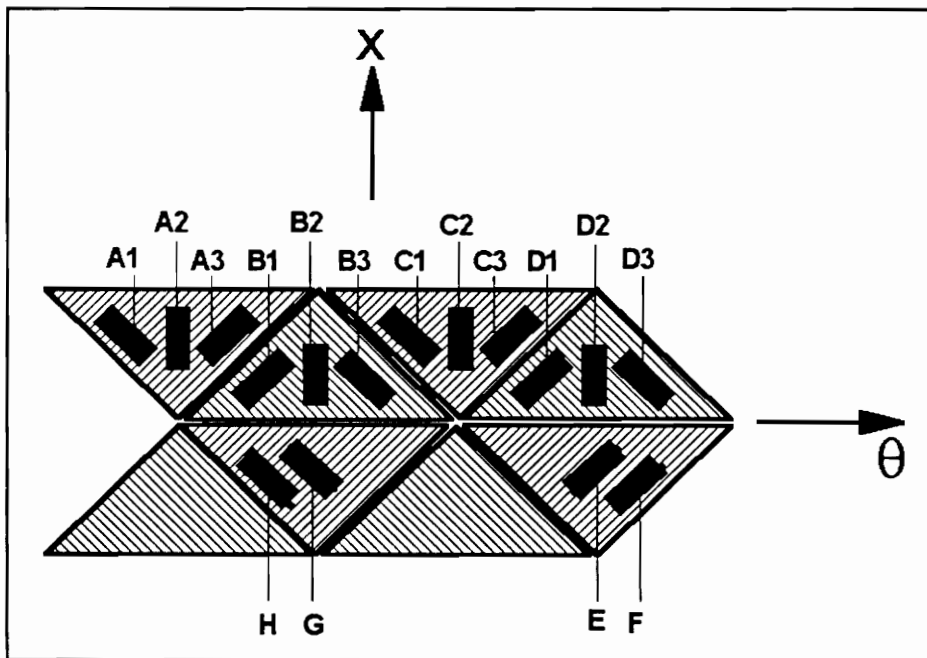


Figure C.1 Strain Gauge Positions, Specimen 67A

Gauges E and F are aligned with the fibers and therefore measure  $\epsilon_1$  while gauges G and H are perpendicular to the fibers and measure  $\epsilon_2$ . Gauges E and G are located at the center of the patch and gauges H and F are close to the edges.

Note that Fig. D.1 is not to scale. Gauges E, F, G, and H are substantially larger than those composing the strain gauge rosettes (A-D) above them. The off-axis gauges for the rosettes are also not exactly aligned with the fiber direction and are much further from the patch edges than gauges F and H.

Four loads were considered; tension, compression and  $\pm$  torsion. Four trials were done for each of the axial loads and three trials were recorded for each of the torsional loads. Plots of the first trial of each load are now presented.

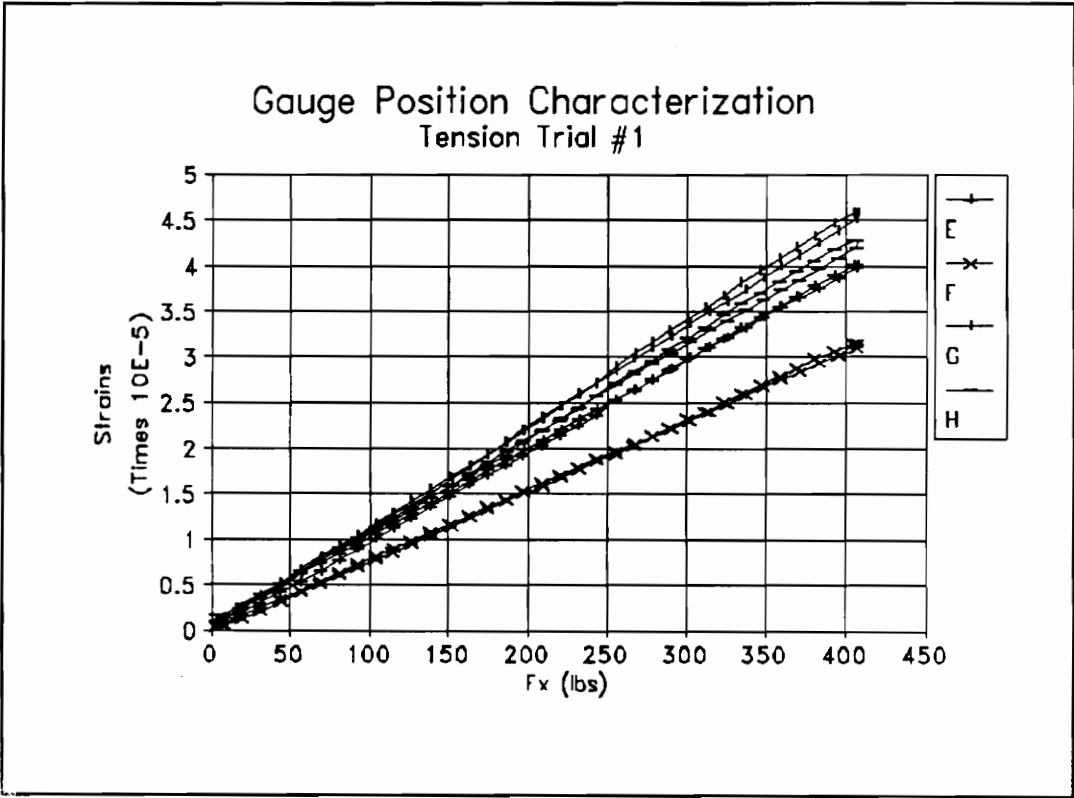


Figure C.2 Sample Tension Trial, Gauges E, F, G, H

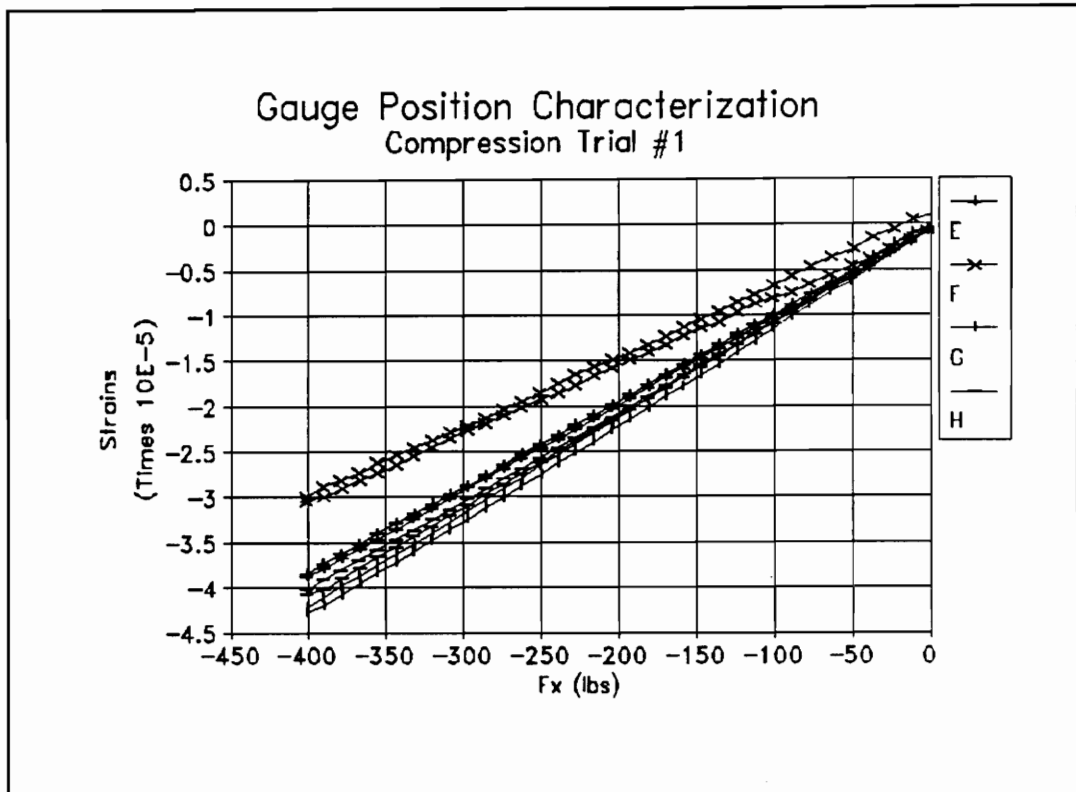


Figure C.3 Sample Compression Trial, Gauges E, F, G, H

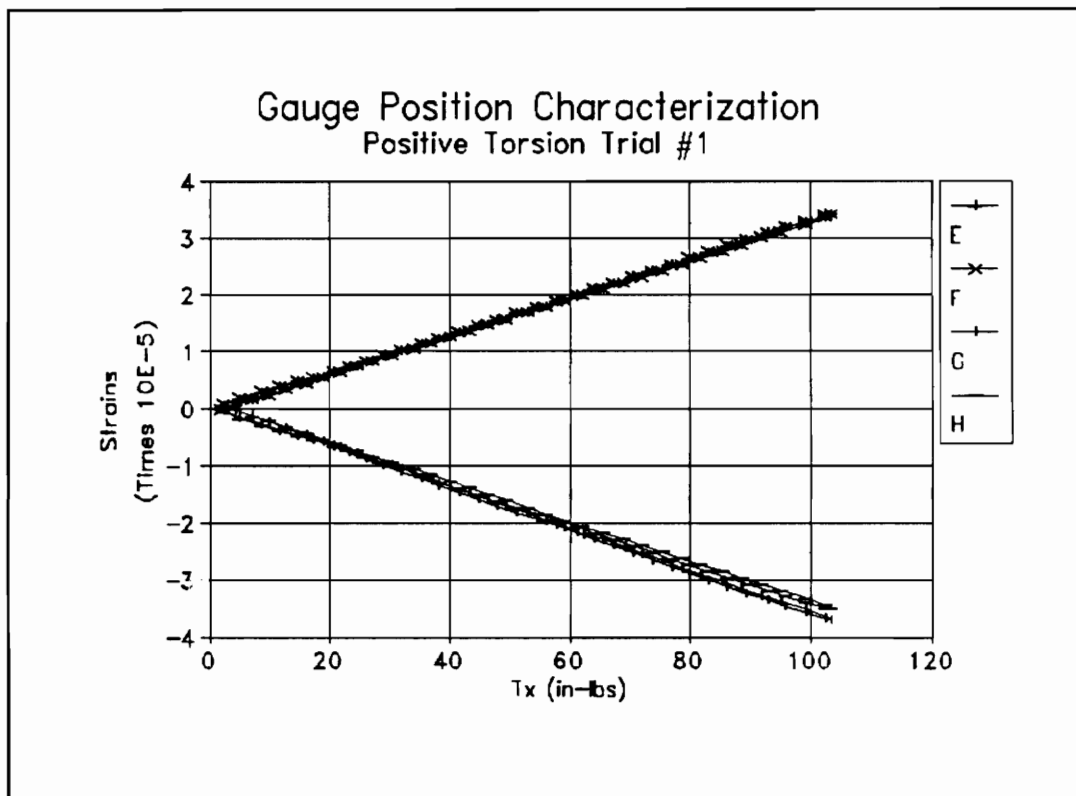
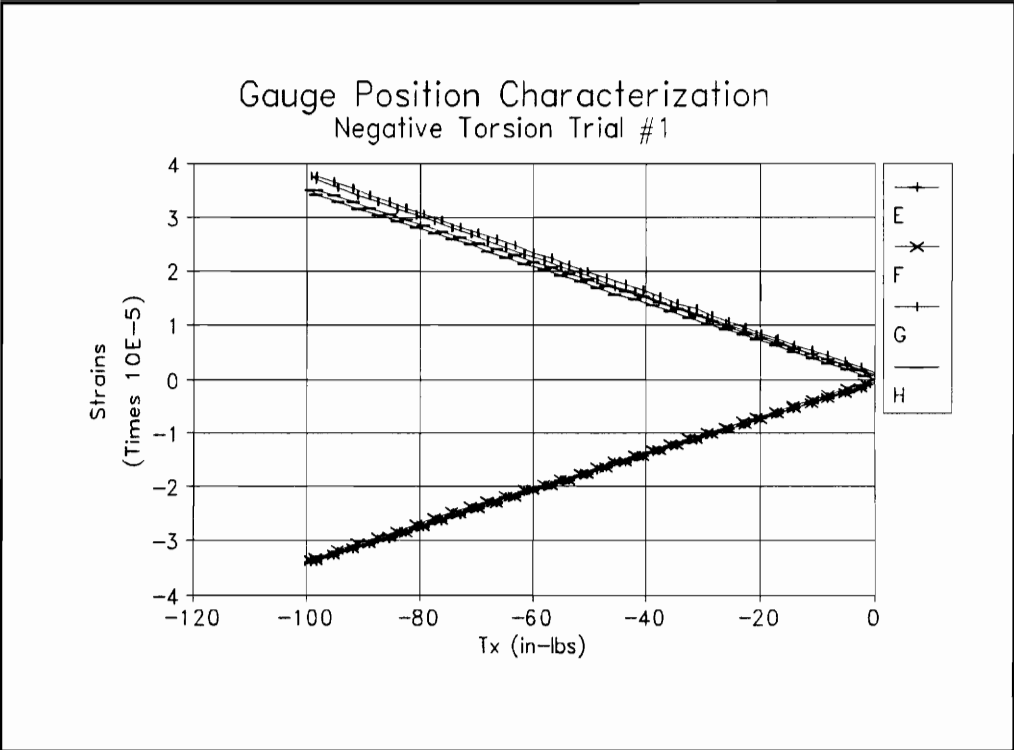


Figure C.4 Sample Positive Torsion Trial, Gauges E, F, G, H



**Figure C.5** Sample Negative Torsion Trial, Gauges E, F, G, H

Two parameter linear regressions are now fit to the data to enable a more quantitative examination. All axial trials are lumped together as are all torsion trials. The y intercept was subsequently neglected (as discussed in ch. 5). The linear regression data is presented below.

**Table C.1** Comparison of Patch Edge and Patch Center Strains, Axial Load

<b><u>Axial Loading</u></b>		<b>m</b>	<b>±Error</b>
$\epsilon_1$	<b>Center (E)</b>	9.89520e-08	1.30346e-10
	<b>Edge (F)</b>	7.75233e-08	8.70825e-11
	<b><u>Edge/Center</u></b>	<b><u>0.783</u></b>	
$\epsilon_2$	<b>Center (G)</b>	1.08692e-07	1.33417e-10
	<b>Edge (F)</b>	1.00576e-07	1.71662e-10
	<b><u>Edge/Center</u></b>	<b><u>0.925</u></b>	

**Table C.1** Comparison of Patch Edge and Patch Center Strains,  
Torsional Load

<b><u>Torsional Loading</u></b>		<b>m</b>	<b>±Error</b>
<b><math>\epsilon_1</math></b>	Center (E)	3.34424e-07	2.06035e-10
	Edge (F)	3.32513e-07	2.92536e-10
	<b><u>Edge/Center</u></b>	<b><u>0.994</u></b>	
<b><math>\epsilon_2</math></b>	Center (G)	-3.71542e-07	3.40356e-10
	Edge (F)	-3.46548e-07	4.85299e-10
	<b><u>Edge/Center</u></b>	<b><u>0.933</u></b>	

Examination of Tables C.1 and C.2 reveals a large effect for fiber direction strain under axial load and a very small effect for fiber direction strain under torsional load. The effect of position on the transverse direction strains is also relatively large at 7 or 8 percent.

Although these cursory results are not quantitatively useful in this study they indicate that this effect may be a major concern for filament wound characterization specimens and should be examined more closely.

# Appendix D

## Computer Codes

The computer codes developed for the project are listed below along with sample input files. The BASIC version (Microsoft QuickBasic Compiler) is listed first followed by a C version (MIX Software Power C and C Math Toolbox) designed to map convergence zones (ch. 6). The final code listed is the pattern search code discussed in ch. 6. The elasticity solution is not listed separately but is included as a subroutine in each of the codes.

### D.1 *BASIC Code*

The following is the input data file used with the basic version of the code in ch. 6. The first two columns are unimportant. The third column list the strains and columns 1-4 list the loads in the following order:  $F_x$ ,  $T_x$ ,  $P_{INNER}$ ,  $dT$ . The C version input file is similar.

---

1	1	3.22359d-7	1.0	0.0	0.0	0.0
2	2	-1.04690d-7	1.0	0.0	0.0	0.0
3	3	1.31797e-8	1.0	0.0	0.0	0.0
4	1	3.11918d-7	0.0	-1.0	0.0	0.0
5	2	-3.30342d-7	0.0	-1.0	0.0	0.0
6	3	1.09655d-7	0.0	-1.0	0.0	0.0

Final Data, (-) Patch

---



The Basic code is now listed, the geometry is that used in ch. 6 for a (-) patch. The geometry is set in the *ELASTCYL* subroutine.

```

DECLARE SUB INPUTSUB (X#(), Expr#(), LOADS#())
DECLARE SUB PHISUB (X#(), LOADS#(), Expr#(), phi#(), PS, Y#)
DECLARE SUB JACOBEAN (X#(), LOADS#(), Expr#(), JCALL#())
DECLARE SUB ELASTCYL (X#(), LOADS#(), i%, Eps#())
DECLARE SUB AmatBvec (J#(), phi#(), A#(), B#())
DECLARE SUB MATRIXSOLVE (B#(), A#(), dX#(), NP%, ENORM#, MCALL$)

COMMON SHARED ND%, NP%, NAP%, Pi#

CLEAR , , 2000

CLS

DEFINT I, K, N
DEFDBL A-H, J, L-M, O-Z

BEEP

'INPUT "ENTER THE NUMBER OF DATA POINTS: ", ND
'INPUT "ENTER THE NUMBER OF PARAMETERS: ", NP
'INPUT "ENTER THE NUMBER OF ACTIVE PARAMETERS: ", NAP
ND = 6
NP = 10
NAP = 5
INPUT "ENTER THE TRACE FILE NAME: ", TRCn$

TRC$ = "C:\thesis\exper\" + TRCn$ + ".TRC"
TRs$ = "C:\thesis\exper\" + TRCn$ + ".TRs"

OPEN TRC$ FOR OUTPUT AS #2
OPEN TRs$ FOR OUTPUT AS #3

DIM J(NAP, ND), Eps(3), X(NP), dX(NAP), A(NAP, NAP), B(NAP), Expr(ND),
phi(ND)
DIM ITP(ND), LOADS(ND, 4)

'NP: # OF PARAMETERS (ELASTIC CONSTANTS)
'ND: # OF DATA POINTS (STRAINS)
'PHI(): VECTOR OF SQUARE ROOTS OF OBJECTIVE FUNCTION TERMS
(Y=PHI()*PHI())
'J(): JACOBEAN MATRIX
'X(): SOLUTION VECTOR (ELASTIC CONSTANTS E1, E2, v12 etc.)
'Expr(): EXPERIMENTAL RESULTS

INPUTSUB X(), Expr(), LOADS()

20 C = C + 1

JCALL$ = "N"

PRINT "Run: "; TRCn$; ".trc"

PHISUB X(), LOADS(), Expr(), phi(), JCALL$, Y

PRINT
PRINT C;
PRINT USING "ENORM=#####.##"; ENORM;
PRINT USING " ENORM/SF=##.##^" ENORM / 1D+25
PRINT
PRINT USING "Y= ##.####^" Y

```

```

IF INT(1E+16 * Y) = INT(1E+16 * ypre) THEN BEEP

ypre = Y

PRINT
PRINT #2, Y;

FOR i = 1 TO NP
    PRINT "x("; i; ")= "; X(i)
    IF i > NAP THEN 1
    dX(i) = 0#
    PRINT #2, ", ";
    PRINT #2, X(i);
1 NEXT i
PRINT

PRINT #2,

JACOBEAN X(), LOADS(), Expr(), J()

AmatBvec J(), phi(), A(), B()

MCALL$ = "Y"

MATRIXSOLVE B(), A(), dX(), NAP, ENORM, MCALL$

FOR i = 1 TO NAP

    dX(i) = dX(i) * 100000#

    IF ABS(dX(i)) > ABS(.25 * X(i)) THEN dX(i) = ABS(.25 * X(i)) *
    SGN(dX(i))

    X(i) = X(i) + dX(i)
NEXT i

X(6) = X(5)
X(7) = X(5)

GOTO 20

END

SUB AmatBvec (J(), phi(), A(), B())

    '[A]=[J][JT]
    '[B]=-[J]{PHI}

    FOR i = 1 TO NAP
        B(i) = 0#
        FOR K = 1 TO NAP
            A(i, K) = 0#
            FOR KK = 1 TO ND
                A(i, K) = A(i, K) + J(i, KK) * J(K, KK)
                IF K > 1 THEN 10
                B(i) = B(i) - J(i, KK) * phi(KK)
10            NEXT KK
        NEXT K
    NEXT i

    ABSF = 1D+25
    ASF = 100000#

    FOR i = 1 TO NAP
        FOR K = 1 TO NAP

```

```

        A(i, K) = A(i, K) * ABSF * ASF
    NEXT K
    B(i) = B(i) * ABSF
NEXT i

END SUB

DEFINT J
DEFDBL N
SUB ELASTCYL (XZ(), LOADS(), IDT, Eps())
'PRINT "ELASTCYL"

'A PLANAR, CYLINDRICAL ELASTICITY SOLUTION FOR LAMINATED COMPOSITE
CYLINDERS
'SUBJECT TO AXIAL, TORSIONAL, THERMAL AND PRESSURE LOADS.

'FROM MASTER'S THESIS BY CARL ROUSSEAU
'"STRESSES AND DEFORMATIONS IN ANGLE-PLY COMPOSITE TUBES"
'ERIC GEORGE

'B1,B2,B3: COEFFICIENTS IN W EQUATION
'**C1: COEFFICIENT OF Eo IN RESPECTIVE STRESS COMPONENTS
'**C2: COEFFICIENT OF (Go R) IN RESPECTIVE STRESS COMPONENTS
'**C3: COEFFICIENT OF (A1 R^(L-1)) IN RESPECTIVE STRESS COMPONENTS
'**C4: COEFFICIENT OF (A2 R^(-L-1)) IN RESPECTIVE STRESS COMPONENTS
'**C5: CONSTANT PORTION OF RESPECTIVE STRESS COMPONENTS
'NOTE: ALL OF THE ABOVE ARE FUNCTIONS OF K

K = 6
KK = 2 * K + 2

DIM CB(K), TH(K), T(K), R(K + 1), A1(K), A2(K), B1(K), B2(K), B3(K),
L(K)
DIM ZZ(K), SXC1(K), SXC2(K), SXC3(K), SXC4(K), SXC5(K), SOC1(K),
SOC2(K)
DIM SOC3(K), SOC4(K), SOC5(K), SRC1(K), SRC2(K), SRC3(K), SRC4(K),
SRC5(K)
DIM TC1(K), TC2(K), TC3(K), TC4(K), TC5(K), EXT(K), EOT(K), ERT(K),
GXOT(K)
DIM A(KK, KK), B(KK), CB11(K), CB12(K), CB13(K), CB16(K), CB22(K)
DIM CB23(K), CB26(K), CB33(K), CB36(K), CB66(K)
DIM X(KK)

Pi = 4 * ATN(1)

'ELASTIC CONSTANTS *****

E1 = XZ(1)
E2 = XZ(2)
E3 = XZ(3)
G12 = XZ(4)
v12 = XZ(5)
v13 = XZ(6)
v23 = XZ(7)
alpha1 = XZ(8)
alpha2 = XZ(9)
alpha3 = XZ(10)
IF INT(E2) = INT(E3) THEN E2 = E2 + 1

'GEOMETRY *****

Ri = .624#
Ro = .72#

T(1) = .016#

```

```

T(2) = .016#
T(3) = .016#
T(4) = .016#
T(5) = .016#
T(6) = .016#

R(0) = Ri
R(K) = Ro

h = Ro - Ri

FOR i = 1 TO K - 1
    R(i) = R(i - 1) + T(i)
NEXT i

'LOADS *****

Fx = LOADS(IDT, 1)
Tx = LOADS(IDT, 2)
dT = LOADS(IDT, 3)
Pin = LOADS(IDT, 4)
Pout = 0#

'PLY ORIENTATION*****

isign = -1

TH(1) = -45.37 * (Pi / 180#) * isign
TH(2) = 46.08 * (Pi / 180#) * isign
TH(3) = -46.78 * (Pi / 180#) * isign
TH(4) = 47.46 * (Pi / 180#) * isign
TH(5) = -48.12 * (Pi / 180#) * isign
TH(6) = 48.77 * (Pi / 180#) * isign

SFSCALE = 1#

' c MATRIX INITIALIZATION SUBROUTINE
GOSUB 100

' C-BAR MATRIX INITIALIZATION SUBROUTINE (ALSO ALPHA's, THERMAL
STRAINS)
GOSUB 110

' STRESS-STRAIN DISPLACEMENT COEFFICIENT SUBROUTINE
GOSUB 120

' SOLUTION MATRIX STACKING ROUTINE
GOSUB 130

MCALL$ = "N"

MATRIXSOLVE B(), A(), X(), KK, ENORM, MCALL$

Eo = X(1)
Go = X(2)

IC = 0
FOR i = 3 TO KK - 1 STEP 2
    IC = IC + 1
    A1(IC) = X(i)
    A2(IC) = X(i + 1)
NEXT i

' STRESS OUTPUT SUBROUTINE
GOSUB 140

```

GOTO 1000

```

100 'c MATRIX SUBROUTINE*****
V = (1 - v12 * (v12 * E2 / E1 + 2 * v23 * v13 * E3 / E1) - v13 ^ 2 * E3 / E1 - v23 ^ 2 * E3 / E2)

C11 = (1 - v23 ^ 2 * E3 / E2) * E1 / V
C12 = (v12 + v13 * v23 * E3 / E2) * E2 / V
C13 = (v13 + v12 * v23) * E3 / V
C23 = (v23 + v12 * v13 * E2 / E1) * E3 / V
C22 = (1 - v13 ^ 2 * E3 / E1) * E2 / V
C33 = (1 - v12 ^ 2 * E2 / E1) * E3 / V
C66 = G12
RETURN

```

```

110 'CBAR MATRIX SUBROUTINE*****
FOR i = 1 TO K
  M = COS(TH(i))
  N = SIN(TH(i))

  CB11(i) = C11 * M ^ 4 + (2 * (M * N) ^ 2) * (C12 + 2 * C66) + C22 * N ^ 4
  CB12(i) = ((M * N) ^ 2) * (C11 + C22 - 4 * C66) + C12 * (M ^ 4 + N ^ 4)
  CB13(i) = C13 * M ^ 2 + C23 * N ^ 2
  CB16(i) = M * N * (C11 * M ^ 2 - C22 * N ^ 2 - (C12 + 2 * C66) * (M ^ 2 - N ^ 2))
  CB22(i) = C11 * N ^ 4 + (2 * (M * N) ^ 2) * (C12 + 2 * C66) + C22 * M ^ 4
  CB23(i) = C13 * N ^ 2 + C23 * M ^ 2
  CB26(i) = M * N * (C11 * N ^ 2 - C22 * M ^ 2 + (C12 + 2 * C66) * (M ^ 2 - N ^ 2))
  CB33(i) = C33
  CB36(i) = M * N * (C13 - C23)
  CB66(i) = (C11 + C22 - 2 * C12) * (M * N) ^ 2 + C66 * (M ^ 2 - N ^ 2)

  EXT(i) = (alpha1 * M ^ 2 + alpha2 * N ^ 2) * dT
  EOT(i) = (alpha1 * N ^ 2 + alpha2 * M ^ 2) * dT
  ERT(i) = alpha3 * dT
  GXOT(i) = 2 * M * N * (alpha1 - alpha2) * dT

NEXT i
RETURN

```

```

120 'STRESS-STRAIN-DISPLACEMENT SUBROUTINE*****
FOR i = 1 TO K
  B1(i) = (CB12(i) - CB13(i)) / (CB33(i) - CB22(i))
  B2(i) = (CB26(i) - 2 * CB36(i)) / (4 * CB33(i) - CB22(i))
  B3(i) = 1 / (CB33(i) - CB22(i))

  L(i) = SQR(CB22(i) / CB33(i))

  ZZ(i) = (CB13(i) - CB12(i)) * EXT(i) + (CB23(i) - CB22(i)) * EOT(i) + (CB33(i) - CB23(i)) * ERT(i) + (CB36(i) - CB26(i)) * GXOT(i)

  SXC1(i) = CB11(i) + B1(i) * (CB12(i) + CB13(i))
  SXC2(i) = CB16(i) + B2(i) * (CB12(i) + 2 * CB13(i))
  SXC3(i) = CB12(i) + L(i) * CB13(i)
  SXC4(i) = CB12(i) - L(i) * CB13(i)
  SXC5(i) = B3(i) * ZZ(i) * (CB12(i) + CB13(i)) - EXT(i) * CB11(i) - EOT(i) * CB12(i) - ERT(i) * CB13(i) - GXOT(i) * CB16(i)

  SOC1(i) = CB12(i) + B1(i) * (CB22(i) + CB23(i))

```

```

SOC2(i) = CB26(i) + B2(i) * (CB22(i) + 2 * CB23(i))
SOC3(i) = CB22(i) + L(i) * CB23(i)
SOC4(i) = CB22(i) - L(i) * CB23(i)
SOC5(i) = B3(i) * ZZ(i) * (CB22(i) + CB23(i)) - EXT(i) * CB12(i) -
EOT(i) * CB22(i) - ERT(i) * CB23(i) - GXOT(i) * CB26(i)

SRC1(i) = CB13(i) + B1(i) * (CB23(i) + CB33(i))
SRC2(i) = CB36(i) + B2(i) * (CB23(i) + 2 * CB33(i))
SRC3(i) = CB23(i) + L(i) * CB33(i)
SRC4(i) = CB23(i) - L(i) * CB33(i)
SRC5(i) = B3(i) * ZZ(i) * (CB23(i) + CB33(i)) - EXT(i) * CB13(i) -
EOT(i) * CB23(i) - ERT(i) * CB33(i) - GXOT(i) * CB36(i)

TC1(i) = CB16(i) + B1(i) * (CB26(i) + CB36(i))
TC2(i) = CB66(i) + B2(i) * (CB26(i) + 2 * CB36(i))
TC3(i) = CB26(i) + L(i) * CB36(i)
TC4(i) = CB26(i) - L(i) * CB36(i)
TC5(i) = B3(i) * ZZ(i) * (CB26(i) + CB36(i)) - EXT(i) * CB16(i) -
EOT(i) * CB26(i) - ERT(i) * CB36(i) - GXOT(i) * CB66(i)

```

```

NEXT i
RETURN

```

### 130 'SOLUTION MATRIX STACKING

SUBROUTINE\*\*\*\*\*

'SF IS A SCALE FACTOR USED TO IMPROVE THE NUMERICAL ACCURACY OF THE SOLVE ROUTINE BY SCALING THE W INTERFACE CONDITIONS CLOSER TO THE REST OF THE MATRIX VALUES.

```

'ERASE A, B, X
'DIM A(KK, KK), B(KK), X(KK)

```

```

B1T2 = 0#
B2T2 = 0#

```

'NEXT TWO LOOPS STACK MATRIX ELEMENTS ASSOCIATED WITH THE INTEGRATED B.C.

```

FOR i = 1 TO K
  A(1, 1) = A(1, 1) + (SXC1(i) * (R(i) ^ 2 - R(i - 1) ^ 2)) / 2
  A(2, 1) = A(2, 1) + (TC1(i) * (R(i) ^ 3 - R(i - 1) ^ 3)) / 3
  A(1, 2) = A(1, 2) + (SXC2(i) * (R(i) ^ 3 - R(i - 1) ^ 3)) / 3
  A(2, 2) = A(2, 2) + (TC2(i) * (R(i) ^ 4 - R(i - 1) ^ 4)) / 4
  B1T2 = B1T2 + (SXC5(i) * (R(i) ^ 2 - R(i - 1) ^ 2)) / 2
  B2T2 = B2T2 + (TC5(i) * (R(i) ^ 3 - R(i - 1) ^ 3)) / 3
NEXT i

IC = 0
FOR i = 3 TO KK - 1 STEP 2
  IC = IC + 1
  A(1, i) = SXC3(IC) * (R(IC) ^ (1 + L(IC)) - R(IC - 1) ^ (1 + L(IC))) / (1 + L(IC))
  A(1, i + 1) = SXC4(IC) * (R(IC) ^ (1 - L(IC)) - R(IC - 1) ^ (1 - L(IC))) / (1 - L(IC))

  A(2, i) = TC3(IC) * (R(IC) ^ (2 + L(IC)) - R(IC - 1) ^ (2 + L(IC))) / (2 + L(IC))
  A(2, i + 1) = TC4(IC) * (R(IC) ^ (2 - L(IC)) - R(IC - 1) ^ (2 - L(IC))) / (2 - L(IC))
NEXT i

B(1) = Fx / (2 * Pi) - B1T2
B(2) = Tx / (2 * Pi) - B2T2

```

'THE NEXT LOOP STACKS THE [A] MATRIX AND {B} VECTOR ELEMENTS ASSOCIATED WITH  
'THE INTERFACE CONDITIONS

```

IC = 0
FOR i = 3 TO KK - 3 STEP 2
  IC = IC + 1
  A(i, 1) = SRC1(IC) - SRC1(IC + 1)
  A(i, 2) = (SRC2(IC) - SRC2(IC + 1)) * R(IC)

  A(i + 1, 1) = ((B1(IC) - B1(IC + 1)) * R(IC))
  A(i + 1, 2) = ((B2(IC) - B2(IC + 1)) * R(IC) ^ 2)

  A(i, i) = SRC3(IC) * R(IC) ^ (L(IC) - 1)
  A(i, i + 1) = SRC4(IC) * R(IC) ^ (-L(IC) - 1)
  A(i, i + 2) = -SRC3(IC + 1) * R(IC) ^ (L(IC + 1) - 1)
  A(i, i + 3) = -SRC4(IC + 1) * R(IC) ^ (-L(IC + 1) - 1)

  A(i + 1, i) = (R(IC) ^ L(IC))
  A(i + 1, i + 1) = (R(IC) ^ (-L(IC)))
  A(i + 1, i + 2) = (-R(IC) ^ L(IC + 1))
  A(i + 1, i + 3) = (-R(IC) ^ (-L(IC + 1)))

  B(i) = SRC5(IC + 1) - SRC5(IC)
  B(i + 1) = ((B3(IC + 1) * ZZ(IC + 1) - B3(IC) * ZZ(IC)) * R(IC))
NEXT i

```

'THE FOLLOWING LINES STACK THE MATRIX ELEMENTS ASSOCIATED WITH THE  
INNER AND  
'OUTER SURFACE PRESSURE B.C.

```

A(KK - 1, 1) = SRC1(1)
A(KK - 1, 2) = SRC2(1) * Ri
A(KK - 1, 3) = SRC3(1) * Ri ^ (L(1) - 1)
A(KK - 1, 4) = SRC4(1) * Ri ^ (-L(1) - 1)

A(KK, 1) = SRC1(K)
A(KK, 2) = SRC2(K) * Ro
A(KK, KK - 1) = SRC3(K) * Ro ^ (L(K) - 1)
A(KK, KK) = SRC4(K) * Ro ^ (-L(K) - 1)

B(KK - 1) = -Pin - SRC5(1)
B(KK) = -Pout - SRC5(K)

```

RETURN

140 'STRESS OUTPUT

SUBROUTINE\*\*\*\*\*

```

  R = Ro
  J = K

  W = B1(J) * R * Eo + B2(J) * Go * R ^ 2 + A1(J) * R ^ L(J) + A2(J)
  * R ^ (-L(J)) + B3(J) * ZZ(J) * R

  Ex = Eo
  Etheta = W / R
  Gxo = Go * R

  M = COS(TH(J))
  N = SIN(TH(J))

  Ep1 = Ex * M ^ 2 + Etheta * N ^ 2 + Gxo * M * N
  Ep2 = Ex * N ^ 2 + Etheta * M ^ 2 - Gxo * M * N
  Gam12 = -Ex * 2 * M * N + Etheta * 2 * M * N + Gxo * (M ^ 2 - N ^

```

2)

```
IF Fx > 0 THEN 150 ELSE 160

150   Eps(1) = Ex
      Eps(2) = Etheta
      Eps(3) = Gxo

      GOTO 170

160   Eps(1) = Ep1
      Eps(2) = Ep2
      Eps(3) = Gam12

170 RETURN

1000 END SUB

DEFINT N
DEFDBL J
SUB INPUTSUB (X(), Expr(), LOADS())

  OPEN "C:\thesis\exper\finalm.dat" FOR INPUT AS #1

  PRINT
  FOR i = 1 TO ND
    INPUT #1, Gigo, GIGO2, Expr(i), LOADS(i, 1), LOADS(i, 2), LOADS(i, 3), LOADS(i, 4)
    PRINT Gigo; GIGO2, LOADS(i, 1), LOADS(i, 2), LOADS(i, 3), LOADS(i, 4)
  NEXT i

  PRINT
  INPUT " ENTER THE INITIAL GUESS FOR E1: "; X(1)
  INPUT " ENTER THE INITIAL GUESS FOR E2: "; X(2)
  INPUT " ENTER THE INITIAL GUESS FOR E3: "; X(3)
  INPUT " ENTER THE INITIAL GUESS FOR G12: "; X(4)
  INPUT " ENTER THE INITIAL GUESS FOR v12: "; X(5)
  INPUT " ENTER THE INITIAL GUESS FOR v13: "; X(6)
  INPUT " ENTER THE INITIAL GUESS FOR v23: "; X(7)
  INPUT " ENTER THE INITIAL GUESS FOR alpha1: "; X(8)
  INPUT " ENTER THE INITIAL GUESS FOR alpha2: "; X(9)
  INPUT " ENTER THE INITIAL GUESS FOR alpha3: "; X(10)

  INPUT "OK", Gigo
  CLS

END SUB

SUB JACOBEAN (X(), LOADS(), Expr(), J())

  DIM XT(NP), FM(ND), FP(ND)

  JCALL$ = "Y"

  FOR i = 1 TO NP
    XT(i) = X(i)
  NEXT i

  h = .0001

  FOR i = 1 TO NAP
    XT(i) = XT(i) - h * X(i)
    PHISUB XT(), LOADS(), Expr(), FM(), JCALL$, Y
```

```

        XT(i) = XT(i) + 2 * h * X(i)
        PHISUB XT(), LOADS(), ExpR(), FP(), JCALL$, Y
        XT(i) = XT(i) - h * X(i)

        FOR K = 1 TO ND
            J(i, K) = (FP(K) - FM(K)) / (2 * h * X(i))
        NEXT K

    NEXT i

END SUB

DEFINT J
DEFDBL N
SUB MATRIXSOLVE (B(), A(), X(), KK, ENORM, MCALL$)

200 'SUBROUTINE FOR SOLVING THE MATRIX EQUATION [A]{X}={B} USING
    GAUSSIAN
    'ELIMINATION AND SCALED PARTIAL PIVOTING. ROUTINE OVERWRITES ORIGINAL
    [A],{B}
    'RETURNS: SOLUTION VECTOR {X}, ERROR NORM ENORM, MAXERROR RESMAX.

    DIM RSUM(KK), RNORM(KK), RES(KK), IP(KK - 1)

    IF MCALL$ <> "Y" THEN 210

        DIM AO(KK, KK), BO(KK)

210 RNMAX = 0#
    FOR i = 1 TO KK
        RSUM(i) = 0#
        FOR J = 1 TO KK
            RSUM(i) = RSUM(i) + A(i, J) ^ 2
            IF MCALL$ <> "Y" THEN 220
                AO(i, J) = A(i, J)
                BO(i) = B(i)
220        NEXT J
        RSUM(i) = RSUM(i) + B(i) ^ 2
        RNORM(i) = SQR(RSUM(i))
        IF RNORM(i) > RNMAX THEN RNMAX = RNORM(i)
    NEXT i

    FOR i = 1 TO KK
        SF2 = (RNORM(i) / RNMAX)
        B(i) = B(i) * SF2
        FOR J = 1 TO KK
            A(i, J) = A(i, J) * SF2
        NEXT J
    NEXT i

    GOSUB 300
    'FACTOR SUBROUTINE

    GOSUB 510
    'SOLVE SUBROUTINE

    IF MCALL$ <> "Y" THEN 1100

    RESSUM = 0#
    FOR i = 1 TO KK
        RES(i) = 0#
        FOR J = 1 TO KK
            RES(i) = RES(i) + AO(i, J) * X(J)
        NEXT J
        RES(i) = RES(i) - BO(i)
    
```

```

    RESSUM = RESSUM + RES(i) ^ 2
NEXT i

ENORM = SQR(RESSUM)

GOTO 1100

300 'FACTOR SUBROUTINE*****
FOR C = 1 TO KK - 1
    IP(C) = C
    FOR ROW = C TO KK - 1
        IF ABS(A(ROW + 1, C)) > ABS(A(ROW, C)) THEN IP(C) = ROW + 1
    NEXT ROW

    IF IP(C) <> C THEN GOSUB 460
    FOR ROW = C + 1 TO KK
        A(ROW, C) = -A(ROW, C) / A(C, C)
        FOR CC = C + 1 TO KK
            A(ROW, CC) = A(ROW, C) * A(C, CC) + A(ROW, CC)
        NEXT CC
    NEXT ROW

NEXT C
RETURN

460 'ROWSWITCH SUBROUTINE
FOR CC = C TO KK
    SWAP A(C, CC), A(IP(C), CC)
NEXT CC
RETURN

510 'SOLVE SUBROUTINE*****
FOR RR = 1 TO KK - 1
    SWAP B(RR), B(IP(RR))
    FOR ROW = RR + 1 TO KK
        B(ROW) = A(ROW, RR) * B(RR) + B(ROW)
    NEXT ROW
NEXT RR

X(KK) = B(KK) / A(KK, KK)
X(KK - 1) = (B(KK - 1) - A(KK - 1, KK) * X(KK)) / A(KK - 1, KK - 1)

FOR ROW = KK - 2 TO 1 STEP -1
    FOR C = ROW + 1 TO KK
        X(ROW) = X(ROW) + A(ROW, C) * X(C)
    NEXT C
    X(ROW) = (B(ROW) - X(ROW)) / A(ROW, ROW)
NEXT ROW
RETURN

1100 END SUB

DEFINT N
DEFDBL J
SUB PHISUB (X(), LOADS(), Expr(), phi(), JCALL$, Y)

    DIM CompR(3), Rerr(3)

    Y = 0
    Merr = 0

    FOR i = 1 TO ND STEP 3
        ELASTCYL X(), LOADS(), i, CompR()

        phi(i) = Expr(i) - CompR(1)

```

```

        phi(i + 1) = ExpR(i + 1) - CompR(2)
        phi(i + 2) = ExpR(i + 2) - CompR(3)
IF LOADS(i, 1) <> 0 THEN phi(i + 2) = phi(i + 2) * 10000#
    IF JCALL$ = "Y" THEN 2000
        Y = Y + phi(i) ^ 2 + phi(i + 1) ^ 2 + phi(i + 2) ^ 2
        FOR II = 0 TO 2
            Rerr(II + 1) = (ExpR(i + II) - CompR(II + 1)) / ExpR(i + II)
            IF ABS(Rerr(II + 1)) > Merr THEN 1990 ELSE 1992
1990            Merr = ABS(Rerr(II + 1))
                IMAX = i + II
1992 'PRINT (I + II), ;
        PRINT USING "##.###^" " "; ExpR(II + i); CompR(II + 1); Rerr(II +
1)
        NEXT II

    PRINT #3, CompR(1); ", "; CompR(2); ", "; CompR(3); ", ";
2000 NEXT i

    IF JCALL$ = "Y" THEN 2040

    PRINT
    PRINT "MAXERROR = "; IMAX, Merr

PRINT #3,
2040 END SUB

```

## D.2 C Code

The C code developed is listed below. The matrix equations are solved by the *Lineqn()* function available in the MIX Software C/Math Toolchest. The organization of the program is similar to the BASIC program but this version is set up to map areas in search of consistent data (ch. 6).

---

### Header File

```
#include <stdio.h>
#include <stdlib.h>
#include <math.h>
#include <mathlib.h>
#include <bios.h>

#pragma library "C:\\powerc\\mathlib\\mathlib.lib"

char gigo;

#define Pi 3.141592654
#define PAUSE scanf("%c",&gigo);

#define K 6          /* # of plies */
#define KK ((2*K)+2) /* size of elasticity solution matrix */
#define ND 6         /* # of data points */
#define NAP 5        /* # of active parameters */
#define h .0001      /* size of % interval used in jacobian
N-derivatives */

void lstsq(double *Y, double E[], double Expr[][3], double eload[][5],
double th[], double r[], int *conv);

void input(double E[], double th[], double r[], double Expr[][3], double
eload[][5]);

double phisub(double E[], double r[], double th[], double eload[][5],
double Expr[][3], Real_Vector phi, int jcall, int *crsh);

void jacobian(double E[], double r[], double th[], double eload[][5],
double Expr[][3], Real_Matrix jaco);

void elastsub(double E[], double r[], double th[], double load[], double
Rc, double Ep[], int *crsh);

void c(double E[], double cm[]);

void cb(double cm[][4], double th[], double E[], double dT, double
cbm[][4][4], double et[][4]);

void stress(double cbm[][4][4], double et[][4], double l[], double
bc[][4], double sc[][4][5], double th[], int *crsh);

void mat_stack(double sc[][4][5], double l[], double bc[][4], double
r[], double load[], Real_Matrix A, Real_Vector B);

void output(Real_Vector x, double th[], double Rc, double l[], double
bc[][4], double Ep[], double load[]);
```

## Main Program File

```
#include "viz.h"
#include "lstsqrv.c"
#include "elastsub.c"
#include "input.c"
#include "phisub.c"
#include "jacobean.c"

int useinput_ = 1;          /* causes lineqn() to overwrite inputs */

main()
{
    int i, j, ii, ij, c, conv;

    double avgele2, E[10], Eo[10], Expr[ND/3][3], eload[ND/3][5], th[K],
    r[K+1], Y;

    FILE *OUTFILE;

    if((OUTFILE = fopen("output.dat", "w")) == NULL)
    {
        printf("Cannot open data file, program aborted");
        exit(0);
    }

    c = 0;

    input(Eo, th, r, Expr, eload);

    avgele2 = (Expr[1][0]-Expr[1][1])/2;

    for(i=0; i<10; i++)
        E[i] = Eo[i];

    for(i=0; i<50; i++)
    {
        Expr[0][2] = 1e-11 + i * 1.8e-12;

        for(j=0; j<50; j++)
        {
            c++;
            printf("\n%d\n", c);

            Expr[1][0] = avgele2 - (1.2e-8 + j * 1e-11);
            Expr[1][1] = -avgele2 - (1.2e-8 + j * 1e-11);

            lstsq(&Y, E, Expr, eload, th, r, &conv);

            if(conv==1)
                printf("\nCONVERGED\n");
            else
                printf("\nFAILED\n");

            printf("\ni = %d, GammaXY(Fx) = %1.6e\n", i, Expr[0][2]);
            printf("j = %d, Epsilon1(Tx) = %1.6e\n", j, Expr[1][0]);
            printf("j = %d, Epsilon2(Tx) = %1.6e\n\n", j, Expr[1][1]);

            printf("Y = %1.6e\n\n", Y);

            for(ii=0; ii<NAP; ii++)
                printf("E[%d] = %1.8e\n", ii, E[ii]);
            printf("\n");
        }
    }
}
```

```

        fprintf(OUTFILE, "%1.8e %1.8e %1.8e %1.6e %d ", Expr[0][2],
Expr[1][0], Expr[1][1], -log10(Y), conv);
        for(ii=0; ii<7; ii++)
        {
            if(ii<NAP)
                fprintf(OUTFILE, "%1.9e ", E[ii]);

            E[ii] = Eo[ii];
        }
        fprintf(OUTFILE, "\n");
    }
}

```

## **Subroutines**

```

void lstsqqr(double *Y, double E[], double Expr[][3], double eload[][5],
double th[], double r[], int *conv)
{
    int itr, i, j, jcall, crsh;

    double Ypre;

    Real_Vector phi, B1;
    Real_Matrix jaco, A1;

    phi = valloc(NULL, ND);
    jaco = mxalloc(NULL, NAP, ND);

    for(itr=0; itr<23; itr++)
    {
        crsh = 1;

        /* printf("%d ",itr); */

        jcall = 0;

        *Y = phisub(E, r, th, eload, Expr, phi, jcall, &crsh);

        if(crsh!=1)
            goto CRASHED;

        if(itr!=0)
        {
            if(fabs(1-(*Y)/Ypre) < .0001)
                goto CONVERGED;
        }

        Ypre = *Y;

        jacobean(E, r, th, eload, Expr, jaco);

        A1 = mxmul2(jaco, jaco, NAP, ND, NAP);

        B1 = vscale(vmxmul(jaco, phi, NAP, ND). NAP, -1.0);

        lineqn(A1, B1, NAP);

        for(i=0 ; i<NAP ; i++)
        {
            if(fabs(B1[i])>(.25*E[i]))
                B1[i] = .25*E[i]*(B1[i]/fabs(B1[i]));
            E[i] += B1[i];
        }
    }
}

```

```

        E[5] = E[4];
        E[6] = E[4];

        vfree(B1);
        mxfree(A1);
    }

    CRASHED:
        *conv = 0;
        goto OUT;

    CONVERGED:
        *conv = 1;

    OUT:

    mxfree(jaco);
    vfree(phi);
}

```

```

void input(double E[], double th[], double r[], double Expr[][3], double
eload[][5])
{
    int i, j, ic, dnum, dtyp, rnum;

    double thdp, thdm, dat, t[K];

    FILE *DataF;

    printf("Elastic constant initial estimates:\n\n");

    printf("Enter E1: ");
    scanf("%lf", &E[0]);

    printf("\nEnter E2: ");
    scanf("%lf", &E[1]);

    printf("\nEnter E3: ");
    scanf("%lf", &E[2]);

    printf("\nEnter G12: ");
    scanf("%lf", &E[3]);

    printf("\nEnter v12: ");
    scanf("%lf", &E[4]);

    printf("\nEnter v13: ");
    scanf("%lf", &E[5]);

    printf("\nEnter v23: ");
    scanf("%lf", &E[6]);

    printf("\n\nThermal expansion constants:\n");

    printf("\nEnter alpha 1: ");
    scanf("%lf", &E[7]);

    printf("\nEnter alpha 2: ");

```

```

scanf("%lf", &E[8]);

printf("\nEnter alpha 3: ");
scanf("%lf", &E[9]);

printf("\n\nTube geometry input:\n");

/* printf("\nEnter the inside radius: "); */
/* scanf("%lf", &r[0]); */

/* printf("Enter the outside radius: "); */
/* scanf("%lf", &r[K]); */

th[0] = 45.365*Pi/180;
th[1] = -46.081*Pi/180;
th[2] = 46.779*Pi/180;
th[3] = -47.459*Pi/180;
th[4] = 48.122*Pi/180;
th[5] = -48.769*Pi/180;

t[0] = .016;
t[1] = .016;
t[2] = .016;
t[3] = .016;
t[4] = .016;
t[5] = .016;

r[0] = .624;
r[K] = .72;

for(i=1 ; i<(K+1) ; i++)
{
    r[i] = r[i-1] + t[i-1];
    printf("r[%d] = %1.6e\n", i, r[i]);
}

PAUSE

printf("\n\nElastic constant echo:\n");

printf("\nE1 = %g", E[0]);
printf("\nE2 = %g", E[1]);
printf("\nE3 = %g", E[2]);
printf("\nv12 = %g", E[3]);
printf("\nv13 = %g", E[4]);
printf("\nv23 = %g", E[5]);
printf("\nG12 = %g", E[6]);

printf("\n\nThermal expansion echo:\n");

printf("\nAlpha 1 = %g", E[7]);
printf("\nAlpha 2 = %g", E[8]);
printf("\nAlpha 3 = %g", E[9]);

PAUSE

printf("\n\nTube geometry echo:\n");

printf("\nK= %d", K);
printf("\ninner radius = %g", r[0]);
printf("\nouter radius = %g\n\n", r[K]);

PAUSE

for(i=0 ; i<K ; i++)

```

```

    printf("PLY %d: theta = %f, Ri= %f, Ro= %f\n", i, th[i]*180/Pi,
r[i], r[i+1]);

    PAUSE

    clrscrn();

    if((DataF = fopen("finalm.dat", "r")) == NULL)
    {
        printf("Cannot open data file, program aborted");
        exit(0);
    }

    ic = -1;
    for(i = 0 ; i<ND ; i += 3)
    {
        ic++;
        for(j = 0 ; j<3 ; j++)
        {
            rnum = fscanf(DataF, "%d %d %lf %lf %lf %lf", &dnum, &dtyp,
&Expr[ic][j], &eload[ic][2], &eload[ic][3], &eload[ic][4]);
            if(rnum != 6)
                printf("File read error, check format");
            printf(" %d %d %1.8e %6.1f %6.1f %6.1f\n", dnum,
dtyp, Expr[ic][j], eload[ic][2], eload[ic][3], eload[ic][4]);
        }
        eload[ic][0] = 0;
        eload[ic][1] = 0;
    }
    fclose(DataF);

    printf("read ok");
}

```

```

double phisub(double E[], double r[], double th[], double eload[][5],
double Expr[][3], Real_Vector phi, int jcall, int *crsh)
{
    int i, ic;
    double Eps[3], Y;

    Y = 0.0;

    ic = -1;

    for(i=0 ; i<ND ; i+=3)
    {
        ic++;

        elastsub(E, r, th, eload[ic], r[K], Eps, &crsh);

        phi[i] = Expr[ic][0] - Eps[0];
        phi[i+1] = Expr[ic][1] - Eps[1];
        phi[i+2] = (Expr[ic][2] - Eps[2]);

        if(i==0)
            phi[i+2]=phi[i+2]*1000;
    }
}

```

```

        if(jcall==0)                                /* skip block if called by jacobian */
        {
            Y += phi[i]*phi[i] + phi[i+1]*phi[i+1] + phi[i+2]*phi[i+2];
/*          printf("%1.8e      %1.8e\n",Expr[ic][0], Eps[0]);
            printf("%1.8e      %1.8e\n",Expr[ic][1], Eps[1]);
            printf("%1.8e      %1.8e\n\n",Expr[ic][2], Eps[2]);
            PAUSE */
        }
    }
    if(jcall==0)                                    /* skip block if called by jacobian */
        return Y;
}

/*a planar, cylindrical elasticity solution for laminated composite*/
/*subject to axial, torsional, thermal and pressure loads.*/

void elastsub(double E[], double r[], double th[], double load[], double
Rc, double Ep[], int *crsh)
{
    int i, j;

    double cm[4][4], cbm[K][4][4], sc[K][4][5], bc[K][3], et[K][4], l[K];

    Real_Matrix A;
    Real_Vector B;

    A = mxalloc(NULL, KK, KK);
    B = valloc(NULL, KK);

    /*input section *****/
    /*elastic parameters *****/

    /* E[0]:  E1      */
    /* E[1]:  E2      */
    /* E[2]:  E3      */
    /* E[3]:  G12     */
    /* E[4]:  v12     */
    /* E[5]:  v13     */
    /* E[6]:  v23     */
    /* E[7]:  ALPHA1  */
    /* E[8]:  ALPHA2  */
    /* E[9]:  ALPHA3  */

    if(E[1] == E[2])
        E[2] += 1;

    /*loads*****/

    /* load[0]:  Pout */
    /* load[1]:  Pin  */
    /* load[2]:  Fx   */
    /* load[3]:  Tx   */
    /* load[4]:  dT   */

```

```

/*main body *****/
c(E, cm);

cb(cm, th, E, load[4], cbm, et);

stress(cbm, et, l, bc, sc, th, &scrsh);

mat_stack(sc, l, bc, r, load, A, B);

lineqn(A, B, KK);
mxfree(A);

output(B, th, Rc, l, bc, Ep, load);
vfree(B);

} /*end *****/

void c(double E[], double cm[][4])
{ /*c MATRIX SUBROUTINE*/

    double v;

    v = (1 - E[4] * (E[4] * E[1] / E[0] + 2 * E[6] * E[5] * E[2] / E[0]) -
E[5] * E[5] * E[2] / E[0] - E[6] * E[6] * E[2] / E[1]);

    cm[0][0] = (1 - E[6] * E[6] * E[2] / E[1]) * E[0] / v;          /* c11 */
    cm[0][1] = (E[4] + E[5] * E[6] * E[2] / E[1]) * E[1] / v;      /* c12 */
    cm[0][2] = (E[5] + E[4] * E[6]) * E[2] / v;                    /* c13 */
    cm[1][1] = (1 - E[5] * E[5] * E[2] / E[0]) * E[1] / v;        /* c22 */
    cm[1][2] = (E[6] + E[4] * E[5] * E[1] / E[0]) * E[2] / v;     /* c23 */
    cm[2][2] = (1 - E[4] * E[4] * E[1] / E[0]) * E[2] / v;        /* c33 */
    cm[3][3] = E[3];                                                /* c66 */
}

void cb(double cm[][4], double th[], double E[], double dT, double
cbm[][4][4], double et[][4])
{
    /*c-bar MATRIX SUBROUTINE*/

    int i, ii, j, jj, k;
    double m, n;

    for(i=0; i<K; i++)
    {
        if(i>1)
        {
            for(j=0; j<2; j++)
            {
                if(th[i]==th[j])
                {
                    for(ii=0; ii<4; ii++)
                    {
                        for(jj=0; jj<4; jj++)
                        {
                            cbm[i][ii][jj] = cbm[j][ii][jj];
                        }
                        et[i][ii] = et[j][ii];
                    }
                    goto end_loop_cbm;
                }
            }
        }
    }

    m = cos(th[i]);

```

```

    n = sin(th[i]);

    cbm[i][0][0] = cm[0][0]*pow(m,4) + (2*pow(m*n,2))*(cm[0][1] +
2*cm[3][3]) + cm[1][1]*pow(n,4);
    cbm[i][0][1] = pow(m*n,2)*(cm[0][0] + cm[1][1] - 4*cm[3][3]) +
cm[0][1]*(pow(m,4) + pow(n,4));
    cbm[i][0][2] = cm[0][2]*m*m + cm[1][2]*n*n;
    cbm[i][0][3] = m*n*(cm[0][0]*m*m - cm[1][1]*n*n - (cm[0][1] +
2*cm[3][3])*(m*m - n*n));
    cbm[i][1][1] = cm[0][0]*pow(n,4) + (2*pow(m*n,2))*(cm[0][1] +
2*cm[3][3]) + cm[1][1]*pow(m,4);
    cbm[i][1][2] = cm[0][2]*n*n + cm[1][2]*m*m;
    cbm[i][1][3] = m*n*(cm[0][0]*n*n - cm[1][1]*m*m + (cm[0][1] +
2*cm[3][3])*(m*m - n*n));
    cbm[i][2][2] = cm[2][2];
    cbm[i][2][3] = m*n*(cm[0][2] - cm[1][2]);
    cbm[i][3][3] = (cm[0][0] + cm[1][1] - 2*cm[0][1])*pow(m*n,2) +
cm[3][3]*pow((m*m - n*n),2);

    for(j = 1; j<4 ; j++)
        for(k = 0; k<j ; k++)
            cbm[i][j][k] = cbm[i][k][j]; /*stacks symmetric terms*/

    et[i][0] = (E[7]*m*m + E[8]*n*n)*dT; /*X      thermal strain*/
    et[i][1] = (E[7]*n*n + E[8]*m*m)*dT; /*THETA  thermal strain*/
    et[i][2] = E[9]*dT; /*R      thermal strain*/
    et[i][3] = 2*m*n*(E[7] - E[8])*dT; /*X-THETA thermal strain*/

end_loop_cbm:
}
}

void stress(double cbm[][4][4], double et[][4], double l[], double
bc[][3] , double sc[][4][5], double th[], int *crsh)
{
    /* stress coefficients */

    int i, ii, j, jj;
    double zz;

    for(i=0 ; i<K ; i++)
    {
        if(i>1)
        {
            for( j=0 ; j<2 ; j++)
            {
                if(th[i]==th[j])
                {
                    for(ii=0; ii<4; ii++)
                    {
                        for(jj=0; jj<5; jj++)
                        {
                            sc[i][ii][jj] = sc[j][ii][jj];
                        }
                        if(ii<3)
                            bc[i][ii] = bc[j][ii];
                    }
                    l[i] = l[j];
                    goto end_loop_stress;
                }
            }
        }
    }

    bc[i][0] = (cbm[i][0][1] - cbm[i][0][2]) / (cbm[i][2][2] -

```

```

cbm[i][1][1]);
bc[i][1] = (cbm[i][1][3] - 2 * cbm[i][2][3]) / (4 * cbm[i][2][2] -
cbm[i][1][1]);
bc[i][2] = 1 / (cbm[i][2][2] - cbm[i][1][1]);

zz = (cbm[i][0][2]-cbm[i][0][1])*et[i][0] +
(cbm[i][1][2]-cbm[i][1][1])*et[i][1] +
(cbm[i][2][2]-cbm[i][1][2])*et[i][2] +
(cbm[i][2][3]-cbm[i][1][3])*et[i][3];

bc[i][2] *= zz;

if(*crsh != 0)
{
if((cbm[i][1][1] / cbm[i][2][2]) <= 0)
*crsh = 0;
}

l[i] = sqrt(fabs(cbm[i][1][1] / cbm[i][2][2]));

for(j = 0; j<4 ; j++)
{
sc[i][j][0] = cbm[i][0][j] + bc[i][0]*(cbm[i][1][j] +
cbm[i][2][j]);
sc[i][j][1] = cbm[i][j][3] + bc[i][1]*(cbm[i][1][j] +
2*cbm[i][2][j]);
sc[i][j][2] = cbm[i][1][j] + l[i] * cbm[i][2][j];
sc[i][j][3] = cbm[i][1][j] - l[i] * cbm[i][2][j];
sc[i][j][4] = bc[i][2]*(cbm[i][1][j] + cbm[i][2][j]) -
et[i][0]*cbm[i][0][j] - et[i][1]*cbm[i][1][j] - et[i][2]*cbm[i][2][j] -
et[i][3]*cbm[i][j][3];
}

end_loop_stress:
}
/*j=0: SIGMax      coefficients */
/*j=1: SIGMATHeta  coefficients */
/*j=2: SIGMAR      coefficients */
/*j=3: TAUx-theta  coefficients */
}

void mat_stack(double sc[][4][5], double l[], double bc[][3], double
r[], double load[], Real_Matrix A, Real_Vector B)
{
/*subroutine for stacking the components of the linear equations
[A]{x}={B}*/

int i, j, ic;
double r3, rp3, blt2, b2t2;

for(i = 0; i<KK ; i++) /*initialize [A], {B}*/
{
B[i] = 0.0;
for(j = 0; j<KK ; j++)
A[i][j] = 0.0;
}

blt2 = 0;
b2t2 = 0;

/*next two loops stack elements associated with the integrated B.C.*/
for(i = 0; i<K ; i++)
{
rp3 = r[i+1] * r[i+1] * r[i+1];

```

```

    r3 = r[i] * r[i] * r[i];

    A[0][0] += (sc[i][0][0]*( r[i+1]*r[i+1] - r[i]*r[i] )) / 2.0;
    A[1][0] += (sc[i][3][0]*( rp3 - r3 )) / 3.0;
    A[0][1] += (sc[i][0][1]*( rp3 - r3 )) / 3.0;
    A[1][1] += (sc[i][3][1]*( rp3*r[i+1] - r3*r[i] )) / 4.0;

    blt2 += (sc[i][0][4]*( r[i+1]*r[i+1] - r[i]*r[i] )) / 2.0;
    b2t2 += (sc[i][3][4]*( rp3 - r3 )) / 3.0;
}

ic = 0;

for(i = 2; i<(KK-1) ; i += 2)
{
    ic++;

    A[0][i] = sc[ic-1][0][2]*(pow(r[ic], 1+l[ic-1]) - pow(r[ic-1],
1+l[ic-1])) / (1+l[ic-1]);
    A[0][i+1] = sc[ic-1][0][3]*(pow(r[ic], 1-l[ic-1]) - pow(r[ic-1],
1-l[ic-1])) / (1-l[ic-1]);
    A[1][i] = sc[ic-1][3][2]*(pow(r[ic], 2+l[ic-1]) - pow(r[ic-1],
2+l[ic-1])) / (2+l[ic-1]);
    A[1][i+1] = sc[ic-1][3][3]*(pow(r[ic], 2-l[ic-1]) - pow(r[ic-1],
2-l[ic-1])) / (2-l[ic-1]);
}

B[0] = load[2] / (2 * Pi) - blt2;
B[1] = load[3] / (2 * Pi) - b2t2;

/*next loop stacks the elements associated with the interface
conditions*/

ic = 0;

for(i = 2; i<(KK-3) ; i += 2)
{
    ic++;

    A[i][0] = sc[ic-1][2][0] - sc[ic][2][0];
    A[i][1] = ( sc[ic-1][2][1] - sc[ic][2][1] ) * r[ic];

    A[i + 1][0] = ( bc[ic-1][0] - bc[ic][0] ) * r[ic];
    A[i + 1][1] = ( bc[ic-1][1] - bc[ic][1] ) * r[ic]*r[ic];

    A[i][i] = sc[ic-1][2][2] * pow(r[ic], (l[ic-1] - 1) );
    A[i][i+1] = sc[ic-1][2][3] * pow(r[ic], (-l[ic-1] - 1) );
    A[i][i+2] = -sc[ic][2][2] * pow(r[ic], (l[ic] - 1) );
    A[i][i+3] = -sc[ic][2][3] * pow(r[ic], (-l[ic] - 1) );

    A[i+1][i] = pow(r[ic], l[ic-1] );
    A[i+1][i+1] = pow(r[ic], -l[ic-1] );
    A[i+1][i+2] = -pow(r[ic], l[ic] );
    A[i+1][i+3] = -pow(r[ic], -l[ic] );

    B[i] = sc[ic][2][4] - sc[ic-1][2][4];
    B[i+1] = ( bc[ic][2] - bc[ic-1][2] ) * r[ic];
}

/*next lines stack the matrix elements associated with the pressure
B.C.*/

A[KK-2][0] = sc[0][2][0];
A[KK-2][1] = sc[0][2][1] * r[0];
A[KK-2][2] = sc[0][2][2] * pow(r[0], (l[0] - 1) );

```

```

A[KK-2][3] = sc[0][2][3] * pow(r[0], (-l[0] - 1) );
A[KK-1][0] = sc[K-1][2][0];
A[KK-1][1] = sc[K-1][2][1] * r[K];
A[KK-1][KK-2] = sc[K-1][2][2] * pow(r[K], ( l[K-1] - 1) );
A[KK-1][KK-1] = sc[K-1][2][3] * pow(r[K], ( -l[K-1] - 1) );

B[KK-2] = -load[1] - sc[0][2][4];
B[KK-1] = -load[0] - sc[K-1][2][4];
}

void output(Real_Vector x, double th[], double Rc, double l[], double
bc[][3], double Ep[], double load[])
{
double Ex, Eo, Gxo, w, m, n;

w = bc[K-1][0]*Rc*x[0] + bc[K-1][1]*x[1]*Rc*Rc + x[2*(K-1)+2]*pow(Rc,
l[K-1]) + x[2*(K-1)+3]*pow(Rc, -l[K-1]) + bc[K-1][2]*Rc;

Ex = x[0]; /* Ex: Epsilon x */
Eo = w/Rc; /* Eo: Epsilon theta, Er: Epsilon r */
Gxo = x[1]*Rc; /* Gxo: Gamma x-theta */

m = cos(th[K-1]);
n = sin(th[K-1]);

if(load[2]==0)
{
Ep[0] = Ex*m*m + Eo*n*n + Gxo*m*n; /* Epsilon 1 */
Ep[1] = Ex*n*n + Eo*m*m - Gxo*m*n; /* Epsilon 2 */
Ep[2] = 2*m*n*(Eo - Ex) + Gxo*(m*m - n*n); /* Epsilon 12 */
}
else
{
Ep[0] = Ex; /* Epsilon X */
Ep[1] = Eo; /* Epsilon Y */
Ep[2] = Gxo; /* Epsilon XY */
}
}

void jacobean(double E[], double r[], double th[], double eload[][5],
double Expr[][3], Real_Matrix jaco)
{
int i, j, jcall, Gint;

double Etemp[10];

Real_Vector PHIminus, PHIplus;

PHIminus = valloc(NULL, ND);
PHIplus = valloc(NULL, ND);

for(i=0; i<10; i++)
Etemp[i] = E[i];

jcall = 1;

for(i=0; i<NAP; i++)
{

```

```

Etemp[i] -= h * E[i];
phisub(Etemp, r, th, eload, Expr, PHIminus, jcall, &Gint);

Etemp[i] += 2.0 * h * E[i];
phisub(Etemp, r, th, eload, Expr, PHIplus, jcall, &Gint);

Etemp[i] -= h * E[i];

for(j=0; j<ND; j++)
    jaco[i][j] = (PHIplus[j] - PHIminus[j])/(2 * h * E[i]);
}

vfree(PHIplus);
vfree(PHIminus);
}

```

## D.3 Pattern Search Code

The following is a listing of the header and main program files of the Pattern Search program developed to find regions of high data consistency (ch. 6). Many of the subroutines are not listed as they are identical to those listed for the C version of the Least-Squares code listed above. For a description of the algorithm see reference 9.

---

### HEADER FILE

```
#include <stdio.h>
#include <stdlib.h>
#include <math.h>
#include <mathlib.h>
#include <bios.h>

#pragma library "C:\\powerc\\mathlib\\mathlib.lib"

char gigo;

#define Pi 3.141592654
#define PAUSE scanf("%c",&gigo);

#define K 6          /* # of plies */
#define KK ((2*K)+2) /* size of elasticity solution matrix */
#define ND 6         /* # of data points */
#define NAP 5        /* # of active parameters */
#define h .0001      /* size of % interval used in jacobian
N-derivatives */

double lstsq(double E[], double X12[], double Expr[][3], double
eload[][5], double th[], double r[], int *conv);
void Pattern(double Xb[], double Yb, double X[], double *Y, double
deltaF, double deltaT, double E[], double Expr[][3], double eload[][5],
double th[], double r[]);

void input(double E[], double th[], double r[], double Expr[][3], double
eload[][5]);

double phisub(double E[], double r[], double th[], double eload[][5],
double Expr[][3], Real_Vector phi, int jcall, int *crsh);

void jacobian(double E[], double r[], double th[], double eload[][5],
double Expr[][3], Real_Matrix jaco);

void elastsub(double E[], double r[], double th[], double load[], double
Rc, double Ep[], int *crsh);

void c(double E[], double cm[]);

void cb(double cm[][4], double th[], double E[], double dT, double
cbm[][4][4], double et[][4]);

void stress(double cbm[][4][4], double et[][4], double l[], double
bc[][4], double sc[][4][5], double th[], int *crsh);
```

```

void mat_stack(double sc[][4][5], double l[], double bc[][4], double
r[], double load[], Real_Matrix A, Real_Vector B);

void output(Real_Vector x, double th[], double Rc, double l[], double
bc[][4], double Ep[], double load[]);

```

## Main Program File

```

#include "search.h"
#include "lstsq.c"
#include "elastsub.c"
#include "input.c"
#include "phisub.c"
#include "jacobian.c"
#include "pattern.c"

int useinput_ = 1;          /* causes lineqn() to overwrite inputs */

main()
{
    int i, j, ii, c, *conv;

    double E[10], Eo[10], Expr[ND/3][3], eload[ND/3][5], th[K], r[K+1];
    double Xb[2], Yb, Xt[2], Yt, X[2], Y, deltaF, deltaT, DR;

    c = 0;

    input(Eo, th, r, Expr, eload);

    /*Expr[1][2] = -1.2e-5;*/

    for(i=0; i<10; i++)
        E[i] = Eo[i];

    printf("Enter the starting pt. for the pattern search.\n");
    printf("GammaXY(Fx) :");
    scanf("%lf", &Xb[0]);
    printf("\nDiff :");
    scanf("%lf", &Xb[1]);
    printf("\n\nInitial delta (GammaXY(Fx)):");
    scanf("%lf", &deltaF);
    printf("\n\nInitial delta (Diff):");
    scanf("%lf", &deltaT);
    printf("\n\nDelta reduction percentage :");
    scanf("%lf", &DR);

    Yb = lstsq(E, Xb, Expr, eload, th, r, &conv);
    printf("\nInitial Y: %1.6e\n", Yb);

PT1:

    Pattern(Xb, Yb, X, &Y, deltaF, deltaT, E, Expr, eload, th, r);
    printf("First Pattern Y: %1.6e\n", Y);

    if((Xb[0]==X[0])&&(Xb[1]==X[1]))
    {
        deltaF *= DR;
        deltaT *= DR;
        printf("\nReducing delta, deltaF = %1.6e\n", deltaF);
        printf("\nReducing delta, deltaT = %1.6e\n\n", deltaT);
        printf("GammaXY(Fx) = %1.8e\n", X[0]);
    }
}

```

```

        printf("Diff = %1.8e\n\n", X[1]);
        for(i=0; i<NAP; i++)
            E[i] = Eo[i];
        goto PT1;
    }

PT2:

    Xt[0] = 2*X[0]-Xb[0];
    Xt[1] = 2*X[1]-Xb[1];

    Xb[0] = X[0];
    Xb[1] = X[1];

    Yb = Y;

    Yt = lstsq(E, Xt, Expr, eload, th, r, &conv);
    printf("Temp Head Y: %1.6e\n",Yt);

    Pattern(Xt, Yt, X, &Y, deltaF, deltaT, E, Expr, eload, th, r);
    printf("Temp Head Pattern Y: %1.6e\n",Y);

    if(Y>Yb)
    {
        printf("\nStarting New Pattern, Y = %1.6e\n", Y);
        printf("GammaXY(Fx) = %1.8e\n", X[0]);
        printf("DIFF = %1.8e\n\n", X[1]);
        goto PT1;
    }
    else
    {
        printf("\nExtending Pattern, Y = %1.6e\n", Y);
        printf("GammaXY(Fx) = %1.8e\n", X[0]);
        printf("Diff = %1.8e\n\n", X[1]);
        goto PT2;
    }
}

```

## Subroutines

```

void Pattern(double Xb[], double Yb, double Xl[], double *Yl, double
deltaF, double deltaT, double E[], double Expr[][3], double eload[][5],
double th[], double r[])
{
    double Xp[2], Xm[2], Yp, Ym;
    int *conv;

    Xp[0] = Xb[0]+deltaF;
    Xm[0] = Xb[0]-deltaF;

    Xp[1] = Xb[1];
    Xm[1] = Xb[1];

    Yp = lstsq(E, Xp, Expr, eload, th, r, *conv);
    Ym = lstsq(E, Xm, Expr, eload, th, r, *conv);

    if((Yp<Yb)&&(Yp<Ym))
    {
        Xl[0] = Xp[0];
        *Yl = Yp;
    }
    else

```

```

    {
        if((Ym<Yb)&&(Ym<Yp))
        {
            Xl[0] = Xm[0];
            *Yl = Ym;
        }
        else
        {
            Xl[0] = Xb[0];
            *Yl = Yb;
        }
    }

    Xp[1] += deltaT;
    Xm[1] -= deltaT;

    Xp[0] = Xl[0];
    Xm[0] = Xl[0];

    Yp = lstsq(E, Xp, Expr, eload, th, r, *conv);
    Ym = lstsq(E, Xm, Expr, eload, th, r, *conv);

    if((Yp<*Yl)&&(Yp<Ym))
    {
        Xl[1] = Xp[1];
        *Yl = Yp;
    }
    else
    {
        if((Ym<*Yl)&&(Ym<Yp))
        {
            Xl[1] = Xm[1];
            *Yl = Ym;
        }
        else
            Xl[1] = Xb[1];
    }
}

double lstsq(double E[], double Xl2[], double Expr[][3], double
eload[][5], double th[], double r[], int *conv)
{
    int itr, i, j, jcall, crsh;

    double Ypre, Y, avg;

    Real_Vector phi, B1;
    Real_Matrix jaco, A1;

    phi = valloc(NULL, ND);
    jaco = mxalloc(NULL, NAP, ND);

    avg = (Expr[1][0]-Expr[1][1])/2;

    Expr[0][2]=Xl2[0];

    Expr[1][0]= avg - Xl2[1];
    Expr[1][1]= -avg - Xl2[1];

    for(itr=0; itr<21; itr++)
    {
        crsh = 1;

        jcall = 0;

```

```

Y = phisub(E, r, th, eload, Expr, phi, jcall, &crsh);

if(crsh!=1)
    goto CRASHED;

if(itr!=0)
{
    if(fabs(1-Y/Ypre) < .0001)
        goto CONVERGED;
}

Ypre = Y;

jacobeau(E, r, th, eload, Expr, jaco);

A1 = mxmul2(jaco, jaco, NAP, ND, NAP);

B1 = vscale(vmxmul(jaco, phi, NAP, ND), NAP, -1.0);

lineqn(A1, B1, NAP);

for(i=0 ; i<NAP ; i++)
{
    if(fabs(B1[i])>(.3*E[i]))
        B1[i] = .3*E[i]*(B1[i]/fabs(B1[i]));
    E[i] += B1[i];
}
E[5] = E[4];
E[6] = E[4];

vfree(B1);
mxfree(A1);
}

CRASHED:
    *conv = 0;
    goto OUT;

CONVERGED:
    *conv = 1;

OUT:

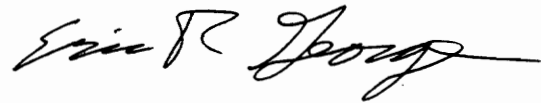
mxfree(jaco);
vfree(phi);

return Y;
}

```

## Vita

Eric Roger George was born on 18 April 1969 in Reading, Pennsylvania. After graduating from Northwestern Lehigh High School in 1987 he attended Virginia Polytechnic Institute and State University on an Air Force scholarship. He graduated with a B.S. in Aerospace Engineering in December, 1991 and was commissioned in the United States Air Force. The author then continued his studies at Virginia Tech in January, 1992 in pursuit of a Master's degree in Engineering Mechanics. The degree was completed in December, 1993.

A handwritten signature in black ink, reading "Eric R. George". The signature is written in a cursive, flowing style with a long horizontal stroke at the end.